THE
PHYSICAL REVIEW

A journal of experimental and theoretical physics established by E. L. Nichols in 1893

SECOND SERIES, VOL. 74, NO. 5 SEPTEMBER 1, 1948

Photographic Plates for Use in Nuclear Physics†

J. H. WEBB
Research Laboratories, Eastman Kodak Company, Rochester, New York
(Received April 13, 1948)

The registration of charged particles by the photographic emulsion is considered from the standpoint of their space rate of energy loss on passage through matter. On the basis of the highest-energy particles that can be recorded as recognizable tracks, an energy-loss value of 0.013 Mev per centimeter of air path is taken as an approximate threshold sensitivity value of the best present-day nuclear-particle emulsions. This energy-loss value corresponds to alpha-particles of energy >400 Mev, deuterons of 100 Mev, protons of 50 Mev, and electrons of 20 kev. Some evidence is cited to show that these limiting energy values are in accord with experience.

Range-energy curves for alpha-particles, protons, deuterons, and mesons in high silver halide concentration emulsions are given, based on constant stopping-power values of the emulsion. A relative stopping-power value of 1800 is used for alpha-particles, and a value of 2000 is used for protons, deuterons, and mesons.

Data on the composition, physical characteristics, and sensitivity, and also recommended uses of some of the commercially available nuclear-particle emulsions are presented.

A theoretical calculation of the stopping power of the photographic emulsion relative to that of air is given. Curves of stopping power *versus* energy for alpha-particles and protons in a high silver halide content emulsion are calculated and compared with published experimental values.

Grain density and its variation in the recorded tracks of nuclear particles in the photographic emulsion are discussed. It is pointed out that the grain density for low-energy particles approaches a maximum value determined by the grain population of the unexposed emulsion. A qualitative discussion is given to show why grain spacing varies with particles of differing ionizing power.

Finally, the mechanism of latent-image formation is considered from the standpoint of ion-pair production in the grain. Using the energy-loss value of 0.013 Mev per centimeter as a threshold limit and a value of 7.6 ev for the energy required to produce an ion pair in silver bromide, it is shown that about 150 ion pairs must be produced in a single grain to form the latent image.

IN 1896 Becquerel discovered that uranium salts emit radiations capable of blackening a photographic plate. In the early work in radioactivity, the photographic plate was, in fact, about the only means of detecting the radiations from these newly discovered materials. Later, however, as more quantitative work on radiations associated with radioactivity came to be done, other methods of measurement came into general use.

In 1911 Wilson introduced the cloud chamber which was the first instrument actually to show the paths of individual nuclear particles. It was at about this same time that the photographic emulsion was first shown to be capable of registering the paths of nuclear particles. In 1910 Kinoshita[1] demonstrated that photographic grains were affected by alpha-particles and, furthermore, that the impact of a single alpha-particle was probably sufficient to produce a developable latent image in a grain. In 1912 Reinganum[2] showed that the path of an alpha-

† Communication No. 1182 from the Kodak Research Laboratories.

[1] S. Kinoshita, Proc. Roy. Soc. (London) **83A**, 432 (1910).
[2] M. Reinganum, Physik. Zeits. **10**, 1276 (1911).

particle in an emulsion could be registered as a line of developable grains. Since this discovery, many workers have made use of the photographic plate for the registration and study of single nuclear events. Among the pioneers in this field the names of Blau and Wambacher and Wilkins are to be especially pointed out. For a summary of all work along these lines up to 1941 the reader is referred to the excellent review by Shapiro.[3]

The photographic plate resembles very closely the cloud chamber in its ability to record individual nuclear events, but it does not give the fine distinction between tracks of different types of particles nor the possibility of recording the bending of particles in a magnetic field as does the cloud-chamber technique. However, because of its higher stopping power, continuous sensitivity, and simplicity, the photographic plate offers certain advantages not possessed by the cloud chamber. Particles that can be observed in the cloud chamber are alpha-particles, protons, deuterons, positrons, electrons, and mesotrons. It is highly desirable that the photographic plate should be developed to a point where it will record all these particles over wide ranges of energy. Obviously, a photographic plate that could achieve this goal, together with its higher stopping power and permanent record, would be an exceedingly important tool for the nuclear physicist.

It is the purpose of the present paper to show how far the photographic plate has been developed in this direction, what is available now, and what are the prospects for the future. A general outline is given of the mechanism by which charged particles affect the photographic plate. The composition and structure of present-day nuclear-track plates are discussed and a method of calculating the stopping power of an emulsion of known composition is presented. The question of grain spacing and the factors upon which it depends are considered, and finally some aspects of latent-image formation are discussed, with particular reference to the number of ion pairs required to produce developability in a single grain. In discussing all these topics, an attempt is made to cite experimental evidence to show that the conclusions reached are in line with practical experience. This paper does not purport to present novel and unusual experimental results. (While the present paper was in course of preparation, two excellent papers on this same general subject have appeared by Demers[4] and by Lattes, Fowler, and Cüer.[5] These two papers present considerably more experimental data on the nuclear-particle plates than are given here and are highly recommended to the reader, Also, the beautifully illustrated book just published by Powell and Occhialini[6] is recommended to the worker in this field.) Rather, the subjects treated and the experimental data presented are intended as a guide to an understanding of the action of the photographic plate as a tool in nuclear research.

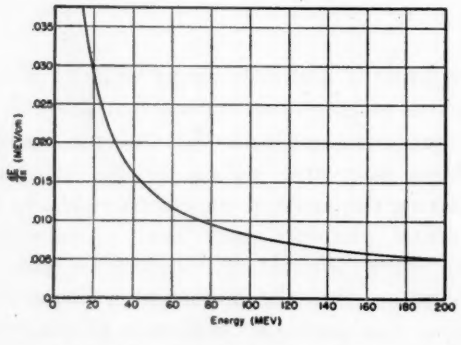

FIG. 1. Theoretical curve of space rate of energy loss for protons in air according to Eq. (1). From calculations by J. H. Smith, Phys. Rev. 71, 32 (1947).

SPACE RATE OF ENERGY-LOSS AND RANGE-ENERGY CURVES FOR CHARGED PARTICLES IN AIR

In Fig. 1 is shown a curve of energy loss per centimeter of path on passage of a proton through air. This curve gives the loss of energy in Mev per centimeter as a function of the energy of the proton in Mev and was plotted from the theoretical data computed by J. H. Smith,[7] using the following equation[8–10] for the average energy

[3] M. M. Shapiro, Rev. Mod. Phys. **13**, 58 (1941).

[4] P. Demers, Can. J. Research **25**, 223 (1947).

[5] C. M. Lattes, P. H. Fowler, and P. Cüer, Proc. Phys. Soc. (London) **59**, 883 (1947).

[6] C. F. Powell, and G. P. S. Occhialini, *Nuclear Physics in Photographs* (Oxford University Press, London, 1947).

[7] J. H. Smith, Phys. Rev. **71**, 32 (1947).

[8] M. S. Livingston, and H. Bethe, Rev. Mod. Phys. **9**, 263 (1937).

[9] B. Rossi, and K. Greisen, Rev. Mod. Phys. **13**, 249 (1941).

[10] J. Wheeler, and R. Ladenberg, Phys. Rev. **60**, 761 (1941).

loss per unit thickness of stopping material:

$$(dE/dx) = -[4\pi(ze)^2 N/mv^2]\cdot \{Z[\ln(2mv^2/I) - \ln(1-\beta^2) - \beta^2] - C_K\}, \quad (1)$$

in which

ze = charge of the incident particle;
v = velocity of the incident particle;
N = number of atoms per cubic centimeter of stopping material;
Z = atomic number of stopping atoms;
I = average ionization potential of stopping material;
m = electron mass;
$\beta = v/c$, c the velocity of light;
C_K = a corrective term which must be applied in case v is comparable with the velocity of the K electron of the stopping material but large compared with that of all others.

The main portion of the energy loss, suffered by charged particles traversing matter, goes into production of ions through the interaction of the bombarding particles with the electrons of the stopping material. The loss of energy varies directly with the square of the charge, $(ze)^2$, of the incident particle, inversely as the square of the velocity, v, of the incident particle, and directly with the number of electrons per cubic centimeter, (NZ), of the stopping material. The quantity

$$B = Z \ln(2mv^2/I) \quad (2)$$

has been designated as the stopping number of an atom of the stopping material, and the ratio of B for a given material to the B_0 for air as the relative stopping power of the atom of that material; thus,

$$s_a = B/B_0. \quad (3)$$

The range-energy curve for a charged particle in air can be obtained from the rate of energy loss curve from the integral,

$$R = \int_0^E [dE/(dE/dx)]. \quad (4)$$

The range-energy curve for protons in air, as computed by J. H. Smith,[7] is shown in Fig. 2. From the curves for energy loss and range for a

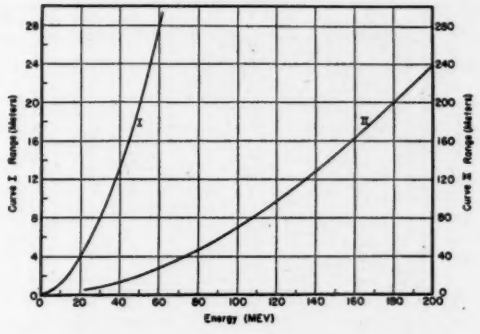

FIG. 2. Theoretical range-energy curves for protons in air according to Eq. (4). From calculations by J. H. Smith, Phys. Rev. 71, 32 (1947).

given type of particle (characterized by a particular value of charge (ze) and mass (M)) it is possible to determine the energy-loss and range curves of other particles of different z and M values by means of relations (5) and (6) given below for alpha-particles and protons as examples. Thus, if an alpha-particle and a proton are assumed to have the same velocities, then

$$(dE/dx)_{\alpha,v} = (z_\alpha/z_H)^2 (dE/dx)_{H,v},$$
$$R_\alpha(v) = (z_H/z_\alpha)^2 (M_\alpha/M_H) R_H(v); \quad (5)$$

or, since particles having the same velocities have energies in proportion to their mass values, the relations (5) can be expressed in terms of energies of the particles:

$$(dE/dx)_{\alpha,E} = (z_\alpha/z_H)^2 (dE/dx)_H \left(\frac{M_H}{M_\alpha}E\right)$$
$$R_\alpha(E) = (z_H/z_\alpha)^2 (M_\alpha/M_H) R_H((M_H/M_\alpha)E). \quad (6)$$

The relations (5) and (6) are very convenient for transposing energy-loss and range values from one particle to another of different z and M values.

In Fig. 3, energy-loss curves in Mev per centimeter of air path for alpha-particles, deuterons, protons, mesons (mass 0.1 of proton), and electrons are shown to the same scale. The proton curve is the same as that shown in Fig. 1, and is therefore accurate with respect to relativity corrections, etc., to the full 400-Mev value shown. The curves for the alpha-particles, deuterons, and mesons were derived from the proton curve by means of the relation (6) and, though not so accurate as the proton curve, are adequate

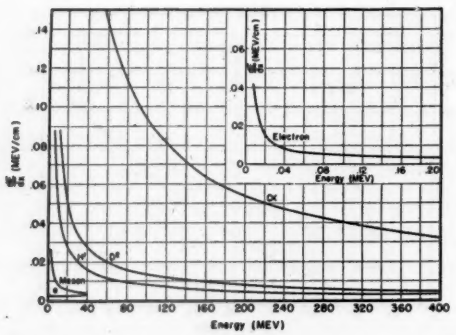

FIG. 3. Theoretical curves of space rate of energy loss for α-particles, deuterons, protons, mesons, and electrons in air.

for the purpose here. The energy-loss curve for the electron is shown on an enlarged scale in the upper right section of Fig. 3.

The reason for showing the energy-loss curves is that they bear a close relationship to the mechanism by which high-velocity charged particles act on a photographic grain to produce developability and therefore will be of material aid in discussing this problem.

PRESENT LIMIT OF PHOTOGRAPHIC SENSITIVITY FOR CHARGED PARTICLES

The threshold sensitivity of nuclear-track plates can best be designated in terms of the lowest rate of energy loss for which a particle will register as a just recognizable line of grains. With the best modern nuclear-track plates, there is evidence to indicate that this limit is reached for deuterons of around 100-Mev and protons of around 50-Mev energy. Thus, on an Eastman NTB plate exposed to the 190-Mev deuteron beam of the University of California cyclotron, individual tracks have been followed in the microscope over path lengths from their stopping end of the order of 2 cm.* Assuming a stopping power of 2000 for the emulsion, this would give an equivalent air path of 40 meters, corresponding to that of a 100-Mev deuteron. The high-velocity end of such a residual track consists of widely and irregularly spaced grains. Therefore, it must be supposed that only those grains of highest sensitivity and those most favorably hit by the charged particles are made developable under these conditions.

* From visual observations through the microscope made in the Kodak Research Laboratories.

Direct evidence on the sensitivity of the nuclear-track plates is given by the pictures shown in Fig. 4. The upper photograph shows an Eastman NTB plate that was exposed edgewise to the 190-Mev deuteron beam in the University of California cyclotron. The deuterons hit the glass plate, on which the emulsion is mounted, edge on, and traveled mostly in the glass. As they emerged through the surface of the glass, they produced tracks in the emulsion that are characteristic of their energy at that point. The darker section at the bottom corresponds to the more intense part of the beam. It can be seen that the darkening of the plate is faint over most of the 6.9-cm range of the particles, but increases steeply near the end of the path, in accordance with the Bragg curve of ionization. It is interesting to note that while the range of the 190-Mev deuterons in glass is 6.9 cm, the range for the same energy deuterons in the photographic emulsion would be 6.4 cm, based on a relative stopping power of 2000. Thus, the stopping power of the glass and that of the photographic emulsion are not very different.

In order to determine how the varying energy deuterons register as tracks on the NTB plate, photomicrographs were made of sample tracks on a plate that had received a somewhat lighter exposure than the above plate, at points 0, 0.5, 1, 2, 4, and 6 cm from the end of their range. These tracks are shown in the lower part of Fig. 4. Only the parallel tracks are to be considered, because the diagonal tracks result from deflected or secondary particles of reduced velocity. It can be seen that dense tracks are obtained at the 0.0- and 0.5-cm positions ($\sim$45 Mev), less dense tracks at the 1-cm position ($\sim$64 Mev), and still less dense, but recognizable, tracks at the 2-cm position ($\sim$95 Mev). At the 4-cm position ($\sim$138 Mev), the tracks have become somewhat tenuous and at the 6-cm position ($\sim$185 Mev) are composed of widely spaced grains. From these pictures it is evident that there is no sharp cutoff in sensitivity with increasing energy. However, when the tracks on these plates are viewed in the microscope it is apparent that the quality of the tracks have deteriorated considerably for energies above 100 Mev.

From the deuteron curve of Fig. 3 it can be seen that a 100-Mev energy corresponds to an

energy-loss value in air of 0.013 Mev per centimeter. Assuming that this is the threshold energy-loss value for which enough grains will respond to give a recognizable track, the following limiting energy values for other particles that will give tracks of comparable quality may be set down:

Deuteron	100 Mev
Proton	50 Mev
α-particle	>400 Mev
Meson (200 Me)	5 Mev
Electron	0.022 Mev

It is of interest to point out that Eastman NTB plates exposed to the 380-Mev alpha-particles of the University of California cyclotron recorded particles of this energy. Though the whole track length (~3.2 cm) corresponding to this energy could not be recorded in the thin emulsion layer, nevertheless it was observed that the beginnings of the tracks of many alpha-particles of this energy were recorded. Tracks of protons of high energy have been recorded on

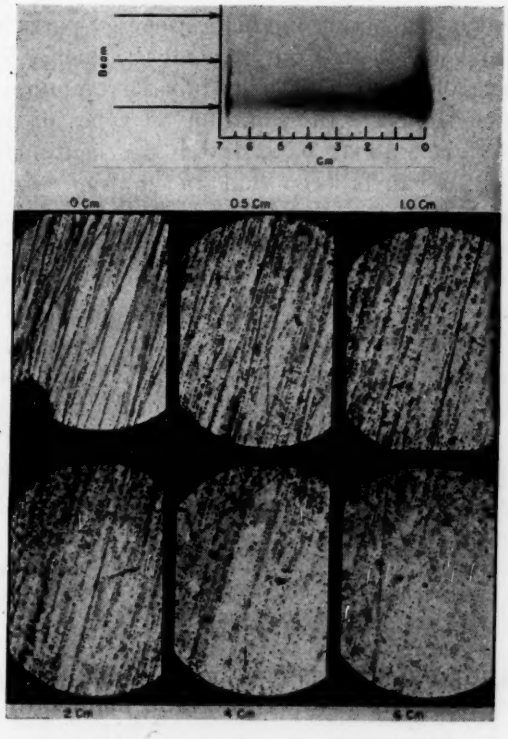

FIG. 4. Photographic effect of 190-Mev deuterons on nuclear-track plates. Upper picture = over-all density due to deuterons as they are slowed. Lower picture = photomicrographs of tracks of deuterons at various distances from the stopping end.

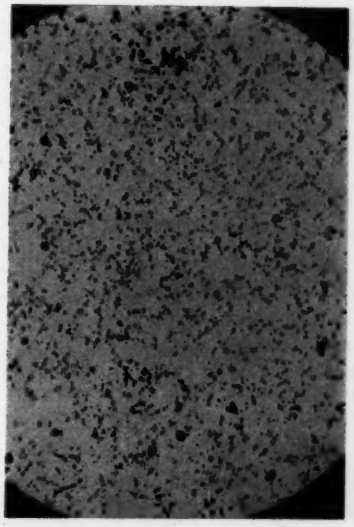

FIG. 5. Photomicrograph of Eastman NTB plate, exposed to 30-kv electrons, showing tracks of 4–5 grain length.

Ilford halftone plates by H. Wambacher.[11] One of these recorded tracks had a path length of 2 cm in the emulsion. If a value of 1300 is taken for the stopping power relative to air for the emulsion used, this would give an air path of 26 meters, corresponding to an energy of 57 Mev. Also, a number of workers[12–17] have given experimental results on meson tracks in emulsions. Lattes, Muirhead, Occhialini, and Powell[12] point out that on the basis of sensitivity estimates mesons of energy higher than 5 Mev probably cannot be detected with Ilford C2 plates. In a later paper by Lattes, Occhialini, and Powell,[16] meson tracks of varying residual ranges were analyzed. The energy can be estimated from the range, if a value for the mass is assumed for the meson. With an assumed mass of 200 electron masses, the tracks corresponded to 4.1-Mev mesons. These results are merely cited as evidence that particles having energies between zero and the limits set above are capable of recording as recognizable tracks in the nuclear-particle plates.

[11] H. Wambacher, Sitz. Akad. Wiss. in Wien, Math.-Naturwiss. Klasse Abteilung IIa, **149**, Heft 3–4, 157 (1940).
[12] C. M. G. Lattes, H. Muirhead, G. P. S. Occhialini, and C. F. Powell, Nature **159**, 694 (1947).
[13] D. M. Bose, and B. Choudhuri, Nature **148**, 259 (1941).
[14] D. H. Perkins, Nature **159**, 126 (1947).
[15] G. P. S. Occhialini, and C. F. Powell, Nature **159**, 186 (1947).
[16] C. M. G. Lattes, G. P. S. Occhialini, and C. F. Powell, Nature **160**, 453 (1947).
[17] C. M. G. Lattes, G. P. S. Occhialini, and C. F. Powell, Nature **160**, 486 (1947).

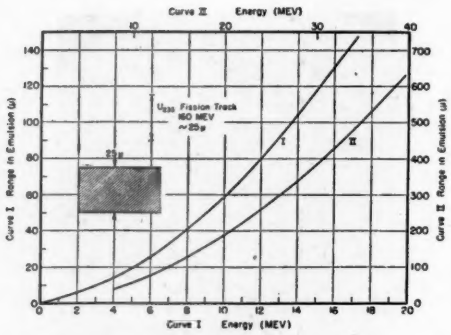

FIG. 6. Range-energy curve for α-particles in nuclear-track plate of high AgBr concentration. Drawn for constant stopping power of 1800.

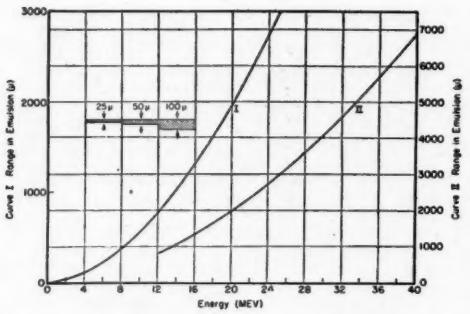

FIG. 7. Range-energy curve for protons on nuclear-track plates of high AgBr concentration. Drawn for constant stopping power of 2000.

Until very recently, indisputable tracks of electrons in emulsions had not been observed. However, in a recent paper Demers[4] stated that with very sensitive emulsions of his own manufacture he had observed faint complicated tracks of a few grains' length which he attributed to electrons. Subsequent to Demers's paper, tracks of electrons were obtained by members of the Eastman Kodak Research Laboratory[18] at Harrow, England, with their high-sensitivity proton plates. Electron tracks have now been observed on the Eastman NTB plates and an illustration is given in Fig. 5. This plate was exposed to 30-kv electrons in the RCA electron microscope, with the electron beam perpendicular to the plate. As can be seen, the tracks are short and wavy and consist of only a few grains each. From the energy-loss curve for electrons shown in Fig. 3, the limiting energy electron that will make a grain developable is about 0.022 Mev. An electron of this energy would have a residual range in air of approximately 0.7 cm. If a stopping power of 2000 is assumed for the emulsion, this would correspond to a path length in the emulsion of 3.5μ. Therefore, only a few grains (three to four) at the very end of the electron path could be made developable. Here, again, the action of the electrons on the emulsion grains appears to be in line with what is to be expected on the basis of energy-loss data.

From what has been said it may be concluded that in the nuclear emulsions being made today a moderate fraction of the grains will be affected by particles whose energy-loss value is as low as 0.013 Mev per centimeter in air. This limit, while somewhat arbitrary, is based on the criterion that the emulsion contains a certain fraction of grains with sufficiently high sensitivity that a particle of this energy-loss value will register as a detectable line of grains.

It is interesting to compare the figure of 0.013 Mev per centimeter with the minimum energy-loss values of the curves of Fig. 3 in order to see how far present-day emulsions are from the point of registering the highest-energy particles. It may be pointed out that all the energy-loss curves of Fig. 3 go through a broad flat minimum, which is closely the same for all types of particles, i.e., about 0.0022 Mev per centimeter. Thus, it can be seen that an emulsion with a threshold sensitivity of some five to six times lower value would be required in order to register particles of any energy value whatever. Even though this ultimate goal may be unattainable, an inspection of the curves of Fig. 3 will show that even slight improvement in the threshold sensitivity value will tend to push upward disproportionately the energy value of particles that can be registered. Considering the short time that serious development work on the nuclear-track plates has been in progress, it does not appear impossible that the sensitivity might be pushed to a point corresponding to an energy-loss value of 0.0022 Mev per centimeter.

RANGE-ENERGY CURVES FOR CHARGED PARTICLES IN A PHOTOGRAPHIC EMULSION

To illustrate the range-energy relationship for nuclear-track plates of high silver bromide concentration, curves showing range in microns (μ) *versus* energy in Mev are given for alpha-particles

[18] R. W. Berriman, Nature **161**, 432 (1948).

and protons, respectively, in Figs. 6 and 7. The curve for alpha-particles shown in Fig. 6 was constructed assuming a constant stopping power of emulsion relative to that of air of 1800. This figure was selected on the basis of the general average of results obtained in tests of Eastman NTA and NTB emulsions exposed to alpha-particles of energy below 9 Mev, obtained from natural radioactive materials such as thorium, polonium, and uranium. Every batch of Eastman NTA plates is given a standard test to polonium alpha-particles (5.3 Mev) and these tests consistently give a range value between 21 and 22μ in close agreement with the stopping power value of 1800.

Data published by Tsien San-Tsiang, Chastel, Faraggi, and Vigneron[19] for alpha-particles on Ilford new halftone concentrated plates are given below:

	E (Mev)	Range in emulsion (μ)	Stopping power relative to air
ThC′	8.77	46.1	1860
ThC	6.05	26.2	1810
Po	5.29	21.4	1790
UI	4.71	18.8	1710
UII	4.15	15.6	1700

These values indicate the falling off of stopping power to be expected at low energies. Later in this paper, the question of stopping power of the emulsion will be discussed more fully and a method will be given for calculating this quantity, using the stopping power of the constituent atoms of the emulsion and the composition of the emulsion.

For energies above 10 Mev there have been so few range-energy measurements made for alpha-particles in emulsions that a curve based on experience cannot be drawn for this region. Therefore, until additional measurements of range-energy values are made for energies above 10 Mev, the curve for this region of Fig. 6 must be considered as an approximation.

The straight vertical arrow in Fig. 6, marked U^{235} fission track, is representative of the range obtained by several workers[20–22] who used photographic emulsions for recording fission tracks. The range (25μ) indicated by the arrow corresponds to the full length of the track for both fragments. One of these tracks, obtained on an Eastman NTC emulsion, is shown in Fig. 19, and it may be noted that the grain density is greatest in the middle portion. The high charge on the fragments immediately after fission causes the heavy initial ionization in spite of the high velocity of the particle. As the fission fragments lose velocity, it might be expected that the ionization would increase. However, the loss of charge of the fragment more than overbalances the effect of reduced velocity, and the net result is a reduction in ionization, as indicated by the lower grain density of the track toward its extremities. It is interesting to estimate the average effective charge of a fission fragment from the observed range of the fragments for U fission, using the relation (6),

$$R_{fiss}(E)=(z_H/z_f)^2(M_f/M_H)R_H((M_H/M_f)\cdot E).$$

Inserting the relative-mass values of fission fragment to proton as 117 and an estimated average value of the charge on the fission fragment of 10, we obtain, for the 160-Mev energy of the combined fission fragments,

$$R_f(160)=(1/100)117R_H(1.36)=4.68 \text{ cm air},$$

or a range in the emulsion, using a stopping power of 1800,

$$R_f=26\mu.$$

Thus, when one assumes an average charge value of 10 for the fission fragments, a range value in close agreement with experiment is found.

Also, a cross section of an emulsion 25μ thick is shown to scale in Fig. 6, for comparison with the track lengths. It can be seen that a 25μ emulsion is thick enough to register alpha-particles of moderate energy value without too much chance of the tracks running out of the emulsion. However, for energy values above 15 Mev, thicker emulsions up to 50 or even 100μ are desirable. In Fig. 7 is given a range-energy curve for protons up to energies of 40 Mev. The curve is drawn for a constant value of stopping power of the emulsion relative to air of 2000 instead of 1800, as used for the alpha-particle curve. This value was chosen from the results of

[19] Tsien San-Tsiang, R. Chastel, H. Faraggi, and L. Vigneron, Comptes rendus **223**, 571 (1946).
[20] P. Demers, Phys. Rev. **70**, 974 (1946).
[21] K. Lark-Horowitz, and W. A. Miller, Phys. Rev. **59**, 941 (1941).
[22] L. L. Green, and D. L. Livesey, Nature **158**, 272 (1946).

tests on Eastman NTB emulsions exposed to protons of energy below 10 Mev. In this connection, Eastman NTB emulsions are regularly tested with 7.0-Mev protons from the University of Rochester cyclotron, and the range values obtained in these tests have averaged 300μ, which, compared with the 60-cm air path for these particles, corresponds closely to a stopping power of 2000. Actually, the stopping power of the photographic emulsion is not a constant value independent of energy of the particle, but increases with energy rather sharply at low energies of the particle and flattens out into a gradually rising curve for higher energies, as shown in Fig. 9. As can be seen from this figure, the plateau region of the stopping-power curve is reached at considerably lower energy values for protons than for alpha-particles and this is in line with the higher stopping-power value of 2000 used in Fig. 7. Owing to the lack of experimental data on the stopping power of the range-energy curve of nuclear plates for energies above 10 Mev and also because of the variation of stopping power at very low energies, the range-energy curves of Figs. 6 and 7 are to be regarded merely as fairly reliable guides to the range-energy relationship.

In Fig. 7, cross sections of emulsions of thicknesses 25, 50, and 100μ are shown for purposes of comparison with the proton tracks of varying energy. Commercial emulsions are now available in thicknesses up to 100μ. For protons of energy above 10 Mev, the 100μ emulsion is required in order to insure that a good fraction of the tracks will fall within the angle tolerance limits afforded by this thickness of emulsion.

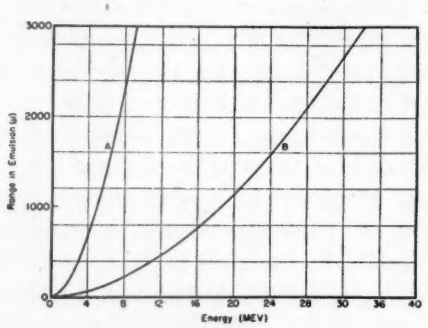

FIG. 8. Range-energy curves for (A) meson (0.1 mass of proton) and (B) deuteron on nuclear-track plates of high AgBr concentration. Drawn for constant stopping power of 2000.

For completeness, range-energy curves for mesons and deuterons in an emulsion are shown in Fig. 8. Both curves were drawn for a constant stopping power of 2000, and the mass assumed for the meson is one-tenth of the proton mass.

According to the foregoing discussion, it is obvious that for the registration of high-energy particles emulsions of much greater thickness than 100μ, in fact, up to several millimeters, would be desirable. Unfortunately, there are several obstacles to the use of emulsions of such great thickness. Coatings of a gelatin emulsion greater than 100μ are exceedingly difficult to deal with mechanically. A 100μ coating on film will cause it to curl and twist to an extent that makes it almost impossible to handle. If placed on glass plates, the gelatin will peel off because the forces exerted are sufficient to fracture the glass surface on which it is mounted. In addition to these troubles, there are formidable difficulties in processing thick emulsions. Both the development and fixing procedures depend upon a process of diffusion of the chemicals into the emulsion layer and of reaction products out of the layer. As the chemical agents become exhausted within the layer, replenishment of fresh chemical is needed, and therefore a process of exchange diffusion is required if the image is to be fully developed and fixed. Even in emulsions of 100μ thickness, development and fixing are carried out with difficulty, and sometimes there is evidence of variation of response at varying depths of the layer because of the non-uniform processing conditions.

Finally, it should be pointed out that the thickness of emulsion that can be examined with the microscope is limited by the working distance of the objective used. With an oil-immersion objective of 1.8-mm focal length and 97 power, the maximum working distance in the emulsion, without a cover glass, is 300 microns.

COMMERCIAL NUCLEAR-RESEARCH EMULSIONS

Nuclear-research emulsions of the type discussed here are manufactured by the Ilford Company and Kodak, Ltd., in England and by the Eastman Kodak Company in America.

The Ilford research laboratory issues a pamphlet describing its emulsions for recording particle tracks and giving photographic charac-

TABLE I. Eastman nuclear plates.

		Type NTA	Type NTB*	Type NTC
Sensitivity	To nuclear particles	Alpha-particles to 200 Mev, Protons to 20 Mev, Deuterons to 20 Mev	Alpha-particles to 400 Mev, Protons to 50 Mev, Deuterons to 100 Mev, Mesons to 5 Mev	Nuclear-fission fragments of high ionizing power only
	To light, gamma rays, and beta rays	low	moderate	very low
Development	To show energy-loss rate by grain spacing	2 minutes at 68°F in D-19		special instructions
	To render tracks very clear for counting	2 minutes at 68°F in D-8** diluted 2:1		special instructions
Recommended fixation		F-5 or 30 percent hypo	30 percent hypo	
Emulsion thickness		25μ regular (to 100μ on request)	50μ and 100μ (process 100μ by special instructions)	25μ
Silver bromide content—percent weight of dry emulsion		83 percent	83 percent	65 percent
Grain size (approx.)		0.2–0.4μ diam.	0.2–0.3μ diam.	0.1–0.4μ diam.

* Recommended for all higher-energy particles of low ionizing power.
** To obtain best response to low ionizing particles such as mesons and electrons the following alternate development is recommended: Soak in water for five minutes; develop in D-19 diluted 1 : 3 for 22 min. at 68°F. Fix in 30 percent hypo for twice the time to clear.

teristics and composition. In the pamphlet accompanying the plates, the Ilford laboratory gives the following list and description of its nuclear-particle emulsions:

"Type B-2—Fine grain and the most sensitive emulsion of the series, giving good tracks of α-particles and 2–4 Mev protons.

"Type C-2—Finer grain than B-2, giving more clearly defined α-particle and proton tracks. Specially made for giving measurable proton tracks.

"Type E-1—Of very slightly finer grain than C-2, giving improved α-particle records, suitable for accurate measurement of range. The tracks formed by protons are poor, thus distinguishing clearly between these and α-particles.

"Type D-1—Of finer grain than E-1. α-particle tracks poor, protons do not record but good fission tracks are obtained.

"The following may perhaps be regarded as obsolescent but are still produced to special order.

"Type B-1—Has grain characteristics similar to B-2 but sensitivity similar to C-2. B-2 and C-2 are believed to be preferable alternatives.

"Type C-1—Similar to E-1 but of slightly coarser grain and slightly greater sensitivity. Gives inferior discrimination between α-particles and protons of low energy.

"Standard emulsion thickness are 50μ and 100μ. All emulsions, except C-1 and D-1 may be supplied loaded with lithium, boron, or beryllium, or with a lower concentration of silver in the gelatin medium. . . .

"All these emulsions, in standard form, have the same chemical composition. This is approximately as follows, in grams of each element per cubic centimeter of emulsion, under normal atmospheric conditions: Ag—1.87; H—0.056; Br—1.36; O—0.24; I—0.053; S—0.014; C—0.33; N—0.083; Ca, P, Cr, Si, Na—traces."

The Ilford Company also publishes tables of range-energy values, based on actual measurement, for the energy range 0–10 Mev and extrapolated range-energy values for the energy range 10–35 Mev, for both alpha-particles and protons.

The range-energy values published by Ilford do not differ greatly from the values given in Figs. 6 and 7 for alpha-particles and protons below 10-Mev energy. However, there are some differences above 10 Mev. This is because the curves of Figs. 6 and 7 were drawn using a constant stopping power for all energy values. In the

TABLE II. Composition of Eastman nuclear-track plates.

Element	NTA and NTB Percent	NTA and NTB Atomic ratio	NTC Percent	NTC Atomic ratio
Ag	47.1	1.0	38.0	1.0
I	1.49	0.027	1.24	0.027
Br	33.9	0.97	27.4	0.979
C	8.47	1.62	16.2	3.83
H	1.17	2.68	2.25	6.38
N	3.06	0.50	6.84	1.17
O	4.80	0.69	9.09	1.62
Relative humidity, percent	Moisture content—percent weight of dry emulsion			
50	2.2		4.5	
70	4.0		8.0	

next section, the matter of stopping power is treated more in detail and curves of range energy, using varying stopping power, are given.

Kodak, Ltd. in England has very recently started to make a nuclear-particle plate designated as NTP-2A. It is a high-sensitivity plate especially recommended for registering high-velocity particles of low ionizing power. In its experimental stage, it was the first plate to register well-recognizable electron tracks. These plates are now marketed as a standard item in size $1''\times3''$ and 50μ thickness. The sensitivity, stopping power, and physical characteristics are closely the same as those of the NTB plate made by the Eastman Kodak Company in America and described in the following paragraphs.

At present, the Eastman Kodak Company is marketing three general types of nuclear-track plates classified under the headings: NTA, NTB, and NTC. The general properties and recommended processing conditions for these emulsions are presented in Table I.

Examples of tracks of different nuclear particles registered on these plates are shown in Figs. 16–19. It should be mentioned that the NTA and NTB plates can be supplied impregnated with the elements, boron, lithium, and beryllium, the amount of impregnating material being specified in milligrams per square centimeter for each batch of plates. Specific instructions for handling and processing these plates are supplied by the manufacturer with each batch of plates.

For certain purposes, it is desirable for the nuclear physicist to have an accurate knowledge of the composition of the photographic plate that he uses. Accordingly, the following figures on the composition of Eastman emulsions are given. All emulsions are essentially mixtures of gelatin and silver bromide. The composition of the gelatin expressed in weight percent is as follows:

Gelatin composition, percent	
Carbon	50.0
Hydrogen	6.7
Nitrogen	18.0
Oxygen	25.0

The nuclear-particle plates have a relatively higher percentage of silver bromide than the normal photographic emulsion. The Eastman NTA and NTB emulsions have the same composition, containing about 83 percent silver halide and 17 percent gelatin. The NTC plate contains about 65 percent silver halide and 35 percent gelatin. In Table II the composition of the Eastman NTA, NTB, and NTC plates is given in terms of percent weight and in terms of atomic ratios, as determined from chemical analysis of the dry emulsions. The atomic composition values must be corrected for moisture content according to the figures in the lower part of Table II, if accurate work is contemplated.

STOPPING POWER OF PHOTOGRAPHIC EMULSION

It seems appropriate to present a calculation of the stopping power of a photographic emulsion, based on the best data available on the atomic stopping power of the constituent atoms of the emulsion.

A method of calculating the stopping power for chemical compounds, when the stopping powers of the constituent atoms of the compound are known, has been outlined by several previous workers.[23,24] A brief review of the method of computing the stopping power of a chemical compound will be given before it is applied to the case of the photographic emulsion. The relative atomic stopping power of one substance, as compared with that of another substance taken as standard, may be defined by the relation

$$R_0/R=(N/N_0)(s/s_0), \tag{7}$$

where R_0 is the range of a charged particle in air,

[23] H. R. Von Traubenberg, Zeits. f. Physik **5**, 396 (1921).
[24] P. Cüer, Comptes rendus **223**, 1121 (1946).

R is the range in the test substance, N_0 is the effective number of atoms per cubic centimeter of air under normal conditions and based on an average atomic weight, and N is the number of atoms per cubic centimeter of the test substance. The quantity, s/s_0, is the atomic stopping power of the substance relative to that of air. As pointed out by Cüer,[24] the quantity usually measured in experimental work is not R_0/R but the relative differential ranges, $\Delta R_0/\Delta R$, for small energy steps. Accordingly, we will change (7) to read

$$\Delta R_0/\Delta R=(N/N_0)(s/s_0), \quad (8)$$

or, since s_0 for air is taken as unity,

$$\Delta R_0/\Delta R=(N/N_0)s. \quad (9)$$

If we replace the quantities N and N_0 by their equivalent values expressed in terms of density and atomic weight, i.e., $N=kd/A$ and $N_0=kd_0/A_0$, then the relationship

$$\Delta R_0/\Delta R=(dA_0/d_0A)s \quad (10)$$

follows. Bragg established the fact that the stopping power of a chemical compound made up of several types of atoms is an additive property. Accordingly, we can write for a compound

$$\Delta R_0/\Delta R=n(N_1s_1+N_2s_2+N_3s_3\cdots+N_is_i)/N_0$$

where N_1, N_2, etc., refer to the number of atoms of each type in one molecule, and n refers to the number of molecules of the compound per cubic centimeter. Since

$$N_0=kd_0/A_0$$

and

$$n=d/(N_1A_1+N_2A_2+\cdots+N_iA_i),$$

we find

$$\frac{\Delta R_0}{\Delta R}=\frac{d\cdot A_0}{d_0}\left(\frac{N_1s_1+N_2s_2+\cdots+N_is_i}{N_1A_1+N_2A_2+\cdots+N_iA_i}\right)=d\cdot A_0S/d_0M, \quad (11)$$

where M in Eq. (11) refers to the molecular weight and s to the molecular stopping power. For purposes of calculation, it is more convenient to write (11) in a slightly different form:

$$\Delta R_0/\Delta R=(d\cdot A_0/d_0)\{(N_1A_1s_1/A_1\textstyle\sum_j N_jA_j)+(N_2A_2s_2/A_2\sum_j N_jA_j)+\cdots+(N_iA_is_i/A_i\sum_j N_jA_j)\}.$$

TABLE III. Composition of emulsion.*

Element	Atoms per molecule of AgBr	Weight per mole of AgBr	P_i weight percent	$\frac{P_i}{A_i}=\frac{\text{fractional weight}}{\text{atomic weight}}$
Ag	1.0	107.88	47.20	0.004375
Br	1.0	79.92	34.95	0.004373
C	1.39	16.70	7.30	0.006083
H	3.06	3.08	1.35	0.013410
N	0.43	6.02	2.64	0.001886
O	0.932	14.90	6.53	0.004081

* This emulsion contains no iodide but this fact affects the stopping power only slightly since bromide replaces the iodide. The effective composition of this emulsion, as it affects stopping power, is closely the same as the Eastman NTA and NTB plates and the Ilford plates.

This relationship may be abbreviated to read**

$$\Delta R_0/\Delta R=(d\cdot A_0/d_0)\{(p_1s_1/A_1)+(p_2s_2/A_2)+\cdots+(p_is_i/A_i)\}, \quad (12)$$

where $p_i=N_iA_i/\sum_j N_jA_j$ represents the fractional weight of each element contained in the compound.

The photographic emulsion is not a chemical compound in the sense that it is a homogeneous chemical combination of atoms composed of identical molecules. Rather, it is a highly dispersed mixture of two compounds, gelatin and silver bromide. The gelatin is a continuous medium in which the silver bromide is suspended in the form of tiny crystals. The physical characteristics of the emulsion, for which stopping-power calculations are here carried out, may be summed up in the following list of values:

Density of emulsion	3.64 g/cc
Percent weight of AgBr in dry emulsion	85.0 percent
Percent weight of gelatin	15.0 percent
Density of silver bromide	6.47 g/cc
Concentration of AgBr in emulsions	3.09 g/cc
Average diameter of grain	0.3μ
Mass of average grain	0.92×10^{-12} g
Number of grains/cc of emulsion	3.36×10^{13} grains/cc
Moisture content (percent weight of dry emulsion)	3.35 percent

If we assume that such a mixture of silver bromide grains and gelatin can be treated as a smoothed-over compound of the various constituent atoms, we can calculate the relative stopping power of an emulsion from Eq. (12), providing we know the atomic composition of the

** This formula was also used by P. Cüer (see reference 24) for calculating the stopping power of emulsions.

TABLE IV. Atomic stopping-power values.

Energy Mev		Atomic stopping power						
E_α	E_H	S_{Ag}	S_{Br}	S_C	S_H	S_N	S_O	S_{air}
2.07	0.52	2.25	2.07	0.94	0.260	1.02	1.10	1.0
4.66	1.17	3.08	2.68	0.932	0.224	1.02	1.10	1.0
8.30	2.09	3.43	2.94	0.921	0.209	1.01	1.10	1.0
12.95	3.26	3.64	3.10	0.914	0.200	1.01	1.09	1.0
18.60	4.70	3.76	3.19	0.908	0.194	1.00	1.09	1.0
33.20	8.36	3.93	3.30	0.899	0.186	1.00	1.08	1.0
51.90	13.06	4.04	3.38	0.892	0.181	.99	1.08	1.0
		Extrapolated						
80.0	20.0	4.12	3.44	0.850	0.170	0.98	1.07	1.0

emulsion and the atomic stopping powers of the atoms involved. To illustrate this, the following calculation of stopping power *versus* energy has been made.***

The atomic composition of an emulsion which is made up of 85 percent silver bromide, has a moisture content of 3.35 percent of the dry weight of the emulsion, and contains gelatin composed of 50 percent carbon, 6.7 percent hydrogen, 18 percent nitrogen, and 25 percent oxygen is given in Table III. A table of atomic stopping powers of the elements hydrogen, carbon, aluminum, copper, silver, and gold as a function of energy for alpha-particles and protons has been published by Bethe and Livingston.[25] By drawing curves relating stopping power and atomic weight from these published values, interpolated values of atomic stopping power for bromine, nitrogen, and oxygen can be obtained. The published values, along with the values obtained therefrom by interpolation, are set down in Table IV.

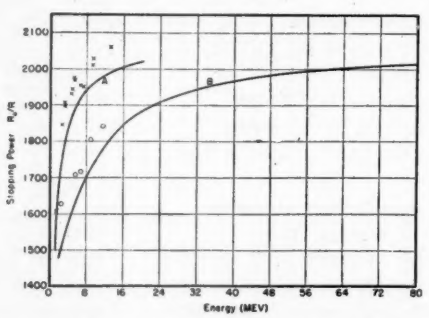

FIG. 9. Calculated integral stopping-power *versus* energy curves for nuclear-track emulsion: (*a*) for protons, (*b*) for α-particles. Experimental points from paper by Lattes, Fowler, and Cüer, Proc. Roy. Soc. **59**, 883 (1947).

The stopping power of the emulsion relative to air was calculated for each energy value in Table IV, using Eq. (12), and values of the constants: average atomic weight of air $(A_0)=14.5$; density of air $(d_0)=0.001205$ g per cubic centimeter; density of emulsion $(d)=3.64$ g per cubic centimeter; and the atomic stopping-power values, s_i, given in Table IV.

The values of the relative stopping power, $\Delta R_0/\Delta R$, so obtained for alpha-particles and protons of various energies are given in Table V.

In Fig. 9 the integral stopping power, R_0/R, for both protons and alpha-particles is plotted as a function of energy in Mev. The values for plotting these curves were obtained as follows: Differential-range values in air over narrow energy steps (2 Mev) were divided by the stopping-power values in Table V to obtain the corresponding range values in the emulsion. These values were then summed over discrete energy steps to obtain integral-range values in the emulsion. The quotients of the integral-range values in air and in the emulsion give the integral stopping-power values. The experimental points shown in Fig. 9 are values of stopping power that were published by Lattes, Fowler, and Cüer[26] for the Ilford B-1 emulsion. The silver halide content of this emulsion, according to the Ilford data given earlier in this paper, is 81 percent. The concentration of silver bromide in the emulsion used in the present calculations (with 3.35 percent water) is, according to Table III, 82.05 percent. Thus, since the silver halide concentration is closely the same in the two cases, the experimental points serve to show the order of accuracy**** to be expected

*** The following procedure for calculating the stopping power of a heterogeneous emulsion follows closely a method worked out (unpublished) by my colleague, Dr. Amos Newton, to whom the author wishes to express his indebtedness.

[25] H. Bethe, and M. S. Livingston, Rev. Mod. Phys. 9, 272 (1937).

[26] C. M. G. Lattes, P. H. Fowler, and P. Cüer, Proc. Phys. Soc. (London) **59**, 883 (1947).

**** The theoretical stopping-power curve of Fig. 9 for alpha-particles also agrees fairly well with the data of Tsien San-Tsiang, Chastel, Faraggi, and Vignoron (see reference 19) on Ilford halftone concentrated plates given earlier in this paper. Peck (see reference 38) made measurements of of stopping power on the Eastman NTB emulsion for protons of energy 2-9 Mev. From 9 Mev to 4 Mev he found a constant value of stopping power of about 2050. However, his measurements showed a sharp rise of stopping power below 4 Mev, going up to 2820 at 2.4 Mev. These results are not understood at present, but since they are in sharp variance with both theory and experimental

from theoretically calculated stopping-power values.

In Figs. 10 and 11, the curves of Fig. 9 have been converted to give stopping power, R_0/R, *versus* range in microns in the emulsion. In Fig. 12, theoretical range-energy curves for protons and alpha-particles in the photographic emulsion are given based on the variable stopping-power values, R_0/R, from the curves of Fig. 9.

It is of interest at this point to give the results of calculations of stopping power, $\Delta R_0/\Delta R$, as a function of energy for pure silver bromide. Using Eq. (12) and values of the atomic stopping power for silver and bromine from Table IV, the values of stopping power shown in Table VI were obtained. It is to be noted that the stopping power for silver bromide is considerably higher (~50 percent) than that for the emulsion itself.

DENSITY OF PHOTOGRAPHIC GRAINS IN TRACKS OF NUCLEAR PARTICLES

The question of the density of developed grains in a nuclear track recorded by the photographic emulsion is of great importance to the nuclear physicist employing the photographic technique for registration of charged particles. By the grain spacing, the type of particle under investigation can frequently be recognized directly. For example, the grain spacing and small angle scatter make it possible to distinguish unmistakably the tracks of a meson and a proton.[13,16] The grain spacing may be assumed to depend upon the energy-loss curves shown in Fig. 3. At points on these curves of the same energy loss, it is to be expected that the grain spacing will be substantially the same, regardless of the type of particle. This is true because the action of the incident particles in producing a latent image in the photographic grain is dependent upon the number of ions produced in the individual grain. In this respect, the process of latent-image formation with particle radiation is not materially different from that in the case of light.

It is now well established[27–29] in the cases of light exposure that the individual grains of the emulsion act as units in exposure. The light quanta strike a silver bromide crystal in succession, and each quantum, upon absorption, raises the energy state of an electron attached to a bromine ion into an empty state of the conduction band of silver bromide. An electron with energy corresponding to a level of the conduction band can move about freely in the crystal and

TABLE V. Stopping power of emulsion.

Energy Mev E_α	E_H	$\Delta R_0/\Delta R$
2.07	0.52	1511
4.66	1.17	1764
8.30	2.09	1868
12.95	3.26	1930
18.60	4.70	1964
33.20	8.36	2009
51.90	13.06	2040
	Extrapolated	
80	20	2065

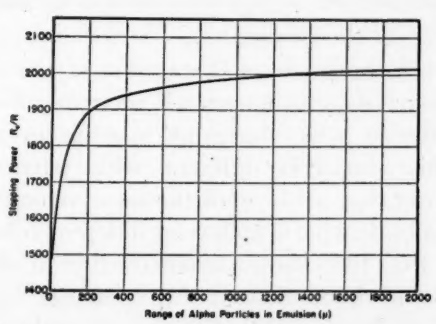

FIG. 10. Calculated integral stopping-power *versus* range curve of nuclear-track emulsion for protons.

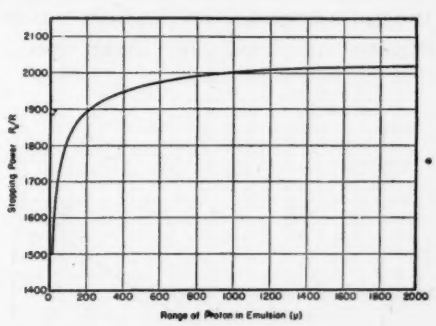

FIG. 11. Calculated integral stopping-power *versus* range curve of nuclear-track emulsion for α-particles.

results of other workers, it would appear that there must have been some unusual circumstances in the experimental work or the particular emulsion used that gave this behavior. Only by further careful measurements along these lines can this problem be cleared up.

[27] R. W. Gurney, and N. F. Mott, Proc. Roy. Soc. (London) **164A**, 151 (1938).
[28] J. H. Webb, J. App. Phys. 11, 18 (1940).
[29] W. F. Berg, and K. Mendelssohn, Proc. Roy. Soc. (London) **168A**, 168 (1938).

TABLE VI. Stopping power of silver bromide.

Energy Mev E_α	E_H	$\Delta R_0/\Delta R$
2.07	0.52	1796
4.66	1.17	2394
8.30	2.09	2648
12.95	3.26	2802
18.60	4.70	2890
33.20	8.36	3006
51.90	13.06	3085
80	20	3164

can be shifted under the action of an electric field. This has been amply demonstrated by experiments on the photo-conductance properties of the silver bromide crystal. Such an electron will move about in the crystal until it comes into contact with a so-called sensitivity speck (a small clump of impurity atoms or a distorted place in the crystal) in the grain, where it becomes trapped in a lower energy level, below the conduction band. An electron trapped in this way is surrounded by an electrostatic field which will attract any positive silver ions in the neighborhood. Since there are always some mobile silver ions present in the silver bromide crystal, as shown by studies on the ionic conductivity of these crystals at room temperature, these ions move up to the charged speck, where they join with the electron to form a silver atom. This process is repeated until a speck of silver is formed large enough to initiate development. It seems likely that exposed grains may acquire a number of silver specks of varying sizes; however, the grain becomes developable only when it has acquired at least one silver speck large enough, and properly located, to initiate development of that grain.

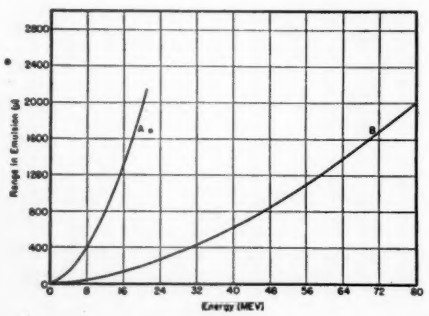

FIG. 12. Calculated range-energy curves for (*A*) protons and (*B*) α-particles in nuclear-track plate. Drawn for variable stopping-power values from calculated curves in Fig. 9.

In the case of exposure of grains to high-velocity, charged particles, the production of electrons in the grain takes place upon passage of the particle through the grain. Electrons freed by such means will behave, in general, like those produced by exposure to light and may be expected to form a latent image. One point of difference should be emphasized, however. With high-energy particles, the electrons are formed within the grain in a very short time, e.g., with a 5-Mev alpha-particle and a grain size of 0.3μ diameter, all the electrons are freed in about 2×10^{-14} second. This rapidity of liberation of the electrons may lead to inefficiency in the photographic process. First, because the positive and negative ions formed by the particle lie along a straight, narrow path through the grain, there will be a tendency for the ions to recombine and thus to be lost for the latent-image formation. Second, it is well known that light exposures become less efficient at very short exposure times (below 10^{-3} second), because of the failure of the reciprocity law in the photo-chemical process of latent-image formation. For the latent-image formation to proceed efficiently, electrons should be freed at such a rate that the ionic movement of the silver ions can keep pace with the electronic process and thus neutralize the electrons as fast as they become trapped. If the exposure is given too fast, the latent-image silver has a tendency to be dispersed throughout the grain, which introduces competition between specks and inefficiency in the process.

The foregoing brief description of the theory of latent-image formation will serve as a basis for considering why the grain spacing in photographic tracks is different with particles of different charge but with the same velocity, and with identical particles having different velocities.

In Fig. 13 is shown schematically an electron revolving about an atom of the stopping material and a charged particle of charge, ze, and velocity, v, passing this electron at a distance, p. The force experienced by the electron while the charged particle is in the vicinity will be of the order of magnitude,

$$F=(ze)^2/p^2.$$

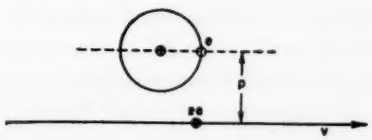

FIG. 13. Schematic diagram to illustrate impulse given to an electron by passage of a charged particle.

The impulse experienced by the electron is given by the product of the force, F, and the time, t, that the particle spends in the neighborhood of the electron. To a first approximation, this time may be taken as

$$t=2p/v.$$

Thus, the impulse is

$$Ft=ze^2/pv. \tag{13}$$

Let us now consider the impulse given to an electron in the two cases: (1) by the passage of a proton, and (2) by an alpha-particle, both of the same range. It is known that an alpha-particle and a proton of the same range have the same velocities. This follows because the alpha-particle, though it has four times the energy of the proton, loses energy at four times the rate of the proton because of its double charge, as can be readily seen by reference to Eq. (1). If, now, we equate impulses in these two cases, we find that

$$2e^2/p_\alpha v=e^2/p_H v,$$

from which

$$(p_\alpha/p_H)^2=4.$$

It is readily seen that p_α and p_H define cylinders of equivalent action of the alpha-particle and proton, respectively. The number of atoms contained in such cylinders will be proportional to the p^2 values. Thus, it may be expected that, for equal velocities, the alpha-particle will ionize approximately four times as many atoms as the proton.

Similarly, it is well known that the velocities of protons and deuterons of the same range have velocities in the ratio, $v_H=1.25v_d$. The ratio of the p values in this case, since the charges are equal, will be 1.25. Consequently, the deuterons will produce $(1.25)^2$, or 1.56 times as many ions as a proton of the same range.

The threshold sensitivity of a photographic grain must depend in first approximation upon the number of ion pairs produced in the grain.

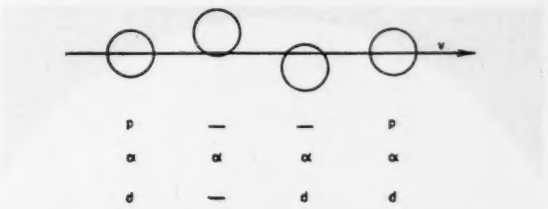

FIG. 14. Schematic diagram to illustrate passage of a charged particle through irregularly distributed photographic grains.

With this basic assumption, the schematic diagram in Fig. 14 can be used to explain crudely the action of different particles on grain spacing. Assume, for example, that a nuclear particle of a given range follows the path shown by the arrow. This path is seen to pass through different thicknesses in different grains, which are irregularly distributed in space. Suppose the particle is a proton and of such velocity that it can produce sufficient ions in the grain to form a latent image only if it passes through a full diameter of the grain. Then, since the path shown passes through the full thickness of the two end grains, a proton following the path would make grains 1 and 4 developable. A deuteron of the same range, having lower velocity, and thus somewhat higher ionizing power, will perhaps affect grains 1, 3, and 4. An alpha-particle of the same range, however, having the same velocity and thus four times the ionizing power of the proton, will affect all grains in the path, 1 to 4.

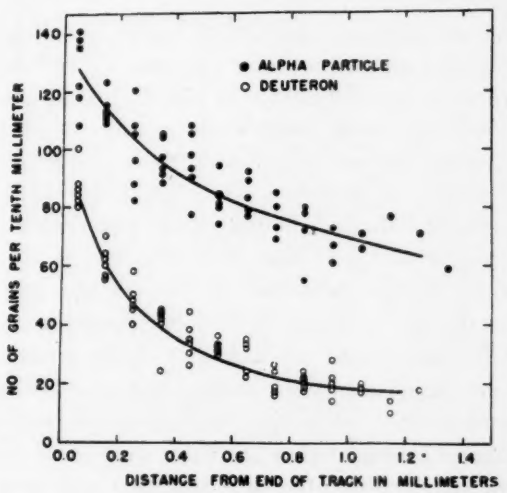

FIG. 15. Curves showing grain spacing as a function of distance from end of particle track. From paper by Brock and Gardner (see reference 32).

FIG. 16. Tracks of Po α-particles obtained with Eastman NTA plate.

Grain spacings in alpha-particle, deuteron, and proton tracks were measured by Wilkins and St. Helens[30] for equal residual ranges, and it was found that the grain density in the proton tracks was about one-half that for the alpha-particle and that the grain density of the deuteron tracks fell between that of the proton and alpha-particle tracks.

When charged particles, such as alpha-particles (<10 Mev) and protons (<3 Mev), have very low velocity, they are highly ionizing and will affect practically every grain with which they come in contact. Under these conditions, the density of grains in a track will approach a maximum value set by the grain population of the unexposed emulsion. Perhaps it will be of interest in this connection to give the maximum grain density in terms of the silver bromide concentration, C, and the diameter of the grain, d, for an emulsion of the conventional type. If it is assumed that all grains are spherical and of diameter, d(cm), then a little reflection will show that the number of grains that will be hit by a particle traveling in a straight path of length, λ(cm), will be equal to the total number of grains whose centers are contained within a cylinder of diameter, d, and length, λ. This number is readily found by dividing the silver bromide concentration of the emulsion, C grams per cubic centimeter, by the mass of one grain and multiplying by the volume of the cylinder of diameter, d, and length, λ. The resulting expression is

$$n=\tfrac{3}{2}(C\lambda/d\rho) \text{ grains per centimeter,} \quad (14)$$

in which ρ represents the density of silver bromide in grams per cubic centimeter. If we take λ to be 1 cm and ρ to be 6.47, we obtain, for the maximum grain density,

$$n=0.23(C/d) \text{ grains per centimeter.} \quad (15)$$

This relation was first given and tested by Idanoff[31] and subsequently tested by Demers.[4] Idanoff, using several emulsions with different values of C and d, tested the relation (15) by measuring the relative grain spacings, Δ. If we set

$$\Delta=1/n=d/0.23C, \quad (16)$$

then

$$\Delta_1/\Delta_2=(d_1/d_2)(C_2/C_1),$$

and the relation between Δ values for different emulsions has been found to hold fairly accurately. Also, Demers[4] tested the relation (16) for a number of commercial emulsions and for special experimental emulsions made by his own formulas and found that the minimum grain-spacing, Δ_0, for alpha-particles near the end of their range was in fair agreement with the theoretical minimum grain spacing, Δ, calculated from (16).

It is of interest to calculate the value of Δ_0 for the emulsion for which the stopping-power calculations were made earlier in this paper. Using the values $C=3.09$ g per cubic centimeter and $d=0.3\mu$, we find that

$$\Delta_0=d/0.23C=0.435\mu.$$

In Fig. 15 are shown experimental data on grain density as a function of residual path length for Eastman NTA plates obtained by

[30] T. R. Wilkins, and H. J. St. Helens, Rev. Mod. Phys. 11, 35 (1940); Phys. Rev. 54, 783 (1938).

[31] A. Idanoff, J. de phys. et rad. 6, 283 (1935); Comptes rendus (Doklady) U.R.S.S. 28, 110 (1940).

Brock and Gardner[32] of the Radiation Laboratory of the University of California. The points represent numbers of grains per 0.1-mm path length for varying residual path for both alpha-particles and deuterons. It may be seen that the grain density for the deuterons is less than that for the alpha-particles throughout the range covered. In the case of the alpha-particles, at the shortest residual ranges measured the grain density is about 1.5 grains per micron, corresponding to a Δ value of 0.6μ.

A useful concept has been employed by Lattes, Occhialini, and Powell[16] for determining from grain density the relative masses of two types of particles of the same charge value. It is a well-known fact (see Eq. 5) that the rate of energy loss of a charged particle having fixed charge value is a function of the velocity of the particle only, irrespective of the mass of the particle. Thus, the rate of energy loss may be written

$$dE/dR=f(v). \tag{17}$$

Since the photographic effect is dependent upon the rate of energy loss, it can be assumed that the grain density along the track will also be a function of velocity, thus

$$dN/dR=f(v).$$

From Eq. (5), it can be seen that the residual track length, R, of a particle of given velocity, v, and fixed charge, is proportional to its mass, M. Thus, the grain density may also be written as a function of residual range divided by M,

$$dN/dR=f(R/M). \tag{18}$$

Integrating, we find that

$$N=M\int_0^{R/M} f(R/M)d(R/M). \tag{19}$$

Since the integral on the right would have a unique value, starting from a point on the track where the velocity has a given value (given R/M value), then, for two different particles having different masses the total numbers of grains, N_1 and N_2, in the residual paths, R_1 and R_2, will be in the ratio of the masses, M_1 and M_2. Thus,

$$R_1/R_2=N_1/N_2=M_1/M_2. \tag{20}$$

[32] R. L. Brock and E. Gardner, Rev. Sci. Inst. 19, 299 (1948).

If it is desired to compare masses of two particles from grain counts, the procedure is to find points along the two trajectories for which the grain densities are equal. Then the relative masses of the two particles will be in the ratio of the two residual paths, or, alternatively, in the ratio of the total numbers of grains in the two residual paths.

ANALYSIS OF NUCLEAR TRACKS AND PLATE CALIBRATION

In analyzing the tracks of nuclear particles recorded in the photographic emulsion, the experimenter must rely upon such features as the recorded range of the particle in the emulsion, small angle scattering along the track, and the grain spacing along the track. The actual range of the particle and the small angle scattering will depend upon the composition of the emulsion and hence may be expected to be constant from one emulsion to another. However, the recorded range of a particle and the grain spacing at the beginning of the track will depend upon the

FIG. 17. Tracks of four α-particles from thorium atom disintegrating through the series: ThX (5.68 Mev), Tn (6.28 Mev), ThA (6.78 Mev) and ThC′ (8.78 Mev).

sensitivity of the individual grains of the emulsion, which is very difficult to reproduce accurately. Accordingly, if the photographic plate is to be used as a quantitative tool to evaluate the properties of a particle through range and grain-spacing measurements, it is essential that the plates used in such experiments be given control exposures to particles of known characteristics, for example, protons or alpha-particles of a series of known energy values, and processed in a controlled manner. All plates coated from a single emulsion batch can be relied upon to give closely uniform results, provided they have been stored under proper temperature and humidity conditions prior to exposure and provided they receive proper and uniform handling during exposure and processing.

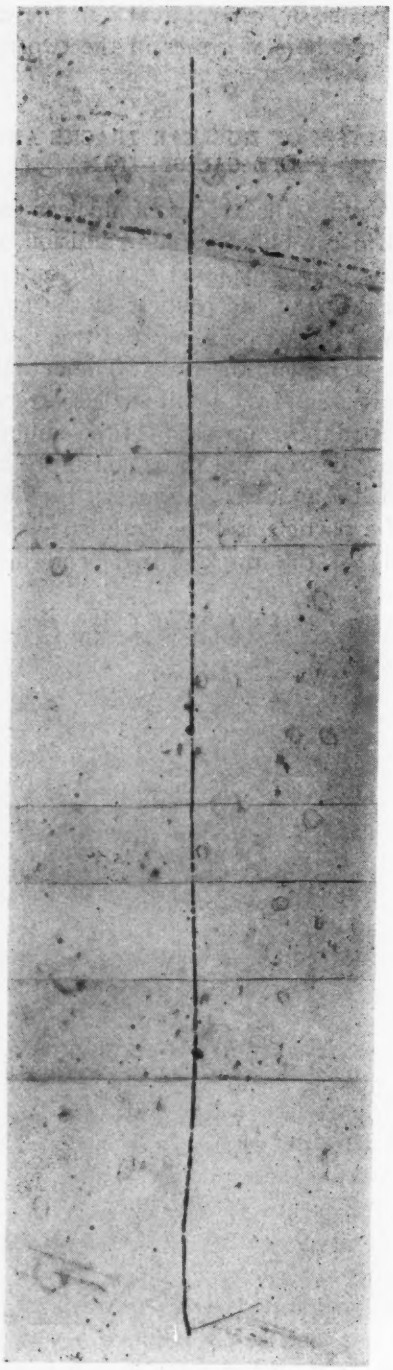

FIG. 18. Track of a 7-Mev proton in Eastman NTB emulsion. Track ends at bottom of figure.

It is highly desirable that emulsions supplied by the manufacturer be constant from batch to batch, so that a minimum of calibration exposures will be required. In the preparation of the nuclear-track plates, serious efforts are being made to achieve this end. However, up to the present time, much experimental work has been necessary to improve these plates in various ways, such as to increase their sensitivity to higher energy particles, to lower the background density, and to reduce the latent-image fading that takes place between exposure and development. During this period of experimentation, the Eastman NTB plate, for example, has been designated as an "experimental plate."

As was stated earlier in this paper, successive batches of Eastman NTA plates are given a standardized test to polonium alpha-particles (5.3 Mev) and the Eastman NTB plates are given a standardized test to 7-Mev protons. These tests are used as a control measure to screen out those emulsions which fall outside certain tolerances in recorded range-value and grain-spacing quality of the tracks. However, it must be pointed out that such tests are inadequate to determine the uniformity of behavior of emulsions when exposed to particles of energy greatly exceeding those used in the tests. For example, it has been found that nuclear-track plates that have shown very uniform grain spacing from one emulsion to another when tested to moderate energy protons may show non-uniform results when exposed to particles of higher energy approaching the threshold sensitivity value of the plate. At higher energies where the grain density in the tracks becomes sparse, the grain spacing becomes much more

critically dependent upon the threshold sensitivity of individual grains and even small differences in sensitivity begin to show up in a measurable way. In the near future. the new cyclotron of the University of Rochester will be in operation, and it is hoped that it will then be possible to give standardized tests to protons over much wider energy ranges than has been possible in the past.

At present, the only safe procedure that can be recommended to the worker in this field is to calibrate the plates of each new emulsion batch in the energy range that the plates are to be used. Accordingly, it is suggested that, if an extended investigation is to be carried out, plates in sufficient quantity to complete the work be acquired in the beginning from one emulsion number and stored at reduced temperature until used.

EXAMPLES OF NUCLEAR TRACKS IN THE PHOTOGRAPHIC EMULSION

As examples of tracks obtained on commercial nuclear-track plates, the pictures in Figs. 16–19 are shown.

The tracks in Fig. 16 were obtained on an Eastman NTA emulsion by means of a weak polonium source of alpha-particles placed practically in contact with the photographic emulsion. The polonium alpha-particles have an energy of 5.3 Mev and, accordingly, a range of about 22μ in the emulsion.

The star tracks in Fig. 17 represent four alpha-particle tracks from a disintegrating thorium atom. An Eastman NTA plate was impregnated with a solution of thorium nitrate, dried, left for a few days, and then washed and processed. A plate so treated will show stars produced by alpha-particles from a single center, corresponding to successive disintegrations of the thorium nucleus. The four tracks shown in this figure correspond to the four successive alpha-disintegrations of thorium *X* (5.68 Mev), thoron (6.28 Mev), thorium *A* (6.78 Mev), and thorium *C'* (8.78 Mev).

Figure 18 shows the track of a 7-Mev proton on an Eastman NTB plate. The grain spacing throughout this track is about constant, indicating that the full grain density was obtained over its entire length. The direction of the proton travel is downward, as shown by the small angle scattering at the lower end which occurs when its velocity is low.

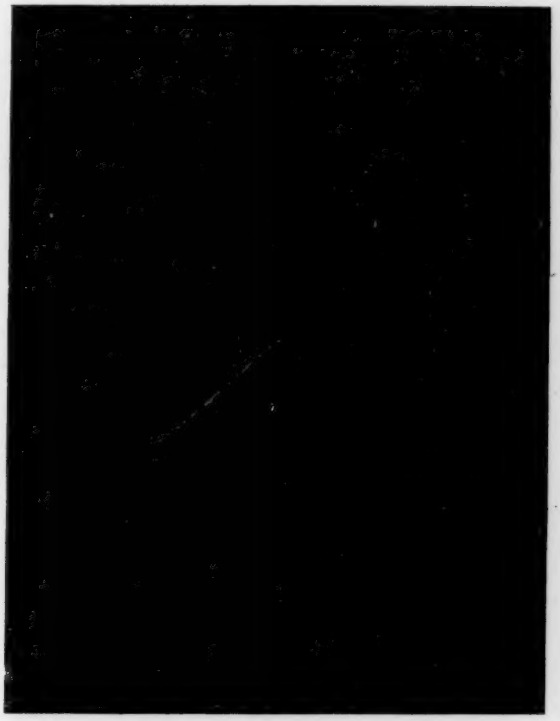

FIG. 19. Track of U^{235} fission on Eastman NTC emulsion, obtained by impregnating emulsion with uranium acetate and bombarding with slow neutrons.

Figure 19 shows the paths of the two fission fragments from a U^{235} atom. An Eastman NTC plate was impregnated with uranium acetate and bombarded with low speed neutrons. The fission of the U^{235} atom occurred near the center of the track and the track itself was produced by the two highly charged fragments flying apart, with a combined energy of 160 Mev. The high charge on these fragments is manifested by the rela-

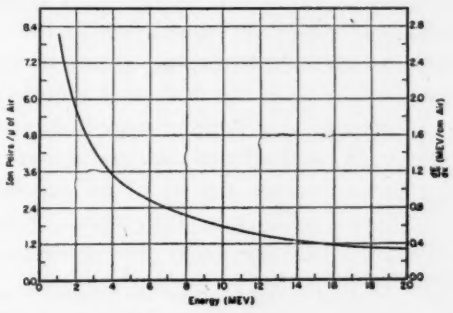

FIG. 20. Ion-pair production *versus* energy curve for α-particles in air.

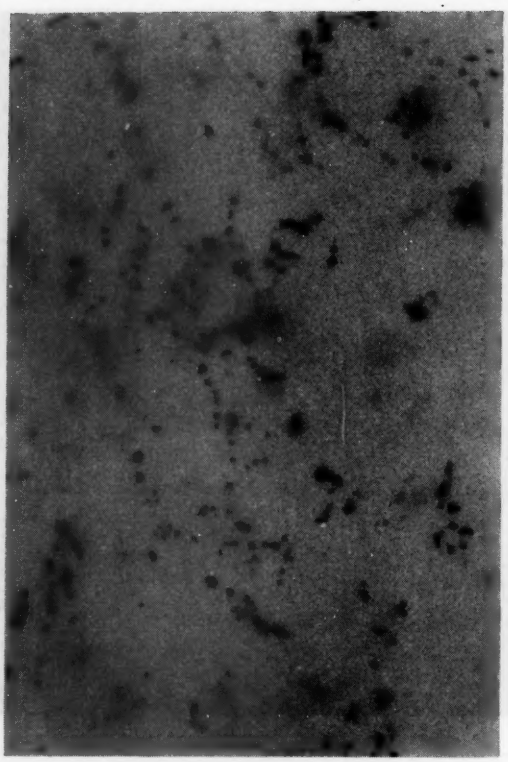

FIG. 21. Tracks of electrons in Eastman NTB emulsion. Plate exposed to 180 kv x-rays to produce photoelectrons.

tively short path of these tracks (25μ for the combined fragments). Also, it is to be noted in this case that the grain density is highest near the center of the track and falls off toward the two extremities as the charge on the fragments, and thus the ionizing power, is reduced.

ION-PAIR PRODUCTION AND LATENT-IMAGE FORMATION

In concluding this paper it seems appropriate to make a few remarks about the mechanism of latent-image formation under the action of charged particles.[33] By analogy with the action of light on the photographic grain, it appears almost certain that the action of charged particles in producing a latent image in the photographic grain results from the production of free conduction electrons just as in an exposure to light. There are certain differences, however, which should be mentioned. In an exposure to light, the quanta are absorbed at random points over the entire grain surface and usually at a moderate rate such that all the quanta received by one grain are absorbed in a time greater than 10^{-3} second. However, as we pointed out earlier in the case of a charged particle of even moderate energy, all ion pairs are produced along a straight line through the grain and in a time less than 10^{-13} second. Under these conditions, formation of the latent image is attended by inefficiency because of ion recombination and reciprocity-law failure. For both these reasons it is to be expected that more electrons must be released in a grain to render it developable with an exposure to a charged particle than is the case in an exposure to light.

In Fig. 20 a curve is shown giving the number of ion pairs formed per micron of path length in air for an alpha-particle of varying energy. This curve was obtained by plotting the differential values of ion-pair production from published tables.[34] This curve is known to follow the same course as the energy-loss curves shown in Fig. 3. Accordingly, a scale has been given on the right-hand ordinate axis of Fig. 20 specifying the energy loss in Mev per centimeter. In air, about 35 ev is required to produce each ion pair, and this figure has been found to be very closely the same, whether the incident particle is an electron, a proton, or an alpha-particle.

The production of ion pairs on passage of a charged particle through solid materials will also take place in accordance with a curve like that of Fig. 20. However, this quantity is not nearly so easily measured in a solid as in a gas, and there are very few data available on the energy required to produce an ion pair in solid materials. Experiments with the recently developed crystal counters, using silver chloride crystals as a solid ionization chamber for the detection of high-energy charged particles, offer the possibility of obtaining the average value of energy required to produce an ion pair in silver chloride. Since silver chloride is very similar to silver bromide, the value obtained in this way will also apply in the photographic case. VanHeerden,[35] who de-

[33] For additional information see the detailed discussions of the problem of latent-image formation by charged particles which have been prepared by P. Cüer, Sci. et Ind. Phot. 18, 321 (1947); 18, 353 (1947).

[34] J. B. Hoag, *Electron and Nuclear Physics* (D. Van Nostrand Company, Inc., New York, 1938), second edition, p. 464.

[35] P. J. VanHeerden, *N. V. Noord-Hollandsche Uitgevers Maatschappy* (Amsterdam, 1945).

veloped the silver chloride crystal counter, found that 7.6 ev is required to produce each ion pair for the case of high-speed beta-particles passing through the silver chloride crystal. More recently, Hofstadter, Milton, and Ridgeway,[36] working with the silver chloride crystal counter and using high-energy electrons, found a series of values for the energy per ion pair with different crystal samples. The lowest value obtained was 13–16 ev, and the authors considered this value to be higher than the true value because of imperfections in the crystal which are known to limit the photo-conductance current. It appears that VanHeerden's value of 7.6 ev is the best available at present for the energy required to produce an ion pair in silver chloride and this value will be used here for the purpose of calculation.

We note from the curve of Fig. 20 that for an 18-Mev alpha-particle, ion-pair production in air amounts to 1 ion pair per micron of air and the energy loss amounts to approximately 0.35 Mev per centimeter of air. If we take the threshold sensitivity value of the photographic grain to be 0.013 Mev per centimeter of air, corresponding to a 100-Mev deuteron, this will give an ion-pair formation rate of 0.037 ion pair per micron of air, since ion-pair production is proportional to energy loss. The maximum number of ion pairs produced in a photographic grain for a particle of this same energy-loss value can be found by multiplying the number of ion pairs per micron of air by the stopping power of silver bromide relative to air ($\sim$3000), dividing by the ratio of electron volt per ion pair in silver bromide to electron volt per ion pair in air, and multiplying by the diameter of the grain (0.3μ). Then we find that

$$\text{Ion pairs/grain AgBr} = 0.037 \times 3000 \times (35/7.6) \times 0.3 = 153,$$

as an approximate value of the threshold number of ions to produce developability of a photographic grain 0.3μ in diameter. This figure must be considered as only approximate, since an accurate threshold cannot be set for the highest energy particle that will produce developability of a grain. All that is known, e.g., is that the

FIG. 22. Track of a negative meson (mass = 300 me) in Eastman NTB emulsion. Range in emulsion 400 microns. Exposure made on University of California cyclotron.

[36] R. Hofstadter, J. C. D. Milton, and S. L. Ridgeway, Phys. Rev. **72**, 977 (1947).

beginnings of tracks of 100-Mev deuterons consist of widely and irregularly spaced grains, thus making it appear that we are reaching the limit at which a useful fraction of grains is being made developable.

It is interesting to compare the figure, 153 ions per grain, with the number of quanta absorbed per grain for developability, as determined from recent work on single-grain-layer plates.[37,38] In this work experimental data indicated that, on the average, 40 quanta had to be absorbed by a grain to produce developability.

Between the time of preparation of this paper and its printing, the sensitivity of nuclear-particle plates has been substantially increased. The highest sensitivity emulsions will now record electron tracks[18] up to 20–30μ, corresponding to 50- to 70-kev energy.

In Fig. 21 are shown electron tracks obtained on an Eastman NTB plate exposed to 180-kv x-rays. The paths of photoelectrons ejected by the x-rays are recorded. The longest tracks registered here have a length of 20μ, corresponding to approximately 50-kev energy. This plate was developed in D-8 developer diluted 2:1 for two minutes. The electron tracks afford such a convenient and sensitive method of testing the threshold sensitivity value of plates that this method is now being used for testing the Eastman NTB plate.

In Fig. 22 is shown the track of a meson recorded on an Eastman NTB plate. The exposure was made to the mesons generated in the University of California cyclotron. The track shown is 400μ in length and corresponds to a negative meson of mass 313 me and energy of approximately 3.6 Mev. It may be observed that the meson track ends in a star formation due to a nuclear reaction set off by the meson.

[37] J. H. Webb, J. Opt. Soc. Am. **38**, 312 (1948).
[38] R. A. Peck, Jr., Phys. Rev. **72**, 1121 (1947).

ACKNOWLEDGMENT

The author desires to express his appreciation to his colleague, Dr. J. Spence, for furnishing various experimental data on the nuclear-track plates, for the preparation of the microscopic pictures of all the particle tracks herein presented, and for valuable discussions throughout the course of the writing of this paper. It is a pleasure to express, on behalf of the Kodak Research Laboratories, appreciation to the Physics Department of the University of Rochester and to the Radiation Laboratory of the University of California for their kind cooperation in exposing Eastman Nuclear Track Plates to charged particles from their high-energy accelerators. In this connection, Mr. Norton, of the University of Rochester, and Dr. E. Gardner, of the University of California, deserve special thanks for their generous and cordial cooperation. The author also desires to express his thanks to Dr. E. Gardner, of the University of California, Dr. Amos Newton, of the Eastman Kodak Company, for helpful suggestions, and to Dr. M. Blau, of Columbia University, for advice on processing of nuclear-track plates.

PHYSICAL REVIEW VOLUME 74, NUMBER 5 SEPTEMBER 1, 1948

The Interaction of Nuclear Electric Quadrupole Moments with Molecular Rotation in Asymmetric-Top Molecules. I*

J. K. BRAGG
Mallinckrodt Chemical Laboratory, Harvard University, Cambridge, Massachusetts

(Received May 17, 1948)

The theory of the interaction of nuclear electric quadrupole moments with molecular rotation is extended to asymmetric-top molecules containing one or two quadrupolar nuclei. The first-order theory is developed in detail, and in a form which makes use of published numerical tables of line strengths of asymmetric-top pure rotation transitions, and involves the second derivatives of the electrostatic potential V taken along the three principal axes of inertia. Only two of these are independent, and $(\partial^2V/\partial z'^2)$ and $(\partial^2V/\partial x'^2)-(\partial^2V/\partial y'^2)$ are a convenient choice of the parameters of the problem. A general formulation of the theory, which includes higher order effects, is given. In case a molecule contains only one quadrupolar nucleus, the structure of the quadrupole multiplets should be sufficient to identify pure rotation transitions.

1. INTRODUCTION

THE theory of the electric quadrupole interaction of nuclei and molecular rotation has been developed for linear and for symmetric top molecules containing one or two quadrupolar nuclei.[1–4] This paper extends the theory to asymmetric-rotor molecules containing one or two such nuclei, in a form which makes use, for first-order work, of previously published numerical tables of line strengths of asymmetric rotors.[5] These tables extend to rotational levels involving $J=12$; a second paper will be concerned with developing convenient asymptotic expressions to be used for rotational levels for which $J>12$. The effects of accidental near degeneracy and the small splitting of the higher levels for a given J are considered.

2. THE FIRST-ORDER HAMILTONIAN

The first-order interaction of nuclear electric quadrupole moments with the electric field of an atom or a molecule is described by the Hamiltonian[1,6]

$$\sum_i[(eQ_i\langle(\partial^2V/\partial z^2)_i\rangle_{Av})/2J(2J-1)I_i(2I_i-1)] \times[3(\mathbf{I}_i\cdot\mathbf{J})^2+\tfrac{3}{2}(\mathbf{I}_i\cdot\mathbf{J})-\mathbf{I}_i^2\mathbf{J}^2] \quad (1)$$

where the $\mathbf{I}_i$ are the nuclear spin angular momentum operators and $\mathbf{J}$ the molecular angular momentum operator. The summation extends over all quadrupolar nuclei present. Q_i, the quadrupole moment of the nucleus, is defined by[1]

$$eQ_i=e\langle 3z_i^2-r_i^2\rangle_{Av}$$

where $\mathbf{r}_i$ is referred to the center of the ith nucleus as origin. The average is taken over the nuclear state $M_I=I$. Also we have[7]

$$\langle\partial^2V/\partial z^2\rangle_{Av}=\langle\textstyle\sum_j e_j(3\cos^2\theta_j-1)/r_j^3\rangle_{Av}.$$

The average is taken over the state $M_J=J$. Here $\mathbf{r}_j$ is the vector from the center of the ith nucleus as origin to the molecular charge e_j; θ_j is the angle between $\mathbf{r}_j$ and the space-fixed z axis.

The first-order problem consists of two parts, (i) the evaluation of the dependence of the $\langle(\partial^2V/\partial z^2)_i\rangle$ on the rotational state, and (ii) the approximate or exact solution of the secular equation obtained from Eq. (1), which involves obtaining the matrices of the operators in square brackets.

* The material of this paper is taken from a thesis submitted to the Faculty of Arts and Sciences of Harvard University for the degree of Doctor of Philosophy in Chemical Physics. Some of the work was supported by the Navy Department through Contract N5ori-76, Task order V, Office of Naval Research.

Part of the material given here was presented at the meeting of the American Physical Society at Columbia University, January 28, 1948.

[1] Kellogg, Rabi, Ramsey, and Zacharias, Phys. Rev. **57**, 677 (1940).

[2] Dailey, Kyhl, Strandberg, Van Vleck, and Wilson, Phys. Rev. **70**, 984 (1946).

[3] D. K. Coles and W. E. Good, Phys. Rev. **70**, 979 (1946).

[4] J. Bardeen and C. H. Townes, Phys. Rev. **73**, 97 (1948).

[5] P. C. Cross, R. M. Hainer, and G. W. King, J. Chem. Phys. **12**, 219 (1944): hereafter called CHK.

[6] H. B. G. Casimir, *On the Interaction between Atomic Nuclei and Electrons*, (E. F. Bohn, Haarlem, 1936).

[7] The components of the dyadic ∇E have everywhere been written in explicitly. For a linear molecule or symmetric top $(\partial^2V/\partial z'^2)$, where z' is a molecule-fixed axis, becomes the q of Bardeen and Townes (see reference 4). In the present problem z' will not in general coincide with an internuclear bond.

The result of the second part is obtained by the same methods used for simpler molecules. This rests on the independence of the operators in square brackets of the symmetric-rotor quantum number K, and hence also of the asymmetric rotor pseudo-quantum number τ. The special dependence of $\langle\partial^2V/\partial z^2\rangle_{Av}$ for the various molecular types introduces only a scale factor into the expressions for the splitting of an energy level.

For molecules containing one quadrupolar nucleus the characteristic value[6] of the operator in square brackets in Eq. (1) is

$$\tfrac{3}{4}C(C+1)-I(I+1)J(J+1), \qquad (2)$$

where $C=F(F+1)-I(I+1)-J(J+1)$ and F takes the values $J+I, J+I-1, \cdots |J-I|$. If two quadrupolar nuclei are present, explicit expressions can be written only in some special cases.[8] In general one may set up the secular equation by the method of Bardeen and Townes.[4] It is also possible to write the secular equation in either of the two vector coupling representations $\mathbf{I}_1+\mathbf{I}_2=\mathbf{I}$, $\mathbf{J}+\mathbf{I}=\mathbf{F}$ or $\mathbf{I}_1+\mathbf{J}=\mathbf{F}_1$, $\mathbf{F}_1+\mathbf{I}_2=\mathbf{F}$. The former scheme is convenient for identical nuclei.[9] The matrices of $\mathbf{I}_1\cdot\mathbf{J}$ and $\mathbf{I}_2\cdot\mathbf{J}$ in these schemes can be obtained from previous work on atomic spectra.[10,11]

The energies for molecules containing three quadrupolar nuclei may also be obtained by using the four-vector scheme of reference (10), but the resulting expressions will be complicated, and their application in analysis of spectra very laborious.

3. ROTATIONAL DEPENDENCE OF $\langle\partial^2V/\partial z^2\rangle_{Av}$

A principal task of this paper is the evaluation of the average value of $(\partial^2V/\partial z^2)$ in terms of rotational quantum numbers and quantities which are constants for a given vibrational and electronic state. In work with asymmetric tops, the expression obtained involves a transformation which depends on the asymmetry of the molecule and the J-value in question. Therefore an equation is derived which involves only quantities which have been tabulated for $J<12$ in CHK in connection with other work on asymmetric tops.

$(\partial^2V/\partial z^2)$ is the zz-component of the dyadic $\nabla\mathbf{E}$ (z here is a space-fixed axis). We may obtain it in terms of the components along molecule-fixed axes $x'y'z'$ (which will be chosen as the principal axes of inertia) by a transformation involving the direction cosines between z and $x'y'z'$. The result is

$$\begin{aligned}\partial^2V/\partial z^2=&\alpha_{zx'}{}^2(\partial^2V/\partial x'^2)+\alpha_{zy'}{}^2(\partial^2V/\partial y'^2)\\&+\alpha_{zz'}{}^2(\partial^2V/\partial z'^2)\\&+2\alpha_{zx'}\alpha_{zy'}(\partial^2V/\partial x'\partial y')\\&+2\alpha_{zx'}\alpha_{zz'}(\partial^2V/\partial x'\partial z')\\&+2\alpha_{zy'}\alpha_{zz'}(\partial^2V/\partial y'\partial z') \qquad (3)\end{aligned}$$

where the α's are direction cosines. According to the definition of $\langle\partial^2V/\partial z^2\rangle_{Av}$, the right side is to be averaged over the state J, τ for which $M_J=J$, and also over the vibrational and electronic state. (This latter averaging is only implicit in our work).

In averaging the right side of Eq. (3), considerable simplification occurs. The matrix elements of $\alpha_{zx'}$ and $\alpha_{zy'}$ in a symmetric rotor representation vanish except for $K'=K\pm1$, and those of $\alpha_{zz'}$ except for $K'=K$.[12] Thus the matrices $\alpha_{zx'}\alpha_{zz'}$ and $\alpha_{zy'}\alpha_{zz'}$ in this representation have non-vanishing elements only for $K'=K\pm1$. They have therefore no diagonal elements in an asymmetric rotor representation, since the transformation to this representation involves either only odd or only even K. The average value of $\alpha_{zx'}\alpha_{zy'}$ is zero in either representation since it is a purely imaginary Hermitian matrix.

Equation (3) thus reduces on averaging to

$$\begin{aligned}\langle\partial^2V/\partial z^2\rangle_{Av}=&\langle\alpha_{zx'}{}^2\rangle_{Av}(\partial^2V/\partial x'^2)\\&+\langle\alpha_{zy'}{}^2\rangle_{Av}(\partial^2V/\partial y'^2)+\langle\alpha_{zz'}{}^2\rangle_{Av}(\partial^2V/\partial z'^2). \qquad (4)\end{aligned}$$

The average is over the state J, τ with $M_J=J$. The fact that the components of $\nabla\mathbf{E}$ are averages over vibrational and electronic states is not

[8] If two identical nuclei of spin 1 or $\frac{3}{2}$ are present in a molecule with C_2 axis, the secular equation factors sufficiently to give explicit expressions for the energies.

[9] H. M. Foley, Phys. Rev. 71, 751 (1947).

[10] M. H. Johnson, Jr., Phys. Rev. 38, 1635 (1931).

[11] E. U. Condon and G. H. Shortley, *The Theory of Atomic Spectra* (Cambridge University Press, Teddington, England, 1935) Chapter III.

[12] The properties of these matrices are given, for instance, in CHK, in addition to a table of the elements in a symmetric rotor representation. All the properties of asymmetric rotors used here are expressed in the formulation of CHK; the notation as regards direction cosines and axes is different, however.

explicitly indicated. Approximate numerical computation of $\langle \partial^2 V/\partial z^2 \rangle_{Av}$ will be described first, since the discussion will indicate in which cases more detailed expressions may be required.

The average of a squared direction cosine appearing in Eq. (4) may be written

$$\langle \alpha^2 \rangle_{Av} = \sum_{J'\tau'} |\alpha_{J\tau J;J'\tau' J}|^2. \quad (5)$$

The direction cosine elements in general exist for $J'=J$ or $J\pm 1$. The restriction that $M_J=J$, however, eliminates the elements $\alpha_{J;J-1}$ and gives

$$\langle \alpha^2 \rangle_{Av} = \sum_{\tau'} \{ |\alpha_{J\tau J;J+1\tau' J}|^2 + |\alpha_{J\tau J;J\tau' J}|^2 \}. \quad (6)$$

However, the line strength of an asymmetric rotor transition $J\tau \rightarrow J'\tau'$ is, in a rigid rotor approximation, proportional to the quantity

$$\lambda_{J\tau;J'\tau'} = 3 \sum_{MM'} |\alpha_{J\tau M;J'\tau' M'}|^2 \quad (7)$$

where α is the direction cosine between z and whichever of x', y', or z' coincides with the dipole moment. The quantities (7) are tabulated numerically in CHK for $J \leq 12$ and for asymmetries $\kappa = -1.0$, -0.5, 0, 0.5, and 1.0, where κ is Ray's asymmetry parameter, defined for instance in CHK.

In order to obtain the average value of a squared direction cosine in terms of these tabulated quantities,[13] we must undo the summation over the Zeeman components in Eq. (7). This can be done explicitly since the M-dependence of the matrix elements of the direction cosines of the asymmetric rotor may be written down in terms of the factors in Table I of CHK. In addition we can make use of a sum rule (Eq. (21), CHK) to eliminate the $J; J+1$ matrix elements in Eq. (6).

The result of all this is

$$\left\langle \frac{\partial^2 V}{\partial z^2} \right\rangle_{Av} = \frac{2J}{(2J+1)(2J+3)} \times \sum_{\tau'} [(\partial^2 V/\partial x'^2)\lambda^{x'}_{J\tau;J\tau'} + (\partial^2 V/\partial y'^2)\lambda^{y'}_{J\tau;J\tau'} + (\partial^2 V/\partial z'^2)\lambda^{z'}_{J\tau;J\tau'}], \quad (8)$$

where the $\lambda^i_{J\tau;J\tau'}$ are Q-branch entries in the table of CHK. These entries are subdivided into a, b, and c sub-branches, where a, b, and c are the principal axes of inertia. The moments of inertia about these axes satisfy $I_a < I_b < I_c$. The $x'y'z'$ axes are to be identified with a, b, and c according to this restriction. In using the tables one must remember, in order to get all the $\lambda^i_{J\tau;J\tau'}$, that $\lambda^i_{J\tau;J\tau'} = \lambda^i_{J\tau';J\tau}$. In practice, the summations seldom include more than two important terms.

The accuracy of any result obtained in this manner depends upon the accuracy with which interpolation may be made in the table. Because of the coarseness of the tabulation this may in many cases not be sufficient, and an expression is desirable which involves explicitly the transformation from a symmetric rotor representation to the representation which diagonalizes the energy of the asymmetric top in question, since the coefficients of this transformation depend upon the particular value of the asymmetry parameter κ.

One may derive such an expression by writing down the complete matrices of the squared direction cosines of Eq. (4) in a symmetric rotor representation, for instance by matrix multiplication of the direction cosine matrices given in Table I of CHK; then using the transformation mentioned above. Using the relation[14]

$$\partial^2 V/\partial x'^2 + \partial^2 V/\partial y'^2 + \partial^2 V/\partial z'^2 = 0 \quad (9)$$

one obtains by this procedure

$$\left\langle \frac{\partial^2 V}{\partial z^2} \right\rangle_{Av} = \frac{1}{(J+1)(2J+3)} \times \sum_K [S_{K\tau}{}^2 (3K^2 - J(J+1))(\partial^2 V/\partial z'^2) - 2 S_{K\tau} S_{K+2\tau} f^{\frac{1}{2}}(J, K+1) \times ((\partial^2 V/\partial x'^2) - (\partial^2 V/\partial y'^2))], \quad (10)$$

where

$$f(J, n) = \tfrac{1}{4}[(J+n)(J+n+1)(J-n)(J-n+1)].$$

[13] The procedure for obtaining squares of individual direction cosine matrix elements from the CHK tables is given by S. Golden and E. Bright Wilson, Jr. in "The Stark Effect for a Rigid Asymmetric Rotor," Appendix C (to be published).

[14] This relation holds because of the way in which the average over the electronic state is carried out. A small sphere surrounding the nucleus is excluded from the integration. The electron distribution within the sphere has spherical symmetry, and its interaction with the nucleus does not affect the fine structure formulas, nor the values of the constants obtained from the measurements of the fine structure.

Here the $S_{K\tau}$ must be evaluated for the asymmetry and the J in question. Such an expression will probably only be useful when, for a low J, a higher degree of precision is required than is available from the CHK table for the particular asymmetry involved. It is completely unsuited for use in analysis of rotational spectra. It furnishes, however, a starting point for development of asymptotic approximations which will be given in the second paper. It should be observed that, for a symmetric rotor, Eq. (10) reduces to the relation

$$\left\langle \frac{\partial^2 V}{\partial z^2} \right\rangle_{Av} = \frac{3K^2 - J(J+1)}{(J+1)(2J+3)} \frac{\partial^2 V}{\partial z'^2}$$

and this could have been obtained from Eq. (4) by writing in the diagonal elements of the α^2 in a symmetric rotor representation. (There are, however, easier methods of obtaining this expression). It further reduces to

$$\left\langle \frac{\partial^2 V}{\partial z^2} \right\rangle_{Av} = -\frac{J}{2J+3} \frac{\partial^2 V}{\partial z'^2}$$

for linear molecules.

Since the CHK tables extend only to $J=12$, and Eq. (10) should be especially tedious to apply for $J>12$, it has seemed advisable to develop asymptotic approximations to $\langle \partial^2 V/\partial z^2 \rangle_{Av}$ for these higher levels. It has so far been possible to obtain such approximation for slight asymmetry and for these levels which are highest or lowest for a given J. These approximations will be published in a later paper.

4. IDENTIFICATION OF ASYMMETRIC ROTOR SPECTRA

One of the uses to which this theory may be put is that of identification and analysis of pure rotation spectra of asymmetric tops containing one quadrupolar nucleus. The structure of a quadrupole multiplet arising from a given transition depends on the scale factors $eQ\langle \partial^2 V/\partial z^2 \rangle_{Av}$ of the initial and final states and on the characteristic value of the operator in square brackets of Eq. (1), given in Eq. (2). This characteristic value depends on I and J, but I is assumed known. The structure thus depends on three unknowns, J and the quadrupole coupling parameters $eQ\langle \partial^2 V/\partial z^2 \rangle_{Av}$. Since for $I=1$ the multiplet will consist of five ($\Delta J=\pm 1$) or six ($\Delta J=0$) components, for $I=\frac{3}{2}$ either nine ($\Delta J=\pm 1$) or ten ($\Delta J=0$) components, and so on, one should in principle have a highly overdetermined set of equations giving the separations of components in terms of the three unknowns.

If the J-values of the transition can be determined in this way, one should also be able to get τ and τ' by a process of elimination in which approximate expected frequencies and selection rules are used, or by comparison of observed values of $eQ\langle \partial^2 V/\partial z^2 \rangle_{Av}$ for initial and final states with those predicted from Eq. (8). In order to make such predictions, there must be available estimates of the second derivatives of the potential along the principal axes.

Dr. C. H. Townes has suggested a way in which to make such guesses. We assume that the component of $\nabla\mathbf{E}$ along the bond from the nucleus in question is the same as that observed experimentally in a linear molecule in which the same nucleus appears, similarly bonded. If we in addition make the approximate assumption that the charge distribution in the vicinity of the nucleus is symmetrical about the bond and use the relation $\nabla^2 V=0$, we can obtain the components of $\nabla\mathbf{E}$ along the principal axes in terms of the components along the bond and the direction cosines between the bond and the principal axes. Then, approximately,

$$\frac{\partial^2 V}{\partial x_i'^2} = -\frac{1}{2} \frac{\partial^2 V}{\partial \zeta^2} [3\alpha_{i\zeta}^2 - 1], \quad i=1, 2, 3 \qquad (11)$$

where ζ is an axis along the bond and x_1', x_2', x_3' are the principal axes of inertia.

5. HIGHER-ORDER TERMS IN QUADRUPOLE COUPLING

The preceding sections have been concerned with developing in detail formulas for the first-order quadrupole contributions to the energy. The problem of calculating higher order contributions will be outlined here. Only the one-nucleus case will be discussed; the extension to

molecules containing two quadrupolar nuclei is immediate.

Bardeen and Townes have developed formulas for the elements of the symmetric rotor quadrupole Hamiltonian which are off-diagonal in J.[15] Their formulas apply when the nucleus in question is on the symmetry axis, so that

$$\partial^2 V/\partial x'^2 = \partial^2 V/\partial y'^2,$$
$$\partial^2 V/\partial x'\partial y' = \partial^2 V/\partial x'\partial z' = \partial^2 V/\partial y'\partial z' = 0. \quad (12)$$

The matrix then turns out to be diagonal in K.

In the present problem these simplifications are absent. In general the quadrupole Hamiltonian will have non-vanishing elements connecting different values of J and τ. While for most nuclei in linear and symmetric tops the second-order effects are small, in asymmetric tops there exists the possibility of near accidental degeneracies, $E_{J\tau} \cong E_{J'\tau'}$, which will make the second-order corrections important. Furthermore, for a given J the highest levels are essentially degenerate in pairs (small K-type doubling) so that for these levels elements off-diagonal in τ must always be taken into account.

The complete quadrupole Hamiltonian may be written

$$\mathbf{H} = \tfrac{1}{6}\mathbf{Q}:\nabla\mathbf{E} \quad (13)$$

where

$$Q_{\mu\nu} = \int \rho(3x_\mu x_\nu - \delta_{\mu\nu} r^2) d\tau,$$

$$(\nabla E)_{\mu\nu} = \sum_j (e_j/r_j^3)(3x_{j\mu}x_{j\nu} - \delta_{\mu\nu} r_j^2), \quad \mu, \nu = 1, 2, 3$$

and the symbol : indicates the inner product of the two dyadics. The matrices of the "scalar product" of two tensors in the $FIJM_F$ scheme have been developed by Racah[16] and his formulas may be used here. The Hamiltonian has the following non-vanishing matrix elements.

TABLE I.

		E	$C_{z'}$	$C_{y'}$	$C_{x'}$
$\alpha_{zz'}{}^2\alpha_{zy'}{}^2\alpha_{zx'}{}^2$	A	1	1	1	1
$\alpha_{xz'}\alpha_{xy'}\ \alpha_{xx'}$	$B_{z'}$	1	1	−1	−1
$\alpha_{yz'}\alpha_{yz'}\ \alpha_{yy'}$	$B_{y'}$	1	−1	1	−1
$\alpha_{zy'}\alpha_{zz'}\ \alpha_{zx'}$	$B_{x'}$	1	−1	−1	1

$$(J\tau F|H|J+2\tau' F) = \frac{eQ(J_\tau J|\nabla E_{zz}|J+2\tau' J)}{16I(2I-1)[(2J+1)(J+1)]^{\frac{1}{2}}} \times[(I+J+F+2)(I+J+F+3)(I-J+F-1)(I-J+F)(J-I+F+1)(J-I+F+2)(I+J-F+1)(I+J-F+2)]^{\frac{1}{2}},$$

$$(J\tau F|H|J+1\tau' F) = \frac{eQ(J_\tau J|\nabla E_{zz}|J+1\tau' J)}{8I(2I-1)J(2J+1)^{\frac{1}{2}}} \times[F(F+1)-I(I+1)-J(J+2)] \times[(I+J+F+2)(I-J+F)(J-I+F+1)(J+I-F+1)]^{\frac{1}{2}},$$

$$(J\tau F|H|J\tau' F) = \frac{eQ(J\tau J|\nabla E_{zz}|J\tau' J)}{8I(2I-1)J(2J-1)} \times[3C(C+1)-4I(I+1)J(J+1)], \quad (14)$$

where Q is defined in Eq. (1). The matrix is diagonal in F and M_F. The $J;J-1$ and $J;J-2$ elements may be determined from Eq. (14) by the Hermitian property of $\mathbf{H}$. The evaluation of the matrix elements of $\nabla E_{zz} = (\partial^2 V/\partial z^2)$ is the difficult problem here, as before. For symmetric tops, using the substitution of Eq. (3), one finds

$$(JKJ|\nabla E_{zz}|J+1KJ) = \frac{3K[(J+1)^2-K^2]^{\frac{1}{2}}}{(J+1)(J+2)[2J+3]^{\frac{1}{2}}} \frac{\partial^2 V}{\partial z'^2},$$

$$(JKJ|\nabla E_{zz}|J+2KJ) = \frac{3[\{(J+1)^2-K^2\}\{(J+2)^2-K^2\}]^{\frac{1}{2}}}{(J+2)(2J+3)[(J+1)(2J+5)]^{\frac{1}{2}}} \frac{\partial^2 V}{\partial z'^2}.$$

Substitution of these into Eqs. (14) leads to the expressions of Bardeen and Townes.

For asymmetric tops the evaluation of $(J\tau J|\nabla E_{zz}|J'\tau' J)$ may be simplified by the use of group theory. The asymmetric top wave functions belong to representations of the four-group D_2; so also do the direction cosines α appearing in Eq. (3). Table I gives the symmetries of the direction cosines and their

[15] J. Bardeen and C. H. Townes, Phys. Rev. **73**, 627 (1948), as corrected in an erratum, p. 1204.

[16] G. Racah, Phys. Rev. **52**, 438 (1942). Racah's formulas were first applied to the quadrupole problem by Bardeen and Townes, reference 5.

products. Thus if the two states have the same symmetry, only those combinations of direction cosines belonging to representation A give non-vanishing elements. If the two states have different symmetries, one of the combinations $\alpha_{zz'}\alpha_{zy'}$, $\alpha_{zz'}\alpha_{zz'}$, $\alpha_{zy'}\alpha_{zz'}$ will give non-vanishing elements.

It is this latter case which is involved in the near degeneracies due to slight K-doubling. This should make possible the individual determination of $(\partial^2 V/\partial x'\partial y')$, etc. It seems reasonable that these "cross-derivates" should be small, but by how much they deviate from the 0 value in symmetric rotors must be found from experiment. Equation (14) shows that in this case the multiplet will have the appearance of a "first-order" quadrupole multiplet, only the scale factor differing. Accidental degeneracy arising from levels involving different J may, however, occur between levels of arbitrary relative symmetries.

The matrices Eq. (14) may be used in the above cases, either to evaluate the second-order energy corrections, or to make possible the treatment of near-degenerate levels by degenerate perturbation theory.

The evaluation of the various matrix elements of the combinations of direction cosines which may occur will not be discussed in detail. Unforunately, it seems that the line-strength tables can no longer be used. Expressions analogous to Eq. (10) may be derived involving explicitly the transformation from symmetric to asymmetric rotor basis. Finally, approximation procedures such as will be the subject of the second paper should be applicable.

ACKNOWLEDGMENTS

The writer gratefully acknowledges the encouragement and assistance of Professors J. H. Van Vleck and E. Bright Wilson, Jr., and the numerous helpful suggestions of Dr. S. Golden.

PHYSICAL REVIEW VOLUME 74, NUMBER 5 SEPTEMBER 1, 1948

The Meson Field and Equations of Motion of Point Particles

R. C. MAJUMDAR AND A. S. APTE*
Department of Physics, University of Delhi, Delhi, India

(Received May 3, 1947)

The equation of motion of a point particle possessing a charge and interacting with a meson field (both vector and scalar) is derived from a generalization of the scheme of Infeld and Wallace for determining the equation of a point electron in an electromagnetic field. The retarded and advanced meson fields of the point particle and the nature of the simultaneous expressions for the symmetric, $\frac{1}{2}$(ret+adv), and radiation, $\frac{1}{2}$(ret−adv), potentials and field intensities are investigated. The simultaneous radiation field is found to be always finite for $r\to 0$, whereas the corresponding symmetric field allows expansion in powers of r with -2 as the lowest, r being the radius of the 3-dimensional sphere surrounding the singularity which represents the point particle. It is shown that the removal of the singularities from the symmetric field leads to the equation of motion given by Bhabha for the vector meson field in the case of the retarded field; the symmetric field, on the other hand, leads to the equation of motion in which the radiation damping is absent. The corresponding equation of motion of a point particle in a scalar meson field is also given.

I. INTRODUCTION

INVESTIGATIONS of the meson field and its scattering by nuclear particles in recent years have led to important developments in the theory of fundamental particles. The highly divergent nature of scattering cross sections for large energies of the meson wave was a puzzle for a long time and was considered to set a limit to the validity of quantum mechanics. It was first realized by Heisenberg[1] and Bhabha[2]

* Scholar, Tata Institute of Fundamental Research, Bombay.

[1] W. Heisenberg, Zeits. f. Physik **113**, 61 (1939).
[2] H. J. Bhabha, Proc. Roy. Soc. **A172**, 384 (1939).

that the increase in the cross section with increasing energy of the incident meson wave was essentially due to the neglect of the reaction of the neutron's own radiated meson field. A completely relativistic invariant theory of the neutron in a meson field, taking account of the reaction of the neutron's own field, was, however, first worked out by Bhabha in the scheme of classical physics by following Dirac's method[3] for obtaining the equation of motion of an electron in an electromagnetic field. In the usual field theory the motion of charged particles, as represented by the singularities of the field, is not determined by the field equations. In Dirac's method, the equation of motion of the point particle is obtained in a simple way from the laws of conservation of the energy-momentum tensor of the field, in which one considers not the total energy of the field, but the manner in which this energy changes. By virtue of this law it is found that the flow of energy and momentum out of a portion of a narrow tube surrounding the world line of the particle representing the singularity of the field depends only on the conditions at the two ends of the tube. The equation of motion was then obtained by Dirac by assuming a simple expression for the flux of energy and momentum out of the tube. It was found, however, that the flux assumes an infinite value when the tube shrinks to the world-line, giving rise to an infinite rest mass for the point particle due to its own field. But as the singular term in the flux was a perfect differential and could therefore be regarded as the change of some quantity which depended only on the state of motion of the point particle, it was possible for Dirac to eliminate it from the equation of motion by subtracting a compensating infinite term from it. This was physically equivalent to postulating an infinite negative mass in the singularity. Although the whole scheme was relativistically invariant, the process of subtracting one infinite quantity from another destroyed the intuitive character of the theory. One would, under the circumstances, expect to get rid of the infinite terms which are entirely spurious by altering the energy-momentum tensor of the field without, however, altering the equation of motion so as to make the flux finite. This obviously involves the reformulation of the energy-momentum tensor of the field itself so that the total energy associated with a point charge becomes finite. This was in principle the method developed by Pryce.[4] Another method of obtaining the equation of motion, free from the difficulty of subtracting two infinite quantities, has been recently suggested by Infeld and Wallace.[5] The method follows closely that employed by Einstein, Infeld, and Hoffmann[6] for determining the equation of motion of point particles in the general theory of relativity. In this method the singularity is surrounded by a small sphere and the equation of motion is obtained from the laws of conservation of energy and momentum tensor together with the generalized Poisson equations expressed in terms of the rate of change of the energy-momentum tensor. Taking a Lorentz frame of reference in which the singularity is instantaneously at rest at the origin at time t, the calculations are conveniently carried out in three-dimensional notation referring to this particular instant t and to this coordinate system. The equation of motion is then obtained from the flow of energy and momentum and the change of the potential functions integrated over the surface of the sphere surrounding the singularity.

In the present paper we shall obtain the fundamental equations of motion of the neutron under the influence of a meson field from a generalization of the scheme of Infeld and Wallace for determining the equation of motion of an electron in an electromagnetic field. As is evident, the equation of motion will depend on the actual field from which the energy-momentum tensor is calculated. We shall divide the field into two parts, the external field (Dirac's incoming field), and the field of the singularity taken as a retarded field. For general discussions we shall further express the retarded field as the sum of two other fields, namely, the symmetric field, defined as half the sum of the retarded and advanced fields, and the radiation field, defined as half the

[3] P. A. M. Dirac, Proc. Roy. Soc. **A167**, 148 (1938).

[4] M. H. L. Pryce, Proc. Roy. Soc. **A168**, 389 (1938).

[5] L. Infeld and P. R. Wallace, Phys. Rev. **57**, 797 (1940).

[6] A. Einstein, L. Infeld, and B. Hoffmann, Ann. Math. **39**, 65 (1938).

retarded minus the advanced field. Because of the special choice of our coordinate system we can conveniently expand the retarded and advanced meson potentials and fields and obtain from them the simultaneous expressions for the symmetric and radiation fields required for the calculations of the energy-momentum tensor. It is found that the simultaneous radiation field is always finite when the radius of the sphere surrounding the singularity tends to zero, whereas the corresponding symmetric field can be expanded in a series in ascending powers of the radius with minus two as the lowest power. The calculations, as presented in the paper, show that the singular term in the flow of energy and momentum through the surface of the sphere enclosing the singularity, which is due to the singular term in the symmetric field, is exactly compensated by the change of the potential function determined from the rate of change of the Poynting vector taken over the entire space, excluding the sphere surrounding the singularity. In case the field of the singularity is taken as a retarded field, the equation of motion obtained for the vector meson is the same as that obtained by Bhabha, but one from which the difficulties of the infinities have been removed. The equation of motion for the scalar meson field, however, differs slightly from the corresponding equation recently derived by Harish-Chandra.[7] But it can be easily verified that the equation given in the text is the simplest form of the equation of motion of a neutron in a scalar meson field. If, on the other hand, the field of the singularity is assumed to be given by that of the symmetric field, the equation of motion which is obtained thereby does not contain the radiation damping term at all.

In Sections II and III we shall formulate the meson potentials and fields of a neutron, and shall evaluate the simultaneous expressions obtained from them for the symmetric and radiation fields by the method of contour integrations. Section IV describes the method of obtaining the equation of motion of a neutron in a meson field by taking account of the reaction of the neutron's own field.

[7] Harish-Chandra, Proc. Roy. Soc. **A185**, 269 (1944).

II. THE MESON FIELD OF A NUCLEON

i. Vector Meson Field

The meson field of a neutron will be assumed to be described by potentials ϕ_μ and field strengths $G_{\mu\nu}$ satisfying the equations

$$G_{\mu\nu}=(\partial\phi_\nu/\partial x_\mu-\partial\phi_\mu/\partial x_\nu)+4\pi S_{\mu\nu}, \quad (1)$$

$$\partial G_{\mu\nu}/\partial x_\nu+\lambda^2\phi_\mu=4\pi M_\mu, \quad (2)$$

where $\lambda=\mu c/\hbar$, μ being the rest mass of the meson. M_μ is a 4-vector describing the effect of the neutron "charge" on the field, and $S_{\mu\nu}$ is an antisymmetrical tensor describing the effect of the neutron dipole moment. For the neutral meson field the quantities in Eqs. (1) and (2) are all real, and we obtain

$$(\partial^2\phi_\mu/\partial x_\nu{}^2)-\lambda^2\phi_\mu=-4\pi M_\mu+4\pi\partial S_{\mu\nu}/\partial x_\nu, \quad (3)$$

$$\partial\phi_\mu/\partial x_\mu=0. \quad (4)$$

We shall use the coordinate system introduced by Proca x_1, x_2, x_3, $x_4=\epsilon ct=\epsilon x_0$, where the quantity ϵ is such that $\epsilon^2=-1$, and in going over to the conjugate complex the sign of ϵ is not changed. We shall take

$$\phi_4=\epsilon\phi_0, \quad G_{4\mu}=\epsilon G_{0\mu}. \quad (5)$$

We now proceed to calculate the meson field produced by the point neutron moving along a classical world line. The field will obviously be given by the solution of the inhomogeneous Eq. (3) which has a singularity[7a] on the world line. The coordinates of the neutron are denoted by z_μ, which can be considered as a function of the proper time, τ, measured from some arbitrary point on the world line of the neutron. In the present paper we shall deal with the field caused by the charge part of the neutron given by the first term of the right-hand side of Eq. (3). We first seek a solution of the homogeneous equation

$$\Box^2\phi-\lambda^2\phi=0. \quad (6)$$

By introducing the four-dimensional distance s given by

$$s^2=s_\mu s_\mu, \quad s_\mu=x_\mu-z_\mu(\tau), \quad (7)$$

[7a] The nature of the singularity must be determined by Green's function for the type of field considered—Ed.

Eq. (6) reduces to[7b]

$$\frac{d^2(\phi s)}{ds^2}+\frac{1}{s}\frac{d(\phi s)}{ds}+\left(i^2\lambda^2-\frac{1}{s^2}\right)(\phi s)=0. \quad (8)$$

This is a form of Bessel's equation of first order, the solution of which has been discussed by several authors.[8] Equation (8) has singularities at

$$\tau=\tau'(\text{ret})=t-r/c \text{ and } \tau=\tau''(\text{adv})=t+r/c. \quad (9)$$

In the complex τ-plane the required solution is readily obtained as

$$\phi_\mu=B\int_{\tau_1}^{\tau_2}\{i\lambda J_1(is\lambda)s^{-1}\log s-s^{-2}\}(dz_\mu/d\tau)d\tau. \quad (10)$$

The retarded potential may be obtained by allowing the path of integration to run along the real axis from $-\infty$ on one sheet of Riemann's surface round τ' to $-\infty$ on a second one. We thus obtain

$$\phi_\mu(\text{ret})=\phi_\mu{}^0(\text{ret})+\phi_\mu{}^\lambda(\text{ret}), \quad (11)$$

where

$$\phi_\mu{}^0(\text{ret})=-B\oint s^{-2}(dz_\mu/d\tau)d\tau=-gv_\mu/(s_\sigma v_\sigma), \quad (12)$$

and

$$\phi_\mu{}^\lambda(\text{ret})=ig\lambda\int_{-\infty}^{\tau'}v_\mu(J_1(is\lambda)/s)d\tau. \quad (13)$$

The contour in (12) runs round the retarded point $s^2=r^2-c^2(t-\tau)^2=0$, $s_0>0$. The advanced potential may be similarly obtained by the choice of a path of integration running along the real axis from $+\infty$ on the Riemann surface round the other singularity $\tau=\tau''$ back to $+\infty$ on a second sheet of the Riemann surface. The meson fields of the neutron are also similarly obtained:

$$G_{\mu\nu}=\frac{\partial\phi_\nu}{\partial x_\mu}-\frac{\partial\phi_\mu}{\partial x_\nu}=G_{\mu\nu}{}^0+G_{\mu\nu}{}^\lambda, \quad (14)$$

where

$$G_{\mu\nu}{}^0=2B\int_{\tau_1}^{\tau_2}s^{-4}(s_\mu v_\nu-s_\nu v_\mu)d\tau, \quad (15)$$

and

$$G_{\mu\nu}{}^\lambda=i\lambda B\int_{\tau_1}^{\tau_2}s^{-2}(s_\mu v_\nu-s_\nu v_\mu)\times\{s^{-1}J_1(is\lambda)-i\lambda J_2(is\lambda)\log s\}d\tau, \quad (16)$$

which for retarded fields reduce to

$$G_{\mu\nu}{}^0(\text{ret})=g\left\{\frac{s_\mu v_\nu-s_\nu v_\mu}{(s_\sigma v_\sigma)^3}(c^2+s_\alpha\dot{v}_\alpha)-\frac{s_\mu\dot{v}_\nu-s_\nu\dot{v}_\mu}{(s_\sigma v_\sigma)^2}\right\}, \quad (17)$$

$$G_{\mu\nu}{}^\lambda(\text{ret})=-\frac{g\lambda^2}{2}\frac{s_\mu v_\nu-s_\nu v_\mu}{(s_\sigma v_\sigma)}+g\lambda^2\int_{-\infty}^{\tau'}\frac{s_\mu v_\nu-s_\nu v_\mu}{s^2}J_2(is\lambda)d\tau. \quad (18)$$

We have put $B=-g/\pi i$. The expressions appearing outside the integrals, as for example (12) and (17) and the first term of (18), are to be taken at the retarded point $\tau=\tau'$. It is to be noticed that $G_{\mu\nu}{}^\lambda$ and $\phi_\mu{}^\lambda$ are finite at all points of space including the world line of the neutron and tend continuously to zero as λ tends to zero. The first term of (18) becomes zero when averaged over-all directions of approach to a point on the world line, and is not single-valued. The only infinities in the potential and the fields are involved in $G_{\mu\nu}{}^0$ and $\phi_\mu{}^0$, which are Maxwell fields for a moving charge. Following Bhabha, we denote the second term of $G_{\mu\nu}{}^\lambda$ by $\bar{G}_{\mu\nu}{}^\lambda$ to mean thereby that it is the value of $G_{\mu\nu}{}^\lambda$ at any point averaged over a small region of space surrounding that point. Since $\bar{G}_{\mu\nu}{}^\lambda$ is continuous everywhere we shall consider it as a part of the external field, and to avoid complication we shall not write it explicitly in the calculations and shall add it only in the final formula. In the following we proceed, therefore, to discuss only the singular part of the fields.

ii. Scalar Meson Field

For the case of the scalar meson field of a neutron, the equations satisfied by the potential, ψ, and the field strength, χ_ν, are given by

$$\partial\chi_\nu/\partial x_\nu+\lambda^2\psi=4\pi gN,\qquad \chi_\nu=-\partial\psi/\partial x_\nu+4\pi M_\nu. \quad (19)$$

We thus obtain

$$(\partial^2\psi/\partial x_\nu{}^2)-\lambda^2\psi=-4\pi gN+4\pi(\partial M_\nu/\partial x_\nu), \quad (20)$$

where N is a scalar and M_ν is a vector describing the effect of neutron dipole moment. The potential is given by

$$\psi=Bc\int_{\tau_1}^{\tau_2}\{i\lambda J_1(i\lambda s)s^{-1}\log s-s^{-2}\}d\tau. \quad (21)$$

[7b] It is assumed here that ϕ is a function of s only—Ed.

[8] R. Courant and D. Hilbert, *Methoden der Mathematischen Physik* II, VI Kapitel; (Julius Springer, Berlin, 1937), S. N. Bose and S. C. Kar, Proc. Nat. Inst. Sci. of India **7**, 93 (1941).

From which it immediately follows that

$$\psi(\text{ret})=\psi^0(\text{ret})+\psi^\lambda(\text{ret}), \tag{22}$$

where

$$\psi^0(\text{ret})=-Bc\oint s^{-2}d\tau=-gc/(s_\sigma v_\sigma), \tag{23}$$

and

$$\psi^\lambda(\text{ret})=ig\lambda c\int_{-\infty}^{\tau'} s^{-1}J_1(is\lambda)d\tau. \tag{24}$$

The meson-field strength is

$$F_\mu=-\partial\psi/\partial x_\mu=F_\mu{}^0+F_\mu{}^\lambda, \tag{25}$$

where

$$F_\mu{}^0=2Bc\int_{\tau_1}^{\tau_2}(s_\mu/s^4)d\tau, \tag{26}$$

$$F_\mu{}^\lambda=i\lambda Bc\int_{\tau_1}^{\tau_2}\{s^{-1}J_1(i\lambda s)-i\lambda J_2(i\lambda s)\times\log(i\lambda s)\}(s_\mu/s^2)d\tau. \tag{27}$$

Thus we obtain

$$F_\mu{}^0(\text{ret})=gc\{(s_\mu/(s_\sigma v_\sigma)^3)(c^2+s_\alpha\dot{v}_\alpha)+v_\mu/(s_\sigma v_\sigma)^2\}, \tag{28}$$

$$F_\mu{}^\lambda(\text{ret})=-\tfrac{1}{2}g\lambda^2(cs_\mu/(s_\sigma v_\sigma))+g\lambda^2 c\int_{-\infty}^{\tau'} s^{-2}s_\mu J_2(i\lambda s)d\tau. \tag{29}$$

As before, we have put $B=-g/\pi i$.

III. SIMULTANEOUS MESON POTENTIALS AND FIELD INTENSITIES[9]

It should be noted that for the evaluation of the energy-momentum tensor we shall require, according to the choice of our special reference system, the simultaneous expressions for the potentials and the field intensities at the instant t. Further, in calculating the energy-momentum tensor it is usual to take the field as the sum of the retarded field of the singularity and the external field incident on the neutron. Equation (3) also permits a solution which is symmetric and is given by $\frac{1}{2}$(ret+adv), and a solution which is responsible for the radiation produced by the neutron and is $\frac{1}{2}$(ret−adv). We shall calculate the two parts separately and separate them by a comma. The sum of these solutions will give the retarded field.

[9] J. Frenkel, *Lehrbuch der Elektrodynamik*, I (Berlin, 1926); L. Page and N. I. Adams, *Electrodynamics* (New York, 1940).

i. Vector Meson Field

The simultaneous expressions for the symmetric and radiation solutions for the potentials and fields can be easily obtained from (12), (13), (15), and (16) by subjecting them to the expansions in powers of $r/c(\tau-t)$ and calculating the residues at $\tau=t$. The contour of integration for the first sum in the expansions is to be taken round the retarded point in the positive sense and that for the second in the negative sense. Both these are then reduced to contours round the point $\tau=t$. Thus expressing

$$\frac{1}{s^2}=\frac{1}{2}\left[\sum_{n=0}^{\infty}\frac{(-)^n r^{n-1}}{c^{n+1}(\tau-t)^{n+1}}-\sum_{n=0}^{\infty}\frac{r^{n-1}}{c^{n+1}(\tau-t)^{n+1}}\right], \tag{30}$$

we get

$$\phi_\mu{}^0(\tfrac{1}{2}\,\text{ret}+\tfrac{1}{2}\text{adv})=(g/4\pi i)\sum_{n=0}^{\infty}\frac{(-)^n+1}{c^{n+1}}\oint\frac{r^{n-1}}{(\tau-t)^{n+1}}\frac{dz_\mu}{d\tau}d\tau. \tag{31}$$

Now by applying Cauchy's formula

$$(d^n f(\tau)/d\tau^n)_{\tau=a}=f^{(n)}(a)=(n!/2\pi i)\oint[f(\tau)/(\tau-a)^{n+1}]d\tau, \tag{32}$$

we can express (31) in the form

$$\phi_\mu{}^0(\tfrac{1}{2}\,\text{ret}+\tfrac{1}{2}\,\text{adv})=g\sum_{l=1}^{\infty}[1/(2l-2)!c^{2l-2}]\times\frac{d^{2l-2}}{d\tau^{2l-2}}(v_\mu(\tau)r^{2l-3}/c), \tag{33}$$

where we have put $n=2l-2$. Similarly, by putting $n=2l-1$, we obtain

$$\phi_\mu{}^0(\tfrac{1}{2}\,\text{ret}-\tfrac{1}{2}\,\text{adv})=-g\sum_{l=1}^{\infty}[1/(2l-1)!c^{2l-1}]\times\frac{d^{2l-1}}{d\tau^{2l-1}}(v_\mu(\tau)r^{2l-2}/c). \tag{34}$$

The fields $G_{\mu\nu}$ may also be calculated in the same

way from (15) and (16)

$$G_{\mu\nu}{}^0(\tfrac{1}{2}\text{ ret}+\tfrac{1}{2}\text{ adv})$$

$$=-\frac{g}{4\pi i}\sum_{n=0}^{\infty}\oint\left\{\frac{(-)^n-1}{c^{n+2}}(n+1)\kappa_{\mu\nu}\frac{r^{n-2}}{(\tau-t)^{n+2}}+\frac{(-)^n+1}{c^{n+1}}\kappa_{\mu\nu}\frac{r^{n-3}}{(\tau-t)^{n+1}}\right\}d\tau \quad (35)$$

$$=\frac{g}{2\pi i}\sum_{l=0}^{\infty}\oint\frac{(2l-1)\kappa_{\mu\nu}}{c^{2l+1}}\frac{r^{2l-3}}{(\tau-t)^{2l+1}}d\tau, \quad (36)$$

where we have put

$$\kappa_{\mu\nu}=s_\mu v_\nu-s_\nu v_\mu. \quad (37)$$

By applying (32) we have

$$G_{\mu\nu}{}^0(\tfrac{1}{2}\text{ ret}+\tfrac{1}{2}\text{ adv})$$

$$=g\sum_{l=0}^{\infty}\left[\frac{2l-1}{(2l)!c^{2l+1}}\right]\frac{d^{2l}}{d\tau^{2l}}(\kappa_{\mu\nu}r^{2l-3}). \quad (38)$$

Similarly, we obtain

$$G_{\mu\nu}{}^0(\tfrac{1}{2}\text{ ret}-\tfrac{1}{2}\text{ adv})$$

$$=-g\sum_{l=0}^{\infty}\left[\frac{2l}{(2l+1)!c^{2l+2}}\right]\frac{d^{2l+1}}{d\tau^{2l+1}}(\kappa_{\mu\nu}r^{2l-2}), \quad (39)$$

and further,

$$G_{\mu\nu}{}^\lambda(\tfrac{1}{2}\text{ ret}+\tfrac{1}{2}\text{ adv})$$

$$=\tfrac{1}{2}\lambda^2 g\sum_{l=1}^{\infty}\left[\frac{1}{(2l-2)!c^{2l-1}}\right]\frac{d^{2l-2}}{d\tau^{2l-2}}(\kappa_{\mu\nu}r^{2l-3}), \quad (40)$$

$$G_{\mu\nu}{}^\lambda(\tfrac{1}{2}\text{ ret}-\tfrac{1}{2}\text{ adv})$$

$$=-\tfrac{1}{2}\lambda^2 g\sum_{l=1}^{\infty}\left[\frac{1}{(2l-1)!c^{2l}}\right]\frac{d^{2l-1}}{d\tau^{2l-1}}(\kappa_{\mu\nu}r^{2l-2}). \quad (41)$$

It is to be noted that all the above quantities are to be evaluated at time $\tau=t$. The energy-momentum tensor of the meson field in a region not occupied by a neutron is

$$T_{\mu\nu}=\frac{1}{4\pi}G_{\mu\sigma}G_{\nu\sigma}-\frac{1}{16\pi}\delta_{\mu\nu}G_{\rho\sigma}G_{\rho\sigma}+\frac{\lambda^2}{4\pi}\phi_\mu\phi_\nu-\frac{\lambda^2}{8\pi}\delta_{\mu\nu}\phi_\sigma\phi_\sigma. \quad (42)$$

From this we obtain at once the stress tensor and the energy density given, respectively, by

$$T_{mn}=(1/4\pi)(G_{mk}G_{nk}-G_{m0}G_{n0})-(\delta_{mn}/8\pi)(\tfrac{1}{2}G_{ik}G_{ik}-G_{k0}G_{k0})+(\lambda^2/4\pi)\phi_m\phi_n+(\lambda^2/8\pi)\delta_{mn}(\phi_0\phi_0-\phi_k\phi_k), \quad (43)$$

$$T_{00}=-T_{44}=(1/8\pi)G_{0k}G_{0k}+(1/16\pi)G_{ik}G_{ik}+(\lambda^2/8\pi)(\phi_0\phi_0+\phi_k\phi_k), \quad (44)$$

whereas the Poynting vector is

$$T_{m0}=(1/4\pi)[G_{mk}G_{0k}+\lambda^2\phi_m\phi_0]. \quad (45)$$

The Greek suffixes run from 1 to 4, whereas the Latin suffixes run from 1 to 3.

ii. Scalar Meson Field

In a similar way the corresponding simultaneous expressions for the potentials and intensities for the scalar meson field can be easily calculated. They are

$$\psi^0(\tfrac{1}{2}\text{ ret}+\tfrac{1}{2}\text{ adv})$$

$$=g\sum_{l=1}^{\infty}\frac{1}{(2l-2)!c^{2l-2}}\frac{d^{2l-2}}{d\tau^{2l-2}}(r^{2l-3}), \quad (46)$$

$$\psi^0(\tfrac{1}{2}\text{ ret}-\tfrac{1}{2}\text{ adv})$$

$$=-g\sum_{l=1}^{\infty}\frac{1}{(2l-1)!c^{2l-1}}\frac{d^{2l-1}}{d\tau^{2l-1}}(r^{2l-2}), \quad (47)$$

and

$$F_\mu{}^0(\tfrac{1}{2}\text{ ret}+\tfrac{1}{2}\text{ adv})=g\sum_{l=0}^{\infty}\frac{(2l-1)}{(2l)!c^{2l}}\frac{d^{2l}}{d\tau^{2l}}(s_\mu r^{2l-3}), \quad (48)$$

$$F_\mu{}^0(\tfrac{1}{2}\text{ ret}-\tfrac{1}{2}\text{ adv})$$

$$=-g\sum_{l=0}^{\infty}\frac{2l}{(2l+1)!c^{2l+1}}\frac{d^{2l+1}}{d\tau^{2l+1}}(s_\mu r^{2l-2}). \quad (49)$$

The energy-momentum tensor of the scalar meson field is

$$T_{\mu\nu}=(1/4\pi)[F_\mu F_\nu-\tfrac{1}{2}\delta_{\mu\nu}(F_\sigma F_\sigma+\lambda^2\psi\psi)], \quad (50)$$

and the Poynting vector is simply

$$T_{m0}=F_m F_0/4\pi. \quad (51)$$

IV. THE EQUATIONS OF MOTION OF A NEUTRON

We are now in a position to derive the equation of motion of a neutron in the meson field from the laws of conservation of energy and momentum as suggested by Infeld and Wallace. Expressing the conservation laws for the energy-

momentum tensor in three dimensional notation, we have

$$\frac{\partial T_{mn}}{\partial x_n}-\frac{\partial}{\partial x_n}\frac{\partial \psi_m}{\partial x_n}=0, \tag{52}$$

$$\frac{\partial T_{0n}}{\partial x_n}-\frac{\partial}{\partial x_n}\frac{\partial \psi_0}{\partial x_n}=0, \tag{53}$$

where ψ_m and ψ_0 satisfy the Poisson equations

$$\Delta\psi_m=-\partial T_{m0}/c\partial t, \tag{54}$$

$$\Delta\psi_0=-\partial T_{00}/c\partial t. \tag{55}$$

Taking the coordinates of the singularity as $\eta_m(t)$, where $\eta(t)=0$, $\dot{\eta}(t)=0$ by the choice of our special reference system, the equations of motion of the neutron are given by

$$m_0\ddot{\eta}_m=-\int(T_{mn}-\partial\Psi_m/\partial x_n)\lambda^n dS, \tag{56}$$

where we have put

$$\psi_m=\bar{\psi}_m+\Psi_m. \tag{57}$$

$\bar{\psi}_m$ are arbitrary harmonic functions, and Ψ_m is the solution of the Eq. (54). It can be shown further by Gauss' theorem that

$$\int(\partial\Psi_m/\partial x_n)\lambda^n dS=\frac{1}{c}\int d(T_{m0})/dt\cdot dV. \tag{58}$$

The integral on the right-hand side of (56) is taken over an arbitrary surface which without loss of generality can be taken to be a sphere of radius r surrounding the singularity and λ^n are the direction-cosines of the outward normal to the surface of integration. The integration in (58) is to be taken over the whole space excluding the sphere of radius r enclosing the singularity.

Now to calculate the integrals we need obviously retain only the terms of order $1/r^2$ in the energy-momentum tensor T_{mn} and of order of $1/r^3$ in the rate of change of the Poynting vector given by dT_{m0}/dt. Since the tensor $T_{\mu\nu}$ contains the fields quadratically and all the expressions in the expansion of the fields have $1/r^2$ as the lowest power of r, we shall retain in $G_{\mu\nu}$ while calculating T_{mn} only the terms of order -2, -1, and 0 in r and in calculating dT_{m0}/dt the terms of order -2, and -1 in r. Although we have chosen the coordinate system such that the singularity is at rest at the origin, we shall retain v_μ and omit only those terms which contain v_k more than once. They will obviously contribute to dT_{m0}/dt. We shall retain terms of order r^0 and lower and make frequent use of

$$\dot{r}=\frac{1}{r}s_k\dot{s}_k=\frac{1}{r}s_kv_k. \tag{59}$$

i. Vector Meson Field

$$\phi_\mu{}^0(\text{simul})=g\left[\frac{1}{c}\frac{v_\mu}{r}-\frac{1}{2c^3}\frac{s_k\dot{v}_kv_\mu}{r}-\frac{1}{c^3}\frac{s_kv_k\dot{v}_\mu}{r},\ -\frac{\dot{v}_\mu}{c^2}-\frac{v_kv_kv_\mu}{c^4}\right], \tag{60}$$

and

$$\begin{aligned}G_{\mu\nu}{}^0(\text{simul})=g\Bigg[&-\frac{s_\mu v_\nu-s_\nu v_\mu}{cr^3}-\frac{v_\mu\dot{v}_\nu-v_\nu\dot{v}_\mu}{2c^3r}+\frac{s_\mu\dot{v}_\nu-s_\nu\dot{v}_\mu}{c^3r^3}s_kv_k+\frac{s_\mu v_\nu-s_\nu v_\mu}{2c^3r^3}s_k\dot{v}_k+\frac{s_\mu(d^2v_\nu/dt^2)-s_\nu(d^2v_\mu/dt^2)}{2c^3r}\\&+\frac{\delta_{\mu\nu,m0}}{8c^5}\Bigg(6\frac{v_\mu\dot{v}_\nu-v_\nu\dot{v}_\mu}{r}s_k\dot{v}_k-3\frac{s_\mu v_\nu-s_\nu v_\mu}{r^3}s_k\dot{v}_ks_l\dot{v}_l+3\frac{s_\mu v_\nu-s_\nu v_\mu}{r}\dot{v}_k{}^2\\&+8\frac{v_\mu(d^2v_\nu/dt^2)-v_\nu(d^2v_\mu/dt^2)}{r}s_kv_k+12\frac{s_\mu\dot{v}_\nu-s_\nu\dot{v}_\mu}{r}v_k\dot{v}_k-4\frac{s_\mu v_\nu-s_\nu v_\mu}{r^3}s_k(d^2v_k/dt^2)s_lv_l\\&+4\frac{s_\mu v_\nu-s_\nu v_\mu}{r}v_k(d^2v_k/dt^2)-12\frac{s_\mu\dot{v}_\nu-s_\nu\dot{v}_\mu}{r^3}s_k\dot{v}_ks_lv_l\Bigg),\\&+\frac{2}{3c^4}(v_\mu(d^2v_\nu/dt^2)-v_\nu(d^2v_\mu/dt^2))\Bigg]+G_{\mu\nu}{}^{\text{ext}},\end{aligned} \tag{61}$$

$$G_{\mu\nu}{}^\lambda=g\left[\frac{\lambda^2}{2c}\frac{s_\mu v_\nu-s_\nu v_\mu}{r},\ 0\right]+\bar{G}_{\mu\nu}{}^\lambda. \tag{62}$$

The terms preceding the comma give the symmetric solution $\frac{1}{2}$(ret+adv) and those after the comma give the radiation solution $\frac{1}{2}$(ret−adv), whereas the complete expression gives the retarded solution. $G_{\mu\nu}{}^{\text{ext}}$ is the incoming external field and $\bar{G}_{\mu\nu}{}^{\lambda}$ is the second term in (18) of $G_{\mu\nu}{}^{\lambda}$

$$\bar{G}_{\mu\nu}{}^{\lambda}=g\lambda^2\int_{-\infty}^{r'}s^{-2}(s_\mu v_\nu-s_\nu v_\mu)J_2(is\lambda)d\tau. \quad (63)$$

This is finite on the world line and, as discussed before, will be omitted henceforth and added in the final result. It is to be noted that the first term in (61) is of the order r^{-2}, the second, third, and fourth are of order r^{-1}, whereas the rest are of order r^0. $G_{\mu\nu}{}^{\lambda}$, which is part of the field depending on λ, is of the order r^0.

Now to calculate the energy-momentum tensor T_{mn}, we need the values of ϕ_0 and ϕ_m and G_{mn} and G_{m0}. It is obvious that the potentials do not contribute to the integration of T_{mn} over the surface. After retaining the relevant terms in G_{mn} and G_{m0} which contribute to the integration in (56), we obtain

$$G_{mn}{}^{0}=g\left[\frac{s_m(d^2v_n/dt^2)-s_n(d^2v_m/dt^2)}{2c^2r},\ 0\right]+G_{mn}{}^{\text{ext}}, \quad (64)$$

$$G_{mn}{}^{\lambda}=0, \quad (65)$$

$$G_{m0}{}^{0}=g\left[-\frac{s_m}{r^3}+\frac{\dot{v}_m}{2c^2r}+\frac{s_ms_k\dot{v}_k}{2c^2r^3}+\frac{1}{8c^4}\left(-6\frac{\dot{v}_ms_k\dot{v}_k}{r}-3\frac{s_ms_k\dot{v}_ks_l\dot{v}_l}{r^3}+\frac{3s_m\dot{v}_k{}^2}{r}\right),\ -\frac{2}{3}\frac{(d^2v_m/dt^2)}{c^3}\right]+G_{m0}{}^{\text{ext}}, \quad (66)$$

$$G_{m0}{}^{\lambda}=-\tfrac{1}{2}g\lambda^2[s_m/r,\ 0]. \quad (67)$$

Substituting these expressions in (43), we obtain after some calculations

$$4\pi T_{mn}=g^2\left(\frac{s_m\dot{v}_n+s_n\dot{v}_m}{2c^2r^4}+\frac{s_ms_ns_k\dot{v}_k}{c^2r^6}\right)-\tfrac{1}{2}g^2\delta_{mn}\left(\frac{s_l\dot{v}_l}{c^2r^4}+\frac{s_l{}^2s_k\dot{v}_k}{c^2r^6}\right)-\frac{g}{r^3}(s_mG_{n0}{}^{\text{ext}}+s_nG_{m0}{}^{\text{ext}}-\delta_{mn}s_lG_{l0}{}^{\text{ext}})+\frac{g^2\lambda^2}{2r^2}\delta_{mn},\ -\frac{2g^2}{3c^3}\frac{s_m(d^2v_n/dt^2)+s_n(d^2v_m/dt^2)-\delta_{mn}s_l(d^2v_l/dt^2)}{r^3}. \quad (68)$$

It should be noted that in obtaining these expressions we have neglected the terms formed of products of even number of s_k's, since when multiplied by λ^n they vanish on integration. The evaluation of the integration for the first term in (56) gives

$$\int T_{mn}\lambda^n dS=-\frac{2}{3}\frac{g^2}{c^2}\frac{\dot{v}_m}{r}-gG_{m0}{}^{\text{ext}},\ -\frac{2}{3}\frac{g^2}{c^3}(d^2v_m/dt^2). \quad (69)$$

To calculate the second term in (56) we need, as mentioned before, only the terms of order r^{-2} and r^{-1} in G_{mn} and G_{m0}. Proceeding in a similar way, we find that

$$\frac{1}{c}\int(dT_{m0}/dt)dV=\frac{g^2}{c^2}\int_r^\infty\left(\frac{\dot{v}_m}{r^2}-\frac{1}{3}\delta_{mk}\frac{\dot{v}_k}{r^2}\right)dr,\ 0=-\frac{2}{3}\frac{g^2\dot{v}_m}{c^2r},\ 0. \quad (70)$$

We therefore finally obtain the equation of motion of the neutron in a meson field, which for the *retarded field* reduces to

$$m_0\dot{v}_m-\frac{2}{3}\frac{g^2}{c^3}\frac{d^2v_m}{dt^2}-g(\bar{G}_{m0}{}^{\lambda}+G_{m0}{}^{\text{ext}})=0, \quad (71)$$

whereas the equation of motion for the *symmetric field* is given by

$$m_0\dot{v}_m-g(\bar{G}_{m0}{}^{\lambda}+G_{m0}{}^{\text{ext}})=0, \quad (72)$$

where $\dot{\eta}_m=v_m$ and $G_{m0}{}^{\text{ext}}$ is evaluated at $x_k=0$ and at the moment t. We now remove the restriction imposed by the choice of a particular coordinate system and pass over to the usual four-dimensional representation. The equations of motion, (71) and (72), assume then the following general forms; for the retarded field

$$m_0\dot{v}_\mu-\frac{2}{3}\frac{g^2}{c^3}\frac{d^2v_\mu}{d\tau^2}+\frac{2}{3}\frac{g^2}{c^5}v_\mu\dot{v}^2+\frac{g}{c}(\bar{G}_{\mu\nu}{}^{\lambda}+G_{\mu\nu}{}^{\text{ext}})v_\nu=0, \quad (73)$$

and for symmetric field

$$m_0\dot{v}_\mu+\frac{g}{c}(\bar{G}_{\mu\nu}{}^{\lambda}+G_{\mu\nu}{}^{\text{ext}})v_\nu=0. \tag{74}$$

These are the fundamental equations of motion of a neutron in a meson field. Equation (73), with $\bar{G}_{\mu\nu}{}^{\lambda}$ given by (63), was first obtained by Bhabha and goes over to Dirac's equation for $\lambda=0$. It is to be noticed that the singularity in (69) has been removed by the singularity in (70), leaving the equation free from divergence. Equation (74), which is derived from the symmetric solution, does not contain the terms representing the reaction of the neutron's own field and passes over to the equation of Infeld and Wallace for $\lambda=0$. It is to be mentioned that the set of Eqs. (53) and (55) does not impose any new restriction upon the motion. It can be easily verified that

$$\int T_{n0}\lambda^n dS=0,$$

and

$$\int\frac{\partial\Psi_0}{\partial x_n}\lambda^n dS=-\frac{1}{c}\int(\partial T_{00}/\partial t)dV=0, \tag{75}$$

and hence the harmonic function must be taken as $\psi_0=0$.

ii. Scalar Meson Field

Proceeding similarly as in the case of a vector meson field and retaining the terms of the order of r^0 and lower, we obtain

$$\psi^0(\text{simul})=g\left[\frac{1}{r}-\frac{s_k\dot{v}_k}{2c^2r},\ -\frac{1}{2c^3}v_k\dot{v}_k\right], \tag{76}$$

and

$$F_\mu{}^0(\text{simul})=g\Bigg[-\frac{s_\mu}{r^3}+\frac{1}{2c^2}\left(\frac{s_\mu s_k\dot{v}_k}{r^3}-\frac{\dot{v}_\mu}{r}\right)-\frac{v_\mu s_k v_k}{c^2r^3}+\frac{1}{8c^4}\Bigg(\frac{12v_\mu s_k\dot{v}_k s_l v_l}{r^3}+\frac{4v_\mu}{r}(s_k(d^2v_k/dt^2)-3v_k\dot{v}_k)$$

$$+\frac{4(d^2v_\mu/dt^2)s_k v_k}{r}+\frac{6s_k\dot{v}_k\dot{v}_\mu}{r}+\frac{s_\mu}{r}(3\dot{v}_k{}^2+4v_k(d^2v_k/dt^2)-s_k(d^3v_k/dt^3))-\frac{3s_\mu s_l\dot{v}_l s_k\dot{v}_k}{r^3}$$

$$-\frac{4s_\mu s_l v_l s_k(d^2v_k/dt^2)}{r^3}\Bigg),\ +\frac{1}{3}\frac{(d^2v_\mu/dt^2)}{c^3}+\frac{2}{c^5}v_k(d^2v_k/dt^2)\dot{v}_\mu\Bigg]+F_\mu{}^{\text{ext}}. \tag{77}$$

$$F_\mu{}^{\lambda}=\tfrac{1}{2}g\lambda^2\left[\frac{s_\mu}{r}+\frac{v_\mu s_k v_k}{rc^2},\ +\frac{v_\mu}{c}\right]+\bar{F}_\mu{}^{\lambda}, \tag{78}$$

where

$$\bar{F}_\mu{}^{\lambda}=g\lambda^2 c\int_{-\infty}^{\tau'}\frac{s_\mu J_2(i\lambda s)}{s^2}d\tau. \tag{79}$$

Substituting these expressions in (50) and retaining the terms which contribute to the integrations in (56), the energy-momentum tensor is found to be

$$4\pi T_{mn}=g^2\left(\frac{s_m\dot{v}_n+s_n\dot{v}_m}{2c^2r^4}-\frac{s_m s_n s_k\dot{v}_k}{c^2r^6}\right)-\frac{g}{r^3}(s_m F_n{}^{\text{ext}}+s_n F_m{}^{\text{ext}}-\delta_{mn}s_l F_l{}^{\text{ext}}),$$

$$-\frac{g^2}{3c^3r^3}(s_m(d^2v_n/dt^2)+s_n(d^2v_m/dt^2)-\delta_{mn}s_l(d^2v_l/dt^2)), \tag{80}$$

which gives on integration

$$\int T_{mn}\lambda^n dS=\frac{g^2\dot{v}_m}{3c^2r}-gF_m{}^{\text{ext}},\ -\frac{g^2(d^2v_m/dt^2)}{3c^3}. \tag{81}$$

Similarly, we obtain

$$\frac{1}{c}\int\frac{dT_{m0}}{dt}dV=\frac{g^2}{3}\frac{\dot{v}_m}{c^2r}. \tag{82}$$

The equation of motion of the neutron in a scalar meson field is therefore:

For retarded field

$$m_0\dot{v}_m-\frac{1}{3}\frac{g^2(d^2v_m/dt^2)}{c^3}-g(\bar{F}_m{}^{\lambda}+F_m{}^{\text{ext}})=0, \quad (83)$$

and for symmetric field

$$m_0\dot{v}_m-g(\bar{F}_m{}^{\lambda}+F_m{}^{\text{ext}})=0 \quad (84)$$

or, expressed in terms of the usual four-dimensional notation, they respectively reduce to

$$m_0\dot{v}_\mu-\frac{1}{3}\frac{g^2}{c^3}\frac{d^2v_\mu}{d\tau^2}+\frac{1}{3}\frac{g^2}{c^5}v_\mu\dot{v}^2$$

$$-\frac{g}{c^2}(\bar{F}_\mu{}^{\lambda}+F_\mu{}^{\text{ext}})(c^2\delta_{\mu\nu}+v_\mu v_\nu)=0, \quad (85)$$

and

$$m_0\dot{v}_\mu-\frac{g}{c^2}(\bar{F}_\mu{}^{\lambda}+F_\mu{}^{\text{ext}})(c^2\delta_{\mu\nu}+v_\mu v_\nu)=0. \quad (86)$$

Equations (85) and (86) are the fundamental equations of the motion of the neutron in a scalar meson field. Equation (85) is practically the same as the corresponding equation of motion which has been recently derived by Harish-Chandra for the scalar meson field, provided we absorb the term proportional to acceleration in the definition of the inertial mass. It is obvious that Eq. (85) represents the simplest equation of motion of a point particle in a scalar meson field.

ACKNOWLEDGMENTS

One of us (A.S.A.) is grateful to Professor H. J. Bhabha, Director of the Tata Institute of Fundamental Research, Bombay, for kindly awarding him a scholarship to enable him to work in the University of Delhi during Professor Bhabha's absence from India. He also wishes to acknowledge his indebtedness to Professor D. S. Kothari, Dean of the Faculty of Science, University of Delhi, for allowing him the use of the facilities of the University Department of Physics.

Study of the Beta-Spectra of C^{14} and S^{35}

C. SHARP COOK, LAWRENCE M. LANGER, AND H. CLAY PRICE, JR.
Indiana University, Bloomington, Indiana

(Received May 20, 1948)

Using sources of high specific activity, the beta-spectra of C^{14} and S^{35} have been investigated in a large magnetic spectrometer. Since the distributions are measured under essentially identical conditions, a direct comparison of the data is possible. The S^{35} spectrum is in agreement with that predicted by the Fermi theory for energies from $W=1.15$ mc^2 to the end point at $W_0=1.331$ mc^2. Below this region, there is a deviation from the theory the exact nature of which is unfortunately somewhat masked by distortions due to source thickness and backing. The C^{14} spectrum has a shape which is slightly different from that which would be predicted for an allowed transition. The experimental shape is not consistent with that calculated for a second forbidden transition using Fermi selection rules. The extrapolated end point for C^{14} is at $W_0=1.306$ mc^2. From the shape of the S^{35} spectrum in the neighborhood of the end point, an upper limit is obtained for the mass of the neutrino as less than one percent the mass of the electron.

1. INTRODUCTION

THE momentum distribution of the negatrons emitted by C^{14} and S^{35} have been investigated in a magnetic spectrometer under rather favorable experimental conditions. Both of these isotopes emit beta-particles having approximately the same maximum energy and since the measurements of the spectra were accomplished under essentially identical conditions, a comparison of the results for the two elements may be made directly. The half lives are such that the 87 day S^{35} involves an allowed transition, whereas the 5100-year C^{14} is at least second forbidden.

Several experimenters[1-7] have made attempts to determine the end point energies of these transitions. The main purpose of the present investigation was to study the shape of the momentum distributions and to obtain some additional information on the influence of source thickness and backing on the experimental measurement of such low energy spectra.

Previous results[8] indicate that an allowed transition does not necessarily yield a spectrum in agreement with the Fermi theory at low energies. Furthermore, many forbidden transitions which might be expected to yield spectra quite different from the allowed shape seem to give a straight line Fermi plot over a large part of the high end of the distribution.[9]

2. EXPERIMENTAL METHOD

The spectra were investigated in a high resolution, 40-cm radius of curvature, shaped field magnetic spectrometer.[10] The large size of this instrument and the use of strategic baffles make the effects of scattering completely negligible.

The same end window G-M counter which was used for the measurements on the shape of the Cu^{64} spectra,[8] was used for the measurements on S^{35} and C^{14}. It has a very thin Zapon window capable of transmitting electrons having an energy as low as 2.0 kev. The supporting grid for the Zapon foil is of such a thickness and design that the transmission is not dependent on energy.

In order to obtain adequate intensity from a thin source, a source and detecting slit were used which were somewhat wider than those used for the Cu^{64} work. In the present investigation sources 0.5 to 1.2 cm wide were used in conjunction with a detector slit width of 0.6 cm. Because of the large value of the radius of curva-

[1] A. K. Solomon, R. G. Gould, and C. B. Anfinsen, Phys. Rev. **72**, 1097 (1947).
[2] S. Ruben and M. D. Kamen, Phys. Rev. **59**, 349 (1941).
[3] P. W. Levy, Phys. Rev. **72**, 248 (1947).
[4] M. N. Lewis and M. Paul, Phys. Rev. **73**, 1269 (1948). W. E. Stephens and M. N. Lewis, Phys. Rev. **72**, 526 (1947).
[5] W. F. Libby and D. D. Lee, Phys. Rev. **55**, 245 (1939).
[6] A. K. Saha, Proc. Nat. Inst. Sci. India, **12**, 159 (1946).
[7] M. D. Kamen, Phys. Rev. **60**, 537 (1941).
[8] C. S. Cook and L. M. Langer, Phys. Rev. **73**, 601 (1948).
[9] K. Siegbahn, Phys. Rev. **70**, 127 (1946).
[10] L. M. Langer and C. S. Cook, Rev. Sci. Inst. **19**, 257 (1948).

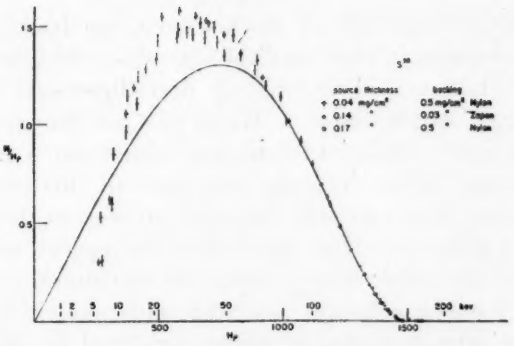

FIG. 1. Momentum distribution of the negatrons of S^{35}. The relative number per unit momentum interval is plotted as ordinate against the momentum in units of gauss-cm. The solid curve is the distribution for an allowed transition according to the Fermi theory. The experimental data have been adjusted to the same intensity at 100 kev.

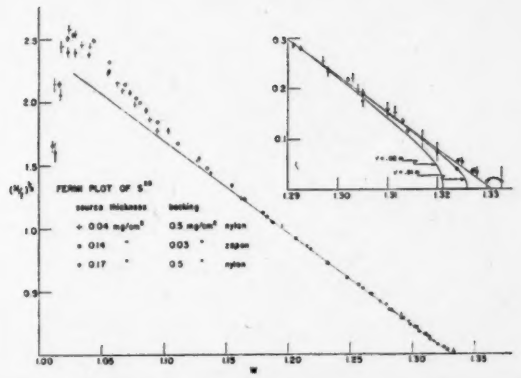

FIG. 2. Fermi plot of S^{35} negatron spectrum. The extrapolated end point is at $W_0=1.331$ mc² corresponding to a kinetic energy of 169.1 kev. The enlarged section in the vicinity of the end point shows the theoretical distribution calculated for a neutrino mass, ν, equal to zero, one percent and two percent the mass of the electron. The arrows indicate the corrections applied for finite resolution.

ture, the resolution under these conditions is still quite adequate, e.g., of the order of one percent.

Relative measurements of the magnetic field were made with a flip coil and ballistic galvanometer. The absolute calibration is in terms of the photoelectrons ejected from a Pb radiator by the 0.5108 Mev annihilation radiation of Cu^{64}. The energizing current for the magnet is stabilized electronically, and the magnetic field remained constant to better than 0.1 percent during the one and two hour runs necessitated by the low counting rates. Several ballistic galvanometer readings were taken during each run, and the calibration of the ballistic galvanometer was checked after each such deflection against a standard mutual inductance. The magnetic field was further monitored continuously by a rotating pick-up coil whose generated voltage is inductively coupled to a crystal rectifier and type K potentiometer.

3. PREPARATION OF SOURCES

Both the C^{14} and S^{35} sources were obtained by (n,γ) reactions in the pile at Oak Ridge. The C^{14} was the very high specific activity material made available by Norris and Snell.[11] For each source which was prepared, a fraction of the finely divided barium carbonate sample was suspended in a few drops of alcohol. This suspension was then diluted to seven times its original volume by the addition of distilled water. Several drops of the final suspension were then deposited on a 0.02 mg/cm² Zapon backing. The source was dried under an infra-red lamp, and the barium carbonate seemed to settle out rather uniformly over the entire area. The several sources which were used were compared by measuring the counting rate in a fixed position under a thin window monitor counter. One source was weighed in order to determine its average thickness. The average thickness of the other sources was deduced from the relative activities.

The S^{35} was obtained as NaS in a 0.1 N solution of NaOH. Since it was found that a Zapon foil would not resist the NaOH, it became necessary either to use a different backing material or to neutralize the solution. Both methods were used. Some of the sources were prepared by spreading the solution of NaS in NaOH over a 0.5 mg/cm² Nylon backing. Since this backing is considerably thicker than those usually used, it was thought desirable to investigate any effects caused by this change in the thickness of the backing. Other sources were therefore prepared by neutralizing the NaOH solution with HNO_3 and spreading on 0.03 mg/cm² Zapon. For the sulfur sources, the average thickness was calculated from the assay made at Oak Ridge and checked by weighing.

[11] L. D. Norris and A. H. Snell, Phys. Rev. **73**, 254 (1948); L. D. Norris and A. H. Snell, Bull. Am. Phys. Soc., No. 3, p. 46, April 1948.

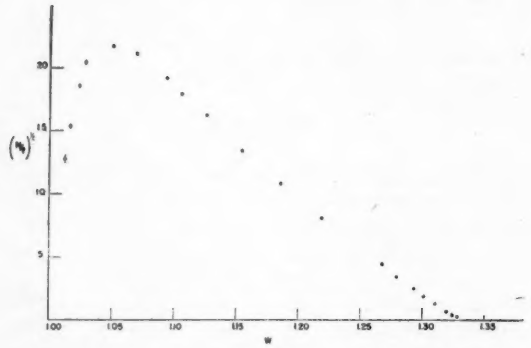

FIG. 3. Fermi plot of S^{35} spectrum for data obtained with a 0.56 mg/cm² source on a 0.5 mg/cm² Nylon backing.

4. RESULTS

The great advantage of measuring C^{14} and S^{35} under essentially identical conditions is that in this way any difference between them may be compared, and a comparison with theory takes on added significance.

The momentum distribution of the S^{35} negatrons obtained for different source thicknesses and backings is shown in Fig. 1. The curve is the distribution predicted by the Fermi theory. Fig. 2 is a Kurie plot of the experimental data. It is significant that the experimental data for all the sources are in good agreement with the theory for all energies above $W=1.15$ mc². Below this energy, the experimental points rise above the theoretical straight line and then fall rapidly for energies below about 15 kev. The deficiency at very low energies is probably due largely to the attenuation of the counter window.

It should be noted that is is possible under certain conditions of thick source and backing to completely eliminate the rise observed below $W=1.15$ mc². This effect is best illustrated in Fig. 3 which shows a Kurie plot of the data obtained with a 0.56 mg/cm² source on a 0.5 mg/cm² Nylon backing. The data, in this case, do not yield a straight line plot but instead there is a slight curvature away from the energy axis over the entire upper end of the distribution. If such a measurement were made with poor resolution and statistics, it might very well be misinterpreted as a straight line and the rise at lower energies would then not be recognized.

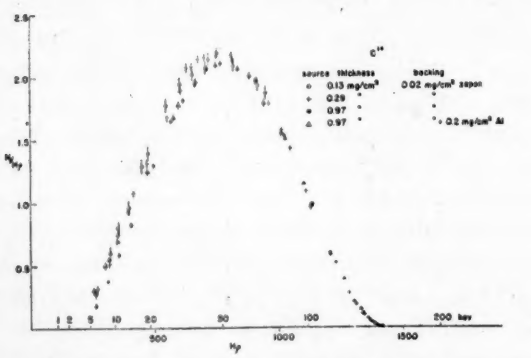

FIG. 4. Momentum distribution of the negatrons of C^{14}. The relative number per unit momentum interval is plotted as ordinate against the momentum in units of gauss-cm. The data have been adjusted to the same intensity at 90 kev.

The momentum distributions of the negatrons of C^{14} are shown in Fig. 4. The corresponding Kurie plots are shown in Fig. 5. In this case it is significant that the data from all the sources give essentially identical results for all energies above $W=1.12$ mc². In this region the Kurie plot is not a straight line but curves very slightly away from the energy axis. Since this curvature is the same for a wide variation of source thicknesses which have quite different influences at low energy, and since the sources of C^{14} were of comparable thinness and backing to those which yielded straight line plots over the same energy region for S^{35}, it is felt that this curvature in the case of C^{14} may indeed be real. One cannot, however, eliminate the possibility that this curvature may yet be caused by some unknown effect arising from the fact that the C^{14} source was prepared from a suspension whereas the S^{35} was deposited from a solution. It is quite possible that although the average thickness would indicate a "thin" source, the thickness of the individual grains may be such as to give a thick source effect.

The low energy region below $W=1.12$ mc² shows an effect caused by differences in source thickness and backing. It is seen that for the same backing, the drop in the low energy region of the Kurie plot occurs at somewhat higher energy for thicker sources. Further, for the same source thickness an increase in backing causes the fall off to occur at lower energy. This is illustrated by the solid circles and the triangles in Fig. 5. The run represented by the solid circles was taken with a source whose average thickness was 0.97 mg/cm² on a Zapon backing of 0.02 mg/cm². The run represented by the triangles

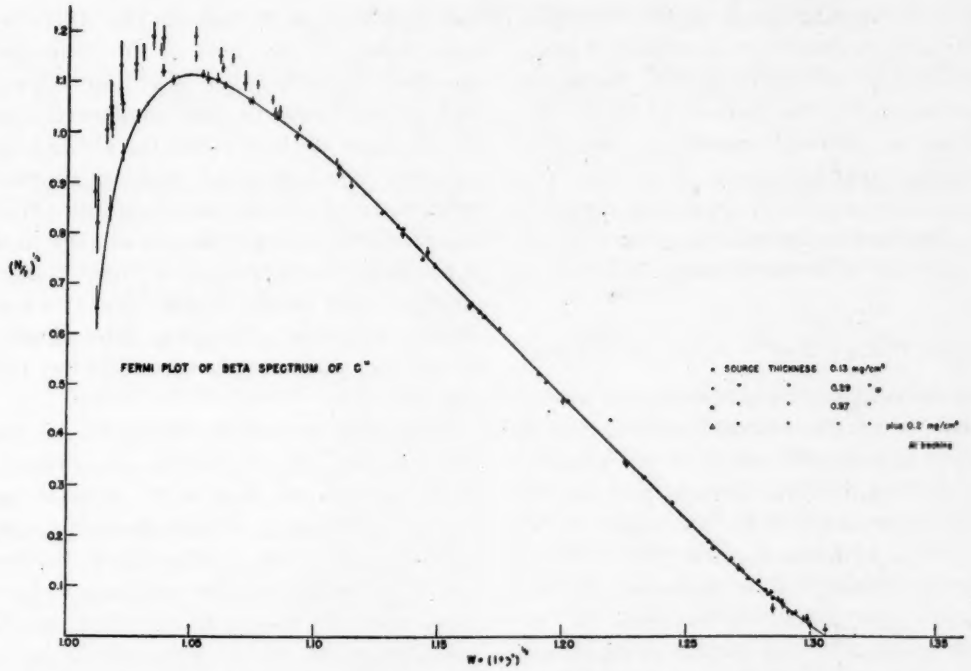

FIG. 5. Fermi plot of C^{14} negatron spectrum. The extrapolated end point is at $W_0=1.306$ mc² corresponding to a kinetic energy of 156.3 kev.

was obtained with the same source after an aluminum foil 0.18 mg/cm² had been placed in contact with the source.

The maximum energy of the negatron spectrum of S^{35} obtained by extrapolating the straight line part of the Kurie plot is $W_0=1.331$ mc². This corresponds to a kinetic energy of 169.1 ± 0.5 kev. This value is in agreement with the values recently reported by Berggren and Osborne[12] and by Solomon, Gould, and Anfinsen.[1]

For C^{14}, the end point obtained from the Kurie plot is $W_0=1.306$ mc² which corresponds to a kinetic energy of 156.3 ± 1.0 kev. This is also in agreement with the value found by Berggren and Osborne.

Because of the finite width of the source and the detecting slit, those beta particles whose momenta are in the immediate vicinity of the end point enter the detector after traversing a trajectory having a slightly different *effective* radius of curvature. Because of the high resolution employed in the present instrument, this effect is very small. The magnitude of this correction has been calculated by integrating the theoretical distribution over the width of the source and the detector slit. The theoretical allowed shape of the momentum distribution for zero neutrino mass was used for this calculation for S^{35}. The shift in the position of the last three points is indicated by the arrows on the enlarged plot in Fig. 2.

[12] J. L. Berggren and R. K. Osborne, Bull. Am. Phys. Soc. No. 3, p. 46, April 1948.

5. CONCLUSIONS

(a) Sulfur 35

As seen in Fig. 2, the S^{35} spectrum shows agreement with the Fermi theory for an allowed transition for energies above $W=1.15$ mc². Below this energy, a rise begins which is very similar to the effect observed in the spectrum of the Cu^{64} negatrons.[8] The effect involves much higher energy electrons in Cu^{64} (up to 1.37 mc²) but leaves a major portion of the energy spectrum undisturbed, just as we find in S^{35}. In the latter case, however, the real nature of the deviations from the Fermi theory is complicated by some distortion due to source thickness and backing.

The shape of the S^{35} spectrum in the vicinity of the end point can be used to set an upper limit on the rest mass of the neutrino. In Fig. 2,

the region of the distribution in the neighborhood of the end point is shown on an enlarged scale. In addition to the experimental points, calculated curves are shown for the theoretical Fermi distribution for an allowed transition calculated for an assumed neutrino mass, ν, of zero, one percent and two percent the mass of the electron. The distribution formula used here for N, the intensity in unit momentum interval, is given by:

$$Nd\eta = \text{const.} F(Z,\eta)\eta^2 K(K^2-\nu^2)^{\frac{1}{2}}(1-\nu/WK)d\eta$$

where F is the coulomb factor ($F\eta^2 \equiv f$, as used in the graphs), η is the electron momentum in units of mc, $W=(1+\eta^2)^{\frac{1}{2}}$ and K is the neutrino energy in mc^2 units. This formula includes the relativistic factor $1-\nu/WK$. The sign in this factor conforms with the form of the theory as discussed by Pruett.[13] The inclusion of this factor makes the difference between the extrapolated end point and the theoretical true end point equal to $\nu/2$. If this relativistic factor is neglected, as was done by Kofoed-Hansen,[14] this difference would be equal to ν.

The experimental points in Fig. 2 are consistent with a neutrino rest mass of zero. Within the limits of error one can certainly say that the mass of the neutrino is less than one percent the mass of the electron.

(b) Carbon 14

The C^{14} disintegration has an extremely long mean life for its energy release and is therefore classified as highly forbidden. On the other hand, recent measurements have determined the spin of C^{14} as zero.[15] This, together with the known spin, 1, of N^{14}, shows that there is only a spin change of one unit in the transition. The so-called Gamow-Teller selection rules permit such a spin change to yield an allowed transition. On the basis of these rules, the C^{14} case must be regarded as an unsolved problem together with other members of the $4n+2$ family. The Fermi selection rules permit no spin change in allowed transitions. Furthermore, if there is no parity change, they would make the C^{14} transition second forbidden, bringing into closer agreement the theoretical expectations with the observations.

Ordinarily, no unique shape can be predicted theoretically for a forbidden transition.[16] However, it turns out that in the special case of a second forbidden $0\rightarrow 1$ transition with the Fermi (polar-vector) form of interaction, the spectrum can be predicted without ambiguity. The calculation was carried out by Pruett,[17] who found a spectrum shape which, when plotted on a Kurie diagram, shows a concavity toward the energy axis, in disagreement with the present experimental observation of the spectrum. The latter, as shown above, shows a very slight convexity toward the energy axis. In comparison with the measurements on S^{35}, it would appear likely that this slight curvature in C^{14} is real.

We are grateful to Professor E. J. Konopinski for many stimulating discussions. We also wish to thank Dr. A. H. Snell and Dr. L. D. Norris for making available the high specific activity C^{14} used in these experiments.

This work is supported by a grant from the Frederick Gardner Cottrell Fund of the Research Corporation and by the U. S. Navy under Contract N6ori-48, T.O. I.

[13] J. R. Pruett, Phys. Rev. **73**, 1219 (1948).
[14] O. Kofoed-Hansen, Phys. Rev. **71**, 451 (1947).
[15] F. A. Jenkins, Phys. Rev. **73**, 639 (1948).
[16] E. J. Konopinski, Phys. Rev. **60**, 308 (1941).
[17] J. R. Pruett, private communications.

The Scattering of 2.4- to 3.5-Mev Protons by Protons

J. MORRIS BLAIR, GEORGE FREIER, EUGENE E. LAMPI, WILLIAM SLEATOR, JR., AND JOHN H. WILLIAMS
Department of Physics, University of Minnesota, Minneapolis, Minnesota

(Received June 1, 1948)

Collimated monoenergetic protons, accelerated by the Minnesota electrostatic generator to energies of 2.42, 3.04, 3.27, and 3.53 Mev, were scattered by hydrogen gas and detected at well defined angles from 8° to 45°. The observations at each angle and energy have been reduced to values of the absolute cross section for proton-proton scattering per unit solid angle. These cross sections are considered to be reliable to ±1.6 percent.

I. INTRODUCTION

THE scattering of protons by protons has been investigated extensively during the past decade. The pioneering work of Tuve, Heydenburg, and Hafstad[1] in the energy region from 600 to 900 kev served to demonstrate clearly the existence of an attractive nuclear interaction between two protons. Breit, Condon, and Present[2] showed that the observations of the elastic scattering cross section as a function of proton energy and angle of scattering could be described by a combination of Coulomb scattering and phase shifts of the spherically symmetrical S-wave. They were able to evaluate the interdependent constants for the square well potential function which determine the nuclear scattering, i.e., the radius e^2/m_0c^2, and the depth 10.66 Mev.

The exceedingly careful work of Herb, Kerst, Parkinson, and Plain[3] confirmed the early work and extended the observations up to 2.4 Mev. The results of these experiments were analyzed by Breit, Thaxton, and Eisenbud[4] who found that the dimensions of the square well representing the S-wave interaction could be given with higher precision as $r=e^2/m_0c^2$ and depth 10.50 Mev without Coulomb potential inside the well and that the data could be fitted without assuming any p-wave interaction. Wilson and Creutz[5] investigated the relative cross section for proton-proton scattering as a function of angle with 8-Mev protons. The results could be described in terms of Coulomb and S-wave scattering alone, but the accuracy was not sufficient to exclude a p-wave anomaly.

Wilson[6] next investigated the proton-proton scattering with 10-Mev protons and concluded that the interaction excluded the possibility of an attractive p-wave potential. The evidence from these experiments for a repulsive p-wave potential was not conclusive.[7]

The recent work of Wilson, Lofgren, Richardson, Wright, and Shankland[8] with 14.5-Mev protons has been interpreted by Foldy and by Lopes and Tiomno.[9] These experiments confirm the conclusion that an attractive p-wave interaction is excluded and strengthen the evidence for repulsive p-wave effects.

During the progress of the experiments reported in this paper, the results of Dearnley, Oxley, and Perry[10] with 7-Mev protons scattered through angles in the range 9° to 45° became available. These results indicate a very small deviation from pure S-wave scattering.

The present experiments were undertaken with a purpose of duplicating the highest energy of the Wisconsin group[3] and extending similar

[1] M. A. Tuve, N. P. Heydenburg, and L. R. Hafstad, Phys. Rev. **50**, 806 (1936); L. R. Hafstad, N. P. Heydenburg, and M. A. Tuve, Phys. Rev. **53**, 239 (1938); N. P. Heydenburg, L. R. Hafstad, and M. A. Tuve, Phys. Rev. **56**, 1078 (1939).

[2] G. Breit, E. U. Condon, and R. D. Present, Phys. Rev. **50**, 825 (1936).

[3] R. G. Herb, D. W. Kerst, D. B. Parkinson, and G. J. Plain, Phys. Rev. **55**, 998 (1939).

[4] G. Breit, H. M. Thaxton, and L. Eisenbud, Phys. Rev. **55**, 1018 (1939).

[5] R. R. Wilson and E. C. Creutz, Phys. Rev. **71**, 339 (1947).

[6] R. R. Wilson, Phys. Rev. **71**, 384 (1947).

[7] L. L. Foldy, Phys. Rev. **72**, 125 (1947). R. E. Peierls and M. A. Preston, Phys. Rev. **72**, 250 (1947). L. L. Foldy, Phys. Rev. **72**, 731 (1947).

[8] R. R. Wilson, E. J. Lofgren, J. R. Richardson, B. T. Wright, and R. S. Shankland, Phys. Rev. **71**, 560 (1947); Phys. Rev. **72**, 1131 (1947).

[9] J. L. Lopes and J. Tiomno, Phys. Rev. **72**, 731 (1947).

[10] I. H. Darnley, C. L. Oxley, and J. E. Perry, Jr., Phys. Rev. **72**, 169 (A) (1947). We are also indebted to these authors for a copy of their forthcoming paper in the Physical Review.

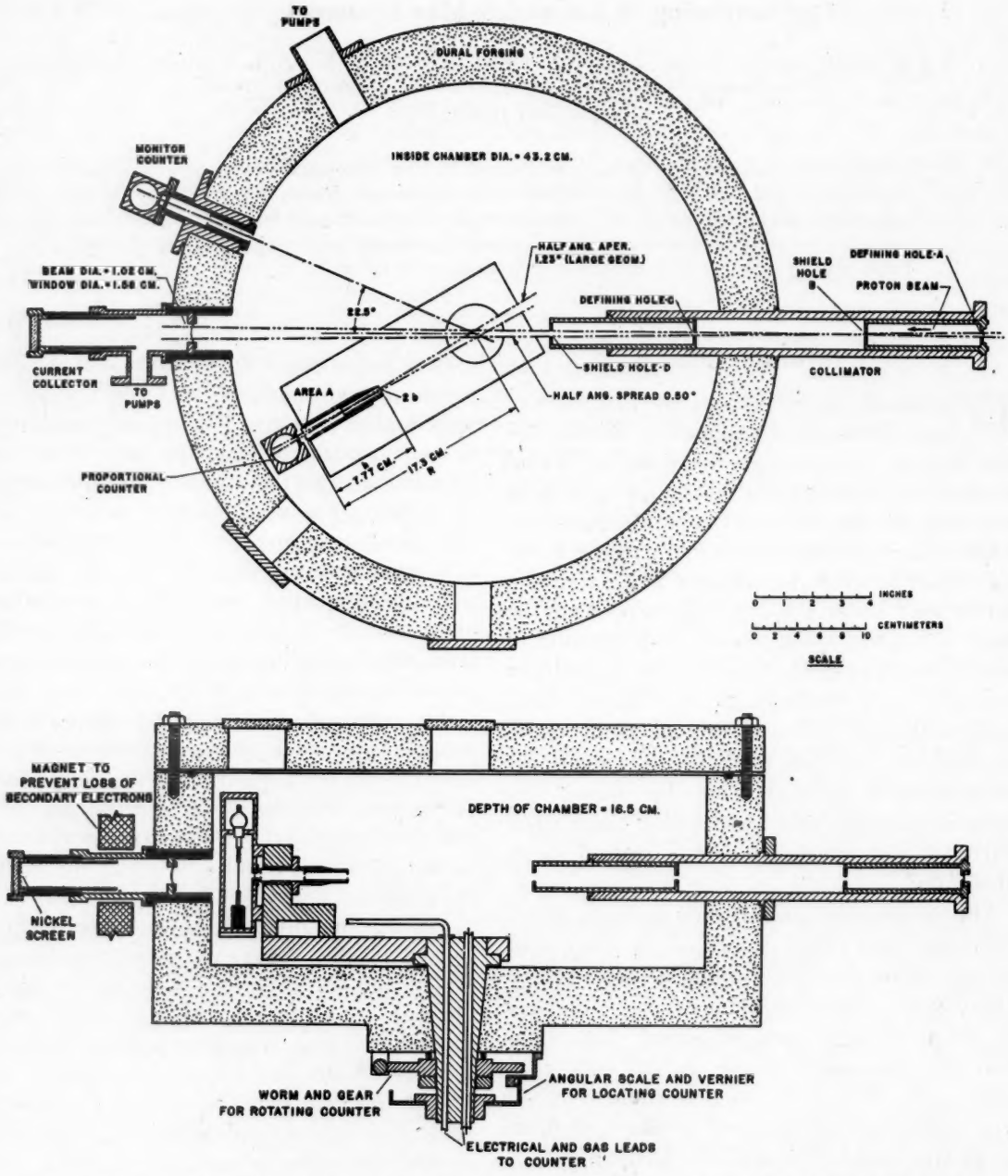

FIG. 1. Plan and elevation of the scattering chamber. Upper figure is a section through the plane of the incident beam and the beam scattered through the analyzer slits and detectors. Elevation is a section through the incident beam. The moveable analyzer slits and detector are not in the same position in the two sections.

observations to higher energies in order to establish more firmly the nature of the *S*-wave interaction. At the suggestion of Professor C. L. Critchfield, we planned to make observations of the absolute cross section for proton-proton scattering at smaller angles, 8°, than had previously been studied, because it is in this angular range that the interference of a small *P*-wave interaction with the Coulomb field would be most evident.

II. DESIGN OF SCATTERING CHAMBER

Our measurements were carried out by a method essentially the same as that of Herb,

Kerst, Parkinson, and Plain[3] (hereafter referred to as HKPP) and the apparatus was in many respects similar to that used by Sherr and coworkers for experiments on proton-deuteron scattering.[11]

The scattering chamber is shown in Fig. 1. It was turned from an aluminum alloy forging and had an outside diameter of 21 inches, walls 2 inches thick, and a depth inside of $6\frac{1}{2}$ inches. The large diameter made possible observations at smaller angles than those available in the previous experiments, and allowed small angular apertures with slits of accurately measurable size.

The beam of protons from the Van de Graaff machine entered the scattering chamber through a series of collimating diaphragms centered in a brass tube which extended radially from one side of the chamber. To reduce slit edge scattering, the diaphragms were shaped so that the edges of the holes were about 0.010 inch thick. The first defining hole, A, was 0.085 inch in diameter. The shield hole, B, 4 inches farther along, was 0.094 inch in diameter. The second defining hole, C, 9.90 inches from the first, was 0.090 inch in diameter. Five inches beyond the second defining hole was the final shield hole, D, whose diameter was 0.180 inch. This diaphragm prevented most of the protons scattered by the edge of the second defining hole from going through the chamber. The maximum spread of the beam of incident protons was 0.55 degree from the axis of the collimator.

Immediately before the incident protons reached the first defining hole they passed through a window of sheet Nylon approximately 0.0002 inch thick. When new, this window had a stopping power of 40 to 50 kev for 2-Mev protons. The stopping power of the window before and after use was measured, as explained below, and the energy of the protons corrected accordingly.

After going across the scattering chamber, the beam of protons passed through another Nylon window into the current collector cup, which is described below in the section on current measurement.

The scattering chamber could be evacuated by an oil diffusion pump and fore pump and isolated from the pumps with a large gate valve. Between the valve and the chamber there was a projecting tube which could be cooled with liquid nitrogen to trap condensable vapors. Near the trap the line from the palladium tube for filling the scattering chamber with hydrogen and the line from the oil manometer for measuring the hydrogen pressure joined the system.

The scattered protons were detected by two proportional counters. One of these, used as a monitor, was mounted on the outside of the scattering chamber with its analyzing slit system projecting through a radial hole in the chamber wall. This slit system had a half-angular aperature of 3.52° and its axis made an angle of $22\frac{1}{2}$° with the central proton beam.

The other proportional counter was mounted inside the chamber on a plate which was fastened to a tapered plug projecting through the center of the bottom of the chamber. The angular position of this counter could be adjusted by a worm and gear outside the chamber and read on a scale and vernier graduated in minutes of arc. During the construction of the chamber great care was taken to make the axis of this plug intersect and be perpendicular to the axis of the collimating diaphragms through which the protons enter the chamber.

The internal dimensions of the two proportional counters were the same, so that they could be filled simultaneously and use the same high voltage supply. The inside diameters were one inch and the wires were 0.010 inch Nichrome. The active lengths of the counters were limited to one inch by pieces of 0.028-inch diameter stainless steel tubing around the wire at each end. The entrance windows were off center by $\frac{1}{8}$ inch so that the incoming protons would not strike the central wire, and were covered with the same Nylon material used for the collimator window.

The analyzing slit system, which defined the region from which particles could be scattered into the movable counter and the solid angle subtended by the counter, consisted of a slit approximately 9.5 cm from the center of the chamber and a round hole approximately 17.3 cm from the center (marked $2b$ and area A, respectively, in Fig. 1). Between them was a larger slit to intercept particles scattered by the wall of the tube.

[11] R. Sherr, J. M. Blair, H. R. Kratz, C. L. Bailey, and R. F. Taschek, Phys. Rev. 72, 662 (1947).

The first slit was made of two pieces of Nichrome, 0.006 inch thick, with edges ground straight and smooth, which were welded to the supporting tube. The width of this slit varied by 1.5 percent from one end to the other, and the average width was $2b=0.10530\pm0.00010$ cm. Because of the great variation with angle of the counting rate of scattered particles, two different defining holes were used, the larger for measurements at angles of 15° and larger, the smaller for angles of 15° and smaller. These holes were bored in brass thimbles which could be interchanged in the supporting tube without disturbing the general line up of the analyzing slit system. The window in the proportional counter was large enough so that all particles passing through the analyzing slit system would enter the counter.

The large hole was found to vary in diameter by 0.3 percent and the average diameter was 0.2283 ± 0.0002 cm. The smaller hole varied in diameter by 1.3 percent with an average diameter of 0.07341 ± 0.00014 cm. The distance between the first slit and the hole, designated by h, was found to be 7.775 ± 0.001 cm with the small hole in place and 7.771 ± 0.001 cm with the large hole. The distance R from the hole to the center of the chamber was determined with the aid of a mandril inserted in the analyzing system and a traveling microscope. $R=17.322\pm0.002$ cm for the small hole and 17.318 ± 0.002 cm for the large hole. In the computation of the data, these dimensions are combined into a geometrical constant

$$G=2bA/Rh, \tag{1}$$

where A is the area of the final hole. G had the value $(3.2036\pm0.0007)\times10^{-5}$ cm when the large hole was used and $(3.3094\pm0.0008)\times10^{-6}$ cm for the small hole. For the monitor counter $G=1.4\times10^{-4}$ cm.

During the assembly of the scattering chamber the bracket supporting the movable proportional counter and the analyzing slit system was shimmed up so that the axis of this slit system intersected the axis of the beam collimator diaphragms to within ±0.005 inch and that of the tapered plug to within ±0.002 inch. This was checked with micrometers and dial gauges and with the aid of a removable pin which could be fitted into a socket in the center of the tapered plug. The accuracy of this centering was checked by revolving the plug while the top of the pin was viewed with a microscope.

These alignments, as well as the zero reading on the scale for measuring the angular position of the movable counter, were further checked by using the collimating and analyzing slit systems to define beams of light which would intersect each other and the end of the removable pin at the center of the chamber. At the center of the chamber the beam of protons was 0.230 inch in diameter, while the regions from which scattered particles could pass through the analyzer and reach the counter were 0.270 and 0.340 inch high when the large and small holes, respectively, were in the analyzer. This assured that every point in the defining hole of the analyzer could "see" all of the proton beam.

III. THE CHARGE MEASURING SYSTEM

To permit accurate measurement of the number of protons which traversed the scattering volume, the collimated beam passed out of the chamber through a Nylon window into an evacuated region and was collected in an insulated cup. The window support and outer case of the evacuated region were also insulated from the scattering chamber so that checks on the efficiency of current collection, production of secondary electrons, ionization currents, etc., could be made. The window diameter was 0.625 inch while the diameter of the proton beam at that point, as determined by the diaphragms in the collimator tube, was 0.40 inch. Calculations showed that the fraction of the beam scattered by the gas beyond the edge of the window was negligible. The checks on the efficiency of current collection were similar to those made on the Los Alamos chamber.[11] As in that case, it was found that a magnetic field across the end of the current collecting cup of approximately 300 gauss was sufficient to prevent secondary electrons from entering or leaving the cup. The potential between the collector cup and the case, to which the Nylon window was sealed, could be varied over a 60-volt range without causing more than 10^{-11} ampere to flow between the cup and the case. During a run the collector cup was not allowed to charge to more than ten volts. While data were being taken, the region around

the collector cup was connected to the oil diffusion pump so that the pressure was approximately 3×10^{-6} mm of Hg. It was found that increasing this pressure to 10^{-5} mm Hg did not cause an appreciable ionization current to flow between the cup and the case. As a result of these tests we concluded that errors in collecting the proton current amounted to less than one-tenth of one percent.

The total number of incident protons in a given observation was determined by allowing the collector cup and a 0.5-μf condenser to build up to a potential of less than ten volts and then discharging this capacitance through a ballistic galvanometer. The calibration of this system was accomplished by two methods. First the system was compared to two "standard" condensers by charging them separately to a potential of 10.50 volts, as determined by a Wolff potentiometer, and discharging them through the ballistic galvanometer.

Since we were not completely confident of the capacitance of these standard condensers, an alternative calibration method was used which simulated the operating conditions more closely. A current of the order of 10^{-7} ampere, supplied by a 2000-volt battery pack and a series resistance of 2×10^{10} ohms, was allowed to flow on to the collector cup condenser system. The exact value of this current was measured by a galvanometer connected between the series resistance and the condenser. Various battery voltages and times of charging were used to determine the constancy of the charge measuring system to make sure the calibration was independent of these factors.

The calibration procedure was as follows. The current was allowed to flow for a given time and read at frequent intervals, the charging circuit was opened, and the ballistic galvanometer was then shorted across the condenser and its deflection recorded. The current galvanometer was then switched into a calibration circuit consisting of a standard one-megohm resistance (several standards intercompared) and a low resistance type K Leeds and Northrup potentiometer used as the source of a known voltage. The potentiometer was adjusted to give galvanometer readings equal to the initial and final deflection when charging the condenser. In this way, the average current used in the condenser charging cycle was determined.

In such calibrations and in the actual employment of a condenser system, extreme care must be taken to avoid effects due to "charge soakage" and leakage resistance. The first effect was minimized during our early scattering observations by removing charge from the previously shorted condenser by carrying the condenser through a "hysteresis cycle" of diminishing amplitude with a six-volt, 60-cycle voltage supply whose output potential was gradually reduced to zero. In later work, a polystyrene condenser* of admirable soakage and leakage properties eliminated most of these uncertainties. In either case the "current-time" method of calibration simulated the operating conditions so closely that errors due to faulty condenser properties were largely eliminated. Other sources of error in this method, such as leakage of charge to ground from the galvanometer in the calibrating circuit, resistance leakage of the condenser, lag of calibrating galvanometer readings behind true current during time of charging, and non-linearity of ballistic galvanometer readings were considered, and minor corrections were applied.

Unfortunately, the two methods of calibrating the charge measuring system gave results which differed by one percent. We attributed this difference principally to a difference between the conditions under which we used the standard condensers and those under which they were calibrated. Therefore, we have based our calibration on the "current-time" method and have estimated a probable error from this cause in the measured cross section of ±1 percent.

IV. MEASUREMENT OF PROTON ENERGY

The voltage of the modified Minnesota electrostatic generator[12] was measured and controlled by means of an electrostatic analyzer of the type described by Hanson.[13] The $Li^7(p,n)Be^7$ reaction threshold was used as a reference point for the calibration of this instrument. Considering recent measurements at Wisconsin,[14] we have taken the threshold of this reaction to be the value 1.883 Mev given by Hanson and Benedict.[15] For con-

* John E. Fast Company, Chicago, Illinois.

[12] J. H. Williams, L. H. Rumbaugh, and J. T. Tate, Rev. Sci. Inst. **13**, 202 (1942).

[13] A. O. Hanson, Rev. Sci. Inst. **15**, 57 (1944).

[14] R. G. Herb, Bull. Am. Phys. Soc. **23**, No. 4, p. 7 (1948).

[15] A. O. Hanson and D. L. Benedict, Phys. Rev. **65**, 33 (1944).

venience in such calibrations and for measuring the thickness of the foil over the entrance to the collimator tube, a nickel screen onto which some LiF had been melted was mounted on an arm which could be turned into position by means of a tapered plug which entered the scattering chamber through the center of the lid. Below the scattering chamber, in line with the axis of the proton beam, there was placed a paraffin-covered BF_3 proportional counter for detecting the neutrons produced in the calibration measurements.

At generator voltages below the threshold for the Li(p,n) reaction the number of counts from the neutron detector was negligible and the rise upon reaching the threshold was sharp and reproducible to one part in five hundred. To calibrate the electrostatic analyzer, a threshold measurement was made with no foil over the collimator. Measurements were also made with a clean piece of Nylon in place and with one which had been used for some time. During use, a layer of carbon collects on such foils, increasing their stopping power.

The energy loss of the protons in traversing the window was obtained from the displacement of the curve for yield of neutrons *vs.* generator voltage taken with a foil in place as compared with the curve taken with no foil. With a foil in place, there was a noticeable tail on the low voltage end of the yield curve indicating a spread in energy of the protons passing through the foil. This variation is included in the energy uncertainty in the tabulated data. The increase in stopping power of the foils was assumed linear with generator running time, and the proton energies were corrected accordingly.

V. DETECTION OF SCATTERED PROTONS

The two proportional counters used to count scattered protons were sufficiently alike so that a common high voltage supply and gas filling could be used. The center wires were held at a potential of about +900 volts with respect to the counter bodies. The gas used was a mixture of argon at 14.5 cm Hg pressure and CH_4 at 0.2 cm Hg pressure. The counter gas was separated from the scattering gas by a Nylon foil of the same thickness as on the other windows. The electrical pulses were taken from the high voltage leads and passed through preamplifiers and amplifiers similar to the Los Alamos type 100 circuits. The pulses were counted by scaling circuits described by Higinbotham, Gallagher, and Sands.[16]

The discriminator bias curves of the counters operated under these conditions had broad, flat plateaus. To check the operation of the movable counter while data were being taken, two identical scale-of-64 circuits were used, one being operated with its discriminator bias set 50 percent higher than the other. Any discrepancy in the number of counts recorded by the two scalers indicated an undesirable variation in the operating conditions so that run would be discarded.

VI. HYDROGEN SUPPLY AND PRESSURE MEASUREMENTS

Before admitting hydrogen to the scattering chamber, it was evacuated with an oil diffusion pump to a pressure of approximately 5×10^{-6} mm Hg. The hydrogen was admitted to the chamber through a heated palladium tube. The pressure of hydrogen in the scattering chamber was measured with a manometer filled with Apiezon oil B. The difference in level between the two sides of the manometer was measured with a cathetometer which could be read to one-hundredth of a millimeter. Measurements were made with a modified Mohr's balance of the density of this manometer oil as a function of temperature. The specific gravity was found to be 0.862 ± 0.001 g/cm^3 at 20°C and the volume coefficient of expansion was found to have the value 83×10^{-5} per degree centigrade.

VII. PROCEDURE

Except for second-order effects, the cross section per unit solid angle for proton-proton scattering is given by

$$\sigma = Y \sin\theta / NnG, \qquad (2)$$

where Y is the number of scattered protons detected by the proportional counter when N protons of energy Ep are incident on $(n/2)$ molecules/cm^3 of hydrogen gas and the detected protons are scattered through a laboratory angle θ. The factor $G=2bA/Rh$ is a measure of the gas scattering volume and solid angle defined by the entrance slits and final aperture of the analyzing system between the scattering volume

[16] W. A. Higinbotham, J. Gallagher, and M. Sands, Rev. Sci. Inst. 18, 706 (1947).

and the counter, and has been described earlier in this report, Eq. (1).

The ratio Y/N was determined by counting the number of scattered protons which entered the slit system and passed through the aperture of area A into the proportional counter during a run of two to five minutes while a charge Q was collected on a condenser attached to the collector cup. Q was determined with the calibrated ballistic galvanometer and could be translated into a value for N with the assumed value of 6.250×10^{12} protons per microcoulomb.

The number of scattering protons per cm^3, n, was determined from the pressure of molecular hydrogen in the scattering chamber as measured by the oil manometer described above and by assuming 6.023×10^{23} molecules in 22,412 cm^3 at normal temperature and pressure.

Any asymmetry of the incident beam and of the analyzing slit system with respect to the central axis of rotation of the detector, and the consequent uncertainty in θ and R, were essentially eliminated by taking observations of Y at approximately equal angles on either side of the experimentally determined zero. This zero was known only to within an accuracy of two or three minutes of arc, but the total included angle, 2θ, between observing positions on the two sides was known to an accuracy limited principally by the accuracy of reading a vernier with graduations of one minute. The absolute angles in the range 8° to 15° were checked by careful triangulation measurements and were found to agree with those read on the scale to within 0.5 minute.

Observations of Y and Q at the two angles $\pm\theta$ were taken for a measured n and a G which was appropriate to the θ under examination. Records were kept of the time of run, time elapsed since filling the chamber with H_2, and the number of protons which entered the monitor counter at $22\frac{1}{2}°$. In general, at least ten thousand scattered protons were observed for each angle at each energy. The counting rates were such that this required several independent sets of observations of Y, Q, and θ, and served to eliminate gross errors of observation.

The observations of Y had to be corrected for a sum of minor background counts. These arose from the following causes and were directly measured and subtracted. With the shutter above the entrance window to the scattering chamber closed, the number of counts per minute due to generator instabilities, alpha-contamination, counter discharges, amplifier noise, etc., was measured. This contribution was, in general, less than 0.1 percent of Y. With the chamber evacuated and cut off from the pumps so that gas contamination could build up, the number of protons scattered from the contaminating gases at each energy was followed as a function of θ for an hour or more. This contribution to Y was kept less than one percent in scattering runs by evacuating and refilling the scattering chamber from fresh H_2 at appropriate intervals.

A small correction, 0.2 percent, was applied to our observations of Y/Q to allow for switching delays in removing the shutter from the beam before turning on the scaling circuits which record Y, and in stopping the recording of Y before the protons were cut off from entering the collector cup.

Other sources of extra and missed counts have been investigated. Since the path through the scattering gas traversed by the primary protons from the collimating apertures to the collector cup is 12.6 inches, and the path of the scattered protons from the center of the chamber to the counter window is 7.07 inches, a possibility of double scattering difficulties exists. In order to evaluate these effects, we have measured the cross section for scattering of 3-Mev protons at 8° as a function of the H_2 pressure in the scattering chamber. Any part of the yield due to double scattering would be expected to depend on the square of the pressure. Changes in pressure by a factor of four are seen from Fig. 2 to produce no appreciable change in the value of the cross section determined under the usual conditions of 16 cm of oil pressure. In fact, the negative

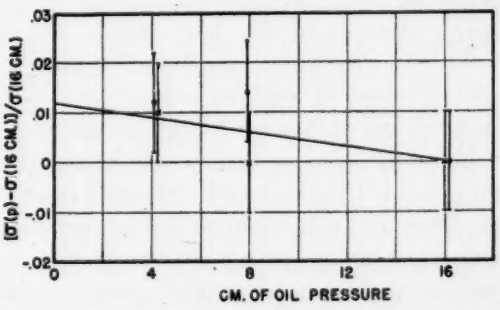

FIG. 2. The fractional change in the measured cross section for scattering through 8° of 2.42-Mev protons as a function of the pressure, p, of the hydrogen filling the scattering chamber.

TABLE I. Proton-proton scattering cross section per unit solid angle in the laboratory system as a function of incident proton energy E_p in Mev and laboratory angle θ. Cross sections are in barns (10^{-24} cm^2).

θ \ E_p	2.42±0.02	3.04±0.02	3.27±0.02	3.53±0.02
8°	7.770±0.100	4.930±0.070	4.390±0.050	3.700±0.060
10°	3.050±0.040	1.990±0.020	1.770±0.020	1.530±0.030
12.5°	1.340±0.020	0.963±0.014	0.864±0.012	0.773±0.012
15°	0.796±0.008	0.626±0.008	0.600±0.005	0.550±0.008
17.5°	0.628±0.007	0.537±0.005	0.512±0.006	0.473±0.005
20°	0.562±0.004	0.493±0.005	0.478±0.006	0.462±0.005
25°	0.528±0.006	0.483±0.006	0.473±0.005	0.442±0.005
30°	0.528±0.010	0.469±0.009	0.450±0.005	0.428±0.005
35°	0.503±0.010	0.450±0.005	0.441±0.005	0.418±0.004
40°	0.475±0.008	0.425±0.008	0.410±0.005	0.397±0.004
45°	0.443±0.006	0.402±0.005	0.380±0.004	0.366±0.004

slope $d\sigma/dp$ is contrary to expectations and is probably not significant.

The scattering of primary protons by the collimating diaphragms directly into the analyzing system and counter was observed by allowing the beam to pass through the evacuated chamber. The detector system could be set down to angles of less than 7° before protons scattered from the slits entered the detector.

A possible contribution to Y could arise from the scattering of protons by the finite thickness, 0.006 inch, of Nichrome metal forming the two sets of slits in the analyzer. In order to measure this, we replaced these slits with special slits made of 0.025-inch Nichrome. A series of observations of the cross section for scattering of 2.4 Mev protons at 8° with these thick slits agreed to within 1½ percent with the average value of the cross sections obtained with 0.006-inch thick slits. Since this is well within the expected reproducibility of independent sets of data, we concluded that contributions from scattering by the 0.006-inch slits were negligible.

We were aware of the difficulties of alignment of a collimating system of the type used in these experiments and, consequently, made several complete changes of the final collimating slit assembly. In particular, the barrel which held the slit of width $2b$ and the hole of area A was changed to one of increased internal diameter to test the possibilities of surface scattering which might possibly have existed in our early observations. None of these changes led to significant differences in the measured cross sections.

One of the disturbing discrepancies which exists in our observations is the disagreement between the values of σ at $\theta=15°$ taken with the two values of G. The larger apertures used in the range 15° to 45° give a more reliable value of $\sigma(15°)$ from a statistical point of view, and we have given these values more weight in arriving at the values listed in Table I. The values for $\sigma(15°)$ at various energies for two values of G, which differ by an order of magnitude, are shown in Table II. There is no significant evidence indicating an error in the relative G values, but the differences in $\sigma(15°)$ between the two experimental conditions certainly exceed the differences expected on the basis of the reproducibility of the data. A partial explanation may be that the values of E_p were not exactly the same under both conditions of observation.

VIII. RESULTS

Values of σ, the cross section per unit solid angle for protons of energy E_p scattered at the laboratory angles θ, are given in Table I. The uncertainties shown for the values of σ in this table were determined by the reproducibility of values of σ from week to week. The uncertainties given for the values of E_p are estimates of our lack of knowledge of the beam energy at the center of the scattering chamber due to the non-uniformity of Nylon windows, lack of information on the exact amount of carbon deposited on these windows at the time of the observation, and fluctuations in the accelerating potential. The non-uniformity of the windows makes it difficult to specify E_p exactly, and we have chosen to give a value of E_p which is a minimum value. From the appearance of the Li(p,n) threshold curves taken with the protons passing through typical Nylon foils, we judge that approximately ten percent of the protons may have had energies as much as 10 kev greater than the value listed. Values for the cross section per unit solid angle in the center of mass system have been calculated by multiplying the values given in Table I by ¼ sec. θ. These center of mass cross sections are plotted as a function of $\Theta=2\theta$ in Fig. 3.

In addition to the experimental uncertainties described in the previous paragraph, there are inherent errors in measuring N, n, and G. We estimate as discussed previously that the probable error in these factors is 1.0, 0.2, and 0.25 percent, respectively. The combined probable error of the cross sections as read from a smooth

curve drawn through the points in Fig. 3 is therefore thought to be ±1.6 percent.

The values shown in Table I for σ have been corrected for second-order geometry effects due to the finite solid angles subtended by the detector system and to the spread of the incident beam of protons. These calculations have been made by Professor C. L. Critchfield and are similar to, but more complete, than those discussed by Breit, Thaxton, and Eisenbud.[4] The percentage correction by which the observed σ's calculated from Eq. (2) are reduced is, of course, a function of E_p, θ, and G and is, at most, about two percent at 8° and is negligible above 30°.

In addition to the data shown in Table I and Fig. 3, we have made less careful measurements of the cross sections at 8° and 10° for protons of energy, 2.05, 1.76, 1.32, 1.12, and 0.915 Mev. These results serve to extend the observations of HKPP to smaller angles than the minimum value of 15° used in their experiments. These low energy results have been compared to those of HKPP by interpolating the value of K_0, the phase shift of the S-wave, from the phase shift values calculated by Breit, Thaxton, and Eisenbud. This interpolation was necessary because our values of E_p did not agree exactly with those used by HKPP. Our results are in excellent agreement with those expected from an extension of the HKPP observations.

At 2.42±0.02 Mev our measurements can be directly compared to those of HKPP, whose highest energy was given as 2.392 Mev. There is reason to believe[14] that this energy, on the new voltage scale, should be interpreted as 2.42 Mev. The surprising agreement to within ⅓ of one percent between our observations in the angular region from 15° to 45° and those of HKPP is probably fortuitous since neither set of data is thought to be accurate to better than one percent.

The interpretation of the data presented here is being undertaken by Professor C. L. Critchfield and will appear in a later publication. These experiments confirm and extend the earlier data on proton-proton scattering in the energy region where S-wave nuclear interaction is preponderant. It is expected that an analysis of the results will increase our knowledge of the range and strength of the proton-proton interaction.

TABLE II. Experimental results of the cross section for scattering through 15° per unit solid angle, in barns, at different values of incident proton energy, E_p in Mev, for the two analyzing slit geometries described in the text.

E_p	2.42	3.04	3.27	3.53
Small	0.788±0.008	0.638±0.008	0.600±0.005	0.560±0.009
Large	0.802±0.008	0.618±0.005	0.600±0.005	0.544±0.005

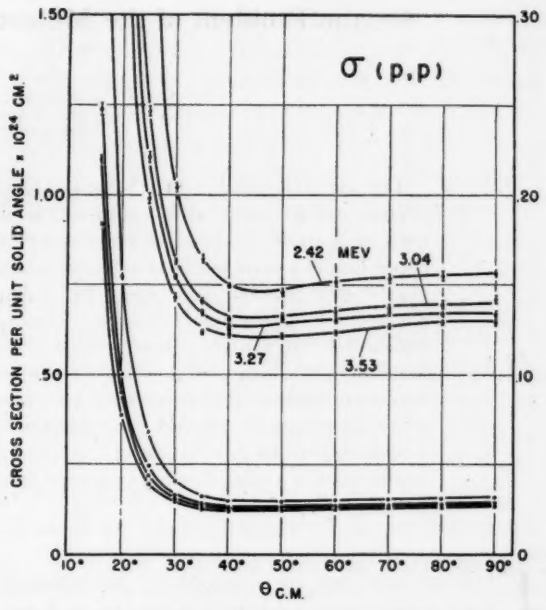

FIG. 3. The cross section per unit solid angle in the center of mass system of coordinates as a function of angle, with parameters of incident proton energy in the laboratory system. The lower curves are to the vertical scale shown on the left. The upper curves are to the scale shown on the right.

ACKNOWLEDGMENTS

We are pleased to express our thanks to Professor C. L. Critchfield for the many stimulating discussions of this problem. Calculations have been made by Professor Critchfield and Mr. Donald C. Dodder which have helped to guide the course of this investigation. Mr. Rudolph Thorness made significant contributions to the design of the scattering chamber.

This research was done under the partial support of the Office of Naval Research, Contract N5ori-147. It was also materially assisted by the University of Minnesota Technical Research Fund subscribed to by General Mills, Inc., Minneapolis Honeywell Regulator Company, Minneapolis Star Journal and Tribune Company, Minnesota Mining and Manufacturing Company, and Northern States Power Company.

PHYSICAL REVIEW VOLUME 74, NUMBER 5 SEPTEMBER 1, 1948

On the Problem of the Molecular Theory of Superconductivity*

F. LONDON
Duke University, Durham, North Carolina
(Received April 25, 1948)

The electrodynamics and thermodynamics of the superconducting state entail quite definite consequences with regard to the stability character of the supercurrents. In contrast to a recent attempt of Heisenberg, superconductivity is characterized in the present paper not as a state of electronic lattice order in ordinary space, but rather as a kind of condensed state in momentum space which implies a long-range order of the momentum vector $p=mv+(e/c)A$ in ordinary space as a consequence of the requirements of quantum kinematics. Indications are that it is most probably the exchange interaction associated with the Coulombian field which is responsible for this condensation in momentum space. Ferromagnetism and superconductivity thus would play the role of two opposite limiting cases of the same effect depending on whether the exchange interaction, competing with the zero-point energy, promotes parallel orientation of the electronic spins or a coordination of the translational momentum in a state of vanishing total spin.

THE appearance of a paper by Heisenberg[1] on superconductivity gives me a welcome occasion to publish a few remarks concerning some related ideas I have nourished for several years but had thought to withhold until I could make a well substantiated contribution to this subject. Since Heisenberg now employs the same interactions that I had in mind but arrives at an entirely different mechanism which, moreover, in my opinion, does not yield superconductivity, it might perhaps be justifiable and even of interest if I briefly develop my viewpoint. Of course, I am quite aware of the necessarily sketchy character of such a discussion.

I. HEISENBERG'S SUPERLATTICE THEORY

Heisenberg's attempt is admittedly not to be considered as a definite solution of the apparently very difficult problem of a molecular theory of superconductivity. He lays stress upon expressing his intention by saying that he wishes to point out a peculiar feature which perhaps characterizes the place in the theory of metals where one might look for an explanation of this phenomenon.

Heisenberg considers—and in this respect we agree with him—the *Coulomb interaction of the electrons* as essential for the establishment of the superconducting state. He assumes the first-order perturbation caused by this interaction to disappear since it is given by the mean value of the interaction potential taken over the unperturbed system, and this mean value disappears if the metal is supposed to be electrically neutral. Accordingly, only the second-order perturbation is regarded as important. It is given by the well-known expression of quantum mechanics:

$$W_2=-\sum_r{}'|H_{0r}|^2/(E_r-E_0). \tag{1}$$

Here H_{0r} is the transition element of the perturbation matrix between the state 0 and the state r and E_0 and E_r the corresponding unperturbed energy values. For two electrons, 1 and 2, of the momenta p_k and p_l in the state 0 and p_m and p_n in the state r the perturbation matrix has the form:

$$\begin{aligned}H_{0r}=(e^2/V^2)\int\int(1/|r_1-r_2|&\\ \times\exp\{(2\pi i/h)[(p_m-p_k)r_1&\\ +(p_n-p_l)r_2]\}d\tau_1 d\tau_2&\qquad(1')\\ =(4\pi h^2e^2/V|p_n-p_l|^2)\delta(p_k+p_l-p_m-p_n),&\end{aligned}$$

where

$$\delta(p)=\begin{cases}1 & \text{for } p=0,\\ 0 & \text{for } p\neq 0.\end{cases}$$

Here we can no longer agree with Heisenberg. The undisturbed state is highly degenerate as a result of the spin and the identity of the electrons. Consequently there might be a first-order effect in spite of the system's being neutral. On the basis of his argument Heisenberg would entirely invalidate his own well-known

* The work reported here was carried out under contract N7onr-455 with the Office of Naval Research.
[1] W. Heisenberg, Zeits. f. Naturkunde **2a**, 185 (1947).

theory of ferromagnetism,[2] since this theory is essentially based on a *first*-order Coulombian perturbation effect in neutral systems, the so-called exchange effect.

Let us, however, first follow Heisenberg's reasoning to its conclusion. A second-order effect is generally due to a perturbation of the eigenfunctions and thus it is surmised that the plane waves of the ordinary theory of metals may not be a suitable starting point. Particularly the states near the surface of the Fermi lake might be greatly disturbed by the presence of the Coulomb interaction. Consequently, it appears preferable to abandon the perturbation method and to start with more suitable wave functions on the basis of the variation method. Heisenberg considers monoelectronic functions in momentum space of the type

$$\psi(p,\vartheta)=\exp[\alpha(\cos\vartheta-1)-\beta(p-P)], \quad (2)$$

where α and β are the parameters to be determined by the minimum principle, P = the limiting momentum of the Fermi distribution, p, ϑ = polar coordinates in momentum space. By this form for the wave function he anticipates a certain range, β^{-1}, of the momentum distribution. This has the consequence that, in ordinary space, he obtains *wave packets* of the *finite* extension βh instead of the usual plane waves of infinite extension in space.

The result is that these localizable wave packets would be arranged best in a kind of space lattice similar to an earlier attempt of Kronig.[3] One may think of a lattice like the *CsCl*-type in which the electrons of opposite spin correspond to the two kinds of ions (see reference 1, Section 2C).

The decisive question is, of course: Why should such a superstructure of electrons, which in itself may appear quite plausible, entail superconductivity? Heisenberg gives an estimate of the different energy contributions in this superstructure from which he infers (reference 1, Eqs. (62), (63), and (64)) that within a certain temperature range $T_1<T<T_0$ an ordered state with a current would be the thermodynamically most stable one, where T_0 is the transition temperature of the superconductor. But for the *lowest temperatures*, $0<T<T_1$, *he obtains a ground state without currents*. He suggests that even at these lowest temperatures, for which a state without macroscopic current is the thermodynamically most stable one, the presence of a "crystal germ" could give rise to a great number of elementary "current threads" of a fixed current strength and direction playing a role similar to that of the Weiss' domains in the theory of ferromagnetism. Normally these threads would be distributed at random and would not give rise to a macroscopic current. But if these current threads could "freeze out" and form a monocrystal, this system might be unable to rid itself of its macrocurrent by collisions with the lattice of the ions. Apparently in virtue of interactions which are not yet explicitly introduced in the theory (surface effects) it is thought that a macrocurrent might be stable or rather metastable after all.

Heisenberg claims that from this basis he can derive an equation of the type:[4]

$$(\partial/\partial t)(\Lambda j_s)=E, \quad (3)$$

(reference 1, Eq. (71)) where j_s is the density of the macroscopic supercurrent, E is the electric field strength, and Λ a coefficient characteristic of the superconductor. I have not been able to follow Heisenberg's deduction here. But for the sake of argument let us assume that Eq. (3) can be derived on this basis. In fact an equation of this type has been proposed[5] several times as basis of a macroscopic electrodynamics of superconductivity in the sense of describing *infinite conductivity*. But after the so-called Meissner-Ochsenfeld effect[6] had been discovered it became clear that the assumption of Eq. (3) leads to a great number of current distributions which cannot be realized within superconductors and that one has to introduce a *supplementary restriction* in order to obtain only the currents which actually exist. This restriction can be

[2] W. Heisenberg, Zeits. f. Physik **49**, 619 (1928); see also F. Bloch, Zeits. f. Physik **57**, 545 (1929).

[3] R. de Lar Kronig, Zeits. f. Phvsik **78**, 744 (1932); **80**, 203 (1932).

[4] Actually Heisenberg obtains an equation somewhat more complicated than (3) (reference 1, Eqs. (70) and (71)) but for the subsequent discussion this is not essential.

[5] B. L. De Haas-Lorentz, Physica **5**, 384 (1925); R. Becker, G. Sauter, and F. Heller, Zeits. f. Physik **85**, 772 (1933).

[6] W. Meissner and R. Ochsenfeld, Naturwiss. **21**, 787 (1933).

written in the form of the following equation:[7]

$$\text{curl}(\Lambda j_s) = -B/c. \tag{4}$$

Heisenberg infers Eq. (4) from Eq. (3) by a purely thermodynamical consideration (reference 1, Section 4b). This proof is, however, dependent on the *assumption* that here one has to deal with a thermodynamical equilibrium state. But this is precisely the assumption which appears not *a priori* justifiable if one considers, as Heisenberg does, superconductivity as the outcome of a "freezing-out" process. Indeed, from Eq. (3) and from Maxwell's $\text{curl}E = -\dot{B}/c$ one infers, taking the curl on both sides of (3), that:

$$(\partial/\partial t)(\text{curl}\Lambda j_s + B/c) = 0, \tag{5}$$

or integrating with respect to time:

$$\text{curl}\Lambda j_s = (B_0 - B)/c. \tag{5'}$$

Here B_0 is an arbitrary time independent vector field playing the role of a frozen-in magnetic field, entirely in disagreement with the experimental finding of Meissner and Ochsenfeld, though quite in line with the concept of an infinite conductivity implying the existence of *undercooled* states. Assuming the equation $B_0 = 0$ or Eq. (4) would go beyond the contents of (3); this cannot be inferred on merely thermodynamical grounds, at least not in a case in which one has all reason *not* to accept without proof, the realization of true thermodynamical equilibrium.

Actually, Eq. (4) accounts for a fact which is not yet implied by (3), namely that superconductors are not only *ideal conductors* ($j_s \neq 0$, $E = 0$), but, moreover, *ideal diamagnetics* ($H \neq 0$, $B_0 = 0$). The latter property is not a consequence of the former, nor is the former a consequence of the latter.

We will not expatiate upon the strange feature that according to Heisenberg's theory one would have to distinguish between two temperature intervals ($0 < T < T_1$) and ($T_1 < T < T_0$) of entirely different stability character within the superconducting state ($0 < T < T_0$). While nothing is known which would indicate the existence of such a characteristic temperature T_1, one could perhaps say that T_1 might be lower than all temperatures reached so far.** Thus one may assume that actually one has to deal only with the upper one of the two intervals ($T_1 < T < T_0$).

Turning now to the case $T_1 < T < T_0$ we believe that a state endowed with a current, as the thermodynamically stable one within this temperature interval (reference 1, Eqs. (62), (63), and (64)), would not furnish a satisfactory description of superconductivity as we know it today.

Heisenberg thinks of an *asymmetric distribution* in momentum space, the asymmetry depending on the direction of the current (reference 1, Eq. (58)). That such a model would not be compatible with the facts can be seen readily if one realizes that it would again entail a great number of equivalent equilibrium states which are actually not realized in nature. For instance, an isolated superconducting sphere in thermal equilibrium is free of any current as long as no external field is applied, whereas from Heisenberg's model one would infer that a state with spontaneous current should be stable even in absence of any applied magnetic field.

Suppose superconductivity really were to be interpreted by a great number of different *asymmetric equilibrium states* corresponding to the different current threads, as this is the case with ferromagnetism for the different orientations of the magnetic moment. Then one should expect to find *hysteresis* whenever one tries to change the direction or strength of a supercurrent, say, by changing the direction or strength of an applied magnetic field. Nothing of this kind has ever been observed with superconductors and, indeed, any relaxation effect of this sort would be quite incompatible with all available evidence as to the peculiar mobility by which the supercurrents adjust themselves to the slightest changes of an applied magnetic field. It is true, there are hysteresis effects in superconductors. But they are exclusively confined to the transition into the superconducting state. There is no hysteresis as long as one stays within the limits of the pure superconducting state.

The same criticism also applies to a recent attempt by Born and Cheng.[7a] These authors

[7] F. and H. London, Physica **2**, 341 (1935).

** Indeed H. Hoppe in a recent paper, Ann. d. Phys. **1**, 405 (1947), comes to the conclusion that $T_1 = 0$.

[7a] M. Born and K. C. Cheng, Nature **161**, 968 (1948).

again propose an asymmetric momentum distribution (in this case arranged in certain "pockets" of the Brillouin zones) in order to account for different permanent currents in the superconductor. In reality there are no permanent currents but at best permanent magnetic fluxes and these occur exclusively in multiply connected superconducting regions.

It is true that some "frozen-in" magnetic fields are frequently found in simply connected superconductors; but they are, according to all evidence, generally to be attributed to non-equilibrium structures, to porous superconducting regions with non-superconducting inclusions, etc. They can be entirely eliminated by using very pure material and monocrystals. This is at least the interpretation which has been widely accepted and has found its general expression in Gorter and Casimir's thermodynamics[8] and in the electrodynamical equations (3) and (4). One may, of course, question whether these thermodynamics and electrodynamics are the last word concerning the macroscopic interpretation of superconductivity. But Heisenberg does not question this, and we certainly would not expect the macroscopic theory to be so fundamentally wrong.

Supplement to Section I

After conclusion of the present paper I received a copy of a manuscript of a paper, "Ueber das elektrodynamische Verhalten der Supraleiter," kindly sent to me by Professor W. Heisenberg. In this new paper Heisenberg withdraws his previous thermodynamical proof of the Meissner effect criticized above. However, now he even undertakes to prove Eq. (4) and the Meissner effect by considering only the action of the *classical Lorentz force*. This again is only possible by way of an assumption which anticipates what actually is the main point to be proven, namely, that case (A), applying the magnetic field after the superconducting state has been established, leads to the same velocity distribution as case (B) in which the magnetic field is applied already in the normal state and the transition into the superconducting state is done while the external field is kept constant. Heisenberg actually considers only the first case (A) and obtains our Eq. (4). However, it is by no means trivial; on the contrary, it would just be the task of a molecular theory of superconductivity to show why the two cases, A and B, lead to the same result.

[8] C. J. Gorter and H. Casimir, Physica 1, 306 (1934).

II. CONCLUSIONS FROM THE ELECTRODYNAMICS OF THE SUPERCONDUCTOR

Before one undertakes to develop a molecular theory of superconductivity it might be well to see how far the electrodynamics as expressed by Eqs. (3) and (4) already allows one to draw conclusions as to the kind of stability and the type of order realized in the superconducting state. Here we have partly to repeat, partly to supplement, remarks which were published about 13 years ago.[9] Their meaning will perhaps become clearer now when they are discussed in connection with Heisenberg's attempt.

A. Gauge Invariance and Superconductor Potential

We introduce the mean momentum field $\bar{p}_s$ of the superelectrons, defined as

$$\bar{p}_s=(m_s/n_se)j_s+(e/c)A, \tag{6}$$

where m_s is the effective mass of the superelectrons, n_s their number per cm^3 and A the vector potential of the magnetic field ($B=\mathrm{curl}A$). We may then write Eq. (4) simply in the form

$$\mathrm{curl}\bar{p}_s=0, \tag{4'}$$

if we assume

$$m_s/n_s=\Lambda e^2. \tag{7}$$

Accordingly we may express the vector $\bar{p}_s$ as the gradient of a scalar χ

$$\bar{p}_s=\mathrm{grad}\chi. \tag{8}$$

This χ, which we may call the "superconductor potential," is *only defined within the superconductor* and, hence, *needs not be single-valued* in multiply connected superconductors.

The vector potential A is not uniquely defined by the magnetic induction B. It can be replaced, as is well known, by an equivalent A' connected with A by a "gauge transformation" of the form

$$A'=A+\mathrm{grad}k, \tag{9}$$

[9] F. London, Proc. Roy. Soc. **A152**, 24 (1935). See also "Une conception nouvelle de la supraconductibilité," Actualités Scientifiques et Industrielles **458** (1937).

where k is an arbitrary continuous scalar with continuous first and second derivatives. Since k, in contrast to χ, is defined to be free of singularities in *whole* space it has always to be *single-valued*.

If we postulate the supplementary condition

$$\mathrm{div}A=0 \tag{10}$$

for A and for all equivalent A', then k has to fulfill the equation:

$$\nabla^2 k=0. \tag{11}$$

From (9) it follows also that $\bar{p}_s$ is not entirely determined by the definition (6). But the difference $\bar{p}_s-(e/c)A$ has a well defined meaning. If A is transformed according to (9), then p_s has to be transformed likewise by

$$\bar{p}_s'=\bar{p}_s+(e/c)\,\mathrm{grad}k. \tag{12}$$

We may add that, correspondingly, in quantum-mechanics any wave function $\psi(r_1, r_2\cdots r_\alpha \cdots r_N)$ which obeys a Schrödinger equation with the vector potential A is equivalent to a ψ' which is defined by

$$\psi'=\psi\exp[(2\pi ie/hc)\textstyle\sum_\alpha k(r_\alpha)], \tag{13}$$

and which fulfills the corresponding Schrödinger equation with A'.

It is possible and convenient to chose a *standard value* for the vector potential with respect to the superconductor. We may, for instance, always chose A so that on the surface of the superconductor

$$A_\perp=0. \tag{14}$$

Indeed, if we had originally another vector potential A' which did not fulfill (14), it would be connected with A by a transformation of the type of Eq. (9)

$$A'=A+\mathrm{grad}k$$

with Eq. (11)

$$\nabla^2 k=0,$$

where, according to (14), k has to fulfill the boundary condition

$$(\mathrm{grad}k)_\perp=A_\perp'. \tag{14'}$$

From well-known theorems of potential theory it follows that there is just one single-valued solution k within the superconductor which satisfies (11) and (14'). Accordingly, for a given magnetic field B there is just one standard vector potential A which, by the way, is defined so as to disappear for $B=0$.

Consequently, $\bar{p}_s$ is uniquely determined by the current j_s according to (5). Summarizing, we then may say that under stationary conditions the vector $\bar{p}_s$ fulfills the following equations: Within the superconductor:

$$\mathrm{curl}\bar{p}_s=0, \quad \text{(equivalent to (4))} \tag{4'}$$

$$\mathrm{div}\bar{p}_s=0, \quad \text{(because of (10) and of the continuity equation for } j_s) \tag{10'}$$

and at its boundary:

$$\bar{p}_{s\perp}=(m_s/n_s e)j_{s\perp}. \quad \text{(equivalent to (14))} \tag{14''}$$

For a simply connected superconductor these equations have one unique solution, provided $j_{s\perp}$ is given on its whole surface. Especially for an isolated superconductor ($j_{s\perp}=0$) this solution is well known to be

$$\bar{p}_s=0. \tag{15}$$

For a multiply connected superconductor the solution of (4') (13) (14'') is not uniquely determined unless the line integrals

$$\oint_{(k)}\bar{p}_s\cdot ds=(e/c)\phi_k, \tag{16}$$

taken along a curve within the superconductor around every hole, k, are given. The quantities ϕ_k are approximately identical with the fluxes through those holes and at the same time defined as the moduli of the, in this case, multivalued superconductor potential χ:

$$\phi_k=\int_{(k)}(A+\Lambda c j_s)\cdot ds=\iint_{(k)}B\cdot dS+\Lambda c\oint_{(k)}j_s\cdot ds$$

$$=(e/c)\oint_{(k)}\mathrm{grad}\chi\cdot ds=(e/c)\langle\chi\rangle_k.$$

By $\langle\chi\rangle_k$ we denote the modulus of χ, i.e., the increase of χ, when being continued once around the hole k. From the differential equations (3) and (4) it follows that the ϕ_k are constant in time and independent of the path, insofar as the path (k) embraces the hole k just once. In general, the line integral $\Lambda c\oint j_s\cdot ds$ is negligible compared with the surface integral $\int\int B\cdot dS$.

B. Long-Range Order of the Momentum Vector

Equation (15) does not necessarily say that there is no current in a simply connected isolated superconductor. In a magnetic field the momentum vector is not necessarily parallel nor is it proportional to the current vector; according to (4′) we may express (15) in the following way:

$$(c/e)\bar{p}_s \equiv \Lambda c j_s + A = 0,$$

or

$$j_s = -A_s/\Lambda c. \tag{15′}$$

This means that there is a well defined current in a magnetic field and no current in the absence of any magnetic field. In addition, we have the equation of Maxwell's theory (we neglect the displacement current and assume as magnetic permeability $\mu = 1$:

$$\text{curl curl} A = (4\pi/c) j. \tag{17}$$

It can be shown that in a simply connected isolated superconductor Eqs. (15′) and (17) uniquely determine the current by the field in infinity as a kind of surface current located within a layer of the very small depth of $c(4\pi\Lambda)^{\frac{1}{2}}$ behind the surface of the superconductor.

Compare Eq. (15′) with the behavior of an isolated ordinary conductor in a magnetic field: In the absence of an electric field there is no ordinary current; hence we have, in contrast to (15′), in a normal conductor:

$$j_n = 0, \tag{18}$$

and instead of (15):

$$\bar{p}_n = (e/c)A. \tag{19}$$

The latter is a very simple consequence[10] of the fact that the Hamiltonian $\mathcal{H}$ of free electrons in a magnetic field is given by:

$$\mathcal{H} = (p - (e/c)A)^2/2m. \tag{20}$$

Hence a superconductor is distinguished from a normal conductor by the feature that something prevents the momentum $\bar{p}_s$ from assuming the local value of $(e/c)A$ and, hence, from minimizing the kinetic energy expression (20). We may characterize the superconducting state by saying that n_s electrons per cm³ maintain a kind of *long-distance order with respect to their momentum vector p*, quite comparable to the ferromagnetic state, in which case it is the electronic angular momentum which is maintained over long distance by a cooperative order-disorder mechanism.

We have chosen the standard vector potential in such a way (Eq. (14)) that for the isolated simply connected superconductor it is especially the value $\bar{p}_s = 0$ which is maintained by the long range order over the whole body. In general we can only say that the long-range order is expressed by the Eq. (4′), $\text{curl}\bar{p}_s = 0$. For a straight wire of constant cross section, which is fed at its ends by a current, this still means simply $\bar{p}_s$ = constant over the whole diameter and length of the wire whereas the current is very inhomogeneously distributed over the cross section and is appreciable only near the surface.

Thus, summarizing this paragraph we may say that the long-range order characteristic of the superconducting state concerns, according to Eq. (4), the *momentum vector p* rather than the elementary current threads assumed by Heisenberg.

C. The Stability Character of the Supercurrents

According to the macroscopic electrodynamics, superconductivity is described in such a way that an isolated simply connected superconductor has no current unless an external magnetic field is applied. For a given applied field there exists just *one* current distribution.[11] It is true, at first sight it looks as if one could easily conceive of a situation of lower energy, for instance a state in which in an applied magnetic field *no* current would be present. However, such a state is not provided for by the differential equations (3) and (4) of the superconducting state although it would have less electromagnetic and kinetic energy than the existing state with current. The stability of the unique realizable state appears here to be of a quite similar character as it was the case in the older quantum theory of Bohr, where it also was still possible to imagine nonexisting states lower than the ground state, and the stability of the ground state had to be formally accepted from the mere *absence* of such

[10] As long as one can disregard quantum effects this (Eq. (19)) simply follows from the fact that the distribution function, $f(\mathcal{H})$, is an even function of the components of the vector $p-(e/c)A$. Hence $\int (p-(e/c)A) f(\mathcal{H}) dp$, the integral over an odd function, must disappear.

[11] M. von Laue, Nach. d. Akad. der Wiss., Göttingen Math. Phys. Chem. Abt., 86 (1946).

lower states, excluded by the quantum conditions. Indeed, Eq. (4) has very much the *character of a quantum condition*, we called it a "supplementary restriction" and we shall see presently to what implications this will lead.

Summing up we may say that in the case of the isolated simply connected superconductor the currents are stable—not because they are "frozen out" but rather because in the given applied field there is *no other current provided for*, not even zero current.

The case of a multiply connected superconductor, say a ring, requires special consideration. In this case the occurrence of a permanent current is not dependent on an applied magnetic field. The field maintaining the current may here be furnished by the current itself. But such a ring current does not represent a state of minimum free energy. The state in which the ring has no current has, of course, less energy if no external field is applied. Nevertheless, the state with current has a kind of *macroscopic metastability*. The quantities (16)

$$\phi_k=(c/e)\oint_{(k)} p_s\cdot ds=\int\int_{(k)} B\cdot dS+c\int \Lambda j_s\cdot ds$$

are constant in time as a consequence of (3) and (4). It requires a *finite* change of the macroscopic variables, e.g., heating above the transition temperature or the application of a magnetic field stronger than the threshold field, in order to release the free energy locked in by the ring.

It is clear from this remark that it makes little sense to speak of the stability of a single current element. One has to consider the system as a whole including the entire external field and its sources. In fact, each current element has its kinetic energy $\Lambda j_s^2/2$ which has its minimum for $j_s=0$. Nevertheless, a state $j_s\neq 0$ can be entirely stable if it is the only one compatible with the external applied field and with the boundary conditions.

III. QUANTUM-MECHANICAL DESCRIPTION OF SUPERCONDUCTIVITY

In the preceding section we have shown that it is the quantity p_s rather than the current j_s which in the superconducting state appears to be held in a kind of long-range order.

The problem of superconductivity is accordingly reduced to finding the mechanism which at sufficiently low temperature enforces the establishment of this kind of order. Before we come to this point it will be well to recall that Eq. (15) and, for multiply connected superconductors, the general Eq. (8) describe a very characteristic situation if they are expressed in the language of quantum mechanics.

It is well known that in non-relativistic quantum mechanics, which at any rate should be competent for explaining superconductivity, the density of the electric current at the point R in space for a state represented by the wave function in multidimensional configuration space $\psi(r_1, r_2, \cdots r_\alpha, \cdots r_N)$ is given by:

$$j(R)=\sum_\alpha \int \{(he/4\pi im)[\psi^* \operatorname{grad}_\alpha\psi - \psi \operatorname{grad}_\alpha\psi^*]-(e^2/mc)A(R)\psi\psi^*\}\,\delta_{R\alpha}d\tau. \quad (21)$$

Here $\delta_{R\alpha}$ is the three-dimensional Dirac function $\delta(R-r_\alpha)$. The integration is to be extended over the whole $3N$-dimensional configuration space; $\operatorname{grad}_\alpha$ is the operator $(\partial/\partial x_\alpha, \partial/\partial y_\alpha, \partial/\partial z_\alpha)$.

A. Simply Connected Isolated Superconductor

If one substitutes plane waves distributed over a Fermi distribution into the expression (21) the terms with the gradients cancel by reason of symmetry. The sum

$$\sum_\alpha \int \psi\psi^*\delta_{R\alpha}d\tau=n(R) \quad (22)$$

is the particle number per cm³. Hence we obtain

$$j(R)=-(e^2/mc)n(R)A(R). \quad (23)$$

This is identical with Eq. (15′) or, hence, Eq. (15), provided that $n(R)$ is a function sufficiently smooth to be replaced by its "coarse-grained" mean value. In fact, for plane waves $n(R)$ is exactly constant.

To be sure, the plane waves are not eigenfunctions of free electrons in a magnetic field. In reality the eigenfunctions of free electrons do depend very definitely on the magnetic field. What happens is well known: the plane waves coil up and transmute into a kind of wave packets of cylindric shape, the axes oriented parallel to the field. These eigenfunctions closely

correspond to the corkscrew orbits of the classical motion of free electrons in a magnetic field. In thermal equilibrium they arrange in such a way that Eq. (19),

$$\bar{p}=(e/c)A(R),$$

is very nearly fulfilled. As we have seen, for classical mechanics this equation is exactly fulfilled. In quantum mechanics the uncertainty relation entails a little difficulty as p cannot be exactly prescribed at a given point in space R. The result is the appearance of the diamagnetism of free electrons first calculated by Landau.[12] But this is a very small effect and may be discarded here.

However the electrons in the superconducting state are certainly not to be considered as free; they have a lower energy than in the normal state, realizable at the same temperature in a strong magnetic field. If $H_c(T)$ is the so-called magnetic threshold field, which limits the superconducting state, the free energy difference per cm³ between the normal state and the superconducting state is given by

$$F_s-F_n=-H_c^2/8\pi. \tag{24}$$

The existence of an energy difference clearly indicates that the superelectrons have yielded to some interaction. Hence there is no reason to expect them to behave like the coiling wave functions of free electrons in a magnetic field.

Evidently, according to (21), it would be sufficient to show that in the superconducting state, as a result of those interactions, the eigenfunctions would resist coiling when brought into a magnetic field and, in fact, simply stay exactly as they are without magnetic field, i.e., as if they were frozen in. Although this would be by no means the only way of obtaining the result (23) we will here consider this possibility somewhat more closely. It means precisely the opposite of the mechanism proposed by Heisenberg: we would expect sharp wave packets in momentum space, sharp even in the presence of a magnetic field, provided the field is smaller than the threshold field. In ordinary space the wave functions would be very widely extended, just as the plane waves fill the whole available volume. Heisenberg, on the other hand, suggests a certain relative localizability in ordinary space, a super lattice, and, correspondingly, some diffusedness of the momentum distribution as described by the wave function (2). According to our concept the long-distance order of the momentum vector would be due to the wide extension of the individual quantum state, as each plane-wave eigenfunction represents a constant momentum vector throughout the whole volume. We would have one single symmetric quantum state for a simply connected isolated superconductor at 0°A. while Heisenberg proposes a continuum of asymmetric states.

[12] L. Landau, Zeits. f. Physik **64**, 629 (1930).

B. Superconducting Ring

Thus far we have only considered an isolated, simply connected superconductor. In order to discuss the case in which an actual transfer of electricity is brought forward it is simplest to consider the case of a superconducting ring. In a ring the superconductor potential may have a modulus and we have, in general, to deal with Eq. (8) or

$$\bar{p}_s=\Lambda e j_s+(e/c)A=\text{grad}\chi, \tag{8'}$$

where the modulus of χ describes the flux possibly locked in by the ring.

In this case it is instructive formally to divide the magnetic field B and its vector potential A into two parts:

$$B=B_0+B_1, \tag{25}$$

$$A=A_0+A_1, \tag{26}$$

in such a way that the total flux of B and the total flux of B_0 are the same, but B_0 is chosen so as to disappear entirely in the material of the ring. For sake of illustration one may imagine B_0 caught inside a hollow cylindric superconductor which has been put into the hole of the ring. Although B_0 is supposed to disappear within the material, the vector potential, A_0, will not vanish there. This simply follows from the fact that on a closed path located entirely within the material

$$\oint A_0\cdot ds=\int\int B_0\cdot dS\neq 0.$$

Since $\text{curl}A_0=0$ within the material, we may write

$$A_0=\text{grad}\nu, \tag{27}$$

where ν has to be a multivalued function whose

modulus $\langle\nu\rangle$ is just equal to the flux of B_0,

$$\langle\nu\rangle \equiv \oint \text{grad}\nu \cdot ds = \int\int B_0 \cdot dS.$$

In addition ν has to fulfill the equations

$$\nabla^2\nu = 0 \quad \text{in the interior,}$$

and

$$(\text{grad}\nu)_\perp = 0 \quad \text{on the surface.}$$

By these conditions gradν is uniquely determined within the whole ring. Correspondingly, if $\psi_0(r_1, r_2 \cdots r_N)$ is the wave function of the super-electrons in the ring without flux, we have to write, according to (13),

$$\psi = \psi_0 \exp[2\pi i(e/hc)\textstyle\sum_\alpha \nu(r_\alpha)] \qquad (28)$$

for the wave function embracing the field B_0, even though no magnetic field is yet in the material itself. This transformation $\psi_0 \rightarrow \psi$ as expressed by Eq. (28) is, evidently, quite generally valid for any ring-shaped quantum-mechanical system which embraces a magnetic flux in such a way as not to touch the flux itself. We now add the field B_1, supposed to be so small as not to destroy superconductivity, and we further assume that now, as well as before, the superconducting state is characterized by that peculiar rigidity of the wave function in a weak magnetic field. Then we may substitute the ψ of Eq. (28) in the expression for the current (21) and obtain:

$$j = -(ne^2/mc)A_1 = (1/\Lambda c)(\text{grad}\nu - A). \quad (29)$$

This is exactly the relation (8′) for the ring if we put $(e/c)\nu = \chi$. It would accordingly be sufficient to prove this particular rigidity in momentum space for a conveniently shaped, simply connected, isolated superconductor. The properties of the ring, and presumably also those of an open superconducting wire which is fed at its ends, would then follow automatically.

Obviously, the state represented by (28) is not identical with ψ_0; it is a metastable excited state which is entirely determined by the flux of B. We see the requirement that ψ be single-valued imposes to the moduli of ν and to the fluxes ϕ a quantum condition,

$$(e/c)\langle\nu\rangle = (e/c)\phi = \oint p_s ds = Kh,$$

where K has to be an integer.

C. The Superconductor as a Quantum Mechnism of Macroscopic Scale

Summarizing the preceding discussion we may say that the long-range order of the momentum vector $\bar{p}$, implied by the macroscopic electrodynamics (IIB) offers a peculiar possibility of reducing superconductivity to a particularly simple quantum-mechanical model: If the momentum vector statistics of at least a fraction of the electrons is *sharp*, or else forms a sharp lattice in momentum space, the wave function has to be spread, according to the uncertainty relation, over a wide volume in ordinary space, and if, moreover, this fraction of the electronic wave function remains essentially unchanged in a magnetic field ($<H_c$), then Eq. (4) follows from (21). If this interpretation should prove correct, then the characteristic stability and mobility of the supercurrents would be understood at the same time, *viz.*, as the outcome of a quantum-mechanical possibility to which we already have referred (IIC) when we characterized Eq. (4) as something like a *quantum-mechanical restriction:* In a simply connected, isolated superconductor, for instance, all possible currents would be represented by the adiabatic transformations of one single quantum state and would be entirely determined by the *macroscopic boundary conditions*, *viz.*, by the orientation and strength of this applied magnetic field in large distance: There is exactly *one* single current distribution for each applied magnetic field, very much the same as this is the case, say, for the ground state of a diamagnetic atom. Correspondingly, one has stability (absence of dissipation) of this current because there is no state with another current provided for in the given magnetic field. The macroscopic, i.e., electrodynamical, boundary conditions coincide here with the boundary conditions which determine the quantum state. Hence one may also say this interpretation characterizes the superconductor as a pure quantum mechanism of macroscopic scale.

This would be the situation at absolute zero. For a finite temperature there are, of course, excitations to be expected. Below the transition temperature, however, a kind of phase equilibrium will be established between the normal and superconducting electrons, two phases, inter-

penetrating each other in any volume element of ordinary space but separated in momentum space. Only a fraction of the formerly superconducting charges will still be connected with the magnetic field by a relation like (4) and their number n_s will be subject to thermal fluctuations, while other degrees of freedom, the lattice vibrations, will be excited. These excitations cannot serve, however, to dissipate the supercurrent, since the latter would still be connected with the magnetic field as before by Eq. (4) except that n_s will undergo thermal fluctuations around a certain mean value. This is quite comparable with the situation in a diamagnetic molecule, which is also unable to get rid of its diamagnetic current by transitions between its vibrational and rotational states. This is not because these degrees of freedom would be entirely uncoupled from the electronic motion, which is not true, but because in all these states practically the *same* diamagnetic current is maintained by the magnetic field. Of course, there will be fluctuations of this current, as the diamagnetism will not be quite the same in the different vibrational and rotational states; and in the case of the superconductor, there will be current fluctuations in addition, because of the fluctuations of the number n_s. But these fluctuations would vary around a *mean value* of the current density, which is the quantity which appears as j_s in (4); they would not open an opportunity for a transition to a non-diamagnetic state.

We have now to investigate whether a mechanism of this kind can be found among the accepted interactions between electrons in metals.

IV. THE EXCHANGE EFFECT OF THE COULOMBIAN INTERACTION

In Section I we have referred to the exchange effect of the Coulomb interaction playing the basic role in the theory of ferromagnetism. In the case of $p_m = p_l$ and $p_n = p_k$ the matrix element (1′) represents the so-called exchange integral of free electrons,

$$I_{kl} = 4\pi h^2 e^2 / V |p_k - p_l|^2, \qquad (31)$$

corresponding to two states which differ only insofar as two electrons have exchanged their momenta. These two states have the same unperturbed energy. Hence one has a highly degenerate system and in the theory of ferromagnetism one deals with the secular equation defined by these matrix elements. The solutions of this secular problem give the first-order perturbation of the energy. In actual fact, up to the present time no one has succeeded in solving this secular problem rigorously. So far it has been possible only to determine the series of *energy mean values* of those groups of states which have the *same total spin s*. With this simplified energy spectrum the statistics have been worked out in a magnetic field. How far this procedure can be justified we do not know.

The exchange integral (31) is evidently always *positive*. In the case of two electrons with parallel spins it is to be multiplied by a factor -1 in order to give the first-order approximation of the energy and by a factor $+1$ for antiparallel spins. This favors ferromagnetism. Nevertheless, ferromagnetism does not necessarily follow from this model, as was already shown by Bloch,[2] since in order to have parallel spins the electrons in question must have different momenta (Pauli principle) and this may require more kinetic energy than can be gained as exchange energy.

For the mean value of the exchange energy of the group of states which have the total spin s one obtains the following expression:

$$\bar{E}_{\text{exch}}(s, n) = -2 \sum_{\alpha<\beta} I_{\alpha\beta} - \sum_{\alpha, k} I_{\alpha k} - \frac{4s(s+1)+n(n-4)}{2n(n-1)} \sum_{k<l} I_{kl}, \qquad (32)$$

where the Greek indices refer to doubly occupied electronic states and Latin indices to singly occupied ones. n is the number of singly occupied states. I_{kl} is given by Eq. (31). The kinetic energy is, of course, given by

$$E_{\text{kin}} = (1/m)\sum_\alpha p_\alpha^2 + (1/2m)\sum p_k^2 \qquad (33)$$

Bloch[2] determined as condition for ferromagnetism of this model the inequality

$$(N/V)^{-\frac{1}{3}} > (3/4\pi)^{\frac{1}{3}}(1+2^{-\frac{1}{3}})h^2/5me^2 \qquad (34)$$

or

$$N/V < 10^{22}\ \text{cm}^{-3},$$

where N/V is the number of electrons per cm³. Unless this inequality is fulfilled the lowest state of the system has $s=0$.

True, this model has to be taken with several

grains of salt, and indeed it is too crude to give correct conditions for the appearance of ferromagnetism. In fact, it has been improved in many respects particularly by taking account of the lattice structure. Still a closer study of this simple mechanism might be of interest. The general behavior of the exchange integral (31) and the negative factors with which it is multiplied in Eq. (32) show that even in a case in which the exchange interaction is not strong enough to bring the system into a ferromagnetic state this interaction still has the character of a kind of *attraction in momentum space*. All terms in (32) are negative and proportional to $(p_k-p_l)^{-2}$.

One could understand that a mutual attraction in momentum space might bring forward a kind of condensation, something like a solid state in that space, i.e., a state which not only has a relatively sharp momentum distribution (which would not mean anything particular as any Fermi distribution of the ordinary plane waves of free electrons would show this character) but which, moreover, would *maintain* its sharpness with respect to p even in the presence of a not too strong magnetic field. As shown in III a state of this kind would be just sufficient for bringing forth superconductivity.

Hence, all this boils down to the question of whether the exchange effect of the Coulomb field actually entails such a condensation in momentum space as suspected. This is a very difficult question which cannot be answered without entering into a special investigation, which would go beyond the scope of the present paper. Here we shall point only to a few indications which seem to speak in favor of our conjecture, but, as the same time, show that relying on the mean value formula (32), so instructive for discussing ferromagnetism, will most probably be insufficient for solving the problem in question.

That superconductivity occurs at much lower temperatures than ferromagnetism does in no way exclude the possibility that both phenomena might be due to the same kind of interaction. In fact, this difference as to the characteristic temperature is just what one would expect. In the case of ferromagnetism the gain of internal energy is of the order of the *total exchange energy* itself as the parallel orientation of the spins entails, in (32), an increase of the factor $[4s(s+1)+n(n-4)]/2n(n-1)$ from $\frac{1}{2}$ to 1; in addition, it decisively affects the number of states which are doubly occupied. On the other hand, if in the superconducting state the electrons arrange themselves only more closely in momentum space without much change of orientation of their spins, then only a *very small fraction* of the original exchange energy can be released as only a minute diffusedness in the momentum distribution near the surface of the Fermi lake is removed by the condensation in question.

Let us now consider N free electrons in a volume V distributed over an entirely degenerated Fermi distribution of which the maximum momentum p_0 is given by

$$(8\pi/3)p_0^3V=Nh^3. \tag{35}$$

On the basis of Eqs. (31) and (32) it is not difficult to calculate the total exchange energy of a single electron of the momentum p in the field of the N other electrons as function of p and p_0. The result is well known[13] to be given by

$$E_{\text{exch}}(p)=-(2p_0e^2/h)\{1+[(p_0^2-p^2)/2pp_0]\times\ln[(p+p_0)/|p-p_0|]\}. \tag{36}$$

The function (36) has for $p=p_0$ a logarithmically infinite derivative and the components of the so-called mass tensor

$$m_{xy}=(\partial^2E/\partial p_x\partial p_y)^{-1} \tag{37}$$

vanish there as $|p-p_0|$.

A *vanishing effective mass*, as this is expressed by (36) and (37), would imply a finite acceleration by an infinitely small force. Obviously, this is a rather formal result which may only serve to indicate that in the neighborhood of the top of the Fermi distribution the electrons behave very "quantum-mechanically:" The smaller the mass the greater the quantum effects. Accordingly, the familiar mixed procedure, customary in the electronic theory of metals, *viz.*, of first calculating energy bands in p-space (Brillouin zones) and then applying classical mechanics on wave packets is certainly not feasible here if we wish to calculate the behavior of these electrons in a magnetic field.

It is further noteworthy that the formula for the magnetic susceptibility χ of the so-called

[13] P. A. M. Dirac, Proc. Camb. Phil. Soc. 26, 376 (1930).

Landau-Peierls diamagnetism,[14] which in the case $E=E(|p|)$ can be written simply in the form,

$$\chi=-(e^2/18\pi hc^2)(E'+2pE'')_{p\to p_0}, \quad (38)$$

would give, in the present case, an *infinite diamagnetic susceptibility*. Also, this result is entirely formal and nothing but an indication that here again an extreme effect is to be expected. It would be necessary to calculate the simultaneous effect of exchange interaction and magnetic field from the beginning and it would presumably be decisive to take account of the effect of the magnetic reaction field produced by the diamagnetic currents, as the resultant field in the interior of the superconductor would be almost zero. One has here to keep in mind that superconductivity is not correctly described by any value of the magnetic susceptibility alone. Hence, one would not be satisfied by calculating the total magnetization only. It would be necessary to consider the current distribution in all detail.

The *level density* at the top of the Fermi distribution would, according to (36), just disappear, though only as feebly as $1/\ln|p-p_0|$. This indicates that in the interaction field (36) the eigenfunctions near the top are less easily deformed (IIIA) by an external magnetic field than those of free electrons would be, since the spacing of the energy levels (E_0-E_k) is decisive for the first-order perturbations of the eigenfunctions:

$$\psi=\psi_0+\sum_k'[H_{0k}/(E_0-E_k)]\psi_k,$$

where ψ_k are the so-called "right" eigenfunction of "zero" order.

However, it can be anticipated that it will require a better approximation than the one given by the mean value formula of the energy spectrum, at least the exact solution of the first-order secular problem but possibly even a still better approximation which considers the electronic correlation effect more appropriately. The logarithmic singularity of $\partial E/\partial p$ (Eq. (36)) is apparently just too weak to cause a phase transition at a finite temperature. This can be learned from an investigation by Sampson and Seitz[15] who studied the effect of (36) on the magnetic susceptibility of Li and Na on the basis of the so-called Bardeen integral equation. These authors showed that the exchange effect as given by (36) would yield only a small contribution to the magnetic susceptibility proportional to $\ln(e^2p_0/hkT)$ and would not entail the appearance of a discontinuity of the specific heat or a sudden condensation at a finite temperature. However, Sampson and Seitz themselves make several reservations as to the competence of their approximation method and come to the conclusion that even for their very limited aims "the problem of the electron-electron correlations has not yet been solved with sufficient completeness to say accurately to which extent the minimum of the energy level density would be influenced by their effect."

[14] R. Peierls, Zeits. f. Physik **80**, 763 (1933).
[15] J. B. Sampson and F. Seitz, Phys. Rev. **58**, 633 (1940).

CONCLUSION

Thus we come to the conclusion that the problem of the molecular theory of superconductivity has not always been posed quite properly. We tried to show that on the basis of the electrodynamics and thermodynamics of the superconductor one can draw quite definite conclusions with regard to the stability character of the supercurrents. In contrast to earlier attempts our discussion led us to characterize superconductivity, not as a state of electronic lattice order, as this was proposed by Kronig and quite recently by Heisenberg, but rather as a kind of condensed state in momentum space implying a long-range order of the momentum vector in ordinary space, presumably as an outcome of the requirements of quantum kinematics. We assembled indications which suggest that it is most probably the exchange interaction associated with the Coulomb field of the electrons which is responsible for this "condensation in momentum space." Ferromagnetism and superconductivity would then be considered as two opposite limiting cases of the same effect, depending on whether the exchange interaction competing with the zero-point energy promotes parallel orientation of the electronic spins or a coordination of the translational momentum in a state of vanishing total spin. However, it had to be left to the future to decide whether or not this suggestion can be substantiated by a rigorous theory.

PHYSICAL REVIEW VOLUME 74, NUMBER 5 SEPTEMBER 1, 1948

The Specific Primary Ionization and Energy Loss of Fast Electrons in Matter*

FRANK L. HEREFORD
Bartol Research Foundation of the Franklin Institute, Swarthmore, Pennsylvania

(Received May 18, 1948)

By utilizing the dependence of the efficiency of a Geiger-Mueller counter upon the primary ionization of a counted particle, the primary ionization by electrons in hydrogen has been determined for energies in the range 0.2 Mev to 9.0 Mev. The relative stopping powers of carbon and H_2O have also been investigated, the results yielding evidence for the existence of a polarization effect which reduces the energy loss of fast particles in condensed matter. Experimental results are compared with those of the Bethe-Bloch theory and the Halpern-Hall theory which takes into account the polarization properties of the medium.

INTRODUCTION

IN its passage through matter a charged particle creates ion pairs through the ejection of secondary electrons from the molecules in the vicinity of its path. These secondaries may in turn produce ionization; consequently, it is possible to define a *primary* and a *total* specific ionization. Cloud-chamber studies have led further to the specification of a *probable* ionization, defined as the number of ion pairs per cm exclusive of ions in clusters greater than a certain upper limit. It is also possible, however, to count the *primary* ion pairs by expansion of the chamber immediately after the passage of a particle.

Collision theory in its present state predicts a variation of both primary and total ionization roughly as follows. At low energies the ionization decreases as the energy of the incident particle increases since the time integral of the perturbation becomes shorter with increased velocity. At relativistic energies, however, the combined effects of the Lorentz contraction of the field in the direction of motion and certain quantum-mechanical considerations result in an increase of ionization with energy. The treatment given by Bethe, corrected for relativistic effects, gives for the primary ionization in hydrogen,[1]

$$J_p=(2\pi ne^4/mv^2)\cdot(a/I)\times[\log(2mv^2/(1-\beta^2)I)+b-\beta^2]. \quad (1)$$

Here n is the electron density, I the ionization potential, a and b numerical constants. This expression is plotted in Fig. 4 ($I=13.5$ ev).

The existing experimental data has verified the indicated dependence of *total* ionization,[2] but much of the *primary* ionization work[3–5] has been at variance with the theory. It is possible, indeed, to visualize an energy distribution of the secondary electrons which would yield an increase in *total* ionization for a decrease in *primary* ionization with energy. In fact, in one instance[4] results have been interpreted to indicate this.

The principal methods which have been employed in primary ionization investigations have utilized the cloud chamber[6] and the dependence of the efficiency of a Geiger counter upon the primary ionization of a counted particle.[7] Part I of this paper describes the application of the second method to the determination of the primay ionization in hydrogen by electrons of energies from 0.2–9.0 Mev.

The energy loss of the incident particle due to ionization has also been given by Bethe and by Bloch. Though their results differ slightly, the generally accepted Bethe-Bloch expression for the energy loss per unit path may be written as follows:[8]

$$[-(dE/dx)]_{\text{ion}}=(2\pi ne^4/mv^2)\times[\log(mv^2T/I^2Z^2(1-\beta^2))+1-\beta^2]. \quad (2)$$

Here T is the maximum transferable energy to

* Assisted by the Office of Naval Research.

[1] H. A. Bethe, *Handbuch der Physik* (1933), vol. 24, p. 522.

[2] D. R. Corson and R. B. Brode, Phys. Rev. **53**, 773 (1938); W. E. Hazen, Phys. Rev. **67**, 269 (1945).

[3] P. Kunze, Zeits. f. Physik **83**, 1 (1933).

[4] M. G. E. Cosyns, Nature **139**, 802 (1937).

[5] W. E. Hazen, Phys. Rev. **63**, 107 (1943).

[6] E. J. Williams and F. R. Terroux, Proc. Roy. Soc. **126**, 289 (1930).

[7] W. E. Danforth and W. E. Ramsey, Phys. Rev. **49**, 854 (1936).

[8] W. Heitler, *The Quantum Theory of Radiation* (Oxford University Press, London, 1936) p. 218.

an electron in a collision as computed by Bhabha.[9] Recently, however, Halpern and Hall[10] have carried out an investigation in which the polarization properties of the medium traversed are considered. The possibility that polarization of the medium might lead to a reduction in energy loss due to a screening effect was first suggested by Swann[11] and treated quantitatively by Fermi.[12] The subsequent investigation of Halpern and Hall yields a variation of ionization loss with energy of the ionizing particle which departs appreciably from the Bethe-Bloch calculation. It is the purpose of Part II to investigate the validity of these results by comparison of the relative stopping powers of carbon and H_2O at various electron energies. Previous attempts at verification have been successful in one case,[13] inconclusive in another.[14] In hydrogen the reduction in loss due to polarization does not appear at energies below about 100 Mev and, consequently, is of no importance in the primary ionization measurements of Part I.

PART I

Experiment

The method employed in the determination of the primary ionization in hydrogen utilizes the dependence of the efficiency of a Geiger counter upon the primary ionization. This dependence is as follows:

$$\text{Eff.} = 1 - e^{-lJp}. \tag{3}$$

Hence the counting rate for N_0 particles per minute traversing the counter is

$$N = N_0(1 - e^{-lJp}). \tag{4}$$

Here l represents the path length through the counter, J the primary ionization, p the counter pressure in atmospheres. Selection of electron energy ranges was accomplished in two ways.

In the range 0.2–0.75 Mev a magnetic focusing beta-ray spectrometer was employed, following the method of Graf[15] (Fig. 1A). Using various pressures of pure hydrogen in the counter at the collector slit, the counting rate was determined for various energies selected by the magnetic spectrometer. The counter was a thin-wall (0.03 g/cm²) type, the cathode being a coating of Aquadag on the inner surface of the glass envelop. The use of a Neher-Harper quenching circuit and a 64-scalar made possible counting rates high enough to minimize sufficiently the background effects. This data gave a family of curves showing *counts per minute vs. energy* with counter pressure as a parameter. For any energy it was then possible to plot *counts per minute vs. pressure.* The appropriate choice of lJ would then fit expression (4) to each curve, thus determining lJ *vs. energy*. The specification of the path length necessary to determine J was accomplished by normalization with the data at higher energies as discussed below.

For energies exceeding 0.75 Mev the beta-ray spectrometer available was unsuitable, and a coincidence counter method was used. The procedure has been previously described.[16] A fourfold coincidence train of thin-wall counters was employed (Fig. 1B), counters 1, 2, and 4 being filled with an argon-ether mixture at 7 cm Hg, which yielded an efficiency for all particles of very nearly 100 percent, counter 3 containing a pure hydrogen filling at 7 cm Hg. The ratio of

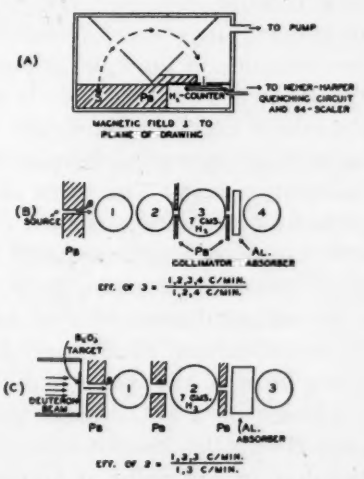

FIG. 1. (A) The beta-ray spectrometer for determination of the primary ionization in the 0.2–0.75 Mev range. (B) The coincidence apparatus for measurements at higher energies. (C) Revised coincidence arrangement using B^{12} beta-spectrum produced by deuteron bombardment of B^{11}.

[9] H. J. Bhabha, Proc. Soc. **164**, 257 (1937).
[10] O. Halpern and H. Hall, Phys. Rev. **57**, 459 (1940); **73**, 477 (1948).
[11] W. F. G. Swann, J. Frank. Inst. **226**, 598 (1938).
[12] E. Fermi, Phys. Rev. **57**, 485 (1940).
[13] H. R. Crane, N. L. Oleson, and K. T. Chao, Phys. Rev. **57**, 664 (1940).
[14] E. Hayward, Phys. Rev. **72**, 937 (1947).
[15] T. Graf, J. de phys. et rad. (Ser. 7) **10**, 513 (1939).
[16] F. L. Hereford, Phys. Rev. **72**, 982 (1947).

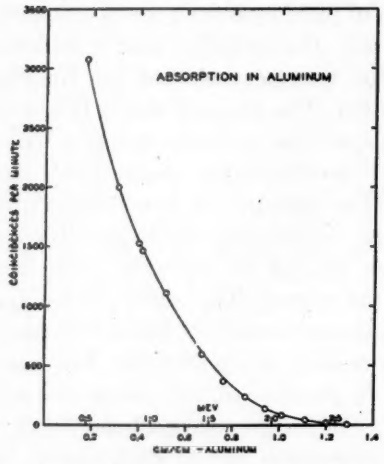

FIG. 2. Absorption in aluminum of beta-rays from the radium source.

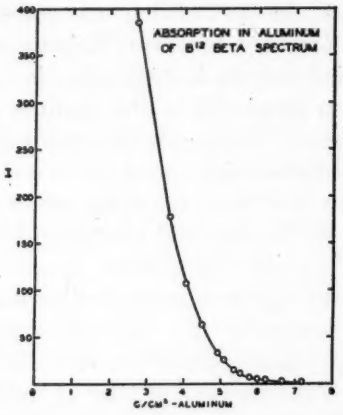

FIG. 3. Absorption in aluminum of beta-rays from B_{12}. See Fig. 7 for end-point determination.

coincidences 1, 2, 3, 4 to coincidences 1, 2, 4 clearly gives the efficiency of counter 3. The path length through this counter was limited to a small region about the diameter by a collimator as shown. Knowledge of the efficiency, counter pressure, and path length then allowed computation by (3) of the primary ionization, J, for any energy distribution of electrons penetrating all counters. Insertion of various thicknesses of aluminum between counters 3 and 4 made possible determination of J for all electrons of energy in excess of that required to penetrate the absorber, counter walls included.

Using first a radium source, J was evaluated for electron energies in the 0.9–2.5 Mev range. The energy spectrum of the source is indicated by the absorption curve in aluminum (Fig. 2), where the end point was determined by the Feather absorption law.[17] The value of l in the beta-ray spectrometer data was then chosen so as to match values of J as determined from the spectrometer and coincidence methods at about 0.8 Mev. For the evaluation of J at higher energies the beta-spectrum of B^{12} was employed. The deuteron beam of the Bartol Van de Graaff generator focused on a B_2O_3 target yielded B^{12} through the $B^{11}(dp)B^{12}$ reaction. The B^{12} spectrum which has an end point at approximately 13 Mev is indicated in Fig. 3.

The short half-life of B^{12} (0.02 sec.) necessitated continuous operation of the generator; the difficulties of prolonged operation made necessary the use of higher counting rates than were previously used. In order to achieve this without loss of genuine counts the hydrogen counter was quenched by a Neher-Harper circuit. Coincidences were recorded by means of the circuit used by Mandeville and Scherb,[18] with which a resolving time of 1.8×10^{-7} second was attained. The consequent low accidental coincidence rate allowed removal of the first counter. Thus the efficiency was determined and primary ionization computed in this case from the ratio of the threefold to twofold coincidences (Fig. 1C).

Results

The collected data for the primary ionization in hydrogen in the energy range 0.2–9.0 Mev are given in Fig. 4 with the theoretical curve of the Bethe-Bloch theory. The ordinate shows the values of E/mc^2 in order that the average value of J for the ionizing component of sea level cosmic radiation can also be indicated. The average value of E/mc^2 in this case is taken to be 20, corresponding to the average energy of the meson component at sea level. The unpublished results of an independent experiment conducted in this laboratory by Mr. Alden Stevenson have shown the primary ionization of the meson component and of the total ionizing component at sea level to be essentially equal. It may be pointed out that the value of J for sea level

[17] N. Feather, Proc. Camb. Phil. Soc. **34**, 599 (1938).

[18] C. E. Mandeville and M. V. Scherb, Phys. Rev. **73**, 90 (1948).

cosmic radiation relative to the minimum ionization (1-Mev electrons) is the same as that previously found[16] in a self-quenching helium-butane counter mixture. Figure 4 also indicates the results of several other experimental investigations for the sake of comparison. The high value of J at the minimum obtained by Cosyns is probably due to an underestimation of scattering effects.

PART II

Experiment

As previously stated Halpern and Hall show that polarization considerations reduce the ionization loss of a fast charged particle traversing a medium. The effect, which is most prominent in condensed substances, yields a 7 percent reduction in the loss of 1-Mev electrons in carbon while in H_2O it becomes appreciable only at higher energies (Fig. 5). Such a reduction alters the relative stopping powers of the two media, which effect should be observable by means of an absorption method.

We have employed[19] a simple scheme in which the reduction in the coincidence rate of a twofold coincidence train was observed upon the insertion of varying thicknesses of carbon and H_2O (Fig. 6). The outstanding difficulty of the method is that a portion of the apparent absorption is due to the scattering of particles out of the solid angle subtended by the second counter. It is possible, however, to choose sample thicknesses

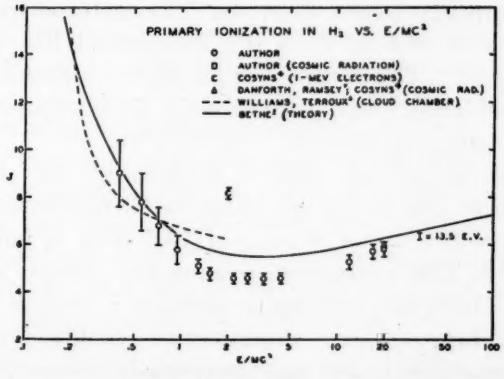

FIG. 4. Results of determinations of the primary ionization, J, in hydrogen. The experimental points may be compared with the curve computed from Bethe's theory.

[19] The details of the procedure have been described and some of these results given previously, F. L. Hereford, Phys. Rev. **73**, 1123 (1948).

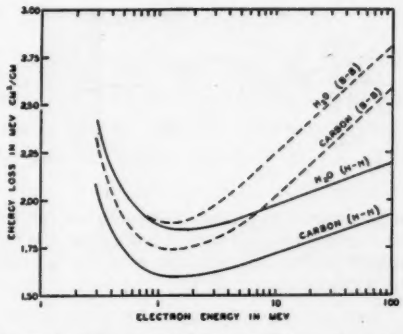

FIG. 5. The theoretical ionization loss for electrons in carbon and H_2O. The Halpern-Hall loss is shown by the solid lines, the Bethe-Bloch loss by the dotted lines.

in such a manner that scattering effects are eliminated.

It is well known that for the case of multiple scattering,[20] if the thickness of a layer is given in "radiation lengths," then the mean square angle of scattering of a monoenergetic beam of particles is independent of the atomic number.[21] Consequently, equal thicknesses of two substances so measured should scatter equivalently a monoenergetic beam. However, in the application here we are concerned with a continuous energy distribution. Hence, if our samples are to exhibit equal scattering effects, in addition to being of equal thicknesses in radiation lengths they must have equal stopping powers, for then the scattering loss will form the same percentage of the apparent absorption in each sample. This condition will exist if, for instance, in the case of carbon and H_2O,

$$S_{H_2O}/S_C = X_C/X_{H_2O},$$

where S and X are, respectively, the stopping

TABLE I.

Thickness of samples			Mean	Stopping power ratio		
Radiation length	H_2O g/cm²	Carbon g/cm	energy Mev	S_{H_2O}/S_C Exp.	S_{H_2O}/S_C Halpern-Hall	S_{H_2O}/S_C Bethe-Bloch
0.0055	0.25	0.29	1.6	1.16±0.02	1.16	1.08
0.0079	0.36	0.41	1.4	1.17±0.02	1.16	1.08
0.019	0.83	0.97	9.0	1.14±0.02	1.15	1.09
0.032	1.37	1.66	7.4	1.16±0.02	1.15	1.09

[20] Williams has given (E. J. Williams, Proc. Roy. Soc. 169, 531 (1939)) as the criterion for multiple scattering,

$$M=(2\pi nZ^{4/3}/\beta^2)(\hbar/mc)^2t\gg 1 \quad (t \text{ in cm}).$$

For all cases considered here, $M\geqq 2\times 10^3$.

[21] B. Rossi and K. Greisen, Rev. Mod. Phys. **13**, 262–265 (1940).

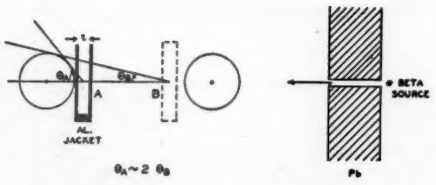

FIG. 6. Schematic diagram of apparatus for investigation of relative stopping powers. θ represents the maximum angle through which an electron may be scattered and still record a coincidence.

power and the radiation length. Fortunately, in the case of carbon and H_2O this requirement is satisfied to within a few percent if we take the value of S_{H_2O}/S_C given by the Halpern-Hall theory.

The experiment then consists only of the observation of the coincidence rates with equal sample thicknesses (in radiation lengths) of carbon and H_2O inserted alternately into a thin-wall aluminum jacket situated at A as shown in Fig. 6. The equivalence of the rates would indicate verification of the Halpern-Hall value of the stopping power ratio.

In the actual experiment this was very nearly the case. The small differences in the rates, however, were evaluated in terms of stopping power by reference to an aluminum absorption curve, the value of S_{H_2O}/S_C taken as the ratio of S_{H_2O}/S_{Al} and S_C/S_{Al}. The procedure was carried through for the electron spectra of both the radium source (Fig. 3) and B^{12} (Fig. 4). In the case of the higher energies of the B^{12} spectrum, the choice of equal sample thicknesses in radiation lengths eliminates confusion between energy loss due to ionization and that due to radiation, the radiation losses being equal. The position of the counters relative to the B_2O_3 target was similar to that shown in Fig. 1C. Coincidence rates were determined relative to the deuteron current striking the target in this case.

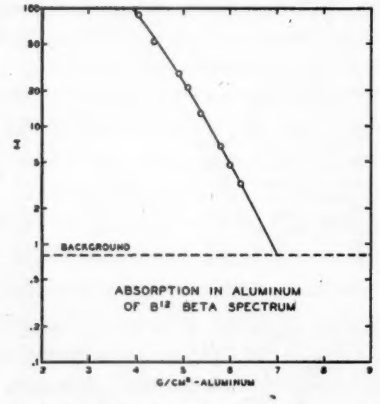

FIG. 7. Logarithmic plot of the higher energy points from Fig. 3 for determination of the end point of the B^{12} beta-spectrum.

The equivalence of scattering in the two samples was demonstrated by shifting each sample to position B (Fig. 6) and observing the increased percentage of intensity scattered out of the counter train. The differential scattering probability depends upon the inverse 4th power of the scattering angle; it can be shown in view of this and the geometry employed that the error in the value of S_{H_2O}/S_C due to scattering was at most 0.2 percent.

Results

The values of S_{H_2O}/S_C as determined for four effective electron energies are given in Table I with the values predicted by the Bethe-Bloch and Halpern-Hall theories shown for comparison. The experimental results clearly favor the Halpern-Hall calculation.

Note on Upper Limit of the B^{12} Beta-Spectrum

As a by-product of the investigations at higher electron energies the end point of the beta-ray spectrum of B^{12} was determined by an absorption method. Figure 7 shows a logarithmic plot of the high energy end of the aluminum absorption curve (Fig. 4). The extrapolated curve is seen to cross the background line at 7.0 g/cm². The background was due to accidental coincidences and coincidences from cascade emission of gammas.

In accordance with a modification of the Feather absorption law given by Glendenin and Coryell[22] a value of E_{max} of 13.3 Mev is indicated. This evaluation assumes the validity of the absorption relation at energies in excess of the range where experimental confirmation exists. This is not too unreasonable since the radiation loss in aluminum for these energies is not appreciable; moreover, it generally appears

[22] L. E. Glendenin and C. D. Coryell, Plutonium Project Record 9B, 2.12 (1946).

as large energy losses by a few particles rather than small losses by many.

The upper limit determined from the cloud chamber data of Bayley and Crane[23] by inspection and by Fermi and K-U extrapolations are given below for comparison.

Inspection	12.0±0.6 Mev,
Fermi Plot	12.4±0.6,
K-U Plot	14.5±0.7,
Above value	13.3±0.5.

[23] D. S. Bayley and H. R. Crane, Phys. Rev. **52**, 604 (1937).

ACKNOWLEDGMENTS

The suggestions and help of Messrs. W. E. Ramsey and M. A. Pomerantz contributed a great deal to the success of the investigation. The author is also indebted to Dr. W. F. G. Swann for his constant interest and frequent advice. Mr. Austin Nester constructed all counters used and Mr. S. H. Forbes assisted in the computations. Thanks are also due to Dr. E. L. Hudspeth and Mr. C. P. Swann for their assistance in the operation of the Bartol Van de Graaff generator.

PHYSICAL REVIEW VOLUME 74, NUMBER 5 SEPTEMBER 1, 1948

Shower Production by Penetrating Particles at 14,000 Feet

H. BRIDGE AND W. HAZEN*
Physics Department and Laboratory for Nuclear Science and Engineering, Massachusetts Institute of Technology, Cambridge, Massachusetts

(Received May 19, 1948)

Showers produced by penetrating particles were studied at 14,000 feet by simultaneous observations with G.M. counters, a cloud chamber, and an ionization chamber in a combined array. At least two-thirds of the observed showers generated by penetrating particles that struck a five-inch lead absorber consisted of a mixture of energetic electrons and particles heavier than electrons. The frequency of these events at high altitude relative to sea level shows that the initiating particles are not ordinary mesons. The presence of heavier particles in the electron shower indicates that the showers result from nuclear interactions in which the nucleus is disrupted rather than from a simple radiation process. Details of the events and their relation to some other cosmic-ray phenomena are discussed.

1. INTRODUCTION

THE production of high energy showers by penetrating particles has been observed with ionization chambers,[1] with cloud chambers,[2] and with counter arrangements.[2]

The observations described in this paper were undertaken in order to study the nature of the showers that have been observed at high altitude under lead shields thick enough to exclude electron or photon initiated showers.[1] For this purpose, the lead was divided into a thick lead shield that was placed above a cloud chamber and a series of lead plates that were placed inside the cloud chamber. A coincident signal from G.M. counters and an ionization chamber controlled the expansion of the cloud chamber. With suitable geometry, this procedure makes possible a detailed study in the cloud chamber of the event responsible for the burst in the ion chamber.[3] Thus it was hoped that the results would provide general information about high energy showers and conclusive evidence as to the nature of the showers studied by Bridge, Rossi and Williams with shielded ionization chambers at high altitudes.[1]

Since the terminology used to describe events

* Now at University of Michigan, Ann Arbor, Michigan. Some of the cloud chamber equipment was constructed during the tenure of a John Simon Guggenheim Memorial Fellowship.

[1] H. Bridge, B. Rossi, and R. Williams, Phys. Rev. **72**, 257 (1947).

[2] See W. B. Fretter, Phys. Rev. **73**, 41 (1948) for cloud-chamber observations and references to previous work.

[3] A brief report of the results was included in a letter by H. Bridge, W. Hazen, and B. Rossi, Phys. Rev. **73**, 179 (1948).

of the type discussed in this paper is by no means standardized, it seems advisable to define terms as they will be used in what follows.

Burst: any event that produces an ionization pulse in an ion chamber.

Nuclear Disintegration: production of secondary particles by a nuclear collision with emission of particles heavier than electrons.

Star: a nuclear disintegration in which only nuclear particles with energies of the order of nuclear binding energies are emitted. These particles have an essentially isotropic angular distribution.

Electronic Shower: a shower of electrons and photons that develops by the ordinary multiplication process.

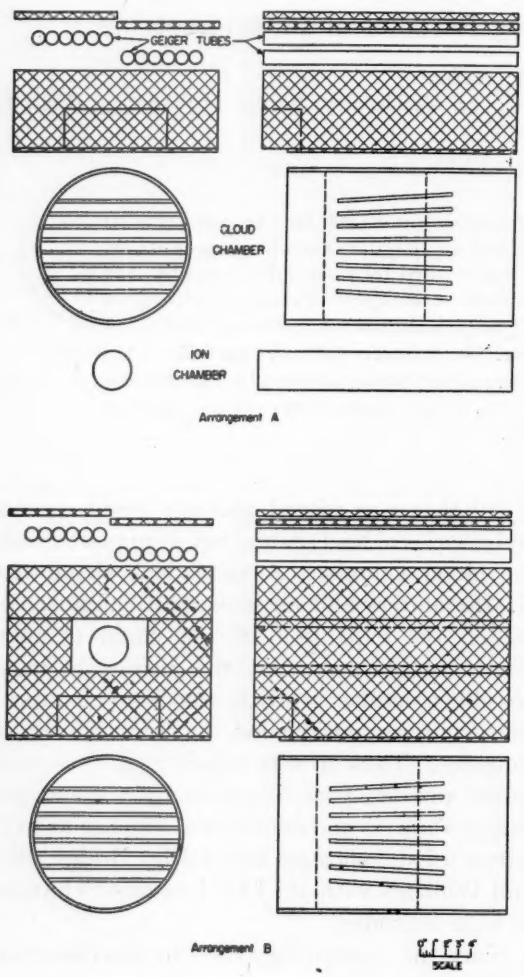

FIG. 1. Experimental arrangements for the two parts of the experiment. The cross-hatched material is lead. The scale is in inches.

Penetrating Shower: a shower consisting primarily of penetrating particles.

Mixed Particle Shower or Mixed Shower: a shower that obviously contains heavy particles as well as energetic electronic radiation.

Air Shower: a shower which has developed at least partly in the air before striking the detecting instrument.

2. APPARATUS AND RESULTS

Apparatus

The two arrangements used in the course of the experiments are shown in Fig. 1. The ionization chamber was filled with purified argon to seven atmos. pressure. The use of electron collection at the wire gave information about the type of ionizing event occurring in the chamber.[4] The cloud chamber contained eight $\frac{1}{4}$-inch lead plates and was filled with argon at about 65 cm pressure. The cloud-chamber photographs were stereoscopic. Signals from the G.M. counters and the ionization chamber were applied to a coincidence stage the output of which triggered the cloud chamber expansion. No pulse was obtained from the coincidence stage unless the pulse from the ionization chamber exceeded a minimum value. In most of the measurements, this value was equivalent to the average pulse produced by 15 fast electrons traversing the ionization chamber perpendicular to the axis. Hence the cloud chamber was insensitive to showers which contained a small number of fast particles. The ion chamber pulses were delayed in time and photographed on an oscilloscope whose sweep was also triggered by the coincidence signal. Air showers were identified by the multiplicity of discharges in the G.M. counter tray and by the appearance of the shower in the cloud chamber.

Reprojection of the stereoscopic views of the cloud chamber allowed an accurate reconstruction of observable penetrating particle tracks, an accurate determination of the position of a shower origin when it was in the cloud chamber, and a moderately good determination of the direction of the shower axis.

The observable depth of the cloud chamber (shown by the dotted lines in Fig. 1) was about

[4] H. Bridge, Phys. Rev. 72, 172A (1947); R. Sherr and R. Peterson, Rev. Sci. Inst. 18, 567 (1947).

eight inches, whereas the lengths of the G.M. tubes and of the ion chamber were about twenty inches. Consequently, the cloud chamber was expanded in many cases as a result of an event that was not seen in the observation region. However, as can be seen from Fig. 1, the geometry was such that any single ionizing particle which discharged a G.M. tube and which was seen in the observable volume of the cloud chamber must have penetrated all of the lead absorber above the cloud chamber. This implies that electrons are excluded as agents responsible for the observed events. Of course, an air shower at a large angle with the vertical can trigger the apparatus and appear in part in the observable volume, but such events are readily identified.

Results Obtained with Arrangement A

Arrangement A (Fig. 1) was intended to be selective for events in which a shower originated in the cloud chamber. Analysis of the records reveals that 20–25 percent of the 700–800 cloud-chamber pictures showed evidence of electron showers and/or groups of penetrating particles. Pictures in which penetrating particles appeared without electrons constituted about 5 percent of the 20–25 percent group. The expressed uncertainty in the figures derives from the difficulty in defining useful pictures (i.e., in determining from the picture alone whether or not the cloud chamber was operating in a satisfactory way), and in applying a criterion for a lower limit to the number of particles which should be required in a photograph to classify the picture as a shower.

Analysis of the 20–25 percent group indicates that about one-half (described under I below) showed particles whose initiators must have been incident on the five-inch lead block, while the other half (described under II below) showed particles that came from the sides, front, or back of the five-inch lead block and entered the cloud chamber at an angle with the vertical such that the initiating rays traversed little or no lead before striking the plates in the cloud chamber.

The large number of pictures which did not show showers (75–80 percent) can be attributed to the following factors:

(a) Accidental coincidences between the ion chamber and the G.M. counters account for 10 percent of the coincidence signals and hence 10 percent of the cloud-chamber expansions were caused by spurious coincidences.

(b) The pulse shape records of the ion chamber signals showed that in 15 percent of the expansions the ion-chamber pulse was caused by a small number of heavily ionizing particles. These cases were presumably the result of a star produced near the ion-chamber wall by a charged particle which had discharged a G.M. tube and penetrated the lead above the cloud chamber.

(c) This leaves 75 percent of the pictures which should have been caused by showers. Of this 75 percent only between $\frac{1}{2}$ and $\frac{1}{3}$ would be seen in the cloud chamber because, as pointed out above, not all triggering events passed through the observation region. Thus between 37 and 25 percent of the pictures should have shown showers. The observed fraction of 20–25 percent is not considered to be in disagreement with the above.

Details of the two classes of events (I and II) in which radiation appeared in the cloud chamber in arrangement *A* are given below.

TABLE I. Events of Class I, Arrangement *A*.

Number of pictures: 68				
Shower origin—(a) in the cloud chamber				25
(b) above the cloud chamber				42
(c) below the cloud chamber				1
Shower Components Observed	*Origin*			*Total*
	a	*b*	*c*	
Penetrating particles only	1	8	1	10
Electron cascade radiation only	6	4	0	10
Mixed particle shower	18	30	0	48
Mixed shower with energetic heavy particles				34
Mixed Showers				
Electrons and fast heavy particles from a common origin				11
Electrons and slow heavy particles from a common origin				12
Electrons and either fast or slow heavy particles from a common origin				16
Associated stars or slow heavy particles				
(1) along the path of the shower				13
(2) other parts of chamber				4

I. *Electron showers and/or groups of penetrating particles in which the initiating particles were incident on the five-inch absorbers*

Illustrations of the events are given in Figs. 2 and 3.

In two short runs where a detailed correlation was made with ion chamber pulses using ar-

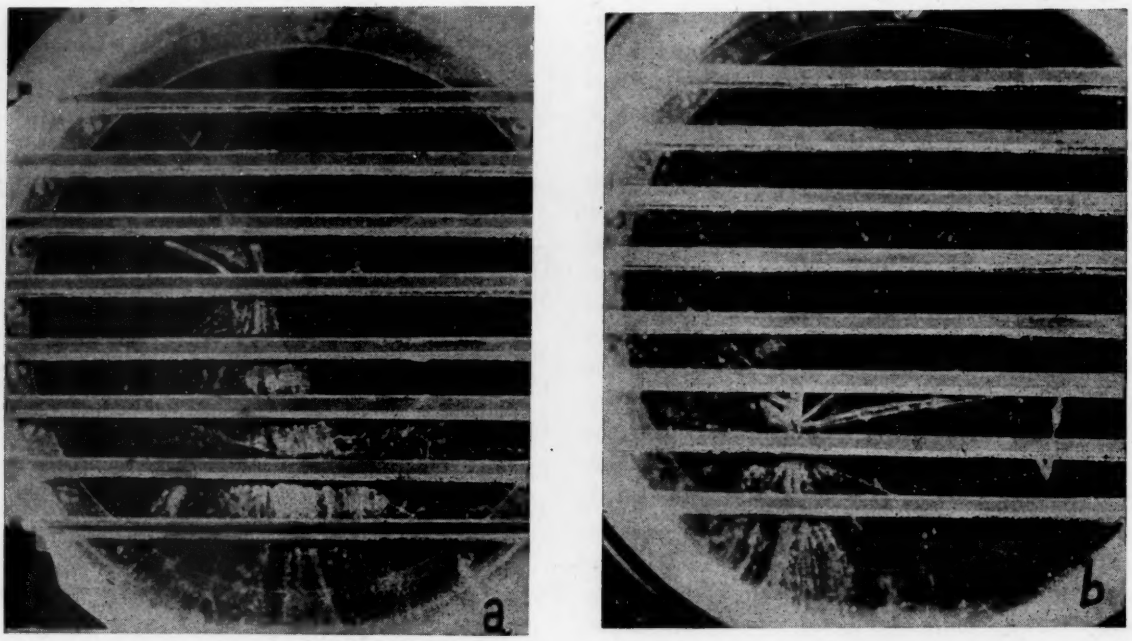

(a) (b)

FIG. 2. (a) Mixed shower originating in the cloud chamber. There are many penetrating particles and an electronic shower component with an energy of the order of one Bev. An originating particle track is visible on the negative. (b) Mixed shower produced by a non-ionizing particle. The G.M. tube was probably triggered by an accompanying air shower particle. It is impossible to tell how many of the shower particles are penetrating but there are either a number of penetrating particles or else a number of widely divergent low energy electrons from the shower origin. At least one of the particles is an energetic electron since there is cascade multiplication in the bottom lead plate.

rangement *A*, the following information was obtained. There were six cases in which the cloud chamber showed that electron showers from initiating particles incident on the five-inch lead block struck the ion chamber. In all six events the shape of the ion-chamber pulse indicated uniform volume ionization. In one case the ion-chamber pulse indicated a mixture of volume and concentrated ionization. Five of the six events resulted in the discharge of no more than two G.M. counters.

II. *Electrons from the Sides, Front, or Back of the Five-Inch Absorber*

As stated earlier, these events occurred with about the same frequency as the events of Class I. In contrast to the events of I, only a very small fraction of these side showers gave any evidence of fast or slow heavy particles associated with the electronic radiation. A correlated ion-chamber, G.M. counter, cloud-chamber record yielded eleven events with the cloud chamber showing side showers of Class II which clearly struck the ion chamber. In all eleven cases the ion-chamber record indicated volume ionization and in only one instance were fewer than 3 G.M. counters discharged.

Results Obtained with Arrangement B

In Arrangement B, Fig. 1, the five-inch lead filter between the ion chamber and cloud chamber was designed to remove the electron component of a burst that struck the ion chamber before the shower products reached the cloud chamber. The ion chamber was well shielded from electron air showers, in contrast to *A*. The geometry was such that we should expect the number of showers observed in the cloud chamber relative to the number of showers detected by the ion chamber to be less in arrangement *B* than in *A*.

The statistics from the 490 photographs with Arrangement *B* are given in Table II.

3. DISCUSSION

1. Initiating Particles

Arrangement A, Class I: In the cases where the cloud-chamber pictures showed bursts in which

the initiating particles were incident on the five-inch absorber, there was seldom a multiple discharge of the G.M. tray above the lead absorber. Therefore, initiating particles were not ordinarily parts of dense electron air showers, either extensive or local. However, one cannot rule out the possibility that the initiating particles were frequently parts of low density air showers.

The initiating particles were certainly not electrons since an electron capable of producing an electron cascade of the observed size under six inches of lead would have to have an energy of the order of 10^{12} ev. It does not seem possible that such electrons occur with the observed frequency of the mixed showers, or that they could account for the heavier particles observed in the showers. The energy of the initiating particles for arrangement *A* Class *I* must have been 1 to 5 Bev in most cases since this energy release was observed in the electron cascades associated with the showers. Because of the method of detection this should also apply to observations with arrangement *B* (i.e., an electron shower in this energy range would be required to affect the ionization chamber).

In the pictures obtained with arrangement *A* where mixed showers were produced above the cloud chamber, it was difficult to decide in some cases whether the penetrating particle component of the mixed shower could have originated at the same point in the five-inch lead block as the electronic radiation or whether the penetrating particles accompanied the particle that produced the electron shower in the five-inch block.

In ten cases of the 42 in this category (Table I), the penetrating particles seem certainly to be parts of air showers rather than products of the shower from the five-inch block, since the penetrating particles were widely separated in position and were far from having a common origin in the vicinity of the apparatus.

Arrangement A, Class II: In the cases where the cloud-chamber pictures showed electronic radiation entering the chamber from the side, front, or back, multiple discharges of the G.M. tray (3 or more tubes), were recorded in ten out

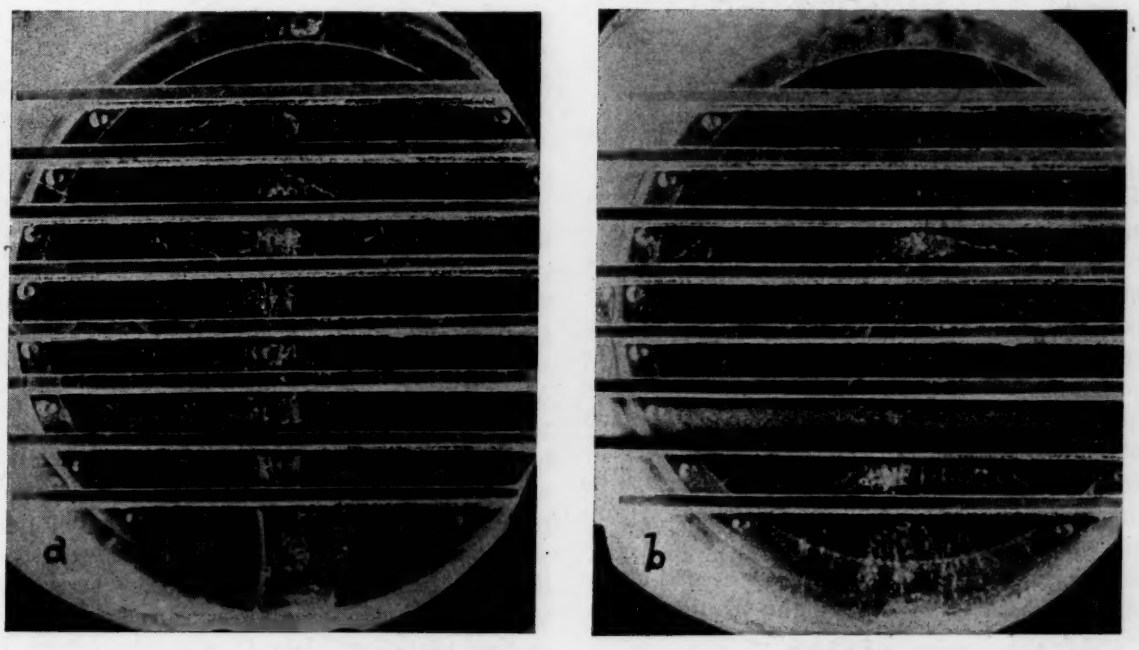

(a) (b)

FIG. 3. (a) Mixed shower originating above the cloud chamber. There appear to be several penetrating particles and two separate electron cascade shower cores. A star is seen to originate in the path of the left shower core in the seventh plate. (b) Penetrating particle shower originating above the cloud chamber. Eight penetrating particles enter the cloud chamber and either a neutron or one of the penetrating particles produces another disintegration of six or more penetrating particles in the third plate. There also appear to be some small electron cascades at the bottom.

TABLE II. Statistics for arrangement *B*.

Two or more penetrating particles from above	21 photographs
Electronic radiation from above (very small showers)	2 photographs
Electronic radiation from side	11 photographs
Few low energy electrons	6 photographs
Mixed showers (all but one from side)	11 photographs

of the eleven cases that were correlated. Therefore, the majority of these events were probably initiated by air showers. There were very few cases of penetrating particles associated with the electron cascades or of heavy particles produced locally by the shower.

Arrangement B: The data from arrangement *B* give additional evidence for occasional association of the shower-producing penetrating particles with low density air showers that contained penetrating particles (see Table II), since there were ten events in which mixed radiation entered the cloud chamber from the side while the ion chamber responded to an associated shower. The data thus show that about one-fourth of the shower-producing penetrating particles are accompanied by other particles within the observed area of roughly 1000 cm².

2. Position of the Shower Origin

The origin of a shower was usually within the three inches of lead nearest the ion chamber. This observation is consistent with the following arguments. If we assume the ion-chamber pulse to be caused by electron showers alone, 15 or more particles that traversed the chamber perpendicularly to its axis would give the minimum required pulse. Thus the average 10^9 ev shower could produce the required pulse only in the immediate vicinity of its maximum at one inch of lead below the shower origin. Therefore, one would expect the origin of such a shower to be in the central plates of the cloud chamber. On the other hand, a shower of 5 Bev energy with an origin in the range $\frac{1}{2}$–$2\frac{1}{2}$ inches of lead above the ion chamber could give the required minimum pulse.

3. Composition of the Mixed Showers

The showers were similar to those recently described by Fretter.[2] Heavily ionizing particles (a), penetrating particles (including a few identifiable mesons) (b), and electron cascade radiation (c), were directly visible; the emission of neutrons (d) is inferred from the presence of time associated stars and single slow heavy particles in parts of the cloud chamber removed from the burst origin.

(a) Heavily ionizing particles were emitted from the shower centers with an essentially isotropic angular distribution. The heavy ionization indicates low energies, perhaps of the order of a few Mev and certainly less than 50 Mev for particles that do not penetrate one plate. There were 21 heavily ionizing particles emitted from the 25 mixed shower origins that occurred in the cloud chamber. Thus the average number of *observed* heavily ionizing particles was about one per shower.

(b) The penetrating particles observed in arrangement *A* had a wider angular divergence than the electronic radiation and in one case a meson was even projected upward with an energy of 40–50 Mev. The lower limits that can be assigned to the energies of the penetrating particles, however, are not high, since the lead absorber in the chamber totaled only two inches and many showers did not originate in the top plates. For protons, the lower limit would be only 200 Mev and for mesons, 100 Mev, even when the origin of the shower was in the top plate. The events observed in arrangement *B*, however, probably represent mixed showers produced near the ion chamber, and thus the penetrating particles which were observed in the cloud chamber with this arrangement must have traversed more than five inches of lead. Therefore they must have had energies of more than 200 Mev if mesons or greater than 350 Mev if protons. The frequency of occurrence of these high energy penetrating particles can be estimated from a comparison of the data for arrangements *A* and *B*. The yield of photographs showing penetrating particles from above was at least four percent in arrangement *B*, whereas the yield of photographs showing showers by penetrating particles (Class I) was ten percent in arrangement *A*. Upon taking into account a factor of about $\frac{2}{3}$ for the difference in efficiencies of the cloud chamber as a detector in the two cases, we can conclude that more than half of the

showers produced by the penetrating particles contained penetrating particles with a range greater than five inches of lead.

The number of penetrating particles per shower is difficult to estimate, particularly in arrangement *A* where the electron component would mask penetrating particles travelling in the same direction. However, the pictures of arrangement *B* indicate that, on the average, each shower contained one penetrating particle which penetrated five inches of lead.

(c) The electron cascade radiation usually exhibited energies in the range 1–5 Bev. These estimates were based on the size of the shower at its maximum and/or the longitudinal development of the electron shower. Since few electrons appeared in the cloud chamber in arrangement *B*, the "range" of the electronic shower component was less than five inches, as expected. Occasionally, a few low-energy electrons were distributed throughout the upper part of the cloud chamber in *B*, which indicated that the incident radiation had produced showers whose low-energy γ-ray residue reached the cloud chamber.

The electron shower component appeared to have a common origin with the penetrating particles in cases where the origin was clearly defined. There is some evidence for multiplicity at the origin which is based on the observation of an unusually wide lateral spread and/or separate shower cores in many of the mixed shower pictures. A direct comparison with showers that seem certainly to be electron or photon initiated leads one to believe that nearly all of the mixed showers are difficult to interpret in terms of a single-particle origin for the electron component. As a reference for electron or photon initiated showers, we select those which are frequently observed in pictures of Class II. These occur at a large zenith angle and hence the initiator misses the lead absorber above the cloud chamber. The electron cascade then originates in the first radiation length and never includes heavy particles. Showers that originate at all depths of lead with approximately equal probability occur much less frequently and, in addition, are usually mixed particle showers. Thus, there is considerable assurance that we actually can select single electron or photon initiated events for use in the observation of the

(a)

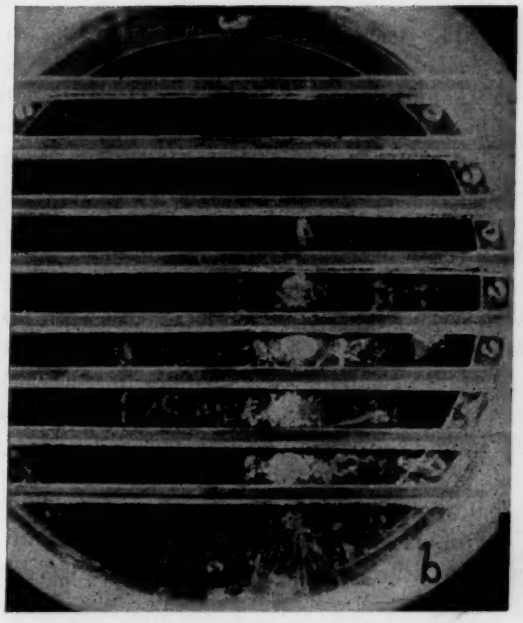

(b)

FIG. 4. (a) One of the cases of an electron shower with an extraordinary lateral spread, and, apparently, more than one shower core. The shower also has a slow heavy particle at the origin and a star in the fifth plate. (b) What is believed to be an ordinary single electron shower. The initiating particle struck the edge of the third plate while travelling down and back 45 degrees from the vertical, thus missing the 5 inch absorber as well as the first and second cloud-chamber plates.

development of a "normal" electron shower without in any way invoking preconceived ideas of the appearance of a "normal" shower as a selection criterion.

Examples of mixed showers where the cascade component is difficult to interpret except in terms of more than one energetic electron or photon at the origin are shown in Figs. 2a, 3a, and 4a. A shower initiated by a single electron is shown in Fig. 4b. The apparently unusual lateral spread of some of the showers may be due to a large admixture of penetrating particles, but the cases of separated cores seem difficult to interpret except as events in which the electron cascades were initiated by more than one ray with an appreciable angular separation at the shower origin.

The relative frequency of occurrence of showers with and without an energetic electron component is impossible to estimate from the present results, since the detecting system was highly selective for showers with a large number of particles.

(d) The occurrence of associated stars and slow heavy particles along the course of the showers and in the other parts of the cloud chamber is most reasonably explained by assuming that neutrons are also emitted in the initial disintegration. Some of the events might well be proton induced but there were two cases in which the star occurred outside the main shower core in a region where the nature of the initiating particle might be ascertained; it was non-ionizing in both cases. There were 15–20 associated stars or slow heavy particles in the photographs of mixed showers. A rough estimate of the number of protons and neutrons emitted from the shower centers can be made by assuming an average path for these particles of 25 g/cm² of lead in the cloud chamber and assuming an absorption coefficient of the order $(100\ \text{g/cm}^2)^{-1}$ corresponding to production of an observable star by energetic protons or neutrons. The result is an average of about one energetic neutron or proton per shower.

Since most of the associated slow particles occurred along the path of the shower or in its immediate vicinity, it is unlikely that they were produced by neutrons from the air. It is also unlikely that they were produced by photons since stars and slow particles occur infrequently in the electron cascades of air showers.

The lateral distribution of the associated slow particles shows that the producing neutrons have a rather wide angular distribution, in contrast to the angular spread of the energetic electronic component of the showers. This is additional evidence that the associated stars and slow heavy particles are not produced by photons.

4. CONCLUSIONS

The showers in Class I that we have observed frequently contained slow heavy particles and fast heavy particles, including occasional identifiable mesons in addition to the electronic radiation that was almost always present. From this we conclude that showers of this type result from nuclear interactions in which electrons and heavier particles are produced. The presence of these heavy particles proves that the electron component of the shower does not arise from simple radiation processes of mesons or any other particle.

5. BURSTS OBSERVED WITH SHIELDED IONIZATION CHAMBERS

Extensive measurements of the burst rates in shielded ionization chambers have been made, both at sea level and at higher elevations, and the fraction of bursts not caused by extensive air showers has been attributed to electromagnetic interactions of mesons.[5] The above conclusion about the nature of showers observed under lead at high altitude is not in agreement with this interpretation and the present results show that a large number of the bursts observed in ionization chambers must be the result of nuclear interactions in which electrons and heavier particles are produced. This applies strictly to showers in which the electron component develops at most to a maximum of 100–200 particles which corresponds to the minimum burst size in most previous ionization chamber measurements.

Even at sea level there is evidence that showers of the mixed particle type may contribute to the observed burst rate. The recent work of Fretter[2] gives evidence that the mixed shower intensity

[5] R. E. Lapp, Phys. Rev. 69, 321 (1946).

is roughly comparable to that of showers containing only electrons and believed to be meson induced. Of 52 showers containing electronic radiation, Fretter observed 30 with a heavy particle component and 22 without, all of which were initiated by penetrating particles in the lead plates of the cloud chamber. Since most of the showers were not very large, those containing penetrating particles would be able to set off the counter control located outside the cloud chamber more often than those that did not. Thus the cloud chamber was biased in favor of these events. However, Fretter points out that a considerable fraction of the mixed showers originated in the last two plates; in these cases the discrimination would be negligible. Thus it appears likely that, even at sea level, the mixed shower contribution to ion chamber bursts may not be negligible.

6. NUCLEAR DISINTEGRATION IN GENERAL

The nuclear disintegrations previously studied by one of us at 10,000 feet[6] showed a rapid increase of intensity with altitude[7] as do the "bursts" we have been discussing above. It was concluded at that time that the ionizing penetrating particles which were observed to produce many of the high energy disintegrations were not mesons because of the rapid altitude variation observed by Anderson.[7] Thus it seems likely that the nuclear disintegrations previously studied[8] and the mixed showers of the present discussion are results of the same type of interaction. The difference evidently is merely one of energy expended in the disintegration.

Thus, the existing evidence indicates that we can make the following tentative summary of the nuclear disintegrations at 10,000–14,000 feet resulting primarily when the strongly altitude-dependent penetrating particles (protons and neutrons?) make nuclear collisions in lead. The disintegrations (stars) where total energies of 50–200 Mev appear in the disintegration products seem to result in the ejection of heavy nuclear particles (protons, α-rays, etc.) and occasional mesons for the higher energy events. The initiating particles are predominantly neutrons but occasionally protons. It is not clear whether or not the initiating particle always loses most of its energy.

When the total energy of the disintegration products is 200–1000 Mev, slow and fast heavy particles, occasional identifiable mesons, and a few electrons are emitted. The initiating particles are about equally divided between neutrons and protons.

When the total energy is greater than 1000 Mev, slow and fast nuclear particles, occasional identifiable mesons, and energetic electronic radiation appear. In the present observations events initiated by ionizing penetrating particles (protons) were selected, but sea level observations without such selection indicate neutron initiation as well.[2]

From the present results one cannot say whether there are a large number of events in this high energy region in which a relatively small number ($\sim$10–20) of high energy penetrating particles are produced without being accompanied by high energy electrons. As has already been pointed out the detecting arrangement was insensitive to such events. Thus the observations seem to be consistent with an increase in the number of constituents with increase in energy released in the disintegration. However, in the case of electrons there may be different origins for low and high energies; the low energy electrons may have their origin in nuclear excitations whereas those of higher energy may originate in the decay of short lived mesons.[9] Hence it is not clear whether the appearance of high energy electrons as we go to high energy showers represents a threshold or a transition effect.

7. INITIAL MULTIPLICITY OF MIXED SHOWER COMPONENTS

There are varying degrees of quality in the evidence for initial multiplicity for the various shower components. It is certain that fast and slow penetrating particles occur multiply; there are a few examples of more than one identifiable meson per disintegration in the literature;[10]

[6] W. E. Hazen, Phys. Rev. **65**, 67 (1944).
[7] C. D. Anderson and S. H. Neddermeyer, Phys. Rev. **50**, 263 (1936).
[8] See also W. M. Powell, Phys. Rev. **69**, 385 (1946).
[9] H. Lewis, J. R. Oppenheimer, and S. Wouthuysen, Phys. Rev. **73**, 127 (1948).
[10] For example, see E. Hayward, Phys. Rev. **72**, 937 (1947).

there is some indication of initial multiplicity of the electron component in the present observations.

The initial angular divergence of penetrating particles appeared to be greater than that of the electron shower particles (assuming that the latter do have a multiple origin). If a sizeable fraction of the penetrating component is composed of mesons, the above observation is in conflict with the neutron meson hypothesis for the origin of the electronic component.[9] However, the apparent difference in angular divergence may not be real since the "range" of an electron of energy 50–100 Mev (which is typical of the energies of the penetrating particles occurring at large angle assuming they are mesons) is so short that it would not even be identified in many cases. It was not possible to compare angular divergences at high energies since the penetrating particles would be concealed by the cascade radiation; it is interesting to note, however, that there were no cases of narrow bundles of penetrating particles observed even under the favorable conditions of arrangement *B*.

8. APPLICATION TO INTERPRETATION OF EVENTS IN THE ATMOSPHERE

The marked altitude dependence of the showers produced by penetrating particles leads one to believe that the showers may be a characteristic of the primary particles or at least that the showers play an important role in determining the relationship among the various cosmic-ray components. If we apply the ideas deriving from observations of interactions in lead to the case of the atmosphere, the following tentative picture suggests itself, at least for initiating energies of perhaps 1–10 Bev. The collision of primary protons, or secondary protons and neutrons, with air nuclei results in multiple production of mesons and, directly or through a short-lived intermediary, in the production of electrons or photons of about the same energy as the mesons. In addition, neutrons and protons are emitted. As already pointed out by Bridge, Rossi and Williams,[1] the production of high energy photons or electrons by nuclear interactions may explain that part of the electron component which does not arise from the decay or other secondary processes of ordinary mesons.[11]

The degradation in energy of the penetrating particles evidently proceeds by more than one large step. The cloud-chamber evidence for this is twofold: first, the present observations and the sea-level observations[2] both showed events in which a penetrating particle that produced a high energy shower in the cloud chamber was accompanied by other penetrating particles (the latter indicating a precursory shower in the air); second, sea level observations[2,12] have produced examples of successive showers in the apparatus itself.

The protons and neutrons produce additional nuclear disintegrations but, because of the low density of electrons in the air shower at the level of observation, these disintegrations will appear to be unassociated with an electronic air shower component. In addition, the low energy disintegrations will occur at large lateral distances from the shower axis, because of the large average value of the initial angular divergence of the low energy neutrons and protons. Thus, as observed,[6,8] we expect the frequent occurrence of stars and low energy nuclear disintegrations that appear to be unassociated with air showers.

Ionization loss causes a rapid attenuation of the proton intensity for energies less than about 500 Mev and hence neutrons will predominate as the star-producing agent at low energies. The transition from production of disintegrations with nearly equal frequency by protons and by neutrons to production predominantly by neutrons does indeed occur at star energies of a few hundred Mev.[6]

The research was partially supported by the U. S. Navy Department, Office of Naval Research, under Contract N5 ORI-78. It is a pleasure to acknowledge the inspiration and ideas given to us by Professor Bruno Rossi: Much of the success of the expedition at Mt. Evans is due to the unfailing cooperation of the University of Denver Staff, particularly Drs. Cohn and Iona.

[11] Bernardini et al., Phys. Rev. **73**, 335 (1948).
[12] W. Fretter and W. Hazen, Phys. Rev. **70**, 230 (1946).

Measurements of the East-West Asymmetry of Cosmic Rays at Hobart, Tasmania

A. G. FENTON AND D. W. P. BURBURY
University of Tasmania, Hobart, Tasmania, Australia

(Received May 3, 1948)

Measurements of the high latitude asymmetry of cosmic rays have been made at Hobart in geomagnetic latitude 51.7° south. A Geiger counter telescope has been used at a zenith angle of 45° with and without 12.5 cm of lead absorber. The asymmetry is increased by a factor just over two when the lead is used. The increase indicates that the hard component of the radiation is responsible for the high latitude asymmetry, and the magnitude of the increase suggests a preferential absorption of negative particles by the lead.

I. INTRODUCTION

THE east-west asymmetry in cosmic-ray intensity observed at latitudes below the knee of the latitude intensity curve, i.e., below about 40–45° geomagnetic latitude, is explained by the deflections of the primary particles in the earth's magnetic field and the excess of positive primary particles, but should disappear at higher latitudes, where field sensitive primaries do not contribute appreciably to the radiation at sea level. A small asymmetry has been observed, however, at higher latitudes[1–5] and T. H. Johnson[6] has given a theory to account for this in terms of the deflection of the secondary penetrating particles while they are being slowed down by ionization in the atmosphere. Data obtained by T. H. Johnson[6] and F. G. P. Seidl[1] between 49° and 54° north geomagnetic latitude support the theory, but the probable errors of some of their results have been too large to test the theory adequately. Experiments have therefore been undertaken here to add to the data of the above workers. The apparatus has been running for some months and some significant results are already available.

The asymmetry is usually given as

$$A=(j_w-j_e)/\tfrac{1}{2}(j_w+j_e).$$

Values of the order of 0.01 have been found at high latitudes by Seidl, Johnson, and ourselves, compared with values more than ten times as large found near the magnetic equator.

II. APPARATUS

Six Geiger counters are used in two banks of three to form a telescope which is mounted in a yoke supported on a turntable. The telescope can be rotated round a horizontal axis to set the zenith angle, and the turntable rotated to obtain the azimuth setting. The axis of the turntable is set within one minute of arc of the vertical, making the zenith angle reproducible after each rotation with this accuracy, and the azimuth setting, which is maintained after each rotation by stops on the turntable, is accurate to within 1°.

The telescope has a sensitive solid angle extending nearly 17° either side of the zenith setting and about 25° either way in the direction perpendicular to this.

The two banks of counters are connected through a coincidence amplifier to a multivibrator which drives a post office call meter. The call meter, and electric clock, a barometer, and an "east-west" indicator are photographed by a 16-mm camera at intervals of four hours. The camera is controlled by a timing unit which also controls the rotation of the turntable from one setting to the other.

Use has been made of voltage regulator tubes to stabilize the various working voltages, and in particular the high voltage supply for the counter tubes uses a series of VR tubes in cascade, the working voltages being tapped from between the tubes or from potential dividers across the tubes.

The functioning of the coincidence circuit is

[1] F. G. P. Seidl, Phys. Rev. 59, 7 (1941).
[2] T. H. Johnson and E. C. Stevenson, Phys. Rev. 44, 125 (1933).
[3] E. C. Stevenson, Phys. Rev. 44, 855 (1933).
[4] J. C. Stearns and R. C. Bennett, Phys. Rev. 43, 1038 (1933).
[5] J. C. Stearns and D. K. Froman, Phys. Rev. 46, 535 (1934).
[6] T. H. Johnson, Phys. Rev. 59, 11 (1941).

TABLE I.

No lead	West	East	Average rate
Total counts	158,782	158,875	
Total time	888.67471 hr.	896.30249 hr.	
Cts/hr.	178.67±0.302	177.25±0.300	177.96±0.21
	$A=(j_w-j_e)/\frac{1}{2}(j_w+j_e)=0.00797\pm0.00239$		

TABLE II.

12.5 cm lead	West	East	Average rate
Total counts	57,491	65,117	
Total time	374.78250 hr.	432.75555 hr.	
Cts/hr.	153.39±0.432	150.47±0.397	151.93±0.29
	$A=0.0192\pm0.0038$		

tested by connecting the two inputs to the X and Y plates of a cathode-ray oscillograph. The separate pulses show as X or Y pips, and a coincidence shows as a pip at 45°. These can be checked against the clicks of the recorder. The coincidence circuit has been tested regularly in this way, and has had to be adjusted to compensate for a slight loss in efficiency on only two or three occasions.

The whole apparatus is housed in a shed built of "Masonite" sheets, situated away from neighboring buildings.

III. COMPUTATION OF THE RESULTS

Data have been obtained by running the telescope alternately in easterly and westerly directions for about four-hourly periods. Because of a slight variation in the timing unit the schedule of the runs tends to precess around the clock, and it has been assumed that this would cause any effect due to a daily variation in the intensity to cancel out over a period. It has also been assumed that, averaged over the time of operation of the apparatus, effects caused by variation of the barometric pressure, changes in the efficiency of the recording circuit, accidental coincidences, and shower coincidences would be small and affect the counting rates from the two directions equally, not influencing the final result very much.

The total counts and total times pertaining to each direction have been used in computing the counting rates, the probable errors of which have been taken as $\pm0.6745j/N^{\frac{1}{2}}$, where N is the number of counts used to obtain j. The probable errors of the asymmetry have been calculated from those of the counting rates.

The data and the results obtained from them are tabulated in Tables I and II. Table II contains those for the period when 12.5 cm of lead were placed between the two banks of counters to absorb the soft component of the radiation. In Fig. 1 these results are shown added to those of Seidl[1] and Johnson.[6]

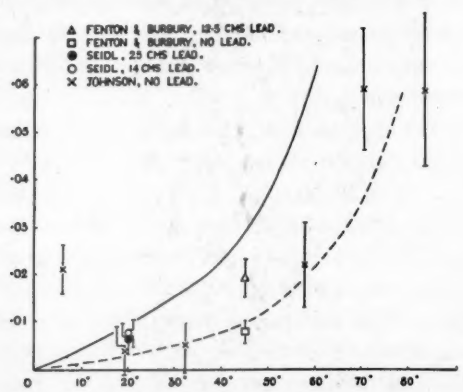

FIG. 1. The high latitude asymmetry of cosmic rays at sea level plotted against the zenith angle. The solid curve gives the values for the hard component of the radiation predicted by Johnson's theory,[6] assuming an energy distribution of mesons proportional to E^{-3} and a lower energy limit of 2.2×10^{8} ev. The broken curve is drawn through the "no lead" values (except that for small zenith angle) and represents the empirical assymmetry of the total radiation, i.e., the hard and soft components taken together.

IV. DISCUSSION

The increase in the asymmetry observed when lead absorber is used agrees with Seidl's observation.[1] The existence of the increase supports the supposition that the asymmetry in these latitudes is due to the hard component of the radiation, but the increase is greater than would be expected if the function of the lead were only to cut out a symmetrical soft component. If we take the intensity of the soft component in our observations to be 26.03 counts per hour (i.e., the difference between the average intensities in the two sets of results) and compute the asymmetry of the hard component by correcting the "no lead" results we find that $A=0.0095$, which is appreciably less than the value observed with the lead absorber. Thus it appears that the lead has enhanced the asymmetry by absorbing more of the radiation when the apparatus faced east than when it faced west. Seidl[1] has suggested that the increase in the observed asymmetry may be

due to a preferential absorption of the negative mesons by the lead, and the present results are in accord with this hypothesis.

If the assumption that the soft component is symmetrical be accepted as true, then the asymmetry of the hard component arriving at the apparatus should be given by calculation from the "no lead" measurements, and in view of the evidence that an absorber influences the results we are of the opinion that this procedure gives a more reliable value than that obtained directly. It is to be noted that this would give values falling on a curve slightly above the broken curve in the figure, and appreciably below the values predicted by Johnson's theory (the solid curve) for a lower energy limit of 2×10^8 ev.

From the data at present available it appears that Johnson's theory gives the form of the asymmetry *vs.* zenith angle curve but the values are slightly large. Further experiments are being conducted, and it may be possible to suggest some modification of the theory when more results are available.

ACKNOWLEDGMENTS

The authors have pleasure in expressing their sincere thanks to Professor A. L. McAulay for his ready advice and for stimulating discussions during the course of the work. We are very grateful to the Electrolytic Zinc Company, Ridson, Tasmania, for a grant for apparatus and to the C.S.I.R. for a grant which enabled one of us (D.W.P.B.) to take part in this research. It is a pleasure to acknowledge the encouragement received from Dr. T. H. Johnson when we first proposed to conduct these experiments. We would also like to thank Mr. R. L. Propsting for his enthusiastic help in the construction of the apparatus.

PHYSICAL REVIEW VOLUME 74, NUMBER 5 SEPTEMBER 1, 1948

A New Radioactive Series—The Protactinium Series*

MARTIN H. STUDIER AND EARL K. HYDE
Argonne National Laboratory, Chicago, Illinois

(Received May 20, 1948)

A new series of radioactive isotopes has been produced by deuteron and helium ion bombardments of thorium. The identity and the properties of the five members of this series, which is a branch of the uranium-radium series and joins it at RaC′, are shown to be the following:

$$\mathrm{Pa^{230}}\xrightarrow[17d]{\beta^-}\mathrm{U^{230}}\xrightarrow[20.8d]{\alpha(5.86\ \mathrm{Mev})}\mathrm{Th^{226}}\xrightarrow[30.9m]{\alpha(6.3\ \mathrm{Mev})}$$

$$\mathrm{Ra^{222}}\xrightarrow[38s]{\alpha(6.5\ \mathrm{Mev})}\mathrm{Em^{218}}\xrightarrow[0.019s]{\alpha(7.1\ \mathrm{Mev})}\mathrm{RaC'}\xrightarrow[1.5\times10^{-4}s]{\alpha}$$

$$\mathrm{RaD}\xrightarrow[22y]{\beta^-}\mathrm{RaE}\xrightarrow[5d]{\beta^-}\mathrm{RaF}\xrightarrow[140d]{\alpha}\mathrm{RaG\ (stable)}$$

A simple electronic device was developed to measure the short half-life of $\mathrm{Em^{218}}$.

1. INTRODUCTION

THREE radioactive series, the thorium series, the uranium-radium series, and the actinium series, are known to occur in nature. These series are often called the $4n$, the $4n+2$, and the $4n+3$ series, respectively, after the general formula for the mass numbers of the isotopes in each of the three series. For a long time a fourth series, the $4n+1$, was predicted and sought for, but it was not until the advent of artificial transmutation that such a series was

* This report is based on work done in 1946 under the auspices of the Manhattan District at the Metallurgical Laboratory, the University of Chicago.

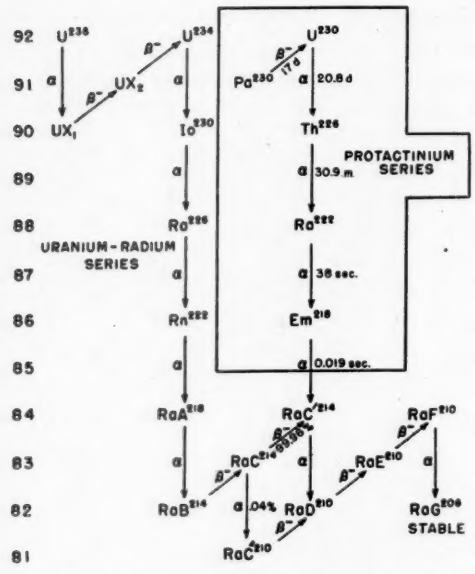

FIG. 1. Relation of the protactinium series to the uranium-radium series.

found.[1,2] This artificially produced decay chain is called the neptunium series after Np^{237}, the long-lived parent of the series.

From time to time individual, synthetically-made isotopes have been added to these main series as extensions or as one-member branches. The existence of a branch of the uranium-radium series consisting not of one but of a whole series of isotopes is reported in this paper. It is proposed to call this new series of synthetically-made isotopes, the protactinium series, after Pa^{230}, its first member.

In Fig. 1 the relation of the protactinium series to the uranium-radium series is presented.

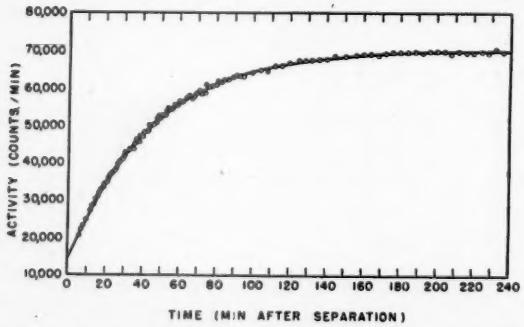

FIG. 2. Growth of alpha-activity in a sample of U^{230}.

[1] F. Hagemann, L. I. Katzin, M. H. Studier, A. Ghiorso and G. T. Seaborg, Phys. Rev. **72**, 252 (1947).

[2] A. C. English, T. E. Cranshaw, P. Demers, I. A. Harvey, E. P. Hincks, J. V. Jelley and A. N. May, Phys. Rev. **72**, 253 (1947).

2. THE PRODUCTION OF THE PROTACTINIUM SERIES

The protactinium series was originally produced by a $d,4n$ reaction in a 100-microampere-hour bombardment of thorium metal with 19 Mev deuterons and by an $\alpha,p5n$ reaction (with probably some contribution from an $\alpha,6n$ reaction) in a 30-microampere-hour bombardment of thorium metal with 38 Mev helium ions. The bombardments were carried out in the 60-inch cyclotron at the University of California by Dr. J. G. Hamilton, T. Putnam and the cyclotron crew. Their assistance is gratefully acknowledged.

The type of nuclear reaction in which more than two particles are ejected had been encountered in only one or two instances at the time that these experiments were begun. The $\alpha,p5n$ and $\alpha,6n$ reactions were probably observed for the first time in this work.

3. THE DISCOVERY OF THE PROTACTINIUM SERIES

The nuclear reactions which produced the protactinium series in the bombardments of thorium metal were accompanied by numerous other reactions such as d,n; d,p; α,n; α,p, etc. In addition, some deuteron and helium ion induced fission of the Th^{232} occurred. The resulting mixture of radioactive isotopes complicated the determination of the decay scheme of the new series.

One of the first clues, leading to the discovery of the new series was the decay of alpha-activity in the pure uranium fraction of the thorium-helium ion bombardment which indicated the presence of an isotope of uranium with a half-life of approximately three weeks. The uranium isotopes which could conceivably be present were those of atomic mass 235 or less; U^{235}, U^{234} and U^{233} are all so long-lived (10^5 years or more) that they would have shown no change in counting rate. A sample of the 70-year[3] U^{232} should show an increase of about ten percent per month from the growth of alpha-emitting daughters. Hence it was necessary to conclude that a new uranium isotope of mass 231 or less was present.

[3] R. A. James, A. E. Florin, H. H. Hopkins and A. Ghiorso, Plutonium Project Record **14B**, No. 22.8; Report CC-3860.

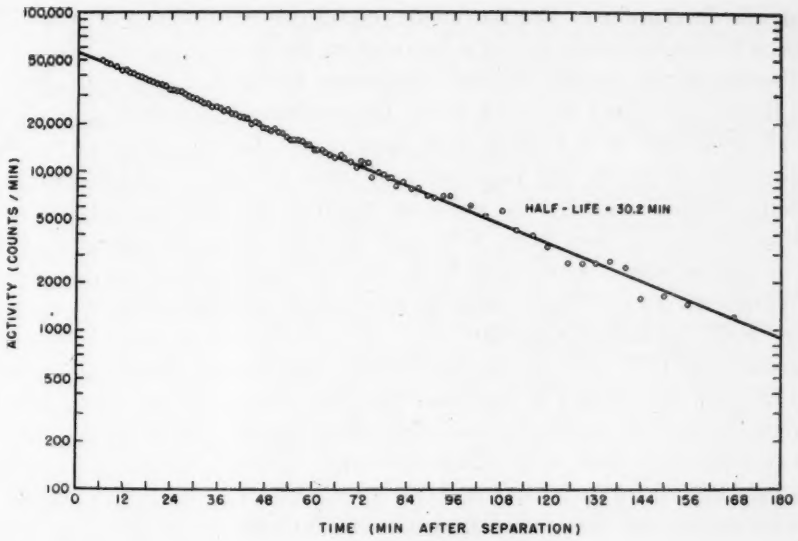

FIG. 3. Complement of the growth curve of a sample of U^{230}.

An examination of the alpha-particle energies of the activity in the uranium fraction a few hours after separation revealed the presence of five equally-abundant activities with energies greater than that of the U^{232} alpha-particle. The growth of the daughters of the uranium isotopes of mass 232 or higher would not be appreciable within a few hours. This is further evidence for a uranium isotope of low mass followed by four daughters with relatively short half-lives.

The rate of growth of daughters was determined by observing the increase of alpha-activity in a uranium sample very soon after purification. By extracting the uranium into ether and evaporating the ether directly on a platinum plate, it was possible to get the sample to an alpha-counter within six minutes after purification. There was an initial rapid growth of alpha-activity which had essentially reached its maximum after four hours, at a level of activity which was five times the activity present at the time of purification. (See Fig. 2.) This is further evidence for the presence of four alpha-emitting daughters of the new uranium isotope. A decay curve which is complementary to the exponential growth of Fig. 2 may be obtained by plotting on semi-logarithmic graph paper the difference between the equilibrium counting rate and the observed counting rate as a function of time. A curve obtained in this manner gave a straight line with a half-life period of one-half hour. (See Fig. 3.) The fact that four alpha-emitters grew in with this half-life indicates that the first daughter of the uranium, a thorium isotope, has the half-hour period and that the others have considerably shorter half-lives. After equilibrium had been reached, the total activity decayed with a half-life of three weeks.

When it was found that the uranium fraction from a deuteron bombardment of thorium also contained five distinct alpha-activities and decayed with the same half-life as the uranium fraction from the helium ion bombardment of thorium, the mass number 231 was eliminated from consideration. The fact that a uranium isotope could not be formed directly by a deuteron bombardment of thorium, but could only result from the beta-decay of a protactinium isotope, together with the fact that Pa^{231} is a long-lived alpha-emitter, justifies this elimination. Therefore the isotope was assumed to be U^{230}.

The next logical step, the search for a uranium daughter in the protactinium fraction, was carried out by isolating a protactinium fraction free from uranium and subsequently extracting a uranium fraction from this after a growth period of several days. The five new alpha-activities and a decay of total activity were observed in the uranium fraction so isolated. This experiment was repeated with the same results on the protactinium fraction of the thorium-helium ion bombardment. This repetition was important since the uranium isotope

in the helium ion bombardment could have been formed directly by an $\alpha,6n$ reaction or indirectly by an $\alpha,p5n$ reaction producing Pa^{230}, followed by a beta decay of Pa^{230}. The evidence indicates that an $\alpha,p5n$ reaction does occur. It does not eliminate the possibility of some U^{230} being formed directly by an $\alpha,6n$ reaction. It was calculated that more U^{230} was isolated in the first uranium separation from the thorium-helium ion target than could be accounted for by Pa^{230} beta-decay on the basis of the later growth of U^{230} into the protactinium fraction. This was interpreted as evidence for the occurrence of an $\alpha,6n$ reaction. Four alpha-disintegrations starting with U^{230} would produce $_{84}Po^{214}$ which is RaC′ of the uranium series. (See Fig. 1.) The energy of the most energetic of the five unknown alpha-emitters is indeed identical within experimental error with the 7.68 Mev energy of the RaC′ alpha-particle. (See Section 4.8.) If the original protactinium isotope were Pa^{229} or Pa^{228}, the resulting polonium isotopes would be Po^{213} or ThC′ with energies (8.28 Mev and 8.776 Mev respectively) much greater than that of RaC′. Furthermore, on theoretical grounds, the $d,5n$, the $d,6n$, the $\alpha,p6n$ and the $\alpha,p7n$ reactions required to produce Pa^{229} and Pa^{228} are probably not energetically possible with 19 Mev deuterons and 38 Mev helium ions.

4. EXPERIMENTAL PROCEDURE

4.1 *Milling and Chemical Treatment.*—The cyclotron targets in these bombardments consisted of thorium metal disks, 8 cm in diameter and 5 mm thick. The 25 by 65 mm rectangular area actually struck by the beam was located by inspection and by radiographs. The top layer of metal was removed from this area by clamping the disk in a special covered mount and milling off 0.030 inch. The millings, which amounted to 15 g of thorium metal, were dissolved and put through an extensive chemical separation scheme to isolate pure protactinium and uranium fractions free from fission products, decay products and other radioactive and inert impurities.

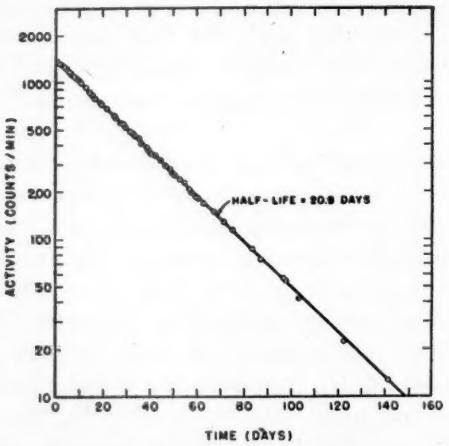

FIG. 4. Determination of the half-life of U^{230} from the decay of alpha-activity of a sample of U^{230} in equilibrium with its daughters.

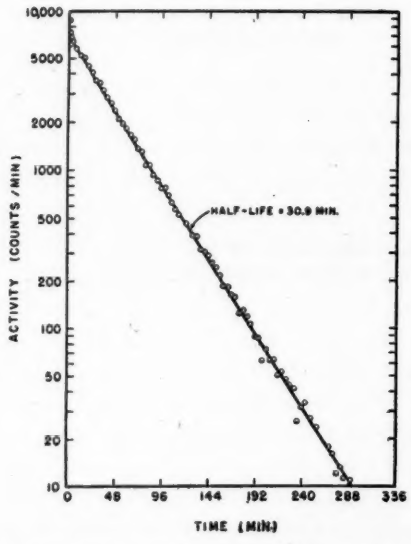

FIG. 5. Determination of the half-life of Th^{226} by the decay of alpha-activity from the recoil atoms of U^{230}.

Samples of these fractions were used in the studies described below.

4.2 *Determination of the half-life of* U^{230}.—Samples of U^{230} were prepared by extracting the uranium which had grown into an originally pure protactinium fraction. Several protactinium isotopes besides Pa^{230} were present. Pa^{233}, Pa^{232} and Pa^{231} were formed in the deuteron bombardment by d,n, $d,2n$ and $d,3n$ reactions, respectively. (In the helium ion bombardment these isotopes were formed by $\alpha,p2n$, $\alpha,p3n$ and $\alpha,p4n$ reactions respectively. The $\alpha,p4n$ reaction was not specifically observed.) Pa^{231} offered no complications because it is a long-lived alpha-emitter. The U^{233} daughter of Pa^{233} is so long-lived that the presence of Pa^{233} does not interfere with the preparation of a U^{230} sample. However, it does complicate the characterization of the beta-

radiation of Pa^{230} since the half-life of Pa^{233} (27.4 days)[4] is close to that of Pa^{230} (17 days). This necessitated the indirect determination of this half-life as described in Section 4.5. The presence of the 1.33 day[5] Pa^{232}, which decays to a 70-year U^{232} daughter, made impossible the isolation of a uranium sample suitable for the half-life determination of U^{230} as long as it was present. This difficulty was eliminated by letting the protactinium activity decay 16 days. By this time the Pa^{232} had decayed to 0.1 percent of its original value while the Pa^{230} had decayed by only about half. At the end of this period the uranium was completely separated and discarded. Pure U^{230} was permitted to grow in for a period of a week and then isolated from the protactinium. Samples of this uranium were mounted on platinum counting disks for following changes in alpha activity.

It was early discovered that samples of U^{230} would leave a residual activity in the counter upon removal. This was first thought to be due to an emanation, but experiments to be described below (Section 4.4) demonstrated that it was due to recoiling nuclei from the energetic disintegrations of U^{230} and its alpha-emitting daughters. This behavior was later found to be very useful (see Sections 4.3 and 4.6), but in counting samples for the decay of U^{230} it was necessary to consider the danger of erratic results due to loss of recoil atoms. This difficulty was resolved in two ways: (1) by permitting the sample to come to equilibrium in the counter before making a count, and (2) by covering the sample with a light film of zapon to prevent the recoil atoms from excaping.

A U^{230} decay curve is shown in Fig. 4. A "least squares" treatment of the data yielded 20.8 days for the half-life.

4.3 *Identification of* Th^{226} *and the determination of its half-life.*—It was postulated above from the characteristic growth of alpha-activity of a sample of U^{230} (Figs. 2 and 3) that the first daughter of U^{230}, Th^{226}, has a half-life of approximately one half-hour. This was shown to be correct by a chemical isolation of the thorium.

The thorium was isolated by coprecipitation with zirconium iodate which is known to be a specific carrier for thorium. Zirconium nitrate was added to a dilute nitric acid solution of U^{230} in equilibrium with its daughters, and zirconium iodate was precipitated by the addition of iodic acid. The precipitate was dissolved with sulfur dioxide, reprecipitated with iodic acid, and mounted on a counting disk. The rate of decay of alpha-activity was determined, and a half-life of 31 minutes was found.

With the Th^{226} positively identified, a more accurate value of the half-life was determined by following the decay of recoil activity left in an alpha-counter after removal of an active sample of U^{230} (100,000 alpha-counts per minute) which had been in the counter for an hour. An initial activity of over 8000 counts per minute decayed to the background of the counter. (Any contribution by "aggregate" recoil to the recoil activity must be negligible since no long-lived

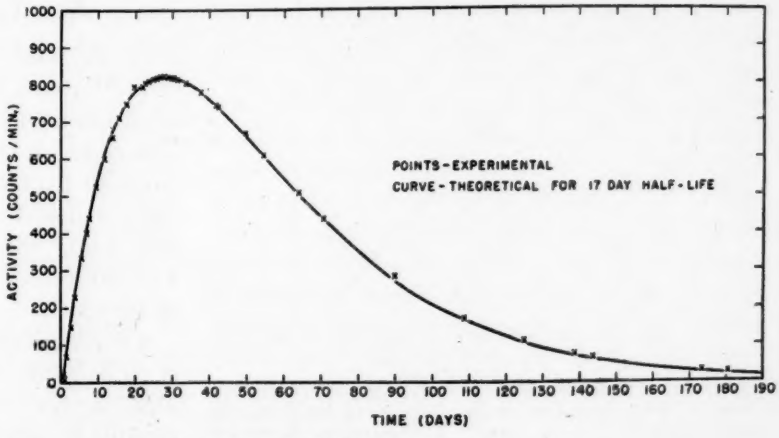

FIG. 6. Determination of the half-life of Pa^{230} from the growth and decay of daughter alpha-activity.

[4] A. V. Grosse, E. T. Booth and J. R. Dunning, Phys. Rev. 59, 322 (1941).
[5] A. H. Jaffey and E. K. Hyde, Plutonium Project Record 17B, No. 9.20; Report ANL-4102.

component due to U^{230} was found in the recoil atom decay curves.) (See Fig. 5.) The small amount of short-lived activity indicated by the beginning of the curve was later shown to be due to Ra^{222}. The half-life obtained for Th^{226} is 30.9 minutes. This is slightly greater than the value obtained from analysis of the growth curve (Fig. 3) because in the latter case the approximation was made that the U^{230} activity was constant during the time of growth.

4.4 *The emanation isotope.*—It was mentioned above that the 30.9 minute contamination of the alpha-counter by samples of U^{230} was thought at first to be due to the emanation isotope, $_{86}Em^{218}$. However, this was shown not to be the case even before the 30.9 minute activity was identified with Th^{226} by the following evidence: (1) Replacing the air in the contaminated chamber did not remove the contamination. (2) Placing in the counter an active U^{230} sample covered with two baffle plates, which permitted the escape of an active gas by an indirect route but offered no direct path for the escape of a recoil atom, did not result in any measurable contamination of the chamber.

These experiments demonstrated that the contamination was due to recoiling nuclei. They do not disprove the existence of an emanation but merely indicate that if it exists it must be short-lived. To set an upper limit on the half-life of the emanation a series of experiments was performed by P. Fineman, B. Weissbourd and T. P. Kohman. They arranged to flush the gas emerging from a boiling solution of U^{230} directly into a special alpha-counting chamber. This was done without detecting any counts above background. From their work they set an upper limit of one second for the half-life of Em^{218}. This half-life was later determined to be 0.019 sec. by an electronic coincidence method. (See Section 4.7.)

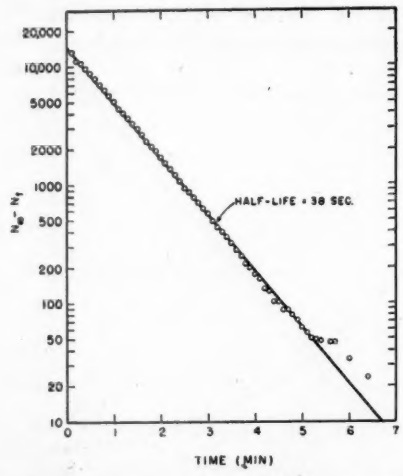

FIG. 7. Determination of the half-life of Ra^{222} by the decay of recoil activity from a Th^{226} sample. N_∞ = total counts observed on complete decay. N_t = total counts observed to any given time.

This short half-life excludes the possibility of chemical identification of Em^{218} and the evidence for the existence of the isotope is indirect, resting on the over-all evidence for the series and particularly on the identification of its RaC′ daughter by energy measurements.

4.5 *Determination of the half-life of* Pa^{230}.—The direct determination of the half-life of Pa^{230} using the protactinium fractions of the thorium bombardments was rendered difficult because of the presence of Pa^{233}. Hence indirect methods were used.

A preliminary value was obtained by extracting and measuring the U^{230} produced in equal periods of time from a sample of protactinium. In this manner a crude half-life value of about two weeks was obtained.

A more accurate value was obtained by mounting a sample of Pa^{230} on a platinum counting disk and following the rate of change of the alpha-activity of the sample. Such a growth and decay curve is shown in Fig. 6. By substituting the half-life of U^{230} determined above into the standard growth equation,

$$N_2 = N_{01}(\lambda_1/\lambda_2 - \lambda_1)(e^{-\lambda_1 t} - e^{-\lambda_2 t}),$$

where N_2 = number of U^{230} atoms, N_{01} = number of Pa^{230} atoms initially present, t = time, λ_1 = disintegration constant of Pa^{230}, and λ_2 = disintegration constant of U^{230}, theoretical curves for various half-lives of Pa^{230} can be calculated and compared with the experimental curves. In this way using three separate samples a value of 17.0 ± 0.5 days was determined for the half-life of Pa^{230}.

4.6 *Identification of* Ra^{222} *and the determination of its half-life.*—From the failure to observe any alpha-activity in a radium fraction, isolated rapidly by chemical precipitation of a barium chloride carrier from an active solution of U^{230}

in equilibrium with its daughters, an upper limit of one minute was set on the half-life of the radium isotope. Although attempts to identify the Ra^{222} chemically were unsuccessful, an alpha-emitting Th^{226} is proof of its existence. It will be recalled that the decay of recoil activity from a U^{230} sample (Fig. 5) indicated the presence of a short lived component with a half-life of the order of half a minute. Since both Em^{218} and RaC′ have half-lives much shorter than a second, this activity must be due to Ra^{222}. It was also noted that a sample of Th^{226} leaves a recoil activity in an alpha-counting chamber after the sample is removed, and the decay of this activity was used to determine the radium half-life.

To get a maximum amount of recoil from a Th^{226} sample, thorium was isolated with a minimum of carrier from a solution containing 100,000 counts per minute of U^{230} and mounted on a platinum disk. By inserting this disk in a standard alpha-counting chamber for a few minutes it was possible, because of the recoil phenomenon, to introduce several thousand counts per minute of Ra^{222} into the chamber. The Th^{226} was then removed and the recoil activity was measured at intervals of 0.1 minute until decay was complete.

It was necessary to measure the activity at such short intervals of time because of the short half-life of Ra^{222}, and as a result the statistical fluctuations were rather severe. An integral decay curve was plotted to minimize the scatter of points. The error, which would result from the use of the usual differential curve because the duration of each measurement was an appreciable fraction of a half-life, was also eliminated. By subtracting N_t, the total number of counts up to a given time, from N_∞, the total number of counts observed on complete decay, and plotting the difference, $N_\infty - N_t$, on a logarithmic scale as a linear function of time, a straight line was obtained, the slope of which determined the half-life. Such a curve is shown in Fig. 7. The half-life of Ra^{222} based on four such determinations is 38.0 seconds.

4.7 *The measurement of the half-life of* Em^{218}.— A simple electronic circuit which can be used to measure the time intervals between the emission of successive alpha-particles was devised to measure the half-life of the emanation isotope.

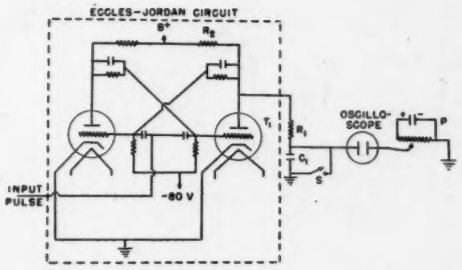

FIG. 8. Diagram of electronic circuit used to measure short time intervals between successive pulses.

In the decay chain

$$A \xrightarrow{\alpha} B \xrightarrow{\alpha} C$$

let A be the (long-lived) parent of B, the half-life of which is to be measured.The instant that the atom A emits an alpha-particle the atom B is formed, and the time elapsing until B emits an alpha particle is the lifetime of B. An average of a number of measured time intervals between the successive disintegrations of A and B gives the mean life of B which is equal to $1/\lambda$ where λ is the decay constant of B. The half-life is then given by $0.693/\lambda$.

A schematic diagram of the circuit which was used for the measurement of the short time intervals between pulses is shown in Fig. 8. A resistor, R_1, in series with a condenser, C_1, was connected between the plate and cathode of one of the tubes, T_1, in the first trigger pair in the scaling circuit of a standard alpha-counter. The horizontal deflecting plates of an oscilloscope were connected across the condenser, C_1, through a potentiometer, P, which was included in the circuit to control the horizontal position of the fluorescent spot on the oscilloscope screen. The scaling pair was of the Eccles-Jordan type[6] with 6C5 triode tubes. Such a trigger pair exhibits two stable states in which one tube is conducting while the other is non-conducting. A pulse fed to the grids of the pair will cause the tubes to reverse from the one stable state to the other in a few microseconds. Because of the potential drop across the plate resistor, the plate voltage of a tube in the conducting state is much lower than that in the non-conducting state. Whenever a pulse is fed to the grids of the scaling

[6] W. H. Eccles and F. W. Jordan, Radio Rev. 1, 143 (1919).

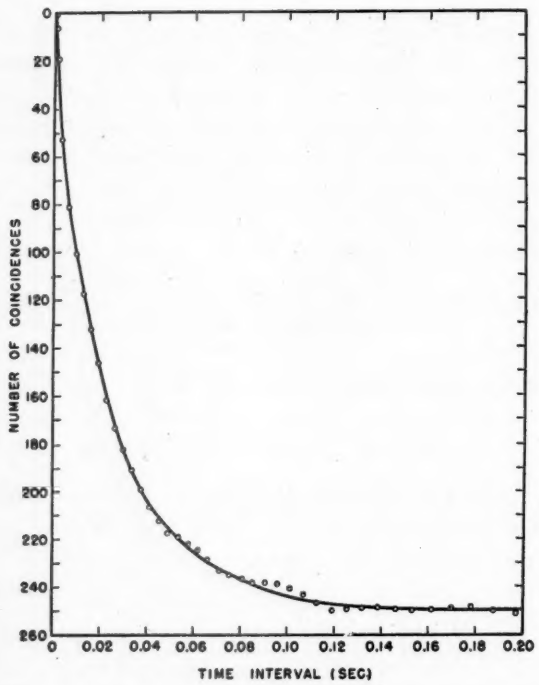

FIG. 9. Integrated frequency distribution of Ra^{222}-Em^{218} coincidences representing the exponential decay of Em^{218}.

pair, there is a sudden change in the plate voltage of tube, T_1, which is reflected in a change in voltage across condenser C_1.

The circuit was operated as follows: The potentiometer, P, was adjusted until the fluorescent spot was at the extreme right of the oscilloscope screen when tube, T_1, was in the conducting state. A pulse caused by alpha-disintegration in the ionization chamber of the counter would cause tube, T_1, to change to the non-conducting state with a consequent sudden rise in plate voltage. Condenser, C_1, would charge through R_1 and R_2 at a rate dependent on the time constant, $(R_1+R_2)C_1$. As the voltage across the condenser increased, the spot moved across the screen. If another alpha-disintegration occurred during the period of the sweep, the stable states of the trigger pair would again reverse and the spot would return to its original position as the condenser discharged. The distance that the spot traveled across the screen was a measure of the time interval between the two successive alpha-disintegrations. Such "coincidences" were observed visually with the aid of a calibrated screen. A sine wave from an oscillator was put in the vertical deflecting plates of the scope to give a moving band which was more easily observed than a moving spot. Resistor, R_1, and condenser, C_1, were so chosen that the sweep was about 0.2 sec. If a single alpha-disintegration occurred, the spot would move across the screen and off the other side. It could be brought back to its original position by shorting out condenser, C_1, with the switch, S.

A time calibration of the sweep is dependent on the time constant of the circuit, the voltage difference between the conducting and non-conducting states of tube, T_1, and the sensitivity of the oscilloscope. The time constant, $(R_1+R_2)C_1$ was 0.1658 second, the voltage difference was 235 volts, and the sensitivity of the oscilloscope was 43 volts per inch. The equation for the instantaneous potential difference between the horizontal deflection plates of the oscilloscope was

$$v=235(1-e^{-t/0.1658}).$$

From the above equation and the sensitivity of the oscilloscope a calibration curve was constructed relating time with sweep distance.

It is necessary to consider the possibility of chance coincidences between alpha-particles arising from the background of the sample and counter. The relative number of such random coincidences can be minimized by using low-counting rate samples and low-background counters. Although it may not be feasible to eliminate the background effect completely, corrections can be made for random coincidences. Since the time distribution of particles emitted from a long-lived radioactive substance is purely random, the probability that n particles arrive in time, t, is given by the Poisson equation,

$$W_n=(x^n e^{-x}/n!),$$

where x is the average number of particles which arrive in time, t. In the experimental apparatus the emission of an alpha-particle starts the sweep on the oscilloscope. Since for a purely random distribution the probability of a future event is not affected by the previous occurrence of an event, the chance that another particle arrives during the period of the sweep is given by the Poisson equation. Thus it is only necessary to determine the number of random alpha-

disintegrations to correct for random coincidences.

In order to obtain a high ratio of true coincidences to random events a high geometry factor is essential. A geometry factor approaching 100 percent was obtained by mounting the samples on a very thin film of zapon supported on a 0.002-in. wire ring about one cm in diameter. The samples were supported in a vertical position between the parallel plate electrodes of the ionization chamber of the counter.

The half-life of Em^{218} was obtained by measuring the time interval up to 0.2 sec. between successive alpha-particles from a sample of U^{230} in equilibrium with its daughters. The half-life of RaC′ is so short and the resolving time of the counter which was used was so long that in most cases the arrival of alpha-particles from Em^{218} and RaC′ were recorded as a single event. When the pulse due to the RaC′ alpha-particle was resolved, it resulted in "triple" coincidences; thus if the Ra^{222} alpha-particle starts the sweep, the Em^{218} alpha-particle reverses it, and the RaC′ alpha-particle reverses it again. Only about three percent of the total observed coincidences were such triple coincidences, and they were neglected. It can be seen from the decay chain that half of the alpha-particles will be observed as true Ra^{222}-Em^{218} coincidences. The half-life of Ra^{222} is so long by comparison with the sweep time that relatively few Th^{226}-

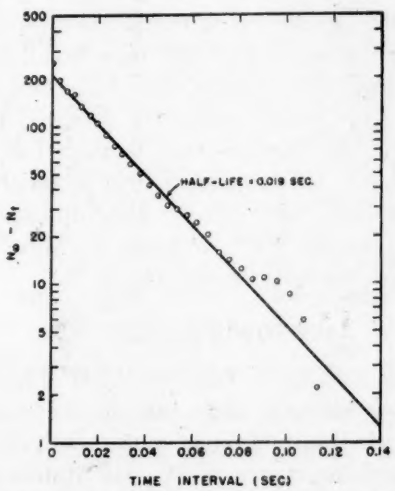

FIG. 10. Decay curve of Em^{218}. N_∞ = total number of observed coincidences. N_t = number of coincidences observed within the time interval, t.

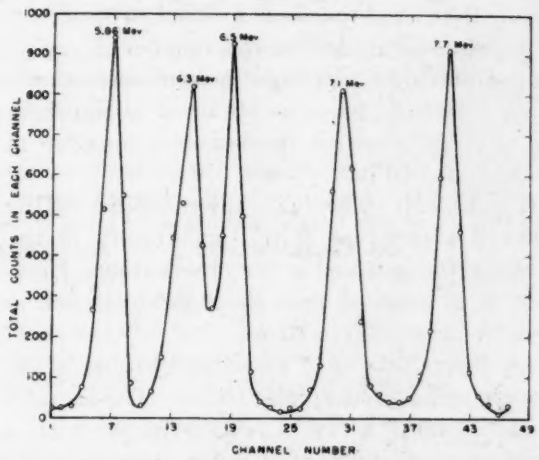

FIG. 11. Alpha-spectrum of the protactinium series as obtained with a multi-channel, differential pulse analyzer.

Ra^{222} coincidences occur. Those that do occur will result in triple coincidences. The total random counting rate is that due to U^{230} and Th^{226}, or half the total counting rate. (The background of the counter was negligible.) Since two alpha-particles are involved in each coincidence, the total number of random events will be twice the number of coincidences. The average total disintegration rate of the sample was 12.3 per minute. The probable number of random coincidences was calculated for the observed time intervals and subtracted from the recorded number of coincidences. The correction varies almost linearly with time over the range represented by the period of the sweep. About 4 percent of the total coincidences observed within 0.2 sec. were estimated to be due to random events.

Figure 9 shows the frequency distribution of the observed time intervals after correction for random events. The total number of observed coincidence periods equal to or less than a given time interval is plotted against the time interval. The integral curve so obtained is exponential within the errors of the experiment and represents the decay of Em^{218}. The mean interval is 0.027 sec. corresponding to a half-life of 0.019 sec.

The same value was obtained by the following graphical analysis. Since the maximum interval observed is greater than ten half-lives of Em^{218}, essentially all of the coincidences which occurred were observed. By subtracting N_t, the number of coincidences observed within a given time in-

terval, from N_∞, the total number of observed coincidences, and plotting this number, $N_\infty - N_t$, against the time intervals on semi-logarithmic paper a straight line was obtained as shown in Fig. 10. The slope of the line is a measure of the half-life of Em^{218}.

It is difficult to evaluate the reliability of the above data because of the uncertainty of the human error involved in the observations. However, it is believed that the half-life is not in error by more than 0.002 sec.

4.8 *Determination of the alpha-energies of the members of the protactinium series.*—The energies of the alpha-particles were determined with a multi-channel, differential pulse analyzer.[7] The instrument which was used has 48 electronic channels which register all the alpha-pulses within a selected range of energies. Each channel records only the pulses falling within a narrow energy band; the 48 channels cover contiguous energy bands of equal width increasing in energy from channel No. 1 to channel No. 48. By plotting the total number of alpha-counts per channel against channel number, a peak will be observed for each alpha group. The position and size of the peak measure respectively the energy and abundance of the alpha group.

Figure 11 shows the entire series of peaks in the protactinium series. These correspond to U^{230}, Th^{226}, Ra^{222}, Em^{218} and RaC′. To determine the energies it was necessary to calibrate the instrument with several isotopes whose known energies are approximately the same as those of the protactinium series. Among these standards was a preparation containing RaC′ which served to establish the identity of the most energetic alpha in the protactinium series. With the aid of these standards the unknown energies were estimated to be 5.8_6 Mev, 6.3 Mev, 6.5 Mev, 7.1 Mev and 7.7 Mev.

The question of the assignment of each energy to the proper isotope remained. The RaC′ assignment was the only certain one in the beginning. The assignment of the energy of the U^{230} alpha-particle was made very definite by means of two experiments:

(1) An active sample of pure Pa^{230} was permitted to decay to U^{230} for several days. Then a rapid extraction was performed to remove uranium. A sample of the U^{230} was quickly inserted in the pulse analyzer instrument and the alpha-spectrum was measured before the daughter isotopes had time to grow into their equilibrium value. The alpha-spectrum was redetermined after several hours when the daughter isotopes were in equilibrium. The 5.8_6 Mev peak, which was prominent in the first curve, was assigned to U^{230} and its relation to the other peaks was established by the second curve.

(2) In a second experiment a two-inch aluminum disk was fastened to the upper electrode of a standard alpha-counting ionization chamber and used to collect recoil atoms from a very active sample of U^{230} placed on the lower electrode. This disk was quickly removed and subjected to pulse analysis. All peaks except the 5.8_6 Mev peak were present, which confirms the assignment of this peak to U^{230}.

Note added in proof: On the basis of a re-analysis of pulse-analyzer data on the protactinium series isotopes, A. H. Joffey reports the following revised figures for the first four alpha-energies: 5.85 ± 0.01 Mev, $6.30 \pm 0.02_5$ Mev, 6.51 ± 0.03 Mev, and $7.12 \pm 0.02_5$ Mev.

This leaves three energies to be assigned. A rigorous assignment is made very difficult because of the short half-lives and because of the rapidity with which these isotopes come into equilibrium with each other. Experimental methods are known by which such a problem may be solved, but up to the present the necessary instruments have not been available to perform such experiments. Hence the remaining energies have been tentatively assigned to the isotopes in the inverse order of their half-lives. Thus the 6.3 Mev alpha-particle is assigned to the 30.9 minute Th^{226}, the 6.5 Mev alpha-particle to the 38 second Ra^{222}, and the 7.1 Mev alpha-particle to the 0.019 second Em^{218}.

ACKNOWLEDGMENTS

Thanks are due A. Ghiorso, A. H. Jaffey and H. P. Robinson for assistance in the measurements with the differential pulse analyzer. The advice and assistance of W. M. Manning and G. T. Seaborg under whose general supervision this work was done are gratefully acknowledged.

[7] A. H. Jaffey, Plutonium Project Record **14A**, Chap. XVI; A. Ghiorso, A. H. Jaffey, H. P. Robinson and B. Weissbourd, Plutonium Project Record, **14B**, No. 16.8.

Radiations from Platinum (193) and Gold (199)*

C. E. MANDEVILLE, M. V. SCHERB, AND W. B. KEIGHTON**
Bartol Research Foundation of the Franklin Institute, Swarthmore, Pennsylvania

(Received May 27, 1948)

The 4-day platinum activity, Pt^{193}, was induced in metallic platinum irradiated by neutrons in the pile at Oak Ridge. This isotope was found to emit conversion electrons of energy 0.115 Mev and x-rays of energy 70 kev. Beta-gamma-coincidence measurements showed that the conversion electrons are coupled with little or no gamma-ray energy. Gamma-gamma-coincidences, probably gamma-(x-ray) coincidences, were found in Pt^{193}.

Aluminum absorption gave a maximum energy of 0.38 Mev for the beta rays of the 3.3-day Au^{199}; lead absorption indicated gamma-radiation of energy 0.18 Mev. Beta-beta- and beta-gamma-coincidences were present in Au^{199}, but no gamma-gamma-coincidences were found. The absorption and coincidence measurements are combined to construct a disintegration scheme for Au^{199}.

1. INTRODUCTION

THE 4-day platinum (193) and the 3.3-day gold (199) were prepared when platinum was irradiated by slow neutrons in the pile at Oak Ridge. Platinum and gold were chemically separated, and the two fractions were subjected to further chemical purification. In the case of both isotopes, measurements of the energies of the beta- and quantum-radiations were carried out by coincidence and absorption methods which have been previously described.[1] For all coincidence measurements, a coincidence resolving time of 0.10 microsecond was employed.

2. PLATINUM (193)

It has been previously shown that the 4-day platinum period emits x-rays, gamma-rays, and soft beta-rays.[2–4] Krishnan and Nahum[3] have obtained a beta-ray energy of 0.12 Mev and have concluded from the shape of the absorption curve that only a line spectrum of conversion electrons is present. They also reported intense x-radiation and have concluded that the isotope decays by K-electron capture. More recently, Wilkinson,[4] has reached the same conclusion by bombardment of platinum by deuterons and fast and slow neutrons, and by bombardment of iridium by deuterons and alpha-particles. He has also reported x-rays, beta-rays of energy 0.1 Mev, and gamma-rays of energy 1.7 and 0.17 Mev.

The platinum fraction of the present experiments was chemically purified for the removal of iron, copper, iridium, and gold. The data of Fig. 1, an absorption curve of the beta-rays of the platinum fraction, were taken eleven days after removal of the platinum from the pile and five days after chemical purification. From the figure, it is clear that the conversion electrons of Pt^{193} have a maximum range of 0.018 g/cm² in aluminum, corresponding to an energy of 0.115 Mev.[5] In addition, it is also evident that a continuum of beta-rays having a visual end point at about 0.16 g/cm² of aluminum is also present. Feather analysis yielded an end point at 0.18 g/cm², corresponding to an energy of 0.56 Mev.[5] This continuum was attributed to the presence of Ir^{192}, indicating an incomplete chemical separation.

The beta-gamma-coincidence rate for Pt^{193} and accompanying iridium contamination is shown in Fig. 2 where it is seen to reach a constant value in the region of 0.018 g/cm² of aluminum placed before the beta-ray counter. The low value of the beta-gamma-coincidence rate at very low absorber thickness is attributed to the presence of the conversion electrons of Pt^{193} which are apparently coupled with less

* Assisted by the Office of Naval Research.
** Also of the Department of Chemistry, Swarthmore College.
[1] C. E. Mandeville and M. V. Scherb, Phys. Rev. **73**, 141 (1948).
[2] E. McMillan, M. Kamen, and S. Ruben, Phys. Rev. **52**, 375 (1937).
[3] R. S. Krishnan and E. A. Nahum, Proc. Camb. Phil. Soc. **37**, 422 (1941).
[4] Geoffrey Wilkinson, Phys. Rev. **73**, 252 (1948).
[5] L. E. Glendenin, Nucleonics **2**, No. 1, 12 (1948).

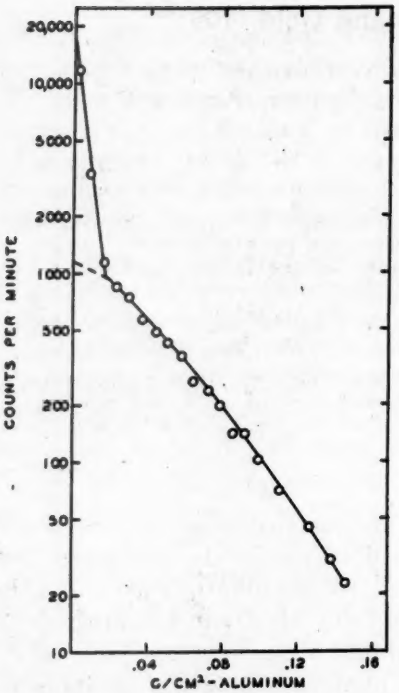

FIG. 1. Absorption in aluminum of the beta-rays of the 4-day Pt^{193}. The curve gives evidence of a line spectrum of conversion electrons of Pt^{193} superposed upon a continuum of low intensity. The continuum is ascribed to the 68-day iridium (192), present as a contaminant.

gamma-ray energy than the nuclear beta-rays of the 68-day iridium contamination. The beta-gamma-coincidence measurements are particularly sensitive to the presence of very small quantities of contamination, since beyond 0.018 g/cm² of aluminum, only the beta-rays of iridium (192) reach the beta-ray counter. The two geometries, *A* and *B*, of Fig. 2 were calibrated by the beta-gamma-coincidence rate of Sc^{46}. It was thus found that on the average, each beta-ray of the contaminant was followed by 0.6 Mev of gamma-ray energy, a known characteristic of Ir^{192}. Furthermore, as the 4-day Pt^{193} continued to decay, the points on the beta-gamma-coincidence curve below 0.018 g/cm² were found to rise to the level of the other points of the curve.

From the beta-gamma-coincidence curve, it can be concluded that the conversion electrons of the 4-day platinum are accompanied by considerably less than 0.6 Mev of gamma-ray energy and probably by no gamma-rays at all. Wilkinson[4] has reported a gamma-ray of energy 1.7 Mev to be related to the 4-day period. This gamma-ray is obviously non-coincident with the conversion electrons. No search for gamma-rays of this energy was made in the course of the investigations described in this paper.

About twelve days after removal of the irradiated material from the pile and six days after chemical purification, a beta-beta-coincidence curve was obtained, using the platinum fraction as a source. These data are given in Fig. 3. The curve is seen to have a peak in the vicinity of 0.018 g/cm² of aluminum. This curve is actually the beta-beta-coincidence curve for the 68-day iridium contamination, the first two points being reduced in magnitude by the presence of the conversion electrons of the 4-day platinum which are apparently not coupled with other beta-rays.†

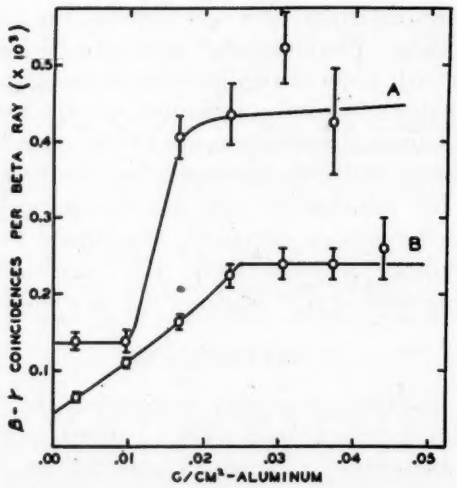

FIG. 2. Beta-gamma-coincidence curve for the platinum fraction. The coincidence rate below 0.018 g/cm² is reduced, owing to the presence of the conversion electrons of Pt^{193}. Beyond this value of absorber thickness, the beta-gamma-coincidence rate indicates that each beta-ray is followed by 0.6 Mev of gamma-ray energy, a characteristic of Ir^{192}. Since the conversion electrons of Pt^{193} are completely stopped by 0.018 g/cm² of aluminum, the remainder of the curve is very sensitive to the presence of any contamination, however small.

Curve *A* was taken with 0.2 g/cm² of aluminum before the gamma-ray counter whereas curve *B* was taken with 2.16 g/cm² of aluminum before the gamma-ray counter. The increased coincidence rate owing to the reduced absorber thickness before the gamma-ray counter simply indicates that the gamma-rays involved are for the most part relatively soft. Both geometries were calibrated by the beta-gamma-coincidence rate of Sc^{46}.

† In making the beta-beta coincidence measurements, the aluminum absorbers were placed before *both* of the beta-ray counters.

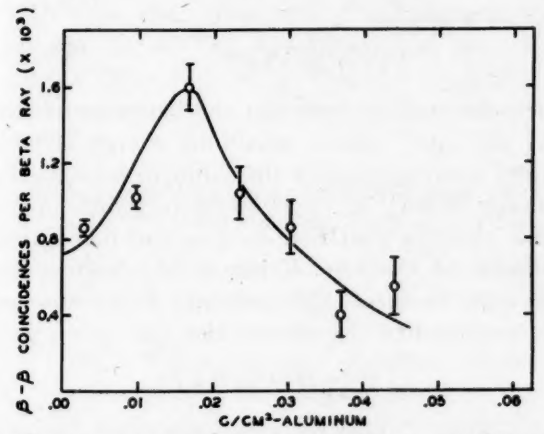

FIG. 3. Beta-beta-coincidence rate of the platinum fraction. As in the case of the beta-gamma-curve of Fig. 2, this curve is in reality characteristic of Ir^{192}. Instead of being purely exponential as is actually the case, the points below 0.018 g/cm² are reduced by the presence of the conversion electrons of Pt^{193} to give a "peaking" effect in the curve.

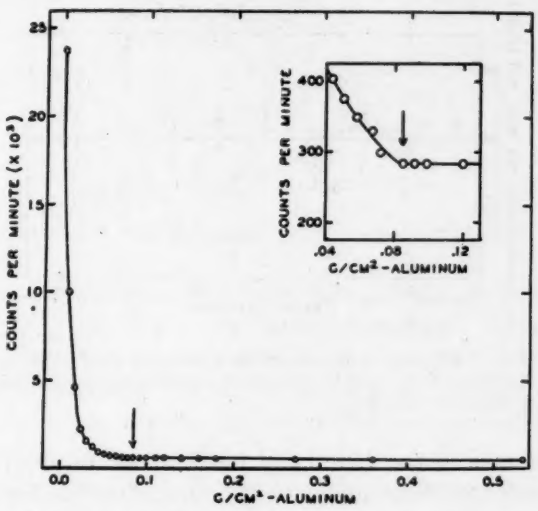

FIG. 4. Absorption in aluminum of the beta-rays of gold (199).

During the early stages of the experiment when the 4-day platinum was the predominant activity, a small amount of the platinum fraction was placed between two gamma-ray counters, each shielded by 0.2 g/cm² of aluminum. A gamma-gamma-coincidence rate of $(0.30\pm0.02)\times10^{-3}$ coincidence per gamma-ray was measured. These were very probably gamma-(x-ray) coincidences and (x-ray)-(x-ray) coincidences.

Absorption of the gamma radiation of Pt^{193} in lead revealed the presence of x-rays having an energy of about 70 Kev.

Finally, in order to ascertain positively that the long period beta emitting contamination was the 68-day iridium (192), the iridium fraction separated from the irradiated platinum metal was purified for the removal of palladium and rhodium. The purified iridium thus obtained gave a maximum beta-ray energy of 0.56 Mev, a beta-gamma-coincidence rate corresponding to 0.6 Mev of gamma-ray energy coupled with each beta-ray, and a beta-beta-coincidence curve, exponential in form, and identical in shape and absolute magnitude with that of Ir^{192} prepared by irradiation of IrO_2 by slow neutrons. These last separations and measurements show conclusively that the contamination was Ir^{192}.

3. GOLD (199)

When platinum is irradiated by slow neutrons, the thirty-minute platinum parent of Au^{199} is formed. The 3.3-day Au^{199} was chemically separated from the platinum activities present, and the nuclear beta-rays were absorbed in aluminum as shown in Fig. 4. The visual limit is 0.085 g/cm², corresponding to 0.32 Mev.[5] A Feather plot gave a maximum beta-ray energy of 0.38 Mev. These beta-rays have been previously reported as "extremely soft"[2] and as of "several hundred kilovolts"[6] energy. Absorption of the gamma-radiation in lead gave evidence of a single gamma-ray having a quantum energy of 0.18 Mev. The beta-gamma-coincidence rate, shown in Fig. 5, was found to be 0.04×10^{-3} coincidence per beta-ray independent of the beta-ray energy, suggestive of a simple spectrum. No gamma-gamma-coincidences were observed in the gold fraction.***

Beta-beta-coincidences were observed in the disintegration of Au^{199}, indicating that the nuclear beta-rays are followed by a partially converted gamma-ray. The beta-beta-coincidence rate is plotted in Fig. 6 where it is seen to drop

[6] R. Sherr, K. T. Bainbridge, and H. H. Anderson, Phys. Rev. 60, 473 (1941).

*** It is here meant that within the sensitivity of the method, no gamma-gamma-coincidences were observed. Gamma-gamma-coincidences between gamma-rays of very low energy (0.1 Mev or less) might have escaped detection owing to the low quantum efficiency of the gamma-ray counters for radiations of that energy.

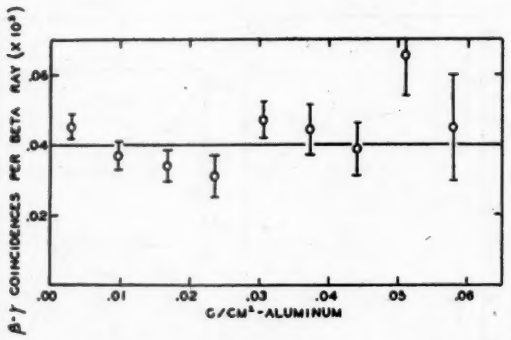

FIG. 5. Beta-gamma-coincidence rate of gold (199) as a function of the surface density of aluminum placed before the beta-ray counter.

to zero in the vicinity of 0.025 g/cm² of aluminum, corresponding to a conversion electron energy of about 0.135 Mev. Extrapolation to zero absorber thickness of the beta-beta- and beta-gamma-coincidence rates on a semi-logarithmic plot yielded a conversion coefficient of 26 percent.††

The coincidence rates and radiation energies of Au^{199} suggest the disintegration scheme of Fig. 7.

Krishnan and Nahum[3] have reported beta-rays of energy 1.01 Mev, gamma-rays of energy 0.45 Mev, and a half-period of 2.6 days for Au^{199} produced by deuteron bombardment of platinum by the Cavendish cyclotron. The reaction would be

$$Pt^{198}+D\rightarrow Au^{199}+n.$$

It is now well known that the beta-rays of the 2.7 day Au^{198} have a maximum energy of 0.97 Mev[7] and that most of the gamma-rays have an energy of 0.41 Mev.[8] It seems probable, therefore, that the radiation energies and half-period assigned to Au^{199} by Krishnan and Nahum are actually those of Au^{198} formed, in the absence of a stable Pt^{197}, by the reaction

$$Pt^{198}+D\rightarrow Au^{198}+2n.$$

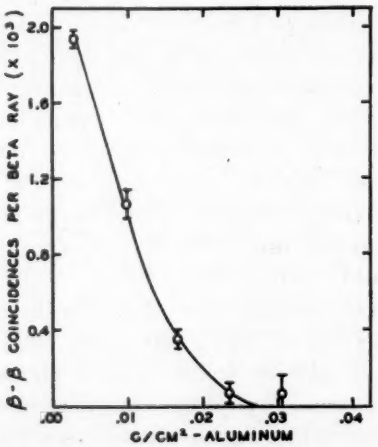

FIG. 6. Beta-beta-coincidence rate for gold (199).

†† This estimate may be regarded only as approximate. The ratio $(N_{\beta\beta}/N_{\beta})/(N_{\beta\gamma}/N_{\gamma})$ from which the conversion coefficient is calculated, is undoubtedly influenced to some extent by coincidences between nuclear beta-rays or conversion electrons and the hard x-rays of mercury which are emitted after internal conversion.

APPENDIX I: CHEMICAL PROCEDURE FOR THE SEPARATION AND PURIFICATION OF GOLD AND PLATINUM

About one-half gram of irradiated metallic platinum was dissolved in *aqua regia*. After expelling the nitric acid by repeated evaporation with hydrochloric acid, the residue was dissolved in one cc of HCl. About 60 mg of gold (as $AuCl_3$ in solution) was added and diluted to 20 cc. The gold was precipitated with SO_2, filtered off, and washed with 0.1N–HCl. The precipitated gold was again dissolved in *aqua regia*; the nitric acid was removed by several evaporations with HCl. The residue was dissolved in 3 cc of HCl, 3 drops of H_2SO_4, and 75 cc of H_2O. The gold was precipitated with oxalic acid and washed with 0.1N–HCl. The precipitated gold should have been free of other metals.

The filtrate of the first precipitation, containing the platinum, was evaporated to dryness with nitric acid and gently ignited. After dissolving in *aqua regia* and destroying the nitric acid, the residue was dissolved in 1 cc of HCl, 9 cc of H_2O, and 4 cc of alcohol. The platinum was precipitated with ammonium chloride as $(NH_4)_2PtCl_6$. This precipitate was thoroughly washed with a 20 percent NH_4Cl solution. The washed precipitate was then decomposed by boiling with ammonium formate solution, and the resulting platinum was thoroughly washed with hot water. It was then boiled with HCl to remove soluble metals. The platinum was again dissolved in *aqua regia*, evaporated with HCl to destroy the HNO_3, and precipitated as $(NH_4)_2$-

[7] P. W. Levy and E. Greuling, Phys. Rev. **73**, 83 (1948).
[8] K. Siegbahn, Proc. Roy. Soc. **A189**, 527 (1947).

$PtCl_6$. This was subsequently decomposed to platinum metal. The same procedure was repeated a third time in an attempt to prepare platinum entirely free of iron, iridium, gold, and copper.

APPENDIX II: CHEMICAL PURIFICATION OF THE IRIDIUM FRACTION

The filtrate from the $(NH_4)_2PtCl_6$ precipitation contained any iridium present, including some added as a carrier before the precipitation with NH_4Cl. Small amounts of palladium and rhodium were added, the solution diluted to 400 ml, and the palladium precipitated with dimethylglyoxime. After standing one hour, the precipitate was separated by filtration and washed with dilute (1:99) HCl and hot water.

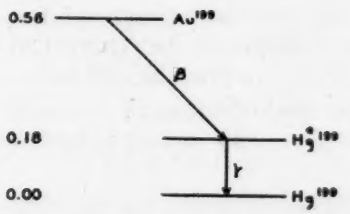

FIG. 7. Disintegration scheme of gold (199).

To the filtrate was added sodium nitrite, then Na_2CO_3 to make the solution neutral. After boiling, the solution was slightly acidified and Na_2S solution added to precipitate rhodium sulfide. The filtrate containing iridium was made alkaline with Na_2CO_3 and iridium sulfide was precipitated with Na_2S. The iridium precipitate was washed and ignited.

PHYSICAL REVIEW VOLUME 74, NUMBER 5 SEPTEMBER 1, 1948

Second-Order Transformations in Two-Component Systems. Application to Solutions of He^3 in He^4

J. W. STOUT
Institute for the Study of Metals, University of Chicago, Chicago, Illinois

(Received May 25, 1948)

A thermodynamic treatment has been made of a second-order transformation in two-component systems. In addition to the requirement that there be no heat of transformation and no volume change, it turns out that the composition is equal in the two phases. Equations have been developed for $(dT/dx)_P$, $(dx/dP)_T$, and $(dP/dT)_x$ along the equilibrium curves. If we assume that the transformation of liquid helium remains second-order on the addition of a mole fraction x of He^3 to a He^4 solution, then for the limit of very dilute solutions

$(dT/dx)_P = 21$ deg. and $(dx/dP)_T = 6\times10^{-4}$ atmos.$^{-1}$.

I. INTRODUCTION

IN order to give a thermodynamic treatment of the change in temperature of the lambda-point of liquid helium with pressure, Ehrenfest[1] was led to the concept of thermodynamic transitions of higher order. In the usual phase transitions there is a discontinuity in the temperature and pressure derivatives of the free energy (the entropy and volume, respectively) but the free energy is equal in the two phases. Such a transformation was called first-order by Ehrenfest. At the lambda-point of liquid helium the free energy and its first derivatives are equal on both sides of the transformation but there is a discontinuity in the second derivatives of the free energy in crossing a line in the pressure-temperature plane along which the transformation occurs. This was called a transformation of the second order. Similarly, a transformation of the nth order is one in which a discontinuity first appears in the nth derivative of the free energy.

Recent experimental investigations of the properties of dilute solutions of the isotope He^3 in ordinary helium make it of interest to investigate the thermodynamics of higher order transitions in systems of more than one com-

[1] P. Ehrenfest, Comm. Leiden Suppl. No. 75b.

ponent. The treatment given will, for reasons of brevity and simplicity, be confined to two-component systems and to a second-order transition. The same methods can be extended to more complicated systems and to higher order transitions.

We take as variables the pressure, P, temperature, T, and the mole fraction of component two in each phase, $x(I)$ and $x(II)$. Of these four variables any two may be independently chosen when the phases are in equilibrium. The conditions for equilibrium between the phases is that the partial molal free energies of each component be equal in the two phases,

$$\bar{G}_1(I)=\bar{G}_1(II) \quad \text{and} \quad \bar{G}_2(I)=\bar{G}_2(II), \tag{1}$$

and that for any variation

$$d\bar{G}_1(I)=d\bar{G}_1(II) \quad \text{and} \quad d\bar{G}_2(I)=d\bar{G}_2(II), \tag{2}$$

if the two phases are to remain in equilibrium.

$$\begin{aligned}&[\partial\bar{G}_1(I)/\partial T]dT+[\partial\bar{G}_1(I)/\partial P]dP\\&\quad+[\partial\bar{G}_1(I)/\partial x(I)]dx(I)\\&=[\partial\bar{G}_1(II)/\partial T]dT+[\partial\bar{G}_1(II)/\partial P]dP\\&\qquad+[\partial\bar{G}_1(II)/\partial x(II)]dx(II)\end{aligned} \tag{3}$$

with a similar equation for $\bar{G}_2$. By eliminating $dx(II)$ between the two equations one obtains

$$\begin{aligned}&[(\bar{S}_1(I)-\bar{S}_1(II))(\partial\bar{G}_2/\partial x(II))\\&\quad-(\bar{S}_2(I)-\bar{S}_2(II))(\partial\bar{G}_1/\partial x(II))]dT\\&\quad-[(\bar{V}_1(I)-\bar{V}_1(II))(\partial\bar{G}_2/\partial x(II))\\&\quad-(\bar{V}_2(I)-\bar{V}_2(II))(\partial\bar{G}_1/\partial x(II))]dP\\&\quad-[(\partial\bar{G}_1/\partial x(I))(\partial\bar{G}_2/\partial x(II))\\&\qquad-(\partial\bar{G}_2/\partial x(I))(\partial\bar{G}_1/\partial x(II))]dx(I)=0,\end{aligned} \tag{4}$$

where the substitutions

$$\partial\bar{G}/\partial T=-\bar{S}, \text{ the partial molal entropy,} \tag{5}$$

and

$$\partial\bar{G}/\partial P=\bar{V}, \text{ the partial molal volume,} \tag{6}$$

have been made. Using the Gibbs-Duhem equation,

$$x(\partial\bar{G}_2/\partial x)+(1-x)(\partial\bar{G}_1/\partial x)=0. \tag{7}$$

Equation (4) becomes

$$\begin{aligned}&[(1-x(II))\Delta\bar{S}_1+x(II)\Delta\bar{S}_2]dT\\&\quad-[(1-x(II))\Delta\bar{V}_1+x(II)\Delta\bar{V}_2]dP\\&\quad-[1-(x(II)/x(I))]\\&\qquad\times[\partial\bar{G}_1/\partial x(I)]dx(I)=0,\end{aligned} \tag{8}$$

where Δ indicates the difference between phases I and II. For a first-order transformation the coefficients of dT, dP, and $dx(I)$ will be finite, and one may immediately write down the expressions for $(dP/dT)_{x(I)}$, $(dx(I)/dT)_P$, and $(dx(I)/dP)_T$. Also, since there is a similar expression for $dx(II)$, the coefficients $(dx(I)/dx(II))_P$ and $(dx(I)/dx(II))_T$ may be obtained.

In a second-order transition the coefficients of dT, dP, and $dx(I)$ will be zero. If the coefficient of $dx(I)$ vanishes, $x(I)$ must equal $x(II)$ or the composition must be equal in the two phases. The coefficient of dT then becomes

$$(1-x)\Delta\bar{S}_1+x\Delta\bar{S}_2=\Delta S,$$

where S is the total entropy per mole. Likewise, the coefficient of dP becomes $-\Delta V$. The requirement that the coefficients of dT, dP, and $dx(I)$ vanish is equivalent to saying there is no entropy change (or no latent heat) and no volume change. $\Delta\bar{S}_1$, $\Delta\bar{S}_2$, $\Delta\bar{V}_1$, and $\Delta\bar{V}_2$ are not individually zero, but are related by the expressions

$$\Delta\bar{S}_1/\Delta\bar{S}_2=\Delta\bar{V}_1/\Delta\bar{V}_2=x/(x-1), \tag{9}$$

and from the Gibbs-Duhem relation

$$\begin{aligned}x/(x-1)&=[\partial\bar{G}_1/\partial x(I)]/[\partial\bar{G}_2/\partial x(I)]\\&=[\partial\bar{G}_1/\partial x(II)]/[\partial\bar{G}_2/\partial x(II)]\\&=[\Delta\partial\bar{G}_1/\partial x]/[\Delta\partial\bar{G}_2/\partial x].\end{aligned} \tag{10}$$

If we require that the transformation remain second-order then the coefficients of dT, dP, and $dx(I)$ in Eq. (8) must remain zero along the transition line. If we call A the coefficient of dT then

$$\begin{aligned}(dA/dx(I))_P=0&=(\partial A/\partial x(I))\\&\quad+(\partial A/\partial x(II))(dx(II)/dx(I))_P\\&\qquad+(\partial A/\partial T)(dT/dx(I))_P.\end{aligned}$$

Since $(dx(I)/dx(II))_P=1$ along the transition line, we obtain

$$(dx/dT)_P=\Delta C_P/T(\Delta\bar{S}_1-\Delta\bar{S}_2).$$

The coefficient of $dx(I)$ in Eq. (8), represented by C, when differentiated in the same fashion as A above does not give a determinate equation since

$$\partial C/\partial T=0$$

and

$$(\partial C/\partial x(I))+(\partial C/\partial x(II))(dx(II)/dx(I))_P=0.$$

However, the requirement that C remains zero

is that $x(I)$ remain equal to $x(II)$, or that $dx(I)=dx(II)$ along the transition curve. Substituting in Eq. (3), we obtain

$$(dx/dT)_P=\Delta\bar{S}_1/(\Delta\partial\bar{G}_1/\partial x)=\Delta\bar{S}_2/(\Delta\partial\bar{G}_2/\partial x)$$
$$=(\Delta\bar{S}_1-\Delta\bar{S}_2)/(\Delta\partial\bar{G}_1/\partial x-\Delta\partial\bar{G}_2/\partial x).$$

In a similar fashion one obtains the equations summarized below.

$$(dT/dx)_P=\Delta(\partial\bar{G}_1/\partial x)/\Delta\bar{S}_1=\Delta(\partial\bar{G}_2/\partial x)/\Delta\bar{S}_2$$
$$=[\Delta(\partial\bar{G}_1/\partial x)-\Delta(\partial\bar{G}_2/\partial x)]/[\Delta\bar{S}_1-\Delta\bar{S}_2]$$
$$=T(\Delta\bar{S}_1-\Delta\bar{S}_2)/C_P$$
$$=-(\Delta\bar{V}_1-\Delta\bar{V}_2)/\Delta(\partial V/\partial T), \quad (11)$$

$$(dx/dP)_T=-\Delta\bar{V}_1/\Delta(\partial\bar{G}_1/\partial x)$$
$$=-\Delta\bar{V}_2/(\partial\bar{G}_2/\partial x)$$
$$=-[\Delta\bar{V}_1-\Delta\bar{V}_2]/[\Delta(\partial\bar{G}_1/\partial x)-\Delta(\partial\bar{G}_2/\partial x)]$$
$$=-\Delta(\partial V/\partial T)/(\Delta\bar{S}_1-\Delta\bar{S}_2)$$
$$=\Delta(\partial V/\partial P)/(\Delta\bar{V}_1-\Delta\bar{V}_2), \quad (12)$$

$$(dP/dT)_x=\Delta\bar{S}_1/\Delta\bar{V}_1=\Delta\bar{S}_2/\Delta\bar{V}_2$$
$$=(\Delta\bar{S}_1-\Delta\bar{S}_2)/(\Delta\bar{V}_1-\Delta\bar{V}_2)$$
$$=\Delta C_P/T\Delta(\partial V/\partial T)$$
$$=-\Delta(\partial V/\partial T)/\Delta(\partial V/\partial P). \quad (13)$$

II. APPLICATION TO DILUTE SOLUTIONS

In the limit of very dilute solutions the preceding equations may be simplified. In the limit of $x=0$, $\bar{S}_1=S$ and $\bar{V}_1=V$ so that $\Delta\bar{S}_1$ and $\Delta\bar{V}_1$ both are zero for a second-order transition. We can also use Henry's law, $f=Kx$, where f is the fugacity.[2] Then, using the well-known thermodynamic treatment of dilute solutions, at $x=0$,

$$\partial\bar{G}_2/\partial x=(RT/x)+RT(\partial\ln K/\partial x),$$
$$(\partial\bar{G}_1/\partial x)=-RT, \quad (14)$$

$$\Delta\bar{S}_2=-RT\Delta(\partial\ln K/\partial T), \quad (15)$$

$$\Delta\bar{V}_2=RT\Delta(\partial\ln K/\partial P). \quad (16)$$

Then Eqs. (11) to (13) become

$$\left(\frac{dT}{dx}\right)_P=-\frac{\Delta(\partial\ln K/\partial x)}{\Delta(\partial\ln K/\partial T)}=\frac{RT^2\Delta(\partial\ln K/\partial T)}{\Delta C_P}$$
$$=\frac{RT\Delta(\partial\ln K/\partial P)}{\Delta(\partial V/\partial T)}, \quad (17)$$

$$\left(\frac{dx}{dP}\right)_T=-\frac{\Delta(\partial\ln K/\partial P)}{\Delta(\partial\ln K/\partial x)}$$
$$=-\frac{\Delta(\partial V/\partial T)}{RT\Delta(\partial\ln K/\partial T)}$$
$$=-\frac{\Delta(\partial V/\partial P)}{RT\Delta(\partial\ln K/\partial P)}, \quad (18)$$

$$\left(\frac{dP}{dT}\right)_x=-\frac{\Delta(\partial\ln K/\partial T)}{\Delta(\partial\ln K/\partial P)}=\frac{\Delta C_P}{T\Delta(\partial V/\partial T)}$$
$$=-\frac{\Delta(\partial V/\partial T)}{\Delta(\partial V/\partial P)}. \quad (19)$$

III. CHANGE TO A FIRST-ORDER TRANSITION

We have treated the case where the transition remains second-order over a finite range of pressure, temperature, and composition. We may consider that the difference in free energy between the two phases is expanded in a Taylor's series around a point where the transition is second-order. The coefficients of the first-order derivatives will be zero and the requirement that they remain zero involves the vanishing of a discriminant of the coefficients of the second-order terms.[3,4]

This condition is expressed by the equality of the various terms in Eqs. (17), (18), and (19). If this condition is not met, then the transition is second-order at only one point and changes to a first-order transition when the composition is changed. For convenience we assume that the singular point is at $x=0$. The fugacities are equal in the two phases so $x(I)K(I)=x(II)K(II)$. Then Eq. (8) becomes

$$\Delta S dT-\Delta V dP$$
$$+RT[1-(K(I)/K(II))]dx(I)=0. \quad (20)$$

The coefficients of dT, dP, and $dx(I)$ are zero, i.e., the transition is second-order, at $x=0$. To determine the slope of the equilibrium line we must determine the limit of the ratios of the coefficients as x approaches zero.

$$K(I)dx(I)+x(I)dK(I)$$
$$=K(II)dx(II)+x(II)dK(II)$$

[2] See G. N. Lewis and M. Randall, *Thermodynamics* (McGraw-Hill Book Company, Inc., New York, 1923) Chapters XVII and XX for the definition of fugacity and the discussion of the laws of the dilute solution.

[3] P. S. Epstein, *Textbook of Thermodynamics* (John Wiley and Sons, Inc., New York, New York, 1937), pp. 128–133.

[4] P. W. Bridgman, Phys. Rev. **70**, 425 (1946).

along the equilibrium line, so when x is small

$$dx(II)/dx(I)=K(I)/K(II)=1, \qquad (21)$$

and we need not distinguish between $dx(I)$ and $dx(II)$.

$$(dT/dx)_P=\operatorname*{Limit}_{x\to 0}RT[(K(I)/K(II))-1]/\Delta S$$
$$=[RT\Delta(\partial \ln K/\partial x)+RT\Delta(\partial \ln K/\partial T)(dT/dx)_P]/[-RT\Delta(\partial \ln K/\partial T)+(\Delta C_P/T)(dT/dx)_P]$$

or

$$(dT/dx)_P=[RT\Delta(\partial \ln K/\partial T)\pm[(RT\Delta(\partial \ln K/\partial T))^2+\Delta C_P R\Delta(\partial \ln K/\partial x)]^{\frac{1}{2}}]/(\Delta C_P/T). \qquad (22)$$

In a like fashion

$$(dP/dx)_T=[-RT\Delta(\partial \ln K/\partial P)\pm[(RT\Delta(\partial \ln K/\partial P))^2-\Delta(\partial V/\partial P)RT\Delta(\partial \ln K/\partial x)]^{\frac{1}{2}}]/\Delta(\partial V/\partial P), \qquad (23)$$

$$(dP/dT)_x=[-\Delta(\partial V/\partial T)\pm[(\Delta(\partial V/\partial T))^2+(\Delta C_P/T)\Delta(\partial V/\partial P)]^{\frac{1}{2}}]/\Delta(\partial V/\partial P). \qquad (24)$$

In these expressions the double sign of the square root corresponds to the existence of two equilibrium lines in the (T, x), (T, P), or (P, x) planes. These lines mark first-order transitions between the phases and at their intersection the transition becomes second-order. If one of the quantities under the square root sign in Eqs. (22)–(24) is zero, then in the corresponding plane the two lines coincide and the transition is second-order in that plane. If any two of the discriminants are zero then the third must be also and Eqs. (17)–(19) are obtained.

If one of the products in a discriminant is zero, then one of the lines in the corresponding plane becomes parallel to an axis. Thus, for example, if in Eq. (22) $\Delta(\partial \ln k/\partial x)=0$, then one of the lines is $(dT/dx)_P=0$.

When the transition is second-order along an equilibrium line, then the extrapolation of the free energies of the two phases would yield the result that one phase is stable on both sides of the line and the other can exist only along the line itself. We must therefore say there is some physical reason not included in the thermodynamic treatment that one phase becomes unstable. This point has been discussed by Bridgman[4] and Keesom.[5] When the transition is second-order only at a point and changes to first-order along two equilibrium lines, we perhaps must discard some regions on the basis of a physical argument.

IV. APPLICATION TO LIQUID HELIUM

The recent measurements of Fairbank, Lane, Aldrich and Nier[6] on the distribution of He^3 between liquid and vapor He^4 may be used for a thermodynamic calculation of the initial slope of the temperature-composition curve for the lambda-transformation. These authors measured C_V/C_L, the ratio of the concentration of He^3 in the vapor and the liquid, as a function of temperature for both helium I and II. We may with sufficient accuracy treat the gases as ideal in which case the fugacity equals the pressure. The solutions were very dilute, around one part per million of He^3, so the limiting laws may be used. Then $f_3=Kx$, $f_4=P$, the vapor pressure of He^4, $C_V=f_3/P$, $C_L=x=f_3/K$, or $C_V/C_L=K/P$. Then

$$d\ln(C_V/C_L)/d(1/T)=[d\ln K/d(1/T)]-[d\ln P/d(1/T)]$$
$$=-[(H_3(\text{gas})-\bar{H}_3)/R]+[(H_4(\text{gas})-H_4(\text{liq.}))/R].$$

When $\ln(C_V/C_L)$ is plotted against $1/T$ one obtains two straight lines which, within the accuracy of the measurements, intersect at the lambda-point, but which are very different in slope. From the data of Fairbank, Lane, Aldrich, and Nier[6] one obtains from the slope above the lamba-temperature,

$$H_4(\text{gas})-H_4(\text{liq.})-(H_3(\text{gas})-\bar{H}_3)=14 \text{ cal. mole}^{-1}.$$

Taking the heat of vaporization of He^4,

$$H_4(\text{gas})-H_4(\text{liq.})=22 \text{ cal. mole}^{-1}$$

at the lambda-temperature, then the partial molal heat of vaporization of He^3, from helium I, $H_3(\text{gas})-\bar{H}_3=8$ cal. mole^{-1}. From the slope

[5] W. H. Keesom, *Helium* (Elsevier Publishing Company, Inc., Amsterdam and London, 1942), Chapter V.

[6] Fairbank, Lane, Aldrich, and Nier, Phys. Rev. **73**, 729 (1948).

below the lambda-temperature

$$H_4(\text{gas}) - H_4(\text{liq.}) - (H_3(\text{gas}) - \bar{H}_3) = -147 \text{ cal. mole}^{-1},$$

and at the lambda-temperature

$$H_3(\text{gas}) - \bar{H}_3 = 169 \text{ cal. mole}^{-1}.$$

Above the lambda-point the heat of vaporization of He^3 from the solution is less than that of He^4 as one might expect from the greater zero-point energy of the lighter isotope. The very large heat of vaporization below the lamba-point is unexplained. It should be pointed out that $\bar{H}_3$ is a measure of the change in enthalpy on the addition of an infinitesimal amount of He^3 to a He^4 solution, and the large energy effect may be because the addition of an atom of He^3 causes a lowering in energy of a large number of He^4 atoms.

The data of Fairbank, Lane, Aldrich, and Nier[6] indicate that at the lambda-point C_V/C_L is equal in the two phases, or that $K(I)=K(II)$. The coefficient of $dx(I)$ in Eq. (20) is therefore zero. ΔS and ΔV are also zero for He^4, and, in fact, remain zero along a curve in the P, T plane, but their derivatives are finite along this curve.

$$\Delta\bar{H}_3 = T\Delta\bar{S}_3 = -RT^2\Delta(\partial \ln K/\partial T) = 161 \text{ cal. mole}^{-1}.$$

The value $\Delta C_P = -7.6$ cal. mole^{-1} deg.$^{-1}$ has been chosen by Keesom[5]. Although it is not possible to assign a very exact value on the basis of the experimental measurements, the value chosen proved to be consistent with the observed discontinuity in $\partial V/\partial T$ and the observed change of the lamba-temperature with pressure as related by Eq. (19). If we assume that the transition remains second-order along a line in the T, x plane, then by Eq. (17) $(dT/dx)_P = 21$ deg. And taking $(dP/dT)_x = -80.8$ atmos. deg.$^{-1}$ from Keesom,[5] by Eqs. (18) and (19), $(dx/dP)_T = 6 \times 10^{-4}$ atmos.$^{-1}$. It should be emphasized that these values apply only to the limiting case of very dilute solutions.

Thus the initial slope of the temperature-composition curve for the lamba-point will be an increase in temperature of about 0.2° per mole percent of He^3 added. The accuracy of the experimental data is not high, but unless the vapor-liquid equilibrium measurements on He *II* are very much in error one can definitely conclude that the lambda-temperature will be raised by the addition of small amounts of He^3, provided the transition remains second-order. There are no available measurements on $\Delta(\partial \ln K/\partial x)$ so the possibility that the transition goes over to a first-order one in the T, x plane in accordance with Eq. (22) cannot be excluded.

ACKNOWLEDGMENT

I am grateful to Dr. Lester Guttman and Dr. Lothar Meyer for many helpful discussions about this problem.

PHYSICAL REVIEW VOLUME 74, NUMBER 5 SEPTEMBER 1, 1948

The Effect of Cold Working on the Magnetic Properties of Pure Metals

JAMES REEKIE
Department of Physics, University of Toronto, Canada

AND

T. S. HUTCHISON
Department of Physics, University of St. Andrews, Scotland

(Received February 18, 1948)

Experiments with aluminum and copper of the highest purity obtainable show that the magnetic susceptibilities of these metals are appreciably altered by cold working. The paramagnetic susceptibility of aluminum is decreased by an amount reaching approximately 15 percent of the original value, and the diamagnetic susceptibility of copper is also, numerically, decreased by nearly the same amount. This strain sensitivity of susceptibility cannot be accounted for by the presence of ferromagnetic impurities, but appears to be related to certain metallurgical changes which occur on cold working. From a consideration of the magnitude of $\Delta\chi$ for different degrees of cold work and the phenomenon of "magnetic self-recovery" (observed in copper but not in aluminum), it is concluded that the combined effects of lattice distortion and fragmentation probably give rise to the observed changes in magnetic susceptibility.

An explanation of the results is suggested in terms of trapping of the "free" electrons in the cold-worked metal at points of considerable internal strain, and a simple application of Stoner's theory of the susceptibility of free electrons appears capable of giving a qualitative indication of why cold working should cause a change of χ towards *increased* paramagnetism in copper but towards *decreased* paramagnetism in aluminum.

I. INTRODUCTION

IT is well known that certain physical properties of metals are markedly affected by the mechanical treatment to which they have been subjected. This is especially significant in the case of the mechanical properties themselves, and while the work-hardening of annealed pure metal is perhaps the commonest observation of this type, changes in electrical resistivity, magnetic properties, and certain thermal properties, as well as in the crystal texture of the metal itself due to cold working, have been recorded by many observers. This present paper is concerned with the effect of cold working on the magnetic properties of pure copper and aluminum; it forms part of a systematic investigation of a number of pure metals and of certain metals with small, known, percentages of iron as impurity. The purpose of the work has been to try to correlate the observed magnetic changes with certain metallurgical changes which are known to occur during cold working, with the ultimate aim of arriving at some understanding of the actual mechanism whereby cold working can bring about such changes.

II. EVIDENCE FOR STRAIN SENSITIVITY OF MAGNETIC SUSCEPTIBILITY

The fact that the magnetic susceptibility of a metal depends in part on its mechanical condition has been known for a long time.[1] For instance, it was found by Bitter,[2] and also by Lowance and Constant,[3] that a relatively small degree of cold working reduced the numerical values of the susceptibilities of the diamagnetic metals, copper, silver, and bismuth, while the paramagnetic susceptibility of platinum was increased. It will be noted that in each case this change of susceptibility could be regarded as a change in the direction of increased paramagnetism. Change towards paramagnetism is not the invariable result however; paramagnetic aluminum, for instance, shows a *reduction* of susceptibility on cold working.

Although the change of magnetic susceptibility with cold work is a well established fact, the reasons for this change are still by no means clear. Attempts have been made to attribute

[1] See, for example, K. Honda and Y. Shimizu, Nature **126**, 990 (1930); Y. Shimizu, Sci. Rep. Tohoku Univ. **20**, 460 (1931).
[2] F. Bitter, Phys. Rev. **36**, 978 (1930).
[3] F. E. Lowance and F. W. Constant, Phys. Rev. **38**, 1547 (1931).

changes in magnetic properties induced by cold work in supposedly pure metals to the presence of minute amounts of ferrous impurity. This impurity is assumed to be in a non-magnetic state in the annealed metal, but to precipitate out in ferromagnetic form on cold working. The very careful work of Kussmann and Seemann,[4] in which susceptibility was measured as a function of the applied magnetic field in the case of cold worked metals containing traces of iron as impurity, lent support to this view.

In the case of a diamagnetic substance, such as copper, precipitation of an iron impurity in ferromagnetic form would result in a change in the observed susceptibility towards increased paramagnetism. If the impurity were present in sufficient quantity the substance might well appear to be paramagnetic, as has often been reported in the case of copper.[2,5] In such a case there would be, however, a marked variation of apparent susceptibility with magnetic field.

Furthermore, in a paramagnetic metal precipitation of ferromagnetic impurity by cold working should result not only in a marked dependence of susceptibility on field strength, but also in an *increase* in apparent paramagnetic susceptibility. We have found, on the contrary, that the paramagnetic susceptibility of aluminum *decreases* considerably on cold working.

In the present work the susceptibility was always measured as a function of field strength, on both annealed and cold-worked specimens, generally in fields up to about 15,000 oersted. The high purity of the metals used, together with the absence of any appreciable field dependence of susceptibility in either the annealed or cold worked states, leads us to conclude that the changes in susceptibility observed require some considerably more fundamental explanation than the presence of impurities. We believe that the magnetic changes can be linked up fairly satisfactorily with certain metallurgical changes which occur as a result of cold working, and an explanation along these lines is attempted. In addition, some degree of correlation with Stoner's theory of free electron susceptibility[6] can be introduced, and the recently reported "self-recovery" effects noted in x-ray observations on cold-worked copper[7] are almost certainly associated with the "magnetic self-recovery" which we recently described as occurring in cold-worked copper.[8]

III. PREPARATION OF SPECIMENS

A. Metals Used

This work has been carried out with copper and aluminum of the highest purity, electrolytically refined "H.S." brand, provided by Johnson, Matthey, and Company, Ltd. of London, England. The metal was obtained in the form of rods 15 cm long and 5 or 6 mm in diameter. The iron content of the materials was stated to be, by chemical analysis, "certainly less than 0.0005 percent," and "not detectable by spectroscopic analysis." From the magnetic measurements it is clear that the iron content must have been much less than the upper limit quoted in the chemical analysis.

B. Heat Treatment

The effect of heat treatment on the magnetic properties of metals containing ferrous impurity can be very considerable, and for this reason the heat treatment used during the present work has followed a relatively simple but standardized procedure.

In the case of aluminum, annealing was always carried out by heating the rod of metal in an atmosphere of hydrogen at a temperature of 500°C for approximately two hours. Annealing of the copper rods was carried out by heating in hydrogen at a temperature of 950°C to 1000°C for a period of approximately ten hours.

Subsequent cooling of the specimens was dependent on the particular investigation being made. If the specimen was required in the "quenched" condition, it was transferred rapidly from the high temperature furnace into water at room temperature; the hydrogen atmosphere was maintained surrounding the metal until it

[4] A. Kussmann and H. J. Seemann, Naturwiss. **19**, 309 (1931); Zeits. f. Physik **77**, 567 (1932). See also, C. S. Smith, Phys. Rev. **57**, 337 (1940).
[5] Y. Shimizu, Sci. Rep. Tohoku Univ. **22**, 915 (1933).
[6] E. C. Stoner, Proc. Roy. Soc. **A152**, 672 (1935).
[7] H. Megaw, H. Lipson, and A. R. Stokes, Nature **154**, 145 (1944); M. Cook and T. Ll. Richards, J. Inst. Metals **70**, 159 (1944); H. Megaw and A. R. Stokes, *ibid.* **71**, 279 (1945); L. L. van Reijen, Nature **157**, 371 (1946); J. L. Miller, L. C. Bannister, and R. M. Hinde, *ibid.* **158**, 705 (1946); W. G. Burgers, *ibid.* **159**, 203 (1947).
[8] J. Reekie and T. S. Hutchison, Nature **157**, 807 (1946).

entered the water. "Slow cooling" was carried out by allowing the metal to cool from its annealing temperature down to room temperature over a period of about eight hours, both for the copper and aluminum, again maintaining a hydrogen atmosphere during the whole period of cooling.

C. Cold Working

Throughout the observations described in the present paper, cold working of the materials has been carried out by drawing the previously annealed rods through hardened steel dies at a uniform rate until the required degree of reduction in diameter was achieved. The direction of draw was always maintained the same, for every specimen, and particular care was taken to avoid any contamination of the pure metals during the drawing processes.[9] The results indicate that no measurable contamination occurred.

No very satisfactory criterion for the specification of the degree of cold working in any simple manner has yet been formulated, though possibly the most logical method would be to determine the amount of stored energy in the cold-worked material, as in the experiments of Taylor and Quinney.[10] However, it has become customary to adopt as an arbitrary measure of cold work the degree of reduction in cross-sectional area of the material, and this definition is adopted in the present paper.

IV. EXPERIMENTAL PROCEDURE

The susceptibility was determined in all cases by the Gouy method, using specimens approximately 12 cm long and of various diameters from about 5 mm down to about 2 mm. In this method it is necessary to measure the force exerted on a specimen of known dimensions when acted on by a magnetic field, and for this purpose we used a small electrodynamic balance and a conventional type of electromagnet. An account of the construction and use of the balance itself has been given elsewhere, and the experimental procedure has been described in previous publications,[11,12] to which reference should be made for details.

V. MEASUREMENT OF MAGNETIC SUSCEPTIBILITY

If a rod of material of uniform cross section α and magnetic susceptibility per unit volume k is suspended so that one end is in a uniform field H and the other in a field H_0, the length of the rod being perpendicular to these fields, then a force is exerted on the material in a direction at right angles to the magnetic field H. The magnitude of this force is given by

$$F=\tfrac{1}{2}(k-k')\alpha(H^2-H_0^2) \text{ dynes}, \qquad (1)$$

where k' is the volume susceptibility of the medium surrounding the rod.

This, as is well known, forms the basis of the Gouy method of measuring magnetic susceptibilities. In the present work the specimen was surrounded by hydrogen gas at a few cm pressure so that no appreciable error was introduced by neglecting k', and the expression for the force can then be written as

$$F=\tfrac{1}{2}m\chi(H^2-H_0^2)/l. \qquad (2)$$

Here m and l are, respectively, the mass and length of the rod, and χ is the susceptibility per gram, i.e., the mass susceptibility.

From this expression it can be seen that if χ is a constant independent of the field, then the force exerted on the specimen should be strictly proportional to the quantity $(H^2-H_0^2)$. This, as has already been indicated, forms a sensitive test for the presence of ferromagnetic impurities, because, in the case of a ferrrous material, χ is a function of the field strength itself, so that F is no longer a linear function of $(H^2-H_0^2)$. However, in such a case, values of χ for the pure material can still be obtained by several well-known methods.[13]

In no instance during the present work could it be said that any definite indication of ferromagnetism was observed, either with the metals in the annealed state or after considerable

[9] See, for example, Philips Technical Review **8**, 315 (1946).
[10] G. I. Taylor and H. Quinney, Proc. Roy. Soc. **A163**, 157 (1937).
[11] J. Reekie, Proc. Roy. Soc. **A173**, 367 (1939).
[12] T. S. Hutchison and J. Reekie, J. Sci. Inst. **23**, 209 (1946).
[13] See, for example, L. F. Bates, *Modern Magnetism* (Cambridge University Press, Teddington, England, 1939), p. 116.

degrees of cold working. In all cases the force exerted on the specimen was found to be, very closely, a linear function of $(H^2-H_0^2)$ over the whole range of fields used, any initial curvature not being outside the experimental error. The fact that χ, as obtained from Eq. (2), shows no evidence of field dependence in any of these measurements must be taken as strong evidence that ferromagnetic impurities play no part in the effects to be described later.

VI. CHANGE OF MAGNETIC SUSCEPTIBILITY ON COLD WORKING

Using a number of specimens annealed in the manner previously described and measured as outlined above, we have found the average value of the susceptibility of pure copper to be -0.085×10^{-6} c.g.s. units per gram at a temperature of about 290°K. Taking into account all sources of error this value is considered to be correct to within about 3 percent.

If any specimen is cold-worked by drawing, the susceptibility is found to decrease (numerically), even for small degrees of cold work. For example, a four percent reduction in area of the specimen reduces the value of mass susceptibility to -0.079×10^{-6}, while at 20 percent reduction in area the susceptibility becomes -0.072×10^{-6}, both values being measured at room temperature. This change is in the direction of increased paramagnetism and, as has been pointed out, is not inconsistent with the possibility of ferromagnetic impurity being precipitated as a result of the cold working.

Equally marked changes are observed in the susceptibility of cold-worked aluminum, but in this case the paramagnetic susceptibility *decreases* with cold working. For example, the annealed metal gives an average value for χ at room temperature of $+0.62\times10^{-6}$ c.g.s. units per gram; seven percent cold working reduces this to 0.60×10^{-6}, while the same specimen cold-worked to 30 percent reduction of area has a susceptibility of 0.54×10^{-6}. It does not seem possible to explain a *decrease* in paramagnetic susceptibility as caused by precipitation of ferrous impurity.

Table I gives the measured values of mass susceptibility of aluminum and copper for a number of different degrees of cold working. These figures refer to one particular specimen of each metal, subjected to successively increasing degrees of cold work. Check measurements on other specimens cold-worked to similar degrees and then re-annealed showed that in all cases annealing caused the susceptibility to revert to its original value, within the limits of accuracy of the measurements. For reasons which will be apparent later, all susceptibility measurements were carried out one hour after the cold working of the metal had taken place.

TABLE I. Mass susceptibility for different degrees of cold working.

Aluminum		Copper	
Cold work: percent reduction of area	$\chi\times10^{+6}$	Cold work: percent reduction of area	$\chi\times10^{+6}$
Annealed	$+0.62_3$	Annealed	-0.085
14.4	0.60_4	2	0.084
18	0.58_6	4	0.079
19	0.56_8	6	0.075
22.6	0.55_2	20	0.073
23.4	0.54_4	34	0.072
32	0.53_8	43	0.074
42	0.53_3	50	0.073
55	$+0.52_8$	59	0.077
		65	0.076
		69	0.076_5
		73	-0.080_5

At this stage, one feature of these results calls for comment. It will be evident in the case of copper that when cold working is in excess of about 45 percent reduction in area the measured susceptibility begins to *increase* (numerically) again. This point appears to be of considerable significance in the explanation of the results and will be discussed later.

The comparative behavior of aluminum and copper is illustrated in Fig. 1, where the percentage change of susceptibility is shown as a function of the degree of cold work. The numerical increase of χ towards its "annealed" value for cold working in excess of 45 percent in the case of copper is also clearly shown in this diagram. (χ_0 represents the susceptibility of the annealed metal, and $\Delta\chi$ the difference between the cold worked and annealed values.)

VII. MAGNETIC SELF-RECOVERY

A. Rate of Recovery of Different Temperatures

During our first investigations on the effect of cold working on the susceptibility of copper it was noted that the numerical value of the suscep-

tibility of the cold-worked metal appeared to increase slowly with time, all other experimental conditions remaining undisturbed. A more detailed investigation of this effect revealed that a noticeable "magnetic self-recovery" takes place in copper,[8] even at temperatures far below that at which recrystallization can occur. The rate of recovery is, as might be expected, dependent on the temperature and can, in fact, be arrested altogether at sufficiently low temperatures. It is because of this magnetic self-recovery that all susceptibilities quoted in the previous section were measured at a specific time, namely, one hour after cold working.

In carrying out these investigations a previously annealed copper rod was cold worked and then assembled in the balance for measurement. The susceptibility was observed one hour after the cold working had been completed, and thereafter at convenient intervals over periods as long in some cases as 100 hours. During the whole time of the measurements on any single specimen the temperature of the specimen was maintained constant. Cold working was, of course, always carried out at room temperature, and, after assembly in the balance, the specimen taken as rapidly as possible to the temperature at which it was desired to carry out susceptibility measurements.

As typical of the recovery effects observed,

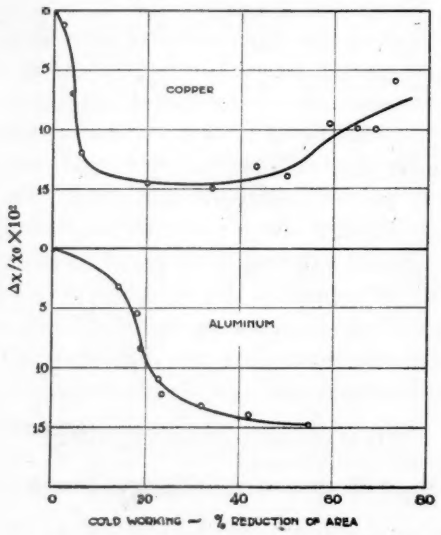

FIG. 1. Percentage change in susceptibility at room temperature as a function of cold working. For copper $\chi_0 = -0.085 \times 10^{-6}$. For aluminum $\chi_0 = +0.62 \times 10^{-6}$.

Fig. 2 shows the change in the measured value of susceptibility as a function of time after cold working, for specimens maintained at three different temperatures. In the diagram $\Delta\chi$ is the actual change in susceptibility and χ the susceptibility of the particular specimen as measured one hour after cold working. During each set of measurements the specimen and the balance remained undisturbed, so that the *relative* accuracy of the points on any particular curve in Fig. 2 is better than $\frac{1}{2}$ percent.

Several features will be evident at once. In the first place, a considerable "recovery" of the susceptibility towards its "annealed" value takes place at room temperature. This recovery can be accelerated by raising the temperature a relatively small amount, while if the specimen is maintained at the temperature of liquid air no measurable recovery takes place. Furthermore, the recovery observed is at most about six percent of the initial value of χ, so that the "recovered" value of susceptibility is still considerably less than the value for the annealed metal at the same temperature. The recrystallization temperature of copper is about 200°C, so that recovery effects of the magnitude observed here cannot be attributed reasonably to recrystallization, nor could any change of state of ferrous impurity occur at these temperatures. It is suggested that this magnetic self-recovery reflects the self-recovery from lattice distortion which recent x-ray observations have made clear.[7] This suggestion will be elaborated when considering the interpretation of the results.

On carrying out similar measurements with aluminum rods cold-worked to varying degrees, no detectable change of susceptibility was noted, even with observations extending over periods of as much as 70 hours at room temperature. Specimens cold-worked up to 50 percent reduction in area were used in these measurements.

The absence of magnetic self-recovery in aluminum may, at first sight, appear difficult to reconcile with the suggested explanation in the case of copper. This is not so however, because the x-ray work of Wood[14] has shown that aluminum is *spontaneously self-recovering during cold*

[14] W. A. Wood, Proc. Roy. Soc. A172, 231 (1939); Proc. Phys. Soc. London 52, 110 (1940). See also A. Taylor, *Introduction to X-ray Metallography* (Chapman and Hall, Ltd., London, 1945), p. 234.

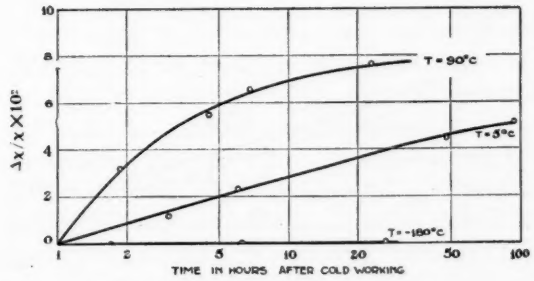

FIG. 2. Magnetic self-recovery of cold-worked copper at various temperatures.

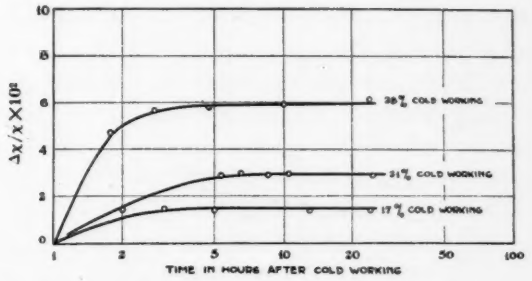

FIG. 3. Magnetic self-recovery of copper at room temperature after various degrees of cold working.

working at room temperature; if magnetic self-recovery is connected with recovery from lattice distortion, one should therefore expect to observe such recovery in copper but not in aluminum, under the present experimental conditions. It is possible that, if the aluminum were cold-worked at some *low* temperature, recovery effects might become observable in this case also.

B. Recovery in Copper as a Function of Cold Working

Some further experiments were carried out to determine to what extent magnetic self-recovery at any given temperature was affected by the degree of cold working. The results of these investigations are summarized in Fig. 3, where the percentage change in χ is shown as a function of time; as before, χ represents the susceptibility of the copper as measured one hour after cold working was carried out.

It should be remarked that, as Fig. 1 shows, the "cold-worked" value of susceptibility for copper appears to be approximately constant for all degrees of cold working between about 10 percent and 50 percent reduction of area. That is, χ in Fig. 3 has the same value (within the limits of accuracy of the measurements) for each curve given, this value being -0.072×10^{-6}. The curves all refer to a temperature of about 290°K and, since the balance and specimen remained undisturbed during any one series of measurements, the relative accuracy of the points on any particular curve is within $\frac{1}{2}$ percent.

Two significant features should be noted in these results. In the first place it is clear that the susceptibility reaches a stable value after an interval of the order of ten hours, and that the extent of the self-recovery depends on the degree of cold work, being greater for greater degrees of cold work. It amounts, however, only to six percent of χ at a 28 percent reduction of area, and from the trend of the curves it seems improbable that the self-recovery would amount to more than about one-half of the initial decrease, even if cold working were continued to 50 percent reduction. Beyond this point, as we have already noted, additional factors evidently contribute to changes in the susceptibility.

The second feature on which we wish to remark is the fact that the time required for self-recovery in these experiments does not appear to depend greatly on the extent of the cold work. In other words, the initial rate of recovery is greater for greater cold working, and at a temperature of 290°K the susceptibility appears to have reached a stable value after some five to ten hours. This time of recovery depends quite markedly, of course, on the temperature, as Fig. 2 shows.

VIII. TEMPERATURE DEPENDENCE OF SUSCEPTIBILITY OF ANNEALED AND COLD-WORKED METAL

A. Copper

In some earlier work[8] it was noted that the temperature variation of susceptibility of cold-

TABLE II. Temperature variation of susceptibility of annealed and cold-worked copper.

Cold work: percent reduction of area	Percent change in χ over temperature range 90°K to 630°K
Annealed and slowly cooled	22
Annealed and quenched	21
5.5	12
19.7	12
26.7	12.5
36.0	13

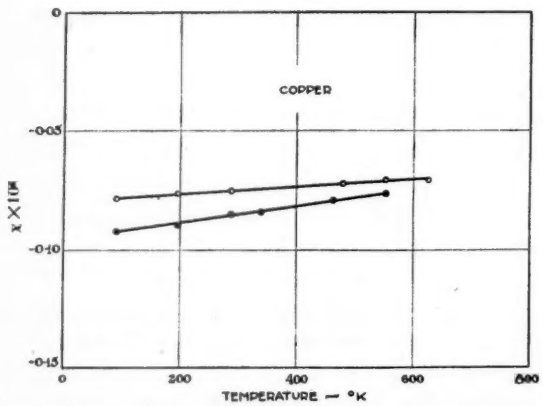

FIG. 4. Temperature dependence of susceptibility of copper. Open circles, copper cold-worked to 5.5 percent reduction of area; filled circles, copper annealed and quenched.

worked pure copper appeared to differ somewhat from that of the annealed metal, and more extensive and systematic investigations of this point are reported here. Over a temperature range from 90°K to about 630°K susceptibility was found to be, in both cases, very nearly a linear function of the temperature; but whereas the annealed metal showed a variation of χ of about 22 percent of its room temperature value over this range, the cold-worked metal showed a variation of only 12 percent. Furthermore, the amount of cold working appeared to have little effect on the form of the curve or on the magnitude of this variation, as is clear from Table II.

Figure 4 shows the susceptibility as a function of temperature in the case of the metal cold-worked to 5.5 percent reduction of area; for comparison the susceptibility of an "annealed and quenched" specimen is shown on the same diagram. It is worth remarking that no measurable difference was observed between the susceptibility *vs.* temperature curves for the "annealed and slowly cooled" and the "annealed and quenched" specimens, nor was any field dependence of χ observed in either case.

TABLE III. Temperature variation of susceptibility of annealed and cold-worked aluminum.

Cold work: percent reduction of area	Percent change in χ over temperature range 90°K to 630°K
Annealed and slowly cooled	28
14	29
33	27.5
62	28

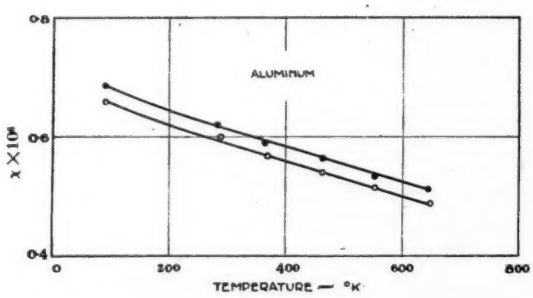

FIG. 5. Temperature dependence of susceptibility of aluminum. Open circles, aluminum cold-worked to 14 percent reduction of area. Filled circles, aluminum annealed and slowly cooled.

Throughout these measurements the specimens were always allowed to stand for 24 hours at room temperature after cold working had been carried out, so that any self-recovery would be effectively complete. The high temperature measurements were made with as little delay as possible after reaching equilibrium, so as to minimize any annealing of the cold-worked specimens. Since the recrystallization temperature of both copper and aluminum is in the neighborhood of 200°C, it is inevitable that some degree of annealing must have taken placed. However, it is believed that this must have been small over the short time during which the specimens were maintained above 200°C, because little change was ever observed in the room temperature, "cold-worked," value of χ after cooling.

B. Aluminum

Similar measurements carried out with pure aluminum showed that the susceptibility was again very nearly a linear function of temperature for both the annealed and the cold-worked metal. In this case, however, the percentage variation of χ over the temperature range used was the *same* for specimens cold-worked to various extents as for the annealed specimens. Table III shows these results. In Fig. 5 curves giving χ as a function of temperature for annealed and 14 percent cold-worked specimens are shown.

Stoner,[6] in work which will be discussed later, has developed expressions for the magnetic susceptibility of free electrons, and has shown that while any variation of electron susceptibility with temperature in a metal is very small, there would,

nevertheless, be an indirect effect due to thermal expansion. This would result in an *increase* in paramagnetic susceptibility with temperature, and such an explanation appears to account reasonably well for the results observed by Sucksmith[15] for alkali metals and by Bates and Baker[16] for mercury. To apply such an explanation to our results for copper would require, however, that the thermal expansion of annealed copper should be nearly twice as great as that of the cold-worked metal. Very simple experiments show that this is not the case, and it is clear that metallurgical processes occurring during the cold working must have some bearing on the explanation of the results. Further, the paramagnetic susceptibility of aluminum *decreases* with increasing temperature.

IX. DISCUSSION AND INTERPRETATION OF RESULTS

We have already, in Section II, to some extent discussed the question as to whether or not ferrous impurities could account for the changes which are definitely observed in the magnetic susceptibility of a supposedly pure metal when it is subjected to cold work. If such impurities do exist and are present in ferromagnetic form, they should have two easily observable consequences: (a) the susceptibility should become field dependent, and (b) the susceptibility should appear more paramagnetic (in any given field) than it would be for the pure parent metal. The purity of the metals used in the present work appears to have been sufficiently high for (a) to have been eliminated, while (b) is not borne out in the case of paramagnetic aluminum.

Further, the solubility curve of iron in copper is such that the amount of iron which could be held in equilibrium in solid solution falls very rapidly as the temperature is reduced, from about 3 percent at 1000°C to an altogether negligible amount in the region of room temperature.[17] Hence, much of the iron present as impurity should precipitate out into either paramagnetic or ferromagnetic form if the metal is very slowly cooled from a high temperature. On the contrary, iron impurity can be retained in solid solution (and hence presumably in a non-magnetic form) if the metal is suddenly quenched from a high temperature. If, therefore, the supposedly pure metal contains iron impurity, it should easily be possible to observe a difference in the magnetic behavior of a specimen when slowly cooled and when quenched. No measurable differences have been observed in the present work, either in copper or aluminum.

In our discussion of the results we shall first consider what happens when an annealed metal is subjected to cold working. In general, three processes occur: (a) lattice distortion, (b) grain fragmentation, and (c) grain orientation. These effects can all be followed by x-ray investigations, as was done by Wood,[14] and the results, very briefly summarized, are as follows. For annealed, pure copper separate sharp reflection spots are obtained, grouped around the positions to be expected for Debye-Scherrer rings. On cold working, a transition to radially diffuse rings gradually occurs, and at the same time change in the diameter of the rings indicates an alteration of the lattice spacing. Wood found that the diffuseness of the rings did not exceed a certain maximum, whatever the degree of cold work, and that the lattice spacing change fluctuated in a periodic fashion.

Fluctuations in lattice spacing similar to the above were found for various other metals, but *not* for aluminum. In the case of aluminum, even after extensive cold working, the lines remained relatively sharp and perfectly resolved. This indicated that not only is the minimum crystallite size resulting from fragmentation considerably larger than in the case of copper, but also that aluminum is spontaneously self-recovering from lattice distortion during cold working at room temperature.

As already noted, recent experiments have been reported[7] showing that cold-worked pure copper also exhibits a "self-recovery" in the sense that a reduction in diffuseness of the lines in x-ray diffraction patterns occurs over a period of some hours, or even days, when the metal is maintained at room temperature. In some instances the reappearance of distinct reflection spots has been noted, indicating that some degree of recrystallization must also have occurred at room temperature.

[15] W. Sucksmith, Phil. Mag. 2, 21 (1926).
[16] L. F. Bates and C. J. W. Baker, Proc. Phys. Soc. London 50, 409 (1938).
[17] M. Hansen, *Der Aufbau der Zweistofflegierungen* (Verlag Julius Springer, Berlin, 1936).

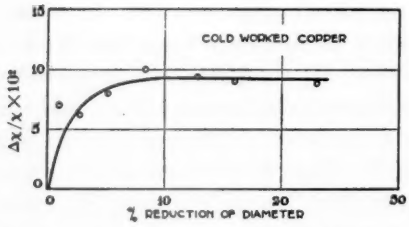

FIG. 6. Percentage change in susceptibility of cold-worked copper as surface layers of metal are removed by etching.

Reverting now to the magnetic measurements, we regard the change in magnetic susceptibility, irrespective of its direction, as due to the combined effects of lattice distortion and fragmentation; and we regard the magnetic self-recovery exhibited by copper to be a direct result of the *lattice* recovery occurring over an interval of the order of some hours. Since aluminum is spontaneously self-recovering *during* cold working at room temperature, we should not expect to find any magnetic self-recovery, but only a stable change of susceptibility due to fragmentation. These features are as we actually observe in cold-worked copper and aluminum.

On the basis of this interpretation we can say, referring again to Fig. 3, that the contribution to $\Delta\chi$ from lattice distortion in the copper increases as the degree of cold work increases, but probably does not exceed one-half of the total change in χ, whatever the degree of cold work. The remaining part of the change in χ must be attributed to fragmentation. Now, when a rod is drawn through a die, cold working is most severe in the surface layers, and it is to be expected that fragmentation is also most severe in this region. Hence, if these surface layers are removed from a cold-worked specimen which has been allowed to recover from the effect of lattice distortion, we might also expect the susceptibility to return to a value approaching that of the annealed metal.

A simple experiment to test this possibility was carried out by gradually etching away the surface from a cold-worked rod of copper with dilute nitric acid. The specimen was cold-worked to 38 percent reduction of area, allowed to recover at room temperature for about 50 hours, and then its susceptibility determined. Successively increasing thicknesses of metal were then etched from the surface, the susceptibility being measured after each etching. The results obtained are shown in Fig. 6. It will be seen that the susceptibility quickly increased (numerically) as the surface layers were etched away and had reached a constant value by the time a ten percent reduction of the diameter had been achieved. Reliable measurements could not be carried beyond about 30 percent reduction of diameter (43 percent reduction of area) because pitting of the surface then became sufficient to produce significant variations in the cross-sectional area of the rod.

It is interesting to consider the relative changes in susceptibility observed in this case. Before etching was commenced the "recovered" value of χ for the 38 percent cold-worked rod was about -0.076×10^{-6}; etching increased this value by about 9 percent, i.e., to -0.083×10^{-6}, which is approaching the observed susceptibility of the annealed metal.

Thus we have a good numerical confirmation of the suggestions outlined above to account for the change in susceptibility of copper. In the case of aluminum the observed, stable, decrease in paramagnetic susceptibility must, on this view, result from fragmentation occurring in the surface layers of the material. It is of interest to note the actual thickness of surface layer removed in the copper specimen before the susceptibility regained its value of -0.083×10^{-6}. The initial diameter of the rod after 38 percent cold working was about 3 mm. A ten percent reduction of this diameter results in removal of a surface layer 0.15 mm thick. Now several investigations[18] by x-ray methods have been carried out to determine how far below the surface of a machined piece of metal the effect of the cutting tool extends. In copper and aluminum subjected to typical machining processes it has been found that the cold work is evident to a depth of approximately 0.25 mm below the surface. This is sufficiently close to the value observed for the "depth of penetration" of the magnetic effect to suggest that the stable portion of the susceptibility change is confined mainly to the region suffering greatest fragmentation.

We are now in a position to remark further on

[18] See, for example, A. Taylor, *Introduction to X-ray Metallography* (Chapman and Hall, Ltd., London, 1945), p. 244.

the form of the curve for copper in Fig. 1, where cold working in excess of 50 percent has been carried out. Normally, recrystallization of a cold-worked metal does not occur until its temperature has been raised above some fairly well defined value which we know as the recrystallization temperature. However, it is well known that if the cold working becomes sufficiently severe, then recrystallization may commence, *even at room temperature.* It is suggested that such "spontaneous recrystallization" at room temperature begins to occur in our specimens of copper when the cold working exceeds about 50 percent reduction of area. Such recrystallization would, if our picture of the process is correct, result in a progressive increase (numerical) in susceptibility as the cold working increased beyond 50 percent. This ultimate increase in susceptibility has been observed in a number of specimens cold-worked beyond 40 to 50 percent reduction of area, and the explanation appears to lie in the direction indicated above. It is very difficult to see how ferromagnetic impurities could revert to non-ferrous form merely as a result of recrystallization at room temperature.

In this discussion we have not so far mentioned the grain orientation which occurs when a rod of polycrystalline metal is cold-drawn. It is well known from x-ray investigations that in cold-drawn wires the crystal grains become so arranged that a definite crystallographic direction tends to lie along the axis of the wire. If the crystal were magnetically anisotropic, this orientation would naturally result in a variation of magnetic properties as the metal was cold-worked. Although in their normal state crystals of both aluminum and copper are isotropic, we do not know to what extent the lattice distortion occurring during cold working may affect this isotropy. It is perhaps possible that that part of the change in susceptibility which we have attributed to lattice distortion may ultimately be related to an actual magnetic anisotropy, but at the present stage of investigations this cannot be regarded as more than speculative.

We have confined our attention so far to a consideration of those processes occurring during cold working which probably give rise to changes of magnetic susceptibility. We shall now consider the manner in which these processes could affect magnetic properties.

The magnitude of the changes in susceptibility brought about by cold working is of the same order as the value of susceptibility calculated by Stoner[6] for free electrons. The electrons in a metal cannot be regarded strictly as "free" electrons, but for many purposes may be considered as approximating to that state, and it is natural to seek first for an explanation of the strain sensitivity of susceptibility along the lines of a variation in the contribution made to the susceptibility by the electrons in the metal. Stoner has derived the following expression for the gram atomic susceptibility of free electrons.

$$(\chi_A)_e \times 10^6 = 32.1(q/V_0) \times \{1 - 6.11 \times 10^{-9}(T/V_0)^2\}, \quad (3)$$

where q is the number of free electrons per atom and V_0 is the maximum electron kinetic energy (in electron volts) at absolute zero. For free electrons V_0 is given by

$$V_0 = 3.62 \times 10^{-15}(q \cdot n)^{\frac{1}{3}}, \quad (4)$$

where n is the number of atoms per unit volume. Equation (3) implies that $(\chi_A)_e$ should decrease with increasing temperature; actually the decrease would, under ordinary conditions, be altogether inappreciable, but Stoner has shown that thermal expansion may change the value of V_0 in such a way as to produce a significant *increase* in $(\chi_A)_e$ with temperature. Thus, for an annealed pure metal we have, from (4),

$$V_0 \propto n^{\frac{1}{3}},$$

and hence, from (3),

$$(\chi_A)_e \propto 1/V_0 \propto n^{-\frac{1}{3}} \propto (1 + \tfrac{2}{3}\alpha_v \cdot T),$$

where α_v is the coefficient of cubical expansion and T the temperature. Hence we have, approximately,

$$\Delta(\chi_A)_e/(\chi_A)_e \cdot \Delta T = \tfrac{2}{3}\alpha_v. \quad (5)$$

This formula accounts fairly well for the observed variation of χ with temperature for the alkali metals[15] and for mercury.[16] Clearly, the temperature variation of χ for aluminum cannot be explained in this way, nor can the difference between the temperature variations of χ for annealed and cold-worked copper. In the former case the variation is in the wrong direction, and

in the latter it would require a coefficient of expansion for the annealed copper 100 percent greater than for the cold-worked metal. Experiments show that the maximum difference in the coefficient of cubical expansion is in the region of 5 percent. This failure to account for the experimental results is not unexpected however, considering the appreciable departure from "free" electron conditions which may exist in these metals.

Referring again to Eqs. (3) and (4) we see that, if we neglect the temperature dependent term in (3), we can write

$$(\chi_A)_e \propto q/V_0 \propto (q/n^2)^{\frac{1}{3}}. \tag{6}$$

Hence $(\chi_A)_e$ will vary with cold working of a metal if either q or n varies. Now we can easily see that both q and n *do* vary when the metal is cold-worked; and whether or not $(\chi_A)_e$ increases or decreases due to the cold working will depend on the relative changes in q and n^2.

When a metal is subjected to cold working, grain fragmentation occurs, with consequent increase in grain boundaries and regions of considerable internal strain. It is generally agreed that grain boundaries and centers of strain form regions in which the "free" electrons of the metal may become "trapped" or perhaps partially bound. Such a trapping of electrons would result in a decrease in the effective value of q and hence of $(\chi_A)_e$. On the other hand, cold working results in a decrease in the density of a metal;[5,19] this implies a decrease in n, which in turn results in an increase in $(\chi_A)_e$. It easily follows from (6) that the fractional *decrease* in electron paramagnetism on cold working would be given by the expression

$$1-\{(q/q_0)\cdot(\rho_0/\rho)^2)\}^{\frac{1}{3}}, \tag{7}$$

where ρ is the density and the subscript "0" refers to the annealed metal. Whether the cold-worked metal appears more or less paramagnetic than when in the annealed state will obviously depend on whether the cube root term in (7) is greater or less than unity. Clearly, therefore, the change in susceptibility could be in either direction, depending on the extent of electron trapping relative to the change in density. Trapping of electrons implies, of course, that q is less than q_0; however, in a cold-worked metal ρ_0/ρ is always slightly greater than unity, so that the sign of the term (7) as a whole will depend on the metal itself.

If we accept the density measurements of Shimizu[5] it appears that $(\rho_0/\rho)^2$ for copper is appreciably greater than for aluminum for similar degrees of cold working. Furthermore, aluminum has three electrons outside a neon-like core while copper has only one outside a newly completed $3d$ shell. Therefore it might not be unreasonable to suppose that trapping of electrons could occur more easily in aluminum than copper; in other words, q/q_0 could conceivably be relatively less for aluminum than for copper. Both effects would tend to make the cube root term of (7) relatively greater for copper than for aluminum, with the possibility that the whole term (7) may be positive for aluminum but negative for copper. Such would be in accordance with our observations. However, it is unjustifiable to carry speculation beyond this stage at present; not only have we neglected to consider what the effect of the "trapped" electrons may be, but also we know little as yet of the actual mechanism by which trapping may occur in cold-worked metals. Nevertheless, the degree of correlation which can be achieved along the lines indicated leads us to consider that the explanation of strain sensitivity of magnetic susceptibility may lie in this direction.

X. ACKNOWLEDGMENTS

This research was carried out in the Physics Department of the University of St. Andrews, Scotland, and was largely supported by the Carnegie Trust. It is a pleasure to record our gratitude to both institutions. We are also very much indebted to the Torpedo Experimental Establishment of the British Admiralty for the loan of high capacity, lead-acid storage batteries, which greatly facilitated the stable operation of the electromagnet used in the work.

One of us (T.S.H.) received a maintenance grant from the Department of Scientific and Industrial Research, and gladly records his thanks to that department.

[19] S. L. Smith and W. A. Wood, Proc. Roy. Soc. **A179**, 450 (1942).

Letters to the Editor

PUBLICATION of brief reports of important discoveries in physics may be secured by addressing them to this department. The closing date for this department is five weeks prior to the date of issue. No proof will be sent to the authors. The Board of Editors does not hold itself responsible for the opinions expressed by the correspondents. Communications should not exceed 600 words in length.

Thermal Consequences of the Capture of Neutrinos by the Earth

A. E. BENFIELD
Department of Engineering Sciences and Applied Physics, Harvard University, Cambridge, Massachusetts
July 22, 1948

IN a recent interesting paper, Crane[1] has used the results of terrestrial heat-flow measurements at the surface of the earth, in order to make deductions about the capture cross section of neutrinos. He argues that neutrinos originating at the center of the sum would produce a maximum heating effect in the earth if the capture cross section were of the order of 10^{-35} cm², and that the consequent rate of heat absorption by the earth would be between 10 and 100 times the rate at which heat is known to be flowing outwards through the earth's surface. He concludes that the cross section, therefore, cannot be 10^{-35} cm².

The purpose of this letter is to point out that the geophysical evidence is, in fact, not as convincing as the above suggests, although it is probably still adequate to draw the conclusion. Our measurements of terrestrial heat flow are limited to a very small part of the earth's surface, and this entirely on the continents. This alone, of course, is not a serious objection, as it is most unlikely that heat flow at the bottom of the oceans will be found to average as much as 10 to 100 times more than the values we already have for the continents.

What is more important, however, is that there would not yet have been enough time, since the earth was created to establish a temperature equilibrium due to neutrino heat. In other words, even if neutrinos have been acting as a source of heat in the body of the earth for as long as the last 3×10^9 years, the temperature gradient at the surface (and hence the observed heat flow) would probably still be far from its final equilibrium value. Slichter[2] and others have considered the related problem of the heat generated in the earth by naturally occurring radioactivity.

In order to make calculations, so as to get an idea of the magnitudes involved, consider the case of a homogeneous solid earth containing a constant uniform source of neutrino heat A cal./cm³-sec. In order to evaluate the effect of the neutrinos alone, we shall assume the sphere (of radius $a>r\geqslant0$) to be initially all at temperature 0°C and that its exposed surface is held at the fixed temperature $T=0$°C. The solution of this problem is given by Carslaw and Jaeger,[3] who show that the temperature in such a sphere may be expressed as

$$T(r,t)=\frac{A}{61}(a^2-r^2)+\frac{2Aa^2}{k\pi^3 r}\sum_{n=1}^{\infty}\frac{(-1)^n}{n^3}\sin\frac{n\pi r}{a}\times\exp\left[-\frac{Kn^2\pi^2 t}{a^2}\right], \quad (1)$$

where k is the conductivity of the solid, K is its diffusivity, and t is time. On differentiating Eq. (1) and setting $r=a$, we find the temperature gradient at the surface to be

$$\frac{\partial T(a,t)}{\partial r}=-\frac{Aa}{3k}+\frac{2}{\pi^2}\frac{Aa}{k}\sum_{n=1}^{\infty}\frac{1}{n^2}\exp\left[-\frac{Kn^2\pi^2 t}{a^2}\right], \quad (2)$$

where the first term represents the equilibrium surface gradient and the second term is the transient. On evaluating this second term of Eq. (2), using $a=6370$ km, $t=3\times10^9$ years, and $K=0.01$ cm²/sec., we find that its magnitude is 84 percent of the first term. That is, the surface gradient would be now only 16 percent of its final value when $t=\infty$.

Because of the assumptions, these figures are rough, and should not be taken as indicating much more than a magnitude. For instance, the value of K is quite uncertain. Also, the earth is not a homogeneous solid; it has layers of different density, and we believe that its deep interior is at least partly fluid. Possible convection currents both in the dense liquid of the core and also in the mantle would speed up the process of heat transfer towards the surface. Slichter[2] discusses the contributions that these possible effects may make to the transfer of heat.

To sum up, it would seem that the geophysical evidence may be used to answer the question of the cross section, but with a significantly smaller margin of safety than has been suggested.

[1] H. R. Crane, Rev. Mod. Phys. **20**, 294 (1948).
[2] L. B. Slichter, Bull. Geol. Soc. Am. **52**, 561 (1941).
[3] Carslaw and Jaeger, *Conduction of Heat in Solids* (Clarendon Press, Oxford, 1947), p. 207.

Notes on the Beta-Spectra of Y^{90} and Sr^{90}

WALTER E. MEYERHOF
Department of Physics, University of Illinois, Urbana, Illinois
July 22, 1948

THE rather wide discrepancies in the literature values of the beta-end-point energy of Y^{90} [1] made it desirable to repeat the measurement of this energy. Since the Y^{90}(60 H) can be obtained in secular equilibrium with Sr^{90}(25 Y) in a practically carrier-free form, a value for the beta-end-point energy of Sr^{90} [2] was obtained also.

Sources of the order of 1 mg/cm² thickness were deposited on 0.02-mg/cm² thick zapon film and mounted in a conventional 180° type spectrometer with a Neary type slit system.[3] An end-window type Geiger counter carrying a fixed slit, which was covered with a 0.8 mg/cm² thick mica window,[4] served as detector. The resolution of the spectrometer was three percent. The magnetic field was

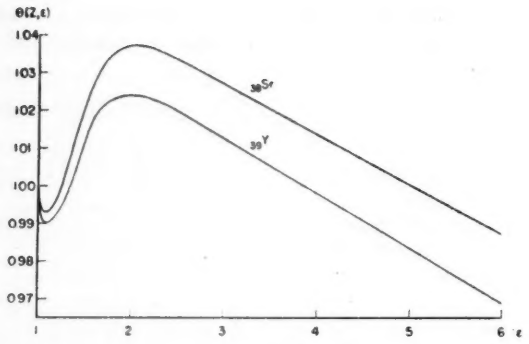

FIG. 1. $\theta(Z, \epsilon)$ for Sr and Y.

measured with a General Electric flux meter, tested for linearity and calibrated absolutely to within one percent with the annihilation radiation from Cu^{64} positrons.

Kurie plots[5] of the beta-spectra gave 2.35 ± 0.03 Mev for the Y^{90} end point and 0.61 ± 0.01 for the Sr^{90} end point.

The Kurie plots of the beta-spectra of Sr^{90}(25 *Y*) and Y^{90}(60 *H*) permit also an interesting comparison of the total beta-intensities by means of the Fermi theory of beta-decay.[6] This comparison is independent of the measurement of the low energy part (<0.2 Mev) of the beta-spectra.

Bleuler and Zünti[7] have been written the Fermi equation for allowed beta-decay in the convenient form,

$$N(\epsilon) \cdot d\epsilon = C(Z) \cdot \theta(Z, \epsilon) \cdot \epsilon^2 (\epsilon_0 - \epsilon)^2 \cdot d\epsilon, \qquad (1)$$

where ϵ is the total energy of an electron in units of its rest mass, ϵ_0 the total beta-end-point energy, and Z the charge of the decaying nucleus. $C(Z)$ depends only on Z and contains the (energy independent) electron-nucleon interaction constant and matrix element. $\theta(Z, \epsilon)$ for Sr and Y is shown in Fig. 1. Since for these elements it is equal to unity within a few percent, it may be replaced by an estimated average, θ_{Av}, and Eq. (1) can be integrated directly to get the total intensity of each beta-spectrum. Now, by making a Kurie plot, i.e., by plotting the quantity $(1/H)(n/\theta(Z, \epsilon) \cdot \epsilon)^{\frac{1}{2}}$ against ϵ, where H is the magnetic field which focuses electrons of energy ϵ and n is the corresponding counting rate of the detector, it can be shown that the intensity of a beta-spectrum may be written

$$I = (K/(\epsilon_0 - 1))^2 \cdot \theta_{Av} \cdot (\epsilon_0^5/30 - \epsilon_0^3/3 + \epsilon_0/2 - 1/5), \qquad (2)$$

where K is the intercept of the Kurie plot on the $\epsilon = 1$ axis. A constant factor has been omitted in Eq. (2).

Figure 2 shows a typical Kurie plot of Sr^{90} and Y^{90} in secular equilibrium; the Sr^{90} plot (reduced scale) was obtained assuming the Y^{90} Kurie plot to be a straight line.

TABLE I. Values of quantities appearing in Eq. (2) for Sr^{90} and Y^{90}.

	Beta-end point ϵ_0	Kurie intercept $K \cdot 100$	θ_{Av}	Intensity $I \cdot 100$	Intensity ratio
Sr^{90}	2.19 ± 0.01	28.0 ± 0.5	1.015	5.4 ± 0.2	1.04 ± 0.10
Y^{90}	5.60 ± 0.02	7.9 ± 0.2	1.005	5.2 ± 0.4	

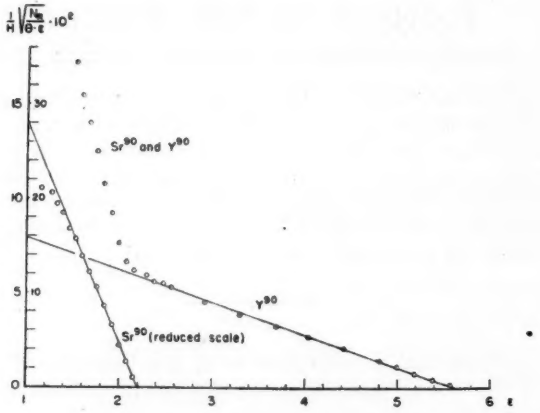

FIG. 2. Kurie plot for Sr^{90} and Y^{90}.

In Table I the values of the various quantities appearing in Eq. (2) are given for Sr^{90} and Y^{90}. Errors were estimated from the extreme ways in which straight lines could be drawn through the experimental points.

Since the Sr^{90} and Y^{90} are in secular equilibrium and since the beta-spectra are simple,[8] the intensity ratio is actually equal to unity. The calculated intensity ratio will only be equal to unity if the Fermi equation, Eq. (1), is correct at all energies. The large experimental error in the above-calculated intensity ratio, which could be reduced by the use of a better spectrometer, permits only the estimation that any deviations from the Fermi equation[9] in Sr^{90} and Y^{90} affect probably less than 1/10 of the electrons.

It is a pleasure to thank Professor C. W. Sherwin and Professor M. Goldhaber for encouragement and advice in this work. This research was supported in part by contract N6-ori-71 between the University of Illinois and the Office of Naval Research. The radioactive isotopes were obtained from the Atomic Energy Commission, Oak Ridge, Tennessee.

[1] Y^{90}: 2.2 (spectr.), 2.45 (abs. Al, Feather plot), 2.55 (abs. Al), 2.6 Mev (cloud ch.), Plutonium Project, Rev. Mod. Phys. **18**, 513 (1946); 2.1 Mev, W. Bothe, Zeits. f. Naturforschung **1**, 179 (1946).
[2] Sr^{90}: 0.6 Mev (abs. Al, Feather plot), Plutonium Project, Rev. Mod. Phys. **18**, 513 (1946).
[3] G. J. Neary, Proc. Roy. Soc. **A175**, 71 (1940).
[4] The author is greatly indebted to Mr. N. Goldstein for the manufacture of these counters.
[5] F. N. D. Kurie, J. R. Richardson, and H. C. Paxton, Phys. Rev. **49**, 368 (1936).
[6] E. Fermi, Zeits. f. Physik **88**, 161 (1934).
[7] E. Bleuler and W. Zünti, Helv. Phys. Acta **19**, 375 (1946).
[8] Plutonium Project, Rev. Mod. Phys. **18**, 513 (1946).
[9] See, e.g., C. S. Cook and L. M. Langer, Phys. Rev. **73**, 601; **74**, 227 (1948).

A Time-of-Flight Mass Spectrometer*

S. A. GOUDSMIT
Brookhaven National Laboratory, Upton, Long Island, New York
July 12, 1948

AMONG the various existing and proposed designs for mass spectrometers I have not found any that make use of the constancy of the time of flight in a magnetic

field. If an ion is released in a homogeneous magnetic field, it describes a helical path. The angular velocity of the helical motion is *independent* of the velocity of the ion and of the direction in which it is released. The time T for a complete revolution is, in round numbers,

$$T=670\ M/H \text{ microseconds.}$$

M is the mass of the ion in atomic weight units and H the field in gauss. For multiple ionization the time of flight is proportionally shorter. For an atomic weight around 150 a field of 100 gauss gives a time of flight of about 1000 microseconds. With a pulsed ion source it should not be too hard to measure this time to about 1/10th of a microsecond. The time interval between different masses is about 7 microseconds per mass unit. If one collects the ions after several revolutions, these time intervals are longer in proportion and a higher accuracy can be obtained.

It is noteworthy that the time of flight increases with the mass M. This means higher relative precision for heavier atoms, for which the methods used so far decrease in accuracy.

Though the time of flight is independent of the velocity of the ions, the dimensions of the apparatus set an upper limit to their speed. For single ions with an energy of V electron volts, the radius R of the helical path is approximately

$$R=145(VM)^{\frac{1}{2}}/H \text{ centimeter.}$$

For a practicable value of R it is necessary to use slow or decelerated ions of less than 100 ev. For multiple ions the radius decreases with the square root of the state of ionization. Too large a value of R may require too high a vacuum.

In addition to the constant time of flight, the helical orbits have a very advantageous focusing property after each complete revolution. All ions from a point source form, after every 360°, a sharp focal line through the source and along the direction of the field. The ion collector can be placed above or below the source, assuming the field H to be vertical. It is intended that the spacing between source and collector can be made large enough to allow the collection of ions which have made several revolutions. A vertical collimation of the ion beam and a controllable vertical deflecting field near the source may give the helical path just the proper pitch.

In the horizontal direction a wide angle can be tolerated, limited only by the dimensions of the magnetic field and its homogeneity. If the radius of the field is R_0 and the radius of the ion path is R, the horizontal half-width of the beam can be $(R_0-R)/R$ radians. Ions outside this angle will hit the wall. Of the magnetic field, only a ring of width $2(R_0-R)$ is used.[1]

The astigmatic focusing in the magnetic field causes the intensity of the various "orders" to go down only with the inverse first power of the number of revolutions. Moreover, the source of ions does not need to be a point. It can be a slit, vertical or horizontal, or an area of arbitrary shape. It is limited mainly by practical geometrical considerations such as difficulty in alignment of the collector, spacing of source and collector, or pulsing or collimating problems. A possible method of pulsing may be to sweep the beam across a slit by means of a modulated or pulsed deflecting field.[2]

Though the actual experiment will present many obstacles, the method described here is so flexible that one expects that such difficulties can be overcome without too much trouble. Moreover, it offers possibilities of expansion which may considerably increase the obtainable precision for measuring masses of heavy atoms. It may be very hard to use this method for absolute measurements. Relative measurements of greatly different masses may not be easy either, because their paths in the field can be very different. For relative masses of heavy elements the time-of-flight method looks most promising. Only after we have finished preliminary experiments, which are now being set up in the simplest possible way, shall we know with some certainty what the limitations of the proposed technique are.

* Research work done at Brookhaven National Laboratory under the auspices of the Atomic Energy Commission.

[1] The focusing at 180° is of no use for our purpose. This is only a focusing in space and not in time.

[2] The picture so far is that of a beam of slow ions describing a helix for which the pitch is much smaller than the radius. For fast ions it may be necessary to have them describe a helix with a pitch much larger than the radius. The field inside a long solenoid or inside a ring solenoid may be suitable for such a case. If, however, the method turns out to be worth while at all, the best way to handle faster ions is most likely the construction of an apparatus with a large radius.

The Abundance and Temperature of Methane in the Earth's Atmosphere

ROBERT R. MCMATH, ORREN C. MOHLER, AND LEO GOLDBERG
McMath-Hulbert Observatory of the University of Michigan, Pontiac, Michigan

July 15, 1948

THE presence of methane in the earth's atmosphere has now been definitely established on the basis of recent spectroscopic evidence.[1] From an analysis of equivalent widths of the lines of the P and R branches of the $2\nu_3$ band at 1.666μ, the writers have obtained estimates both of the abundance of methane and of its temperature in the earth's atmosphere.

The equivalent width of an unsaturated absorption line depends linearly on the number of molecules per unit cross section of the absorbing column, on the theoretical strength, and on the Boltzmann factor. If the theoretical line strengths were accurately known, this relationship could be employed to calculate both the abundance and the temperature from the observed line intensities. In the absence of accurate theoretical strengths, we have compared the atmospheric methane intensities with those produced in the laboratory by the use of an incandescent lamp as a source, together with an absorption cell containing a known quantity of methane at a 25-cm pressure and room temperature.

The mass abundance of methane turns out to be 1.2 parts in a million of the earth's atmosphere. The average temperature of the atmospheric column in which the methane absorption took place is −37°C. The observations

on which the foregoing results are based were obtained on March 28, 1948, between $22^h\ 05^m$ and $22^h\ 53^m$ U.T., with the sun at an average altitude of 14°34′.

The calculated temperature of −37°C is a reasonable value, being that normally found at a height of about 8 km.[2] Pending further study, nothing definite can be stated as to the lateral and vertical distribution of the methane in the earth's atmosphere. The indicated average height of 8 km is reasonable for the relatively light CH_4 molecule. Analysis of tracings made with the sun at various altitudes should provide further information on the vertical distribution.

[1] Marcel V. Migeotte, Phys. Rev. **73**, 519 (1948); McMath, Mohler, and Goldberg, *ibid.* 1203 (1948).
[2] *Smithsonian Physical Tables* (1934), p. 559.

Plasma Oscillations as a Cause of Acceleration of Cosmic-Ray Particles

D. Bohm and E. P. Gross
Princeton University, Princeton, New Jersey
July 12, 1948

ONE of the earliest hypotheses to explain the high energies of cosmic rays postulated weak interstellar electric fields, extending over enormous distances in space. These fields cannot be static because the known concentration of highly mobile ions in space rapidly produces neutralization. On the other hand, if an appreciable number of high energy particles are to be obtained from small oscillatory or fluctuating fields, it seems essential that there be present systematic effects producing cumulative energy transfers of the same sign over a long period of time. We wish to suggest here that plasma oscillations of ion clouds in intra-galactic space can provide such a mechanism of cumulative energy transfers.

About 15 percent of the volume of intra-galactic space is occupied by dust clouds, in which the ion density is of the order of 1 per cm^3. Like any other ion gas, this system constitutes a plasma[1] which can execute longitudinal electronic oscillations of angular frequency,[2]

$$\omega^2=(4\pi n_0e^2/m)+(3kT/m)(2\pi/\lambda)^2,$$

where n_0 is the mean electron density, T the electron temperature, and λ the wave-length. The electron temperature in these gases usually corresponds to a mean kinetic energy of a few ev.

It is found, experimentally[1] and theoretically,[3] that plasma oscillations are readily excited by special groups of electrons which have appreciably more than the mean thermal kinetic energy. To excite the interstellar plasma, one requires electrons of about 5 ev, or more, which can be provided by photo-ionization, and perhaps also by emission of streams of charge from hot stars.

Under the influence of a plasma oscillation of small amplitude, most particles will merely experience correspondingly small oscillatory changes of velocity. A particle which happens to be moving with a velocity close to the phase velocity of the wave, however, can be trapped in the trough of the potential, so that it oscillates about a mean speed equal to that of the wave. If the phase velocity should for any reason increase very gradually in the direction of propagation, this particle would tend to remain trapped, and thus would oscillate about an ever-increasing wave velocity. Inspection of the formula for the plasma frequency shows that such an increase of phase velocity is obtained whenever a wave enters a region of increasing ion density. In fact, as n_0 approaches $(m\omega^2/4\pi e^2)$, the phase velocity grows without limit, thus providing, in principle at least, a mechanism for accelerating particles to arbitrarily high energies. At some point near the above critical density, however, the particle ceases to be trapped, because its mass eventually becomes so great that the electric fields in the wave can no longer supply the mean acceleration needed to match the increase in phase velocity. The maximum energy attainable is determined by the wave amplitude, and this depends on the balance of excitation and damping processes which we hope to investigate in detail.

An important question is whether enough energy can be fed into plasma oscillations to maintain the known flux of cosmic-ray energy. The mean energy density in cosmic rays[4] is about one-fifth that of starlight[5] in interstellar space. If there is a small galactic magnetic field,[6,7] however, as has been suggested on other grounds, each cosmic-ray particle could move in a large orbit making as many as 10,000 revolutions before being absorbed, so that, to maintain the observed flux of cosmic rays, it would be necessary to supply only about 2×10^{-5} of the energy in starlight. It is fairly likely[8] that as much as 10^{-3} of the total energy in starlight goes into photo-ionization; hence this source alone may be adequate.

The final energy spectrum would depend, first, on the details of the acceleration process, and second, on the subsequent degradation in interstellar space.

[1] I. Langmuir, Proc. Nat. Sci. **14**, 627 (1928).
[2] J. J. Thomson, *Conduction of Electricity in Gases* (Cambridge University Press, Teddington), p. 353.
[3] D. Bohm and E. P. Gross, Phys. Rev. (to be published).
[4] L. Janossy, *Cosmic Rays* (Oxford University Press, London, 1947), p. 298.
[5] T. Dunham, Proc. Am. Phil. Soc. **81**, 277 (1939).
[6] H. Alfven, Zeits. f. Physik **107**, 579 (1937).
[7] L. Spitzer, Phys. Rev. **70**, 777 (1946).
[8] L. Spitzer (private communication).

An Investigation of Samarium and Gadolinium by the Photographic Method*

K. K. Keller and K. B. Mather
Physics Department, Washington University, St. Louis, Missouri
July 12, 1948

MÄDER[1] and Taylor[2] reported that long-range particles were emitted by Sm and suspected that these were protons. However, Cuer and Lattes[3] showed that these were not unique to Sm but appeared also from Nd in each instance with a track length corresponding to Po α-particles. They therefore suggested Po contamination as a source of long-range alphas.

A portion of an Ilford C2 Plate was impregnated with $Sm(NO_3)_3$ prepared from pure Sm_2O_3. The plate was examined after 32 days and found to contain many α-tracks with an equivalent range in air of 1.12 cm. In an area containing approximately 4000 Sm tracks, 14 long tracks of varying lengths were found. An equal area of unimpregnated portion of the plate showed 35 long-range tracks. This discrepancy is quite understandable. The nitrate solution has an oxidizing effect on a latent image, and it presumably removed the latent tracks existing in the emulsion at the time of impregnation. The 14 long tracks seen with the Sm α-tracks are probably due to impurities either introduced with the Sm or already existing in the emulsion and decaying during the 32 days. Furthermore, all the long tracks which ended in the emulsion could be identified by their lengths as α-particles from U, Th, or Po. If there are long-range particles from Sm they certainly number less than 0.4 percent of the short α-tracks. There is absolutely no evidence for proton emission.

It has been suggested by E. Feenberg[4] that the isotope $_{64}Gd^{152}$ may possess long-lived α-activity, having escaped detection on account of its low abundance (0.2 percent).

A number of C2 emulsions (100μ) were impregnated with pure Gd_2O_3 by Ilford Ltd., England, during manufacture. Each 3″×1″ plate contained 38±5 mg of oxide. Plates were developed at the end of 4, 9, and 14 weeks after preparation. It was first verified by further impregnating one of these plates with U and measuring its α-tracks that the stopping power of the emulsion had not been altered appreciably by the introduction of the Gd. Hence 1 Mev, α-tracks (and somewhat lower) could have been distinguished clearly. A few tracks were found in the plates having lengths corresponding to the 2-Mev α-particles from Sm. There was no way of proving from our work whether these actually originated from Sm, but as the number of tracks observed corresponds to a Sm impurity in the Gd of less than 10^{-2} percent, the interpretation seems very likely. No other tracks were found which could not be associated with U or Th contamination or reasonably accounted for as due to cosmic rays. Knowing the weight of Gd per plate, the duration of exposure, and the area scanned, it may be said that the half-life of $_{64}Gd^{152}$ must be greater than 10^{15} years and is probably greater than 10^{16} years. These figures can be converted for the other isotopes of Gd knowing their relative concentrations, and hence limits can be placed on their half-lives also. Nothing is gained by exposing longer than about 3 months on account of the fading of α-tracks. It is also unlikely that a large increase can be made in the weight of material introduced into the emulsion without jeopardizing its quality. Hence it seems improbable that the lower limit on half-life quoted above can be increased significantly with the photographic method. The next step in such work must be to use isotopically pure or at least enriched Gd. Assuming a photographic emulsion to be impregnated with a pure isotope, the upper limit of half-life which could be detected by a reasonable amount of scanning is probably of the order of 10^{20} years.

The oxides of Sm and Gd were obtained from Johnson, Matthey, and Company, Ltd., London ("Specpure" Brand). We are indebted to Dr. F. N. D. Kurie for suggesting both these problems. One of us (K.B.M.) acknowledges his Studentship from the Science and Industry Endowment Fund, Commonwealth of Australia.

* This work was supported by Navy Contract N6ori-117, T.O.1.

[1] M. Mäder, Zeits. Physik **88**, 601 (1934).
[2] J. H. Taylor, Nature **136**, 719 (1935).
[3] P. Cuer and C. M. G. Lattes, Nature **158**, 197 (1946).
[4] E. Feenberg, Rev. Mod. Phys. **19**, 239 (1947).

Erratum: Achromatization of Debye-Scherrer Lines

[Phys. Rev. **73**, 1207 (1948)]

H. EKSTEIN AND S. SIEGEL
Armour Research Foundation, Chicago, Illinois

IN the above letter, the relative difference $|\Delta d/d|_R$ of two lattice parameters of the sample giving rise to two lines which are just resolved in the Rayleigh sense should read:

$$\left|\frac{\Delta d}{d}\right|_R = \frac{1.22S}{2F}\cot\theta\cos 2\theta\frac{\cos(\theta m+\alpha)}{\cos(\theta m-\alpha)}.$$

Table of Interplanar Spacings in Angstrom or K.X. Units in Terms of 2θ for Different Target Materials

SUZANNE VAN DIJKE BEATTY
Westinghouse Research Laboratories, East Pittsburgh, Pennsylvania

July 1, 1948

IN view of the widespread and increasing use of the x-ray Geiger counter spectrometer, tables have been computed to expedite the reduction of the diffraction patterns giving line intensities as a function of 2θ.

The tables given in the Internationale Tabellen zur Bestimmung von Kristallstructuren[1] list the d values at intervals of 0.1θ. This requires the reduction of 2θ to θ and interpolation for d. In addition, the volume is scarce and expensive. The tables published by the Advisory Committee for Aeronautics[2] are prepared expressly for use with a Debye-Sherrer camera and give d as a function of R(mm).

The tables here referred to give d values for Mo, Cu, Co, Fe, and Cr targets between the 2θ values 5.0° and 85.0° inclusive. Every tenth of a degree is listed between 5.0° and 70.0°, every two-tenths between 70.0° and 80.0°, and every five-tenths between 80.0° and 85.0°. Since the argument is in angular units, no reductions are necessary to compensate for different counter-arm lengths, motor rates, etc. The values of the interplanar spacings, d, are computed from the Bragg equation, $n\lambda=2d\sin\theta$, where θ is the glancing angle, λ the wave-length of the diffracted target radiation, and n is taken as unity in this case. The tables are available in angstrom units or K.X. units. In either case, conversion curves are given for all five target materials for various values of 2θ.

The tables may be obtained directly from the Westinghouse Research Laboratories in East Pittsburgh, Pennsylvania.

[1] *Internationale Tabellen zur Bestimmung von Kristallstructuren* (Gebruder Borntraeger, Berlin, 1935), Band II, pp. 585–608.
[2] J. H. Kittel, *Table of Interplanar Spacings*, Advisory Committee for Aeronautics (October, 1945).

Erratum: On the Fine Structure in the Inversion Spectrum of Ammonia

[Phys. Rev. **74**, 107 (1948)]

R. S. HENDERSON
Department of Physics, Harvard University, Cambridge, Massachusetts

IN the above letter, numerical values quoted for the constants a and b were interchanged; they should have been given as

$$a=0.0011 \text{ Mc/sec.}, \quad b=0.0057 \text{ Mc/sec.}$$

Spin and Quadrupole Moment of S^{33}*

C. H. TOWNES AND S. GESCHWIND
Columbia Radiation Laboratory, Columbia University, New York, New York

July 12, 1948

QUADRUPOLE effects caused by S^{33} in OCS have been found which show that the spin of S^{33} is $\frac{3}{2}$ and that its quadrupole moment is negative.

Previous evaluation[1] of the mass difference ratio $(S^{33}-S^{32}/S^{34}-S^{32})$ from frequencies of observed $J=1\rightarrow2$ rotational lines of OCS^{32}, OCS^{33}, and OCS^{34} disagreed with other mass measurements. More recent[2] frequency measurements and measurements of the sulfur masses by Davison[3] have served only to increase the discrepancy. Since the most likely explanation of the discrepancy appeared to be a shift of the OCS^{33} line frequency by a quadrupole coupling between the S^{33} nucleus and the molecular field, the OCS^{33} absorption line $J=1\rightarrow2$ was re-examined and a hyperfine structure caused by quadrupole effects found which had previously been overlooked.

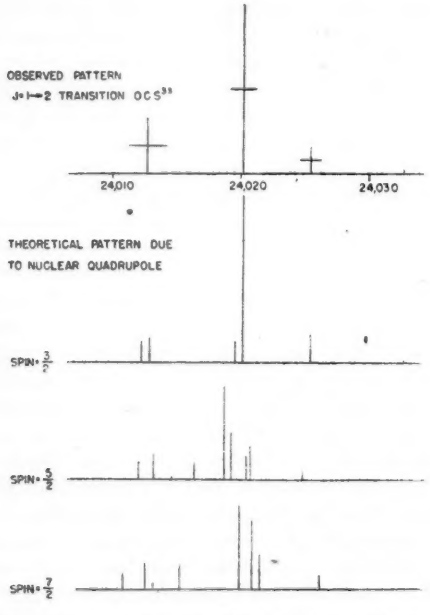

FIG. 1. Comparison of observed OCS^{33} spectrum with theoretical patterns for several assumed values of nuclear spin.

TABLE I. Observed frequencies and intensities compared with theoretical values for a spin of 3/2 and a quadrupole coupling constant of −28.5 mc.

Transition	Observed frequency	Theoretical frequency	Observed relative intensity	Theoretical relative intensity
$(J=1\rightarrow2)$				
$F=1/2\rightarrow3/2$ $5/2\rightarrow5/2$	24,013.04	24,012.85	0.33	0.25
$1/2\rightarrow1/2$ $3/2\rightarrow5/2$ $5/2\rightarrow7/2$	24,020.21	24,020.21	1.0	1.0
$3/2\rightarrow3/2$	24,025.39	24,025.67	0.17	0.16
$3/2\rightarrow1/2$	24,032.75	24,032.48	0.03	0.025

TABLE II. Results of measurements.

Molecule	Rotation-vibration constants in megacycles
OCS^{32}	$a_1=18.12\pm0.06$**
OCS^{34}	$a_2=-10.37\pm0.06$
OCS^{34}	q (l-type doubling constant) 6.07 ± 0.06

The frequencies and relative intensities of the lines found and the theoretically expected values are listed in Table I. That the lines allow a definite determination of the S^{33} spin as $\frac{3}{2}$ may be seen from Fig. 1, where theoretically expected patterns for various spins are compared with the observed spectrum. The horizontal bar through the midpoint of each observed line represents the half-width of the line under conditions of observation. It may be seen that although resolution was not sufficiently good to split the two low frequency components, their combined line is appreciably broadened.

Since the intensity of the OCS^{32} line is known[2] to be 5×10^{-5} cm^{-1}, absorption coefficients for the OCS^{33} lines may be calculated from the isotopic abundance of S^{33} (0.74 percent). It is found that the weakest observed line ($F=\frac{3}{2}\rightarrow\frac{1}{2}$) has a peak absorption coefficient of 5×10^{-9} cm^{-1} or 2.5×10^{-9} neper/cm at room temperature. This is apparently the weakest absorption line so far reported near 1 cm wave-length. The detection system used Stark modulation at 200 kc in a 3-meter wave guide and a phase-detecting or "lock-in" amplifier with a band width of about 20 cycles. The guide was cooled to −78° to enhance the line intensities threefold.

The quadrupole coupling constant $eQ(\partial^2V/\partial z^2)$ is -28.5 ± 0.7 mc. Although the character of the molecular bonds is rather poorly known, the method of determining $\partial^2V/\partial z^2$ previously described[4] appears to allow a definite determination of the sign of the S^{33} quadrupole moment as negative and a determination of the magnitude as -0.05×10^{-24} cm^2 with an accuracy of about a factor of two.

This quadrupole coupling increases the frequency of the strongest line (previously measured) by 0.54 mc. Allowing for this effect and using the latest frequency measurements, the mass ratio $(S^{33}-S^{32}/S^{34}-S^{32})$ can be determined as 0.50066 ± 0.00015. This is in good agreement with the value 0.50060 ± 0.0005 obtained from recent measurements of nuclear reaction energies.

Some additional rotational lines of OCS molecules in excited vibrational states were measured incidentally to this work. They give the results shown in Table II.

* Work supported by the Signal Corps.
** Also recently measured by A. Roberts (private communication).
[1] C. H. Townes, A. N. Holden, and F. R. Merritt, Phys. Rev. **72**, 513 (1947).
[2] C. H. Townes, A. N. Holden, and F. R. Merritt (to be published).
[3] P. Davison, Paper (P5) of Am. Phys. Soc. meeting in Washington (1948).
[4] C. H. Townes, Phys. Rev. **71**, 909 (1947).

The Radioactive Lanthanum and Cerium Isotopes of Mass 137

M. G. Inghram and D. C. Hess, Jr.
Argonne National Laboratory, Chicago, Illinois
July 9, 1948

A SAMPLE of CeO_2 (Hilger Lab. No. 13386) was submitted to long neutron bombardment in a graphite-moderated pile. The activities were studied by the mass spectrographic transfer technique[1] and shown to consist principally of 30.6-day Ce^{141}, 1.4-day Ce^{143}, and 13.5-day Pr^{143}. After the sample had "cooled" for ten months, its isotopic constitution was compared with that of normal cerium using the surface ionization type of mass spectrometer previously described.[2]

Normal cerium showed ion currents at masses 152, 154, 156, and 158, due to the oxide ions $Ce^{136}O^{16}$, $Ce^{138}O^{16}$, $Ce^{140}O^{16}$, and $Ce^{142}O^{16}$. In addition, weak peaks were observed due to the two weaker oxygen isotopes. Pertinent impurities present were Ba, La, and Pr. The lanthanum and praseodymium were detected as $La^{139}O^{16}$ and $Pr^{141}O^{16}$, appearing at masses 155 and 157; the barium, as metallic ions at masses 130 to 138. The bombarded sample showed in addition to the above peaks a new peak at mass 153. That this peak is due to a new isotope of lanthanum was proved by eliminating in turn all the other elements which might give rise to this peak. That it was not cerium was proved by the fact that the ratio of the 152 to 153 peaks varied by a factor of 100 as the temperature of the filament varied. Barium was eliminated because barium ions are emitted as oxides. It is thus concluded that the isotope observed at mass 137 is lanthanum which has been formed by radioactive decay of Ce^{137}. In the particular sample under investigation the ratio of La^{137} to La^{139} was 0.15.

From the fact that at the time of isotopic analysis no Ce^{137} could be detected, it is concluded that the half-life of Ce^{137} is less than two months. By further consideration of the fact that the amount of radioactivity at mass 137 was too small to show by the transfer technique and that all of the La^{137} was the daughter of the Ce^{137} it may be concluded that the half-life of Ce^{137} is less than two weeks. Since the isotopic composition of the barium impurity was not detectably changed as the result of decay of La^{137}, the half-life of La^{137} must be greater than thirty years.

[1] R. J. Hayden and M. G. Inghram, Phys. Rev. **70**, 89 (1946).
[2] M. G. Inghram, R. J. Hayden, and D. C. Hess, Jr., Phys. Rev. **72**, 967 (1947).

The Velocity of Discharge Propagation in Geiger Counters

A. J. Knowles, C. Balakrishnan, and J. D. Craggs
Research Department, Metropolitan-Vickers Electrical Company, Ltd., Trafford Park, Manchester, England
June 2, 1948

THE importance of the finite speed of propagation of the Geiger counter discharge was indicated some years ago by Dunworth,[1] and its existence was indicated by various workers.[1-3]

It was only recently that various and widely different experimental methods have been used by Hill and Dunworth,[4] Huber *et al.*,[5] and Wantuch[6] to measure the velocity of discharge spread along counters filled with self-quenching gas mixtures, such as argon/ethyl alcohol vapor. The results of the above authors disagree to an appreciable extent, as discussed by Wantuch.[6] The purpose of this note is not to comment further on the measurements with self-quenching ("fast") counters, but to submit measurements taken with externally quenched counters containing hydrogen. The use of elementary gases should enable simpler analyses of the results to be made and, it is hoped, might ultimately provide data on photo-ionization in such gases.

The method used in the present experiments was different from any of those used by the above authors and is shown schematically in Fig. 1. A pulse resulting from discharge build-up in one of the short end cylinders ("start cylinder") in the long counter shown (we have used them up to 2 m in length) connects a 4-mc/sec. quartz-controlled oscillator through a gate circuit to a fast scaler and recorder; the discharge then spreads along the counter.

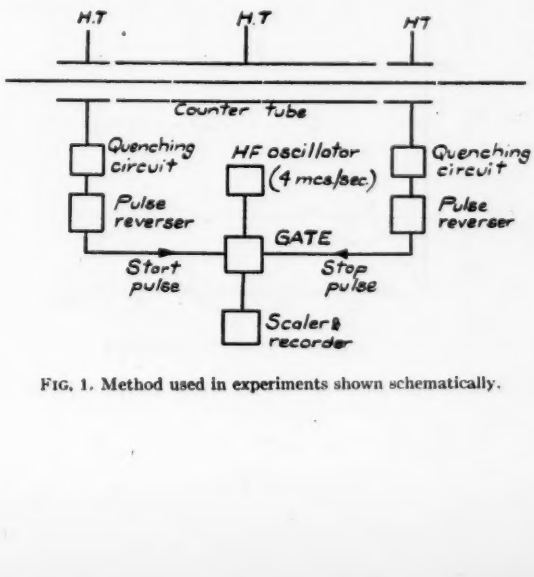

FIG. 1. Method used in experiments shown schematically.

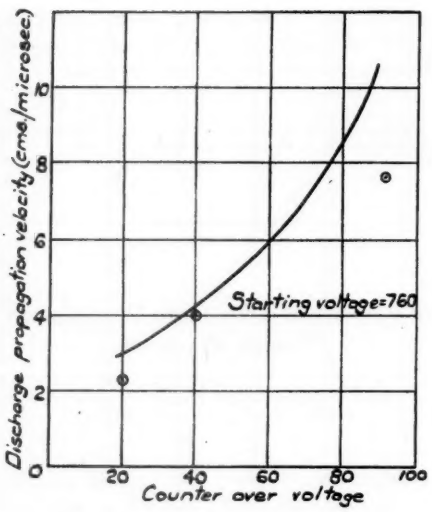

FIG. 2. Results of check measurements taken with an argon/ethyl alcohol-filled counter.

and the subsequent pulse from the other end cylinder ("stop cylinder"), as the discharge reaches it, closes the gate and the intervening number of oscillations, each 0.25μ sec. in duration, is shown upon the recorder.

Some check measurements were taken with an argon/ethyl alcohol-filled counter 1 m in length. Some of the results (9.5 cm Hg argon, 0.5 cm Hg C_2H_5OH) are shown in Fig. 2. The wire and cathode diameters were, respectively, 5 mils (tungsten) and 0.75 inch (copper). The curve in Fig. 2 was taken from the publication of Hill and Dunworth,[4] using an 8-mil wire but with an otherwise similar counter, and the points are the present results. The agreement (see discussion by Wantuch[6]) is considered reasonable.

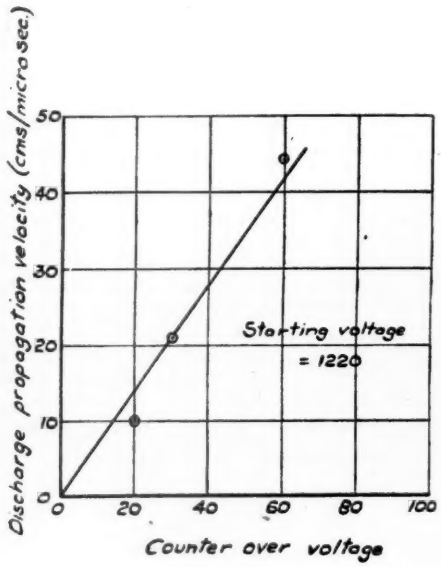

FIG. 3. Results obtained with a counter filling of 10 cm Hg hydrogen.

Using 1-m and 2-m counters (5-mil wire, 0.75-inch dia. cathodes), data have been obtained with certain elementary gases, and Fig. 3 shows some results obtained with a counter filling of 10 cm Hg hydrogen (2 m in length). The speed of discharge propagation is much higher than in Fig. 2, as would be expected in general terms if the discharge spreads along the wire by virtue of a photoionization mechanism, as is generally assumed.[5,7-9]

This simple picture is complicated by various factors which cannot be fully discussed in a note. For example, some discharges start in the long cylinder (see the schematic counter in Fig. 1) as a result the finite background count and, propagating in opposite directions, give short spread times. Discharges propagating by virtue of cathode emission of electrons and by photons covering distances of some cm[9] will also give short times. These and other related matters will be discussed more fully elsewhere, together with a consideration of the mechanism of discharge propagation and more exhaustive experimental data.

We are indebted to Sir A. P. M. Fleming, Director, and Mr. B. G. Churcher, Manager, of the Metropolitan-Vickers Research Department for permission to publish this note.

[1] J. V. Dunworth, Nature **144**, 152 (1939).
[2] W. E. Ramsey and W. L. Lees, Phys. Rev. **60**, 411 (1941).
[3] A. G. M. van Gemert, H. Den Hartog and F. A. Muller, Physica **9**, 556 (1942).
[4] J. M. Hill and J. V. Dunworth, Nature **158**, 833 (1946).
[5] P. Huber, F. Alder, and E. Baldinger, Helv. Phys. Acta **19**, 204 (1946).
[6] E. Wantuch, Phys. Rev. **71**, 646 (1947).
[7] S. A. Korff, *Electron and Nuclear Counters* (D. Van Nostrand Company, Inc., New York, 1946), pp. 95 ff.
[8] W. E. Ramsey, Phys. Rev. **61**, 96 (1942).
[9] C. Balakrishnan, J. D. Craggs, and A. A. Jaffe, Phys. Rev. **74**, 410 (1948).

Erratum: Alkali Halide Scintillation Counters

[Phys. Rev. **74**, 100 (1948)]

ROBERT HOFSTADTER
Princeton University, Princeton, New Jersey

THE Editor regrets that Fig. 1 of the above-named Letter to the Editor was printed upside down. It should have been as follows:

FIG. 1. Oscilloscope screen photographs taken at random for 1/30 second. Above, pulses caused by NaI (Tl) and below, pulses caused by naphthalene under identical circumstances. Sweep calibration: total length of sweep equals 4.3 microseconds.

Negative Energies in Generalized Electrodynamics

JERZY RAYSKI
N. Copernicus University, Toruń, Poland
July 7, 1947

THE "generalized electrodynamics" of Podolsky and Schwed[1] is based on the equation of the fourth order for the potentials:

$$\Box(1-a^2\Box)\varphi_\alpha=0. \tag{1}$$

The general solution of this equation consists of two parts: the "ordinary" field ϕ_α, with the property $\Box\phi_\alpha=0$, and the "extraordinary" field $\langle\phi_\alpha\rangle_N$ obeying the Schrödinger-Gordon-Klein equation $(\Box-(1/a^2))\langle\phi_\alpha\rangle_N=0$. The energy of the field contains subtractively both fields:

$$H=\int\{\varphi_\alpha^*(k)\varphi_\alpha(k)+\varphi_\alpha(k)\varphi_\alpha^*(k)\}k^2dk - \int\{\langle\varphi_\alpha^*\rangle_N(k)\langle\varphi_\alpha\rangle_N(k) + \langle\varphi_\alpha\rangle_N(k)\langle\varphi_\alpha^*\rangle_N(k)\}\langle k^2\rangle_N dk, \tag{2}$$

where the $\varphi_\alpha(k)$ and $\langle\varphi_\alpha\rangle_N(k)$ are the Fourier coefficients of the ordinary and extraordinary fields:

$$\varphi_\alpha(r,t)=(2\pi)^{-\frac{1}{2}}\int\{\varphi_\alpha(k)\exp i(\mathbf{k}\cdot\mathbf{r}-kct) + \varphi_\alpha^*(k)\exp -i(\mathbf{k}\cdot\mathbf{r}-kct)\}dk \tag{3}$$

and a similar equation for $\langle\phi_\alpha\rangle_N$.

In order to simplify the calculations by avoiding a rather complicated auxiliary condition (analogous to the condition $\partial A_\alpha/\partial x_\alpha=0$ of the usual electrodynamics), we may consider a scalar generalized theory with the scalar potential φ. The only difference in the above formulas is that the field quantity appears in (1)–(3) without suffix. In the quantized theory the Fourier coefficients are matrices with the following commutation rules:

$$[\varphi^*(k),\varphi(k')]=(-c\hbar/2k)\delta(k-k'), \tag{4a}$$
$$[\langle\varphi^*\rangle_N(k),\langle\varphi\rangle_N(k)]=(c\hbar/2\langle k\rangle_N)\delta(k-k'). \tag{4b}$$

$\varphi^*(k)$ and $\varphi(k)$ are essentially the well-known matrices denoted usually by $C^*(k)$ and $C(k)$ with the property $[C^*(k),C(k)]=\delta(k-k')$. In close analogy with the procedure applied by Podolsky,[2] we should put in (4b) (apart from a coefficient):

$$\langle\varphi\rangle_N(k)\rightarrow C'(k),\quad \langle\varphi^*\rangle_N(k)\rightarrow -C'^*(k), \tag{5}$$

where

$$[C'^*(k),C'(k)]=\delta(k-k').$$

The relation (4b) is then satisfied and the negative part of the Hamiltonian changes its sign so that the energy becomes positive definite. However, this procedure of avoiding the negative energies is erroneous as the extraordinary field becomes, with (5), imaginary. The only way to satisfy (4b) is to put:

$$\langle\varphi\rangle_N(k)\rightarrow C'^*(k),\quad \langle\varphi^*\rangle_N(k)\rightarrow C'(k). \tag{6}$$

In this case the ordinary and the extraordinary fields are real, but the energy remains non-definite.

The case of a vector field is quite similar, notwithstanding the complications due to the introduction of some auxiliary condition, so that the difficulty with negative energies of the "extraordinary photons" still exists.

[1] B. Podolsky and P. Schwed, Rev. Mod. Phys. 20, 40 (1948).
[2] See reference 1, p. 50, "Concluding remarks."